University of Alberta

Ultra-class Hauler Tire-Rim Interactions

by

Michael Bolster 

A thesis submitted to the Faculty of Graduate Studies and Research in partial fulfillment of the requirements for the degree of Master of Science

in

Mining Engineering

Department of Civil and Environmental Engineering

Edmonton, Alberta

Spring, 2007

Your file Votre référence
ISBN: 978-0-494-29939-5
Our file Notre référence
ISBN: 978-0-494-29939-5

Abstract

In order to gain an improved understanding of the effect of high-g loading on ultra-class rims and tires a series of loading tests were conducted on a 30.00R51 rim and tire arrangement. Using the data collected, graphical analyses were conducted on both the rim and tire for increasing load as well as varying internal tire pressures.

Graphical models were developed using low-g equivalent loads, allowing extrapolation and predictions of high-g loads for specific rim components at various locations around the rim circumference. The research described in this thesis is a starting point in identifying adverse loading leading to potentially unsafe operating conditions. This work will lead engineers and operations personnel concerned with ultra-class hauler performance and specifically tire and rim performance to better understand the impact of high loads on component life.

Table of Contents

List of Figures

List of Tables

List of Symbols and Abbreviations

LTUG	Large Tire User Group
R	Radius
°	Degrees
ϵ	Strain (mm/mm)
$\mu\epsilon$	Microstrain (mm/mmx10^{-6})
σ	Stress (MPa)
g	Gravitational Constant (9.81m/s^2)
ν	Poisson's Ratio
TKPH	Tonne Kilometers Per Hour
TMPH	Tonne Miles Per Hour
CDN	Canadian
SAE	Society of Automotive Engineers
ASTM	American Society for Testing and Materials
U/L	Unloaded
NTS	Not to Scale
LVDT	Linear Vertical Displacement Transducers

1 Introduction

The need for increased production has driven global surface mining operations to move to larger equipment. As a result of this, trucks have moved into the ultra-class category while rim development and knowledge of the interaction between a tire and rim has remained relatively stagnant. More than ever there is the need for increased development and research of rims as many haulers currently operating are exposed to unanticipated high-g loading, especially those operating with soft underfoot conditions; one of the primary causes of high-g loading. As a result, rims are cracking and failing at an unprecedented rate while tires are also experiencing shorter than expected life cycles (LTUG Proceedings, 2005).

The majority of design modifications of the current generation of rims are scale increases of older designs and site specific field fits. This lack of engineered design or understanding of the consequences of high-g loading, has resulted in several instances of rim failure leading to lost production (LTUG Proceedings, 2005), injuries (North Queensland Tyre Fitters Workshop Meeting, 2004), and even fatalities (Occupational Safety and Health Service, Department of Labour, New Zealand, 2004). With an improved understanding of the performance of rims and tires subjected to high-g loading, the knowledge base in this field will be expanded to allow manufacturers to target improved designs that will minimize rim cracks and tire failures that plague today's mining industry.

1.1 Purpose of Research

The end goal of this research is to improve safety conditions at mine sites, as well as to minimize repair and replacement costs of rims and tires for large scale equipment. It is believed that these objectives can be achieved by increasing the understanding of the interaction between the rim and tire of an ultra-class hauler and the effect that a high-g impact has on the interaction. This includes gaining an improved appreciation of the stress/strain concentrations that develop in the rim as a result of loads transferred from the tire and how the shape and magnitude of these stress/strain distributions change as a result of an increase in g load impacts. Therefore, the

purpose of this thesis project is to develop a tool or mechanism, based on the data obtained from research and testing, to accurately predict the impact of high-g loading on ultra-class rims and tires.

Currently, due to the lack of relevant, published material on ultra-class hauler truck and rims, there are misconceptions about the impact of high-g loads on rims and tires. In terms of loading on rims, many people within the mining industry are under the belief that an impact load is not detrimental to a rim, or any stiff component of a hauler, unless it exceeds the plastic limit of the component material. However, mining equipment operates in cycles, and as shown by a representation of cyclic loading for a typical failure curve in figure 1-1, failure in the material can happen as a result of several smaller than peak loads, causing the load/unload curve to traverse in the direction of the strain axis until reaching failure, at a value less than that of the peak limit value. Also, as shown in figure 1-2, for the same material, failure will occur sooner (less cycles) as a result of a larger value of cyclic loading due to the smaller distance underneath the failure curve at higher values of stress. Therefore, not only can repeated loads less than the peak limit, such as the majority of high-g impacts, cause failure in a material as a result of cyclic loading, but the higher the value of load, the fewer the amount of cycles required for failure to occur.

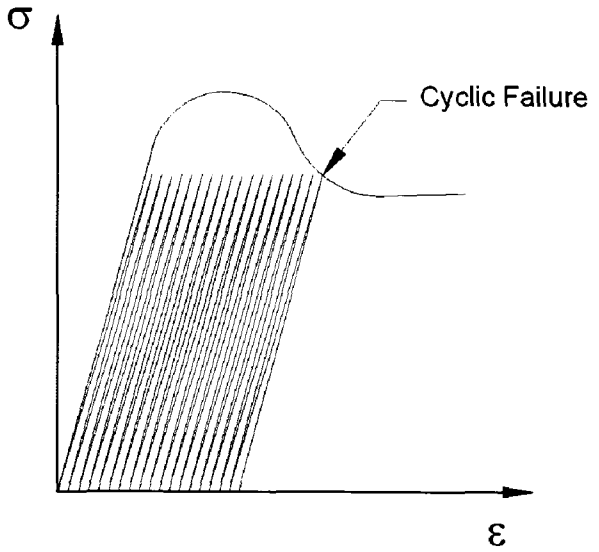

Figure 1-1: Representation of Cyclic Failure for Low Load for Typical Stress/Strain Plot

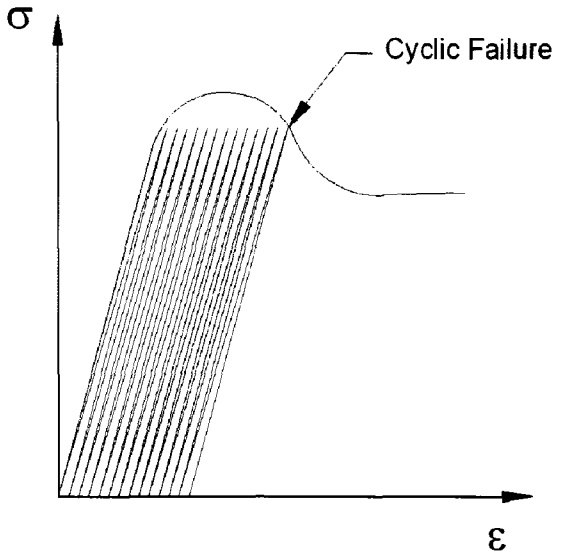

Figure 1-2: Representation of Cyclic Failure for High Load for Typical Stress/Strain Plot

Similarly to rims, the effect of high-g loading on tires is often under estimated, as demonstrated by the calculation of heat build up in tires. Heat build up in tires is estimated using a Tonne Kilometer Per Hour (TKPH) or Ton Mile Per Hour (TMPH) estimate. Each of the tire manufacturers provide different formulas for calculating TKPH or TMPH, however a basic definition is that it is a qualitative measure of heat build-up due to friction in tires and basically states that heat build up is a function of both load and distance traveled for a haul truck. Trade offs can be made: trucks can carry heavier loads but must have their distance traveled reduced, or vice versa. Many mine sites track a running average of TKPH to ensure that their tires do not approach the critical temperature (the temperature at which the tire was cured at and subsequently breaks down at) based on the appropriate TKPH value for their given tires. Once they come close, trucks are generally reassigned to shorter hauls or are instructed to reduce their loads to ensure maximum tire life.

The problem with this method of estimating heat build up is that the value of Qm that is used is measured using a hauler's on-board payload detection system, and therefore, does not represent the value of load experienced by the tire when subjected to a high-g impact. Therefore, if a truck tire experiences a 2g impact, which has an equivalent force of twice that at 1g, the actual TKPH value should be twice that is

measured, and as a result, the actual heat build up in the tire is underestimated. This underestimation of heat build up can lead to premature heat separation (tire temperature exceeding the curing temperature resulting in a separation of the rubber and steel belting), which could be mitigated by a greater understanding of the adverse effect of high g loading on a tire.

1.2 Value to Industry

As commodity prices continue to increase world wide, failures to tires and rims become very costly to mining companies. Increased commodity prices result in higher revenues, however, it becomes essential that a piece of equipment is being used to its full availability to maximize profits and not being parked due to repair or lack of tires and rims. Another negative aspect of higher commodity prices is the increased competition for available rims and tires. In the past several years several mines that were out of operation have come back online, bringing back several hundred pieces of equipment that were sitting idle for years. Also, China's mining industry continues to grow strong and shows no signs of slowing down, increasing the competition for tires and rim components vastly. Finally, as commodity prices increase, so do the prices of tires and rims. As rubber and steel prices have continued to rise the prices of ultra-class heavy hauler rims and tires have increased to $55,000 and $45,000 respectively, or approximately $100,000 per rim/tire arrangement or higher as the market dictates (prices in 2005 CDN dollars). Therefore, based on the high revenue losses for parked trucks, the increased competition for available components and the cost of materials, it is imperative that mining companies maximize the number of hours they can get out of each tire and rim. This can be achieved through a greater understanding of the negative effect of high g loads on rims and tires.

1.3 Research Approach

The I.F. Morrison Laboratory at the University of Alberta was selected as the location to perform the testing for several reasons. The primary reason being that it had the

resources, tools and equipment required to manipulate and test large specimens. Also, it was also the safest place available to test the rim and tire arrangement as it allowed testing to be performed in a large unconfined space, which would minimize any potential damage in the possible event of a tire failure occurring during testing.

With the testing location chosen it was possible to size a tire and rim to test based on the available resources, with the choice of the 30.00 series rim and tire being made. This size was chosen due to the fact that it was the largest sized tire that Kal-Tire had available for testing due to the impending tire shortage that was in its initial stages. Also, this size tire remains relevant in today's mining industry, as it is still in use on haulers in many of the surface coal mines, as well as in some of the larger oil sand operations on gravel and water trucks. With the tire size selected, Rimex fabricated an appropriate sized rim in their manufacturing plant in Surrey, B.C. and shipped it to Kal-Tire's regional office in Kamloops, B.C. There the rim and tire were assembled and an inflation pressure of 30psi was applied, allowing the specimen to be shipped as one component to the The I.F. Morrison Laboratory in Edmonton for testing.

With the testing location set and the tire and rim obtained, the decision of how to test the assembly was required. A test method that provided an accurate simulation of what a rim and tire experienced in the field as a result of high g loading was chosen. The test method also had to be safe to ensure that there would be no harm done to the people or property involved in this project. Therefore it was decided to construct a testing apparatus that loaded the rim and tire similar to a conventional hauler hub assembly, allowing an accurate simulation of the loading experienced by haul trucks during operation. It was also decided to perform the test at lower values of g-load and then to predict the results for high g loads using the trends developed, allowing insight into the effects of high g loading on rims and tires without having the risk associated with producing the high loadings in the test environment. For a description analysis of the test method set up and procedure see Chapter 3. For results and analysis of the testing, see Chapters 4 and 5 respectively.

2 Background

This chapter provides the background information required to fully understand the scope of this research project. This is achieved by examining several key topics. First is a summary of the literature related to the project. This provides a basic understanding of any previous work that has been completed and provides a starting point for the research. In addition to the literature search, an in depth description of heavy hauler tires and rims is provided, which not only describes the components of the rims and tires, but also the common nomenclature that is associated with them. Also, a review of the most common causes of rim and tire damage in the industry is provided based on information from operating mines throughout North America. And finally, a cursory look at the impact of soft ground conditions, such as those found in the oilsands, is presented to set the stage for future work beyond this thesis.

2.1 Literature Search and Consultation of Industry

From the literature it was determined that there is no available literature that pertains to the subject of testing or design of large-scale rims and tires. It is commonly known that several of the tire manufacturers have performed large scale tests and finite element analyses for the current generation of rims and tires but are reluctant to release their results or even an overview of their testing procedures. These companies (Michelin, Bridgestone, and Goodyear) spend millions of dollars a year in terms of research and do not want their information falling into their competitor's hands. Therefore, the data these companies have obtained throughout the years is kept in-house, and is not available to the general public, including end-users of the tires, companies who service and maintain the tires, and educational/research institutes.

An alternative source of information that was examined was the Society of Automotive Engineers' (SAE) standards, specifications, and practices. The SAE regulates all types of automotive vehicles in terms of operating, design, and testing, and therefore seemed to be an ideal source of information for this research project. An examination of this resource did provide some detail in regards to descriptions

and nomenclature that is associated with rims and tires, which will be discussed in detail in the upcoming sections. However, the data that was available in terms of design and testing of rims and tires was either out of date or of too small a scale.

The reason for the lack of information in this field is two-fold: first is that large scale rims and tires are a relatively new technology, having only been in existence for approximately five years. The second reason for the lack of information is that large-scale haulers are a small market when compared to passenger or highway commercial vehicles, and therefore, there has not been the same focus on the rims and tires of heavy haulers that there has been on smaller vehicles.

As there was no previous work done on this subject that was available to the public domain, it was decided to approach manufacturers, service providers, and end users of rims and tires in order to establish what information they found value in. This approach not only provided a starting point for the research but also garnered industry interest and support. The first step taken was a site visit to Kal-Tire and Rimex head offices, located in Vernon, B.C. and Surrey, B.C. respectively. There it was decided to perform a large scale test as both companies pledged their support and materials to be tested. After this, various trips to the sites in Fort McMurray were made, as well as a visit to MineExpo 2004 in Las Vegas, where several visits with service providers and mine operators took place.

As a result of this lack of information for design and testing described previously, as well as direction from discussions with the companies that were consulted, it was decided to develop a large scale loading test based on the direction of industry and the available resources at the University of Alberta.

2.2 Description of tires

In order to adequately describe the test procedure and goals of this project there is a great deal of background information that is required, including an understanding of industrial grade tires. There is a fair amount of information published on highway

size tires, their failures, and testing procedures (Cunagin and Grubbs, 1984; Tielking, 1994; Tielking and Abraham, 1990). However, these sources do not provide a great deal of applicable data due to the large difference in size of ultra-class and highway sized tires. Therefore, the majority of information in regards to ultra-class tires was obtained through conversations with industry (described above), from tire manufacturer's websites and technical manuals (Michelin Earthmover, 2001; Michelin Earthmover, 2005; Bridgestone 2001) as well as SAE standards and practices.

Tire size and design is subject to two primary parameters: highest individual wheel load the tire experiences, as well as the speed range of the vehicle (SAE J1315, 1991). The maximum load that each tire should be subjected to should be less than that specified by the Tire & Rim Association or the manufacturer of a particular tire design, to ensure that tire damage is minimized during operation (SAE J1315, 1991). For a given average vehicle speed, a tire must be selected that will either minimize the build up of heat, or allow an appropriate rate of heat dissipation, preventing tire damage resulting from over vulcanization.

A tire selected for a specific piece of equipment will have an alphanumeric designation based on its nominal section width, nominal rim diameter, carcass strength rating, as well as a service code. This format applies to tires constructed during or after 1988, whereas tires created before this have a slightly different designation (SAE J751, 1997). However, this thesis' focus is primarily on large scale (400+ ton payload) heavy hauler rim damage, which have been in commission since 2000, and therefore will not make use of any tires constructed prior to 1988.

An example of such a tire designation is 48/95R57 ** E-4. The first part, "48/95", relates to the tire's section width, 48 inches in this case, and the aspect ratio, 95% for this tire. The common aspect ratios, the section height divided by the section width, used on today's ultra-class haulers are either 100%, known as conventional, or 80%, referred to as wide base or low profile. The next component of the tire designation

indicates the tire's construction type, which can be either bias ply, indicated by a "–" after the section width reference, or radial, which is indicated by an "R" after the section width. The ultra-class hauler tires used today are all radial in nature, with only small service vehicles making use of bias ply tires in today's mining industry. See figure 2-1 and Table 2-1 for the make-up of a typical radial tire. The next component, the "57" for this example, references the rim diameter in inches, followed by the carcass strength rating, for bias ply tires it is indicated by the initials "PR", whereas radial tires use a rating system of "*'s", as indicated in the above example. Finally, the last component represents a service code; the E-4 in this example indicates that the tire is an earthmoving tire.

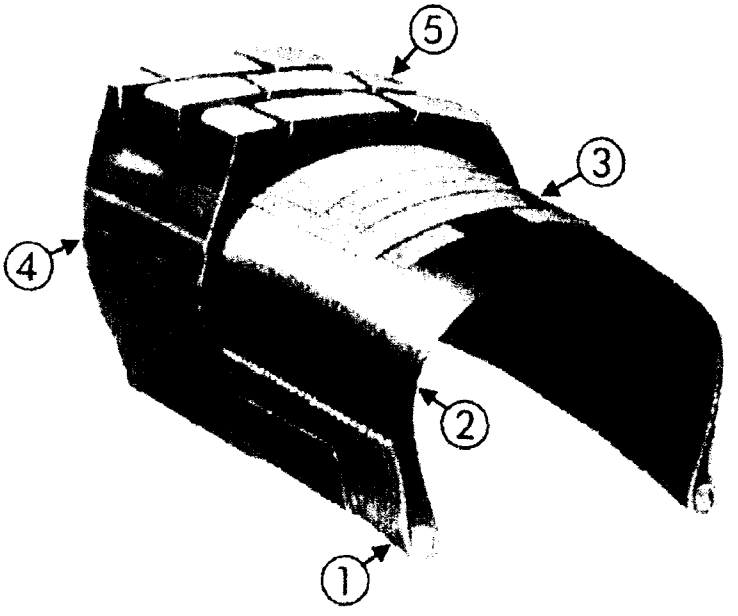

Figure 2-1: Radial Tire (Caterpillar Inc., 2004)

Table 2-1: Figures 2-1 Designations (Caterpillar Inc., 2004)

1.	Beads	2.	Radial Carcass
3.	Belts	4.	Sidewalls
5.	Tread		

2.3 Description of rims

Similar to tires, off-highway rim assemblies also have alphanumeric sequences used to define their contours. These classifications rely on whether the rim is single piece (see figure 2-2), or multi-piece, which can be either two-piece, three-piece, or five piece (see figures 2-3 through 2-5). Single piece rims are designated using their rim diameter and rim width, whereas multi-piece rims are designated by rim width, and either flange or rim profile. The rim width, (A), is defined, in inches, as the distance between the flanges of a rim. The rim diameter, (B), is defined as the distance from the vertical tangent of the flange, to the intersection point of the bead taper of the rim, again in inches. The flange height (C), also measured in inches, is measured from the horizontal tangent of the highest piece of the flange to the point of intersection between the vertical tangent of the flange contour and the bead taper. Finally, the rim profile designation is defined as the rim contour located at the tire to rim interface, and is often used in place of flange height for specifying certain rims (SAE J751, 1997). An example of a single-piece rim designation would be 56.5x20.0, where 56.5 is the rim width, and 20.0 is the rim diameter. An example of a multi-piece rim designation is 49x17.00/3.5, where 49, 17.00, and 3.5 are the rim width, rim diameter, and flange height respectively.

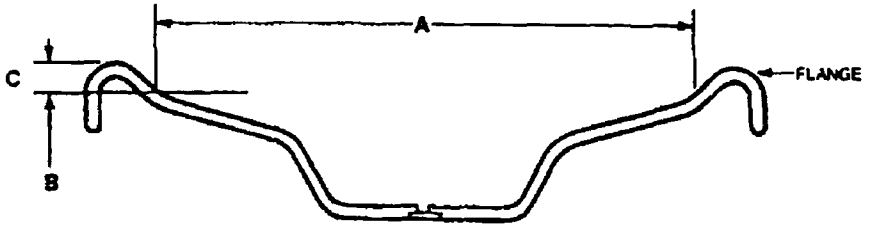

Figure 2-2: Typical 1 Piece Rim (SAE J751, 1997)

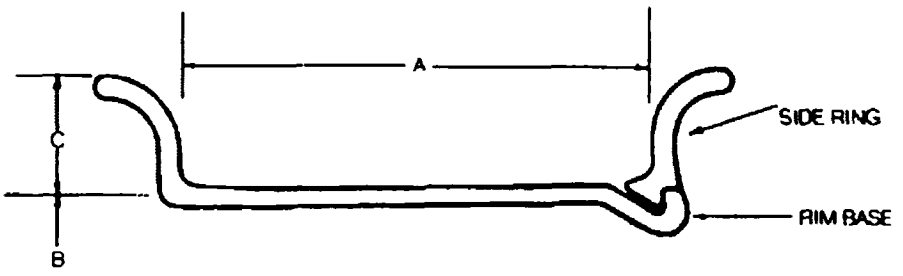

Figure 2-3: Typical 2 Piece Rim (SAE J751, 1997)

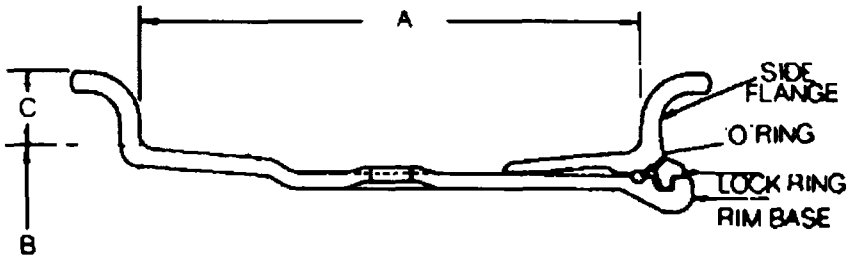

Figure 2-4: Typical 3 Piece Rim (SAE J751, 1997)

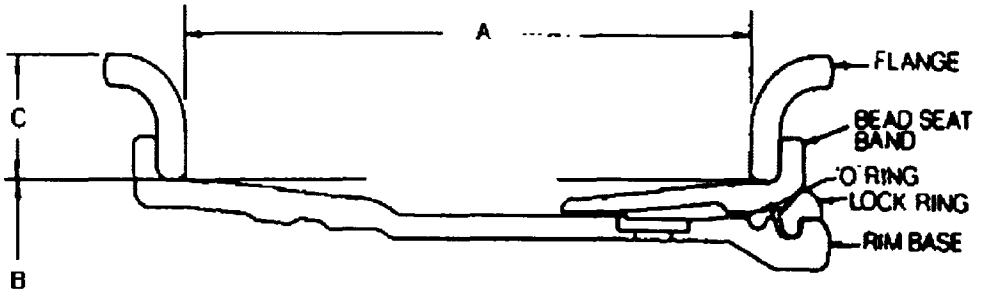

Figure 2-5: Typical 5 Piece Rim (SAE J751, 1997)

For this research project the rims that will be discussed are all multi-piece. The rim that was used for the physical loading test is a 30.00 R51 rim (figure 2-6) and is considered to be a five piece rim. The five pieces are a bead band (figure 2-7), a lock ring (figure 2-8), and two flanges on opposite sides of the rim (figure 2-9), as well as a rim base, which is composed of the back, the gutter, the mounting disc (figure 2-10). Each of these pieces are constructed using ASTM A36 steel, with the following approximate material properties: elastic modulus of 200 GPa, a density of 7860 kg/m^3, and a Poisson's Ratio of 0.29.

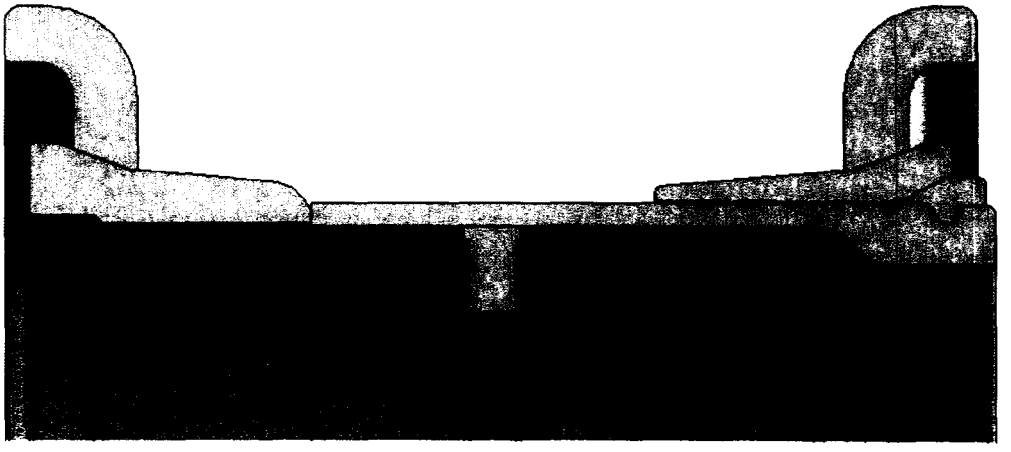

Figure 2-6: Cross Section of 30.00R51 Rim

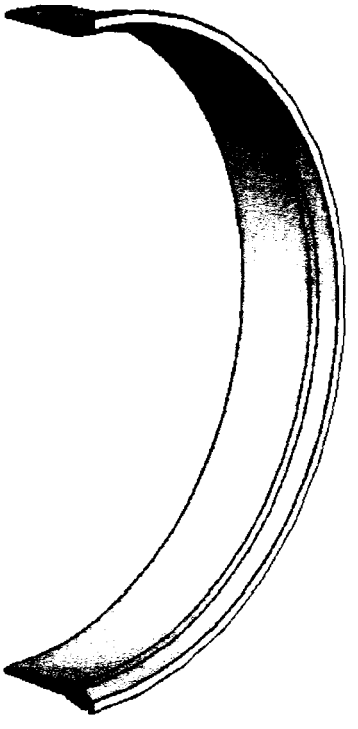

Figure 2-7: Isometric View of Bead Band

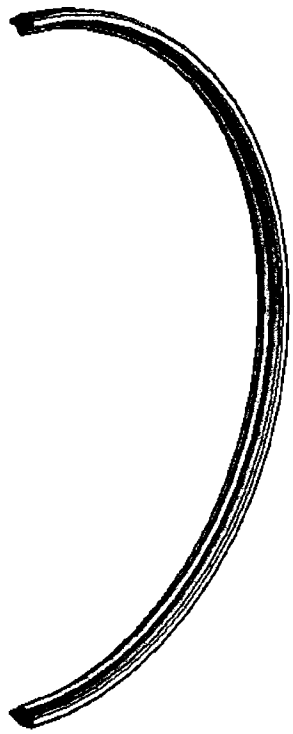

Figure 2-8: Isometric View of Lock Ring

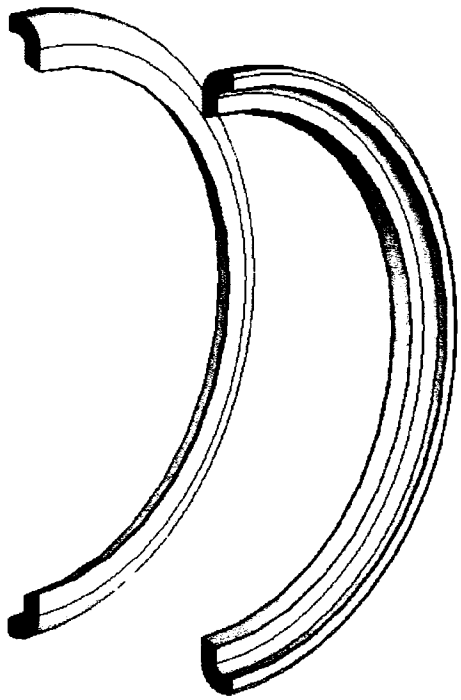

Figure 2-9: Isometric View of Flanges

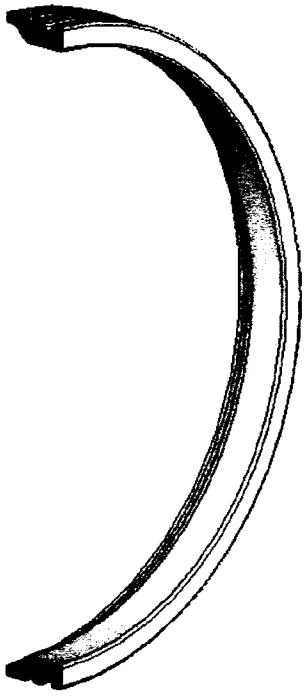

Figure 2-10: Isometric View of Gutter

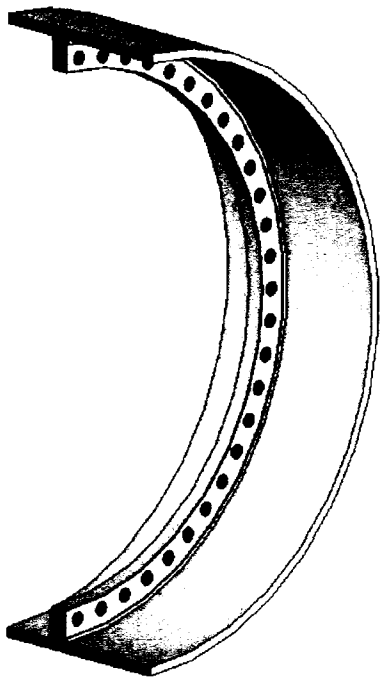

Figure 2-11: Isometric View of Center Band

In terms of the rims that are currently being used on the 400+ tonne haulers, they have the same mechanical properties and a similar design, with subtle differences in geometry and an obvious difference in scale. The rims used on the Caterpillar line of trucks are closest in terms of geometry to the rim that was tested for this project. The major difference being, aside from the scale, is that the center band for the Caterpillar trucks is comprised of a larger amount of smaller sections welded together (figure 2-11). Another noteworthy difference is that the mounting disc is machined as part of the center band, rather than welded on as in the case with the smaller scale rim. The same is true with the rims designed for the Komatsu line of trucks, however, with the Komatsu rims the mounting disc is severely offset (figure 2-12) as the wheel motors need to be accommodated in Komatsu's electric drive trucks, whereas Caterpillar has a mechanical drive system that does not affect the rim mounting.

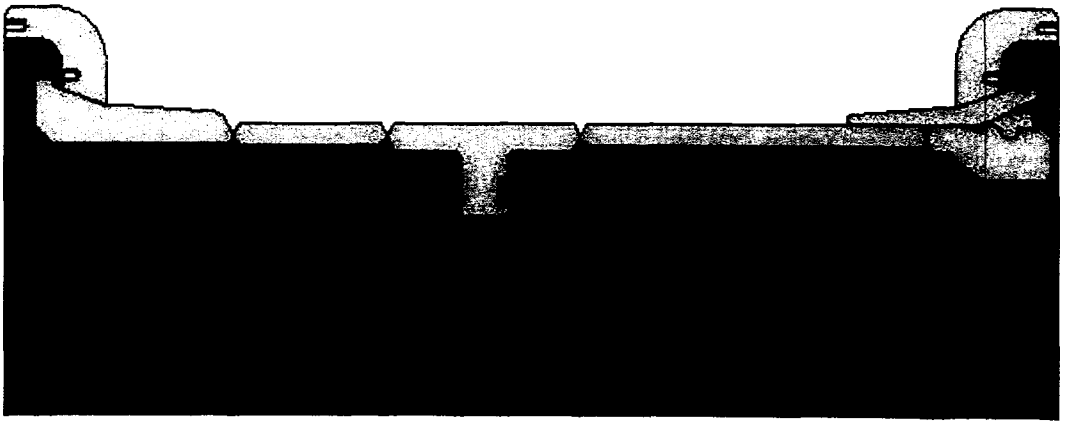

Figure 2-12: Cross Section View of CAT 797B Rim

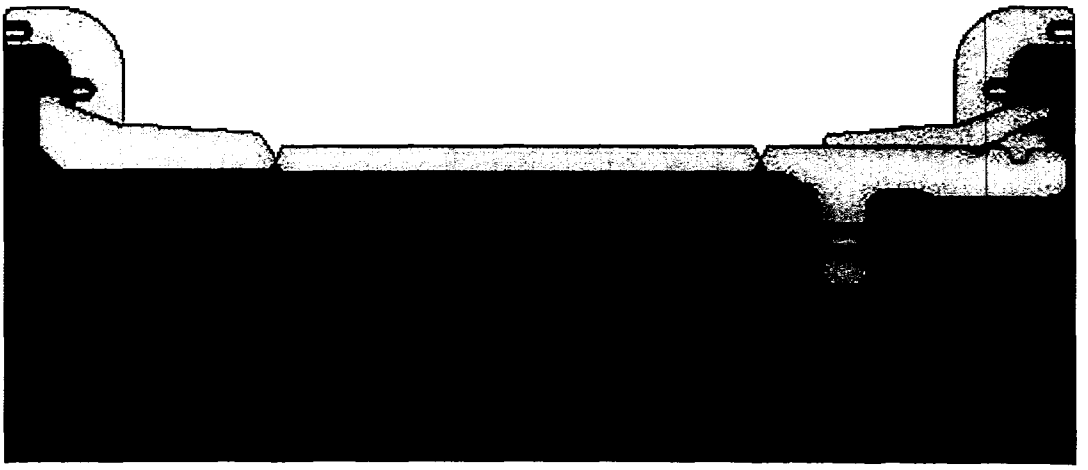

Figure 2-13: Cross Section View of Komatsu 930-E Rim

2.4 Common Causes of Rim Damage in a Mining Environment

Now that the common pieces of the tire and rim assemblies have been described, as well as the nomenclature used, it is important to examine the most common causes of rim failure, as identified by the literature. In terms of a general mining environment, no matter what the ground conditions or operating environment, there four primary causes of rim failures as indicated by SAE J1337, 1997:

- Improper mounting/demounting
- Improper inspection and maintenance
- Improper assembly and inflation
- Improper use during operation

The last item is the one that this research will address, via the loading condition.

During the life cycle of a heavy hauler, maintenance will be required at minimum intervals of every few weeks, or perhaps more depending on the operating conditions.

During these periods of maintenance it will often be required to demount and remount the rim assemblies to either access areas behind them, or perform maintenance on the rims themselves. It is during the demounting and remounting of rims that it is possible to cause damage, either a catastrophic failure, or a minor failure which could result in an unchecked stress concentration, leading to a significant failure at a later date. Therefore, it is important that certain procedures are followed during these periods, such as making sure the machine is properly braked, blocked, and on level ground prior to demounting. Also, all pressure from a tire, or from both tires on a dual rim assembly, must be released prior to work being done on the rim. Both of these precautionary procedures will help to prevent uneven stress distributions on the rim that could result from either the motion of the truck or from excess pressure left in the tire, which could cause the failures described above to occur (SAE J1337, 1997).

Once a rim has been properly demounted and is ready to be inspected or undergo maintenance, there are also certain procedures that must be followed to minimize damage to the rim components. The first and most basic procedure that must be followed during inspection or maintenance is to ensure that the rim components are properly cleaned of all dirt and rust. This is important, as due to the dirt or rust, it is possible to completely miss small cracks or flaws in the rim that may result in a significant failure of the rim at a later date. It is also emphasized that if damage is noticed on a rim component, that it should not be reworked, welded, heated, or brazed by anyone other than an authorize dealer or the manufacturer. Replacement of parts is generally recommended over repair as heat treatment of these pieces can cause significant change in the structural properties of a rim. Also, if it is found that a tire was significantly under inflated during operation, it is vital that all the components of the rim assembly be properly checked by either an authorized dealer or the manufacturer prior to re-inflation of the tire. Even if there appears to be no damage by visual inspection, running an under inflated tire can cause serious damage to a rim as a result of increased stress, and can lead to a future failure of the rim (SAE J1337, 1997).

Similar to the inspection and maintenance of a rim, there are several procedures that must be closely followed during the assembly of the rim and the inflation of the tire that will help minimize rim damage. Although it may sound trivial, it is important that the proper pieces are used during the assembly of the rim. This can be done by checking the markings of each of the components and by verifying the size and shape of the required piece. This is important as mismatched components may fit during assembly and may appear to be in correct order, but during tire inflation may dislodge. Also, when the rim is being assembled steel hammers should not be used, as the metal on metal contact of a steel hammer and the rim can cause distortion of the rim, resulting in improper fitting or rim damage. If hammering is required it is suggested that rubber, plastic, lead, or brass-faced mallets be used, however, if the components are properly matched then they should seat during inflation without hammering. Finally, the rim components should be properly cleaned of dirt and moisture, as well as inflation equipment using an air filter, to prevent corrosion of the rim, which can lead to difficult disassembly or failure of the rim (SAE J1337, 1997).

While improper methods of mounting/demounting, inspecting and maintaining, and assembling rims often result in damage to the rims, the most prominent cause of rim failure is improper operation procedure. These include, but are not limited to: operators driving heavy haulers too fast, carrying too large of a payload, cornering too sharply, operating using an over-inflated/under-inflated tire, or running a dual assembly truck with only one tire. All of these situations either result in an increased un-uniform stress load which exceeds the rim structural capacity, or impact loads which result in deformation and localized stress concentrations causing failures. Therefore, it is vital that the proper operating procedures are followed for each mine site in order to minimize damage and to maximize a rim assembly's lifetime.

2.5 Common Causes of Tire Damage in a Mining Environment

Unlike rim damage, tire damage varies greatly from region to region or with geology, as well as from mine site to mine site. Different types of failures occur more frequently in certain regions as compared to others, but it is also not uncommon to have two mine sites from the same geologic region experiencing different types of failures or a large variation in tire performance.

The most common types of tire failure are: tread wear out, heat and mechanical separation, tread cuts, and sidewall cuts. Tread wear outs occur when the tread of the tire is physically worn down due to the abrasive nature of the ground surface. Heat and mechanical separations occur when a tire's internal temperature reaches the critical temperature at which it is cured (102°C) and the rubber begins to separate from the steel belting. Tread cuts occur when a truck runs over a piece of material and it pierces through the tread material. Sidewall cuts occur when the sidewall of the tire is compromised by a sharp piece of material. This generally occurs when a truck is being loaded or turning a corner and materials spills from the box, contacting the sidewall. Another common instance is when a truck is traveling around a corner to quickly, causing the sidewall to buckle over itself and the tread, allowing for the possibility of contact with sharp materials on the ground.

As a general rule, mine sites that have hard rock conditions typically experience more tread wear outs and heat separations with tire lives in the range of 3,000 hours, while oil sands operations mainly experience sidewall and tread cuts and have tire lives of approximately 5000 hours (LTUG Proceedings, 2005). See Table 2-2 for a summary of the types of tire failures various North American mining operations experience.

Table 2-2: Recorded Tire Failures from Various Mining Operations (LTUG Proceedings, 2005)

Mine Site/Company	Typical Tire Life (hrs)	% Tread Wear Out	% Sidewall Cut	% Tread Cut	% Heat Seperation
Syncrude	4000	-	>50%	>20%	-
Suncor	3500	-	>28%	>43%	>14%
Albian Sands	4000	-	>30%	>37%	>17%
Quebec Cartier Mining	5000	>25%	>24%	-	-
Barrick Goldstrike	4300	>82%	>15%		-
Phelps Dodge Morenci	38000 (miles)	>34%	>55%		-

2.6 Impact of Soft Ground Conditions on Rim and Tire Damage

The causes of damage that were previously discussed during operation can occur in any mining environment, however, the effects observed are amplified when operating on soft ground conditions, where a large number of ultra-class units operate North of Fort McMurray in various oil sands projects. There has been information published in regards to tire/rim and soft ground interactions, but it is in terms of farm and highway sized vehicles (Wiermann, Way, Horn, Bailey and Burt, 1999; Ronai and Shmulevich, 1995), but due to the difference in size these do not provide much relevant information. However, there has been work done previously in regards to large scale mining equipment operating in soft ground conditions (Joseph, 2002; Joseph and Hansen, 2002; Joseph 2003). While they do not touch on ultra-class rims and tires specifically, they provide baseline information in regards to the detrimental effect of soft ground on ultra-class mining equipment.

It has been shown that oil sand is an elasto-plastic strain softening material, which combined with the cyclic nature of mining equipment can result in undulated ground formations on which mining vehicles are forced to operate (Joseph, 2002). This condition worsens in the winter, as the surface of the ground freezes, while the underlying materials retain a strain softening nature, causing some greater extremes in terms of ground undulation. Data collected from a truck operating in such conditions showed that the frame of the hauler experienced ten g-level occurances above 1.5

(forces normalized in terms of the gravitational force) during a period of 13 minutes (Joseph, 2003). It has been estimated that a piece of equipment that experiences 1,000,000 events over 1.5 g will succumb to structural failure, and that a truck frame that is expected to last ten years, will fail closer to the six year mark based on these numbers of g-levels, assuming 80% utilization, 80% availability, and a 350 day/year operation schedule for a specified unit (Joseph, 2003).

Although the rims of a truck will not necessarily experience the same forces as a truck frame, or even react in the exact same manner structurally, it can be assumed based on common sense that if truck frames experience structural damage as a result of undulated, soft ground conditions and high g events, the truck rims will be subjected to similar experiences. Determining the actual magnitude of these forces and the resulting stress that occurs on a hauler rim will be discussed in more detail later in this thesis in the sections pertaining to the loading test. However, as stated above: it can be induced that a clear relationship between the high g loading and structural damage experienced by truck rims exists. Further-more, while the previous example indicates that a truck operating on soft ground conditions will experience structural failure after operating for approximately six years, it has been observed that new trucks are requiring frame repairs after operating for only a few months in the oil sands (Berezan, 2003), and once again it can be concluded that similar adverse loading and damaging events are being inflicted on truck rims.

As discussed previously the majority of tire failures in the oil sands are a result of sidewall and tread punctures. While tires on average have a longer life than those in hardrock conditions, this type of failure being experienced is prematurely ending the majority of tire lifecycles. It does appear however that this is more of an operator issue than a design issue as shown by the discrepancies between the tire data from the different oilsands operations. Also, it is possible to buy tires made from rubbers that are designed to be less susceptible to cuts and punctures, however, these rubbers are more susceptible to heat separation failures.

3 Description of Physical Loading Test

In order to gain an improved understanding of the performance of and interaction between rims and tires, a series of loading tests that simulate the forces ultra-class haul trucks are subjected to on a daily basis was performed. Currently ultra class haulers use 55/80 R63 or 59/80 R63 tires, which have outer diameters of 154" and 159", loaded radii of 64" and 69", and rim diameters of 63" respectively (Bridgestone, 2001 and Michelin Earthmover, 2005). Therefore, in order to perform an accurate loading test as described previously, a 55/80 R63 or 59/80 R63 tire and matching size rim would be the ideal test specimen. However, it would be difficult to test a 55/80 R63 or 59/80 R63 tire and rim at the University of Alberta's I.F. Morrison Laboratory due to its size, but also as mentioned previously, neither of these sizes of tire were readily available due to the tire shortage in the industry. Even if it were possible to obtain a 55/80 R63 or 59/80 R63 tire and rim, the testing facilities that have the available resources to properly test them, those owned and operated by the large tire companies, are located in the southern United States or overseas in Japan, and are therefore not feasibly accessible. Therefore, it was decided to test the largest possible rim and tire that were currently available and could be readily transported to and tested at the University of Alberta. The tire and rim combination was selected was a 30.00 R51 tire, with an external diameter of 112" and a loaded radius of 50", donated by Kal-Tire, and a 51" diameter rim, fabricated and donated by Rimex.

In order to simulate the effect of increased g levels resulting from dynamic loading, the loaded gross vehicle weight was multiplied by the proportion of g loading, applied statically to the rim and tire. The typical payload for a hauler that is used with this sized tire and rim is 170 tons, giving a total gross vehicle weight of approximately 550,000 lbs (Caterpillar Inc., 2004). This results in a loading of 92,000 lbs being experienced by each of the truck's six tires and rims, based on a standard front-to-rear load distribution of 1/3 to 2/3. For the initial 1g loading the rim and tire was loaded to 91,666 lbs, or approximately 410 kN, and then loaded by 0.1g increments up to

1.6g, 146,666 lbs, or 650 kN. The load that a rim and tire experience when a truck travels unloaded (U/L) was also calculated as this presents a low value which is useful for developing trends and also represents the load that a truck carries for half of its cycle. This range will allow a prediction of higher g loading effects based on the trending displayed, while eliminating the safety risk associated with testing the rim and tire at levels around or higher than 2g. See Table 3-1 for complete list of loads/forces applied in both metric and imperial units.

Table 3-1: Summary of Forces for Loading Test

g level	Total (lbs)	Per ram (lbs)	Total (kN)	Per ram (kN)	Approx per ram (kN)
1 U/L	40000	20000	177.9	89.0	90
1.0	91666	45835	407.8	203.9	205
1.1	100835	50415	448.5	224.3	225
1.2	110000	55000	489.3	244.7	245
1.3	119165	59585	530.1	265.0	265
1.4	128335	64170	570.9	285.4	285
1.5	137500	68750	611.6	305.8	305
1.6	146665	73335	652.4	326.2	325

In addition to determining the effect of load on the tire and rim, it was also desired to find the impact of the tire pressure. For this tire type, make and model the nominal pressure is 87 psi (Michelin 2004), however, several mine sites either over or under inflate their tires based on the characteristics of their site. Operations that have haul roads that contain a lot of down hill slopes or tight bends, requiring heavy braking are recommended to run their front tires with an inflation increase of 10% (Michelin 2004). Whereas mine sites that require slow travel speeds or have short cycles are recommended to reduce their tire pressures by 10% (Michelin 2004). Several mine sites also over-inflate their tires to combat the problem of pressure leakage which occurs during operation. Therefore, the series of load increases was performed three times, at 100psi, 90psi, and 80 psi, allowing simulation of a variety of operating conditions.

With the test parameters determined, the next step was to determine the most efficient and safest way to perform the actual loading test. The test was not only chosen to be

conducted at the I.F. Morrison Laboratory due to the abundance of space and equipment, but also due to materials for custom building testing frames as well as the expertise in designing and building loading frames by the technicians who work there. The test set up was built as shown in figure 3-1.

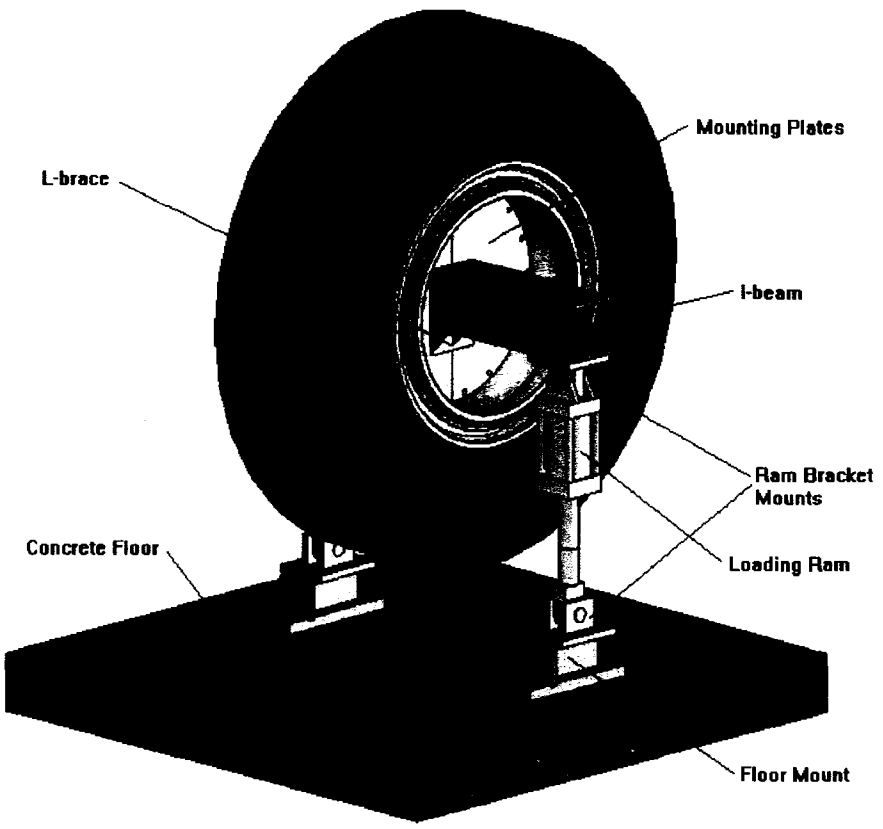

Figure 3-1: Computer Representation of Test Setup

Floor mounts were anchored to the concrete floor with tie rods, attached to these mounts were ram bracket mounts that fit the bolt pattern of the floor mount which slotted onto the bottom of the rams used to provide the load. A similar bracket mount was attached to the top of each of the rams and was bolted on to an I-beam that acted as an axle. For dimensions of the mounts, the loading rams and the I-beam in order of construction from the lab surface up, see figures 3.2 through 3.6 respectively. The I-beam had a width and height of 12" with web and flange thicknesses of 10mm and 7.5 mm respectively. This beam was chosen as it was the smallest size beam that was

available in the lab that could safely withstand the loads that would be required for the test.

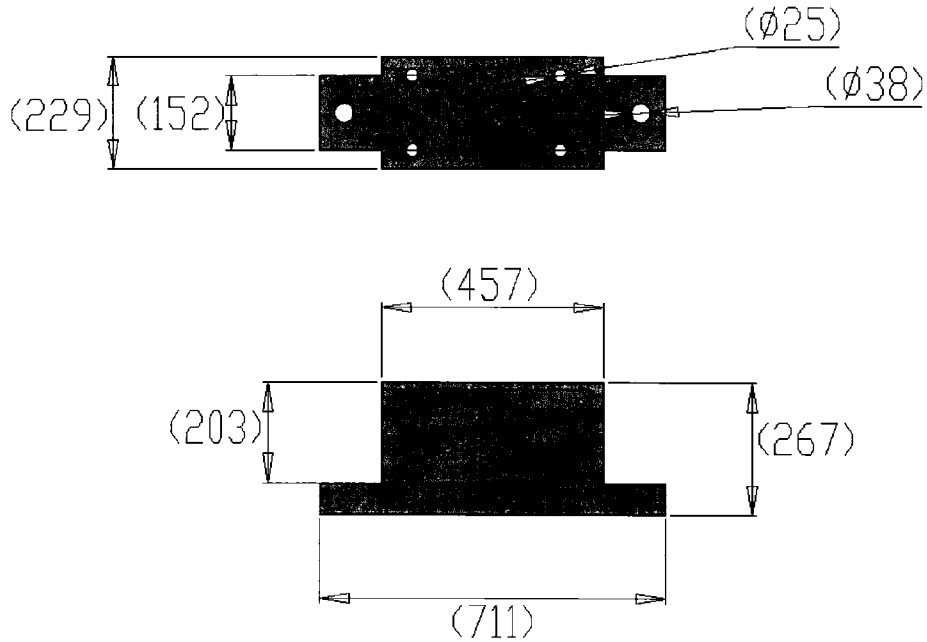

Figure 3-2: Dimensions in Millimeters of Floor Mounts (NTS)

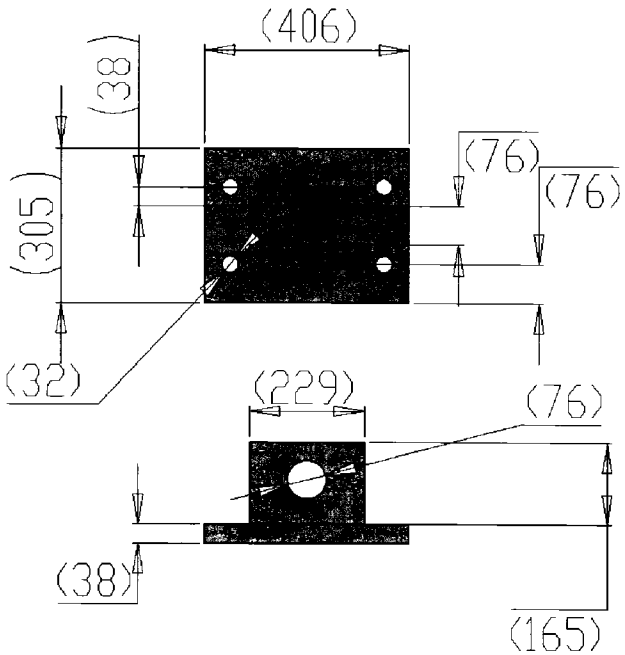

Figure 3-3: Dimensions in Millimeters of Brackets Connecting Floor Mounts to Loading Rams (NTS)

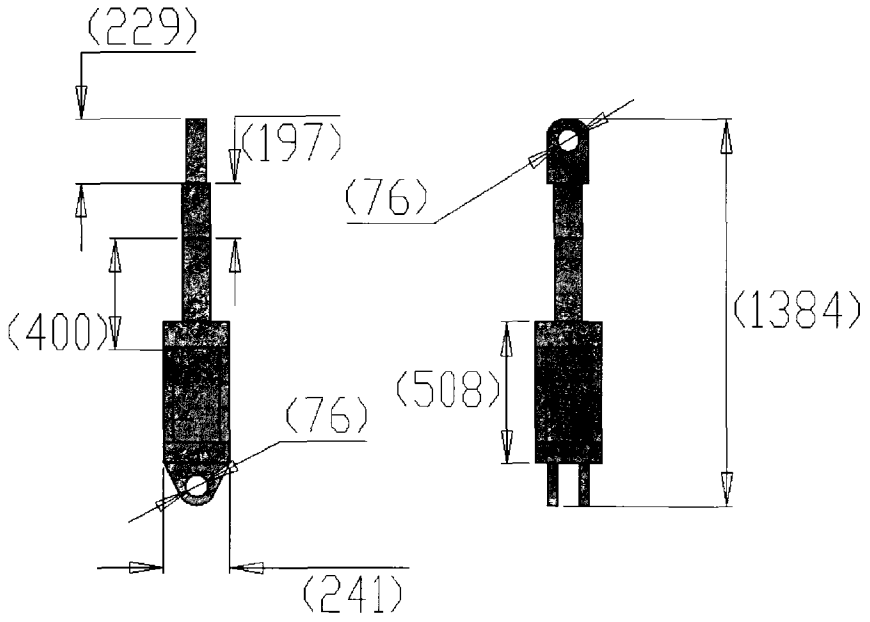

Figure 3-4: Dimensions in Millimeters of Loading Rams (NTS)

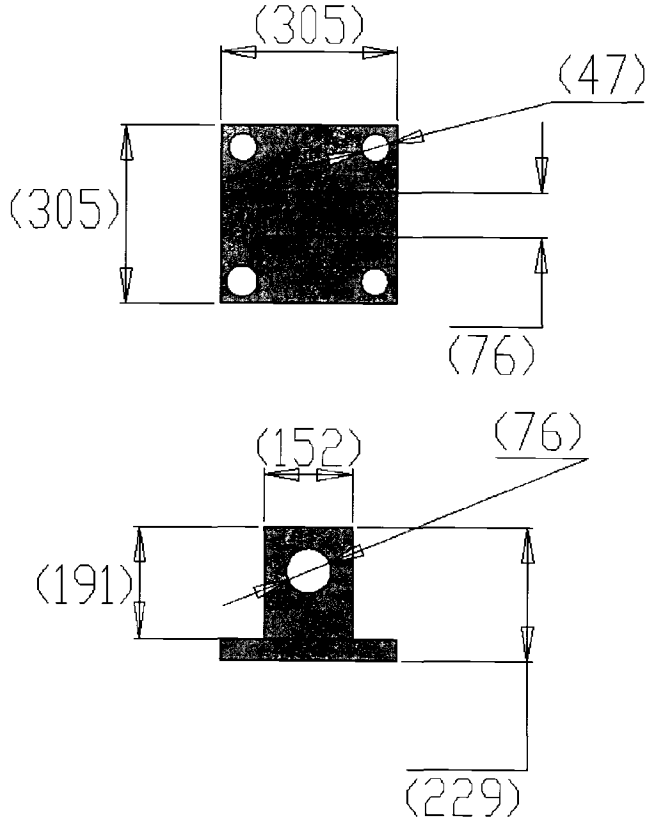

Figure 3-5: Dimensions in Millimeters of Brackets Loading Rams to I-Beam (NTS)

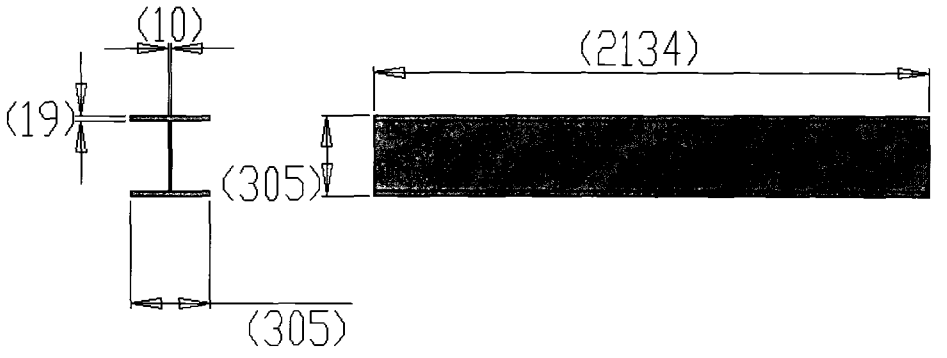

Figure 3-6: Dimensions in Millimeters of I-Beam (NTS)

This I-beam passed through two plates that were bolted to both sides of the rim disc which acted as a wheel hub for the test. Two L-braces, one on each side, were bolted onto the plates and the bottom of the I-beam in order to provide stability preventing any independent movement of the I-beam during loading, however, they offered no structural support. The rim discs had a evenly spaced 18 1" hole pattern rather than the 53 1" pattern of the rim disc. This decrease in the number of bolts used to attach the plates was done as there was less bolting support required for purely vertical loading as was the case with the test, compared to the rotational loading that occurs on a rim that is operating during motion. Even with the reduction in the bolts used it was still decided to keep the bolts evenly spaced to ensure that the force that was applied during loading was evenly distributed throughout the rim as it does with a full bolt pattern. See figures 3-7 and 3-8 for the dimensions of the L-braces and rim discs used during the loading tests.

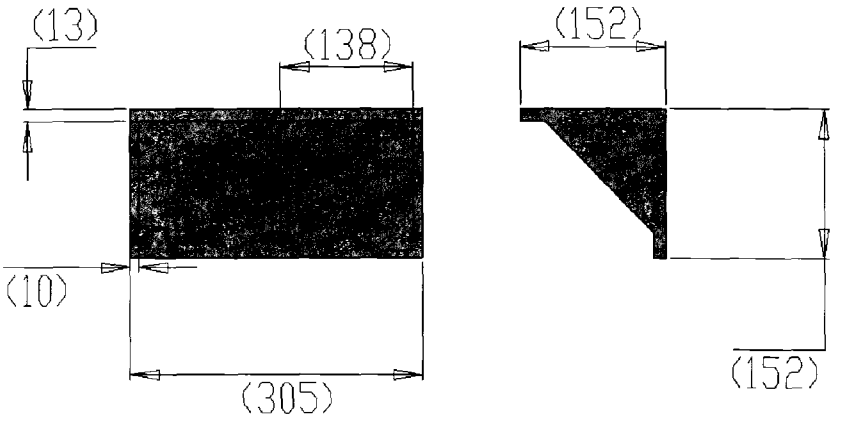

Figure 3-7: Dimensions in Millimeters of L-Brace Support Between I-Beam and Rim Plates (NTS)

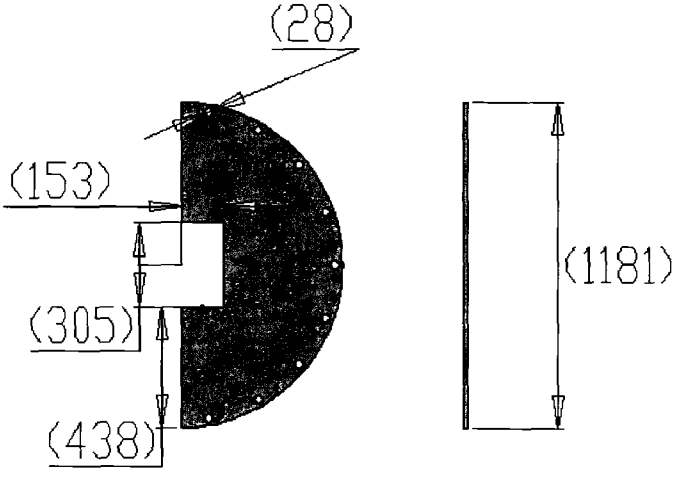

Figure 3-8: Dimensions in Millimeters of Rim Discs (NTS)

The previously described equipment was used to construct the testing frame and to supply the load required to simulate forces experienced by an ultra-class rim and tire. A second group of equipment was required to gather the rim and tire data for the tests, including 52 strain gauges, 2 linear vertical displacement transducers (LVDT's), and 2 load cells. Strain gauges were placed in three main groupings on the rim: on the outer face (the side the faces way from a truck), the inner face (the side the faces inwards towards the truck, and on the inner curve of the rim. On the outer face gauges were placed on the outside flange, the lock ring, and the outside band, as

shown in figure 3-9. For the inner face, gauges were placed along the inside of the rim band, as shown in figure 3-10. Finally, the gauges placed in the inside of the center band were done so at the locations and orientations indicated in figure 3-11. Only one half of the rim was instrumented, as shown in figures 3-9 – 3-11, as the other half will have the same loading curve; a result of symmetry. Also, the majority of the gauges were mounted on the bottom half of the rim as this is where it was believed that the majority of the load would be applied.

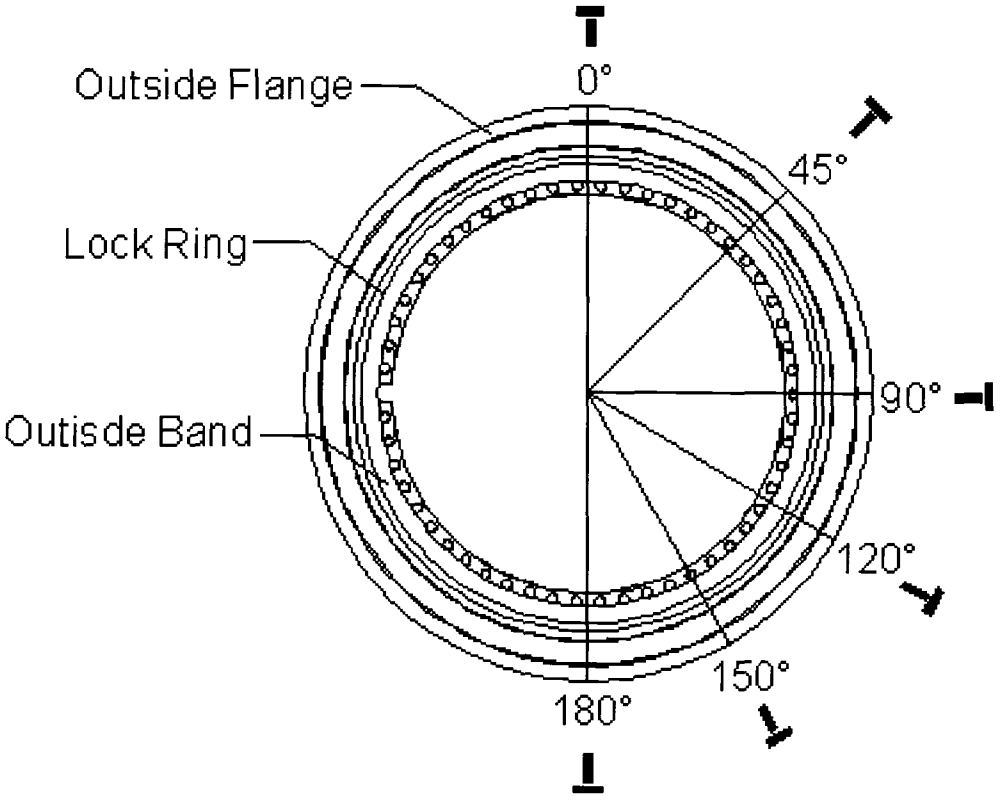

Figure 3-9: Placement and Orientation of Strain Gauges on Outside Edge of Rim

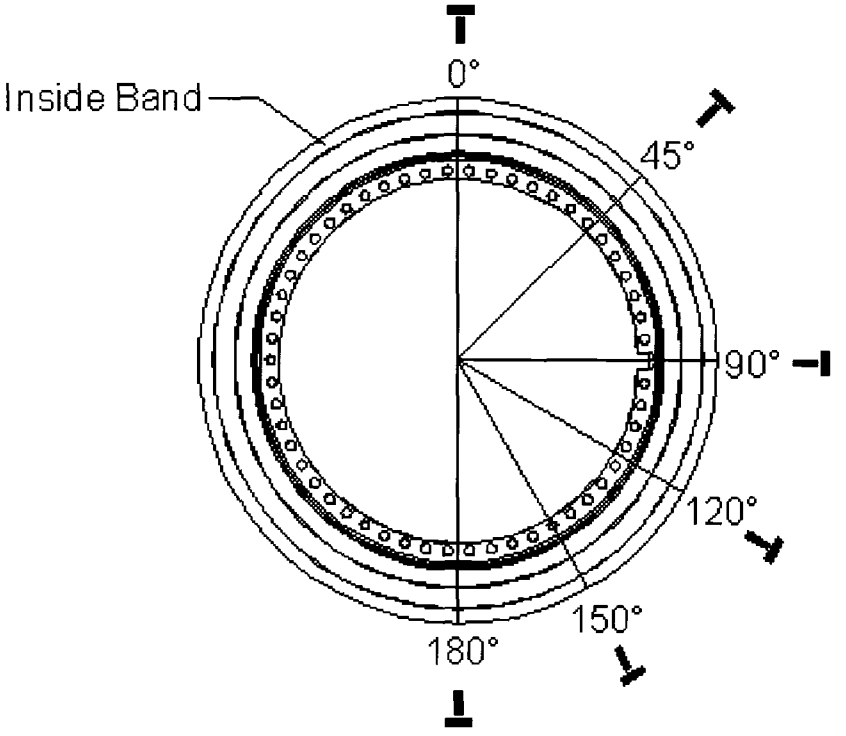

Figure 3-10: Placement and Orientation of Strain Gauges on Inside Edge of Rim

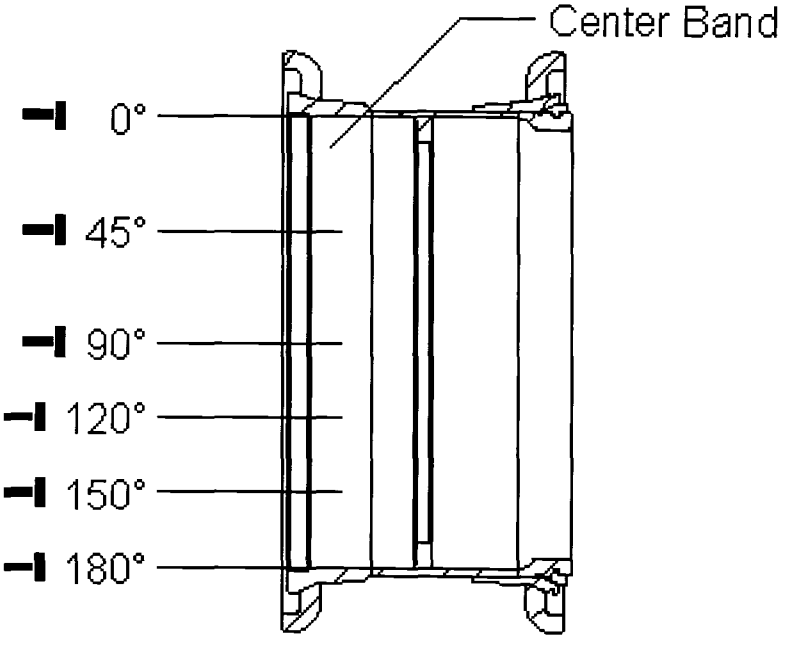

Figure 3-11: Placement and Orientation of Strain Gauges on Inner Surface of Rim

The strain gauges were wired to a Fluke 2400b data acquisition system, hooked up to a PC running Labview (see figure 3-12), allowing for the collection of the rim's strain data. Two LVDT's were placed, one on each side of the I-beam, which allowed accurate, independent measurements of displacement of both sides of the rim/tire configuration. Similarly, two load cells were used, one mounted on each of the loading rams, to measure the actual load that was being applied to each side of the rim and tire.

Figure 3-12: Data Acquisition System

As for the tire, the data from the LVDT's and the load cells described above was used. A carbon paper/plastic sheet was used for creating a footprint while the tire was being loaded and a plumb bob and laser level were used for measuring sidewall bulge during loading. The carbon paper/plastic sheet was constructed by taping several pieces of carbon paper together and placing them beneath a piece of plastic hallway runner with rubber spikes every $1 cm^2$. These rubber spikes reduced the surface area allowing a greater contact pressure, allowing the carbon paper to make a print of the actual tire footprint during loading. For the measurement of the sidewall deflection

the plumb bob was used to mark the furthest point of lateral displacement when the maximum load for each test was reached. The spot marked with the laser level was then compared to the initial point of reference for the unloaded tire.

Up to this point the equipment described has been for either construction of the test frame or for data acquisition. The final pieces of equipment used in order to run the test were: a compressed air pressure panel and a rotation meter. The pressure panel, figure 3-13, used compressed air to apply pressure to the hydraulic fluid within the loading rams, allowing for both extension and compression of each. Due to the fact that the rams operated independently of each other, there was the possibility that one could be extended or compressed significantly more than the other, resulting in an unsafe loading condition. Therefore, a rotation meter was installed on the I-beam when it was level, allowing for a display of the orientation of I-beam during loading, ensuring that the rams were operating in conjunction with one another.

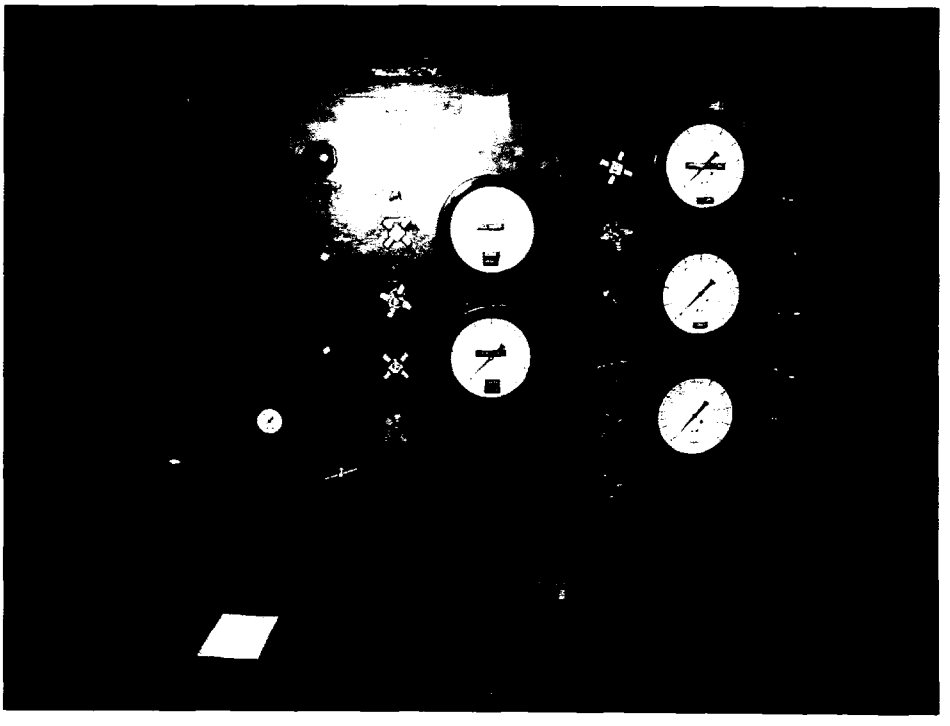

Figure 3-13: Pressure Control Panel

With the test frame constructed, the data acquisition system installed, and the monitoring equipment in place, it was possible to begin testing of the rim and tire. Prior to applying any load on the tire and rim, the rams were fully extended, lifting the tire off of the ground. This allowed for the placement of the carbon paper/plastic sheet mat which would be used to measure the footprint at the maximum load. For each of the three internal tire pressures (100psi, 90psi, and 80psi) the equivalent footprint pressures for a 1.0g, 1.1g, 1.2g, 1.3g, 1.4g, 1.5g, and an unloaded truck weight were then applied by manually increasing the pressure in each of the loading rams from zero to the desired maximum value. An exception to this was for the 80psi tire pressure tests, where due to the lack of tire pressure to bear off against, the loading rams did not have enough stroke to provide a 1.4g or 1.5g equivalent load, and therefore, the maximum load applied was approximately 1.35g.

From zero applied pressure up to the desired maximum load, data from the strain gauges and the LVDT's was recorded at ten second intervals, along with the appropriate applied load. Once the equivalent load g-level was obtained the pressure in the rams was held constant, allowing for several redundant strain and displacement measurements, as this was the critical loading for each of the tests. Also, while the pressure was held constant, the bulge in the tire sidewalls was manually measured by holding a plumb bob against the displaced sidewall and marking the location using a laser level. This location was than compared against the original sidewall displacement at zero loading to obtain a displacement distance for each test. Upon completion of the sidewall measurement the pressure was slowly released in each ram, with strain and displacement measurements again being recorded in ten second intervals. With the load on the tire and rim removed, the rams were again expanded to their full extension, allowing for removal of the carbon paper/plastic sheet mat and measurement the footprint imprint for each test. This was the complete test cycle for each tire pressure/g load combination with the results obtained for the strains in the rim, as well as the displacement, side wall bulge, and footprint area of the tire for each test interval located in Chapter 4.

4 Results of Physical Loading Test

As described in the previous chapter: the loads for each test run were applied gradually, this was due to the fact that the loading rams used to simulate the g-forces were not capable of performing impact loads. Therefore, when the data from the testing was collected, strain values were measured from zero load to the equivalent load for the appropriate g-level, and then measured as the load was backed off to zero again. While this extra data did have a purpose; it provided redundant measurements up to the desired loading ensuring that the testing parameters were consistent; the majority of it was not useful to the analysis of the loading interaction between the rim and the tire. The only data required was the strain values at the equivalent value of force for the g-level test, which was the maximum value in each case. As a result only the maximum strain value was used to represent the equivalent strain for the appropriate g-level and reported in figures 4-1 through 4-10. The rest of the data obtained can be found in Appendix A.

The data below is presented in microstrain versus tire position format for each of the load increments tested. In terms of the tire position, 0° was taken as the top of the tire in the test setup position, and 180° was taken as the bottom value. Data was obtained for each of the pieces strain-gauged, which based on technical advice from Kal-Tire were the outside flange (visible on an operating truck), the inside flange (facing inside on an operating truck), the outside surface of the center band (visible on an operating truck), the interior surface of the center band, and the lock ring (visible on an operating truck). Also, for each piece, gauges were placed in a horizontal and vertical orientation to determine the stress field and the difference of load in the direction of the force and the direction perpendicular to it. See figures 3-9 through 3-11 for a visual representation of the position and orientation of the strain gauges on each of the tested rim components.

4.1 Rim Strain Raw Data

The data presented here is unmodified data obtained from the testing apparatus. The maximum values were used for each data set as described previously.

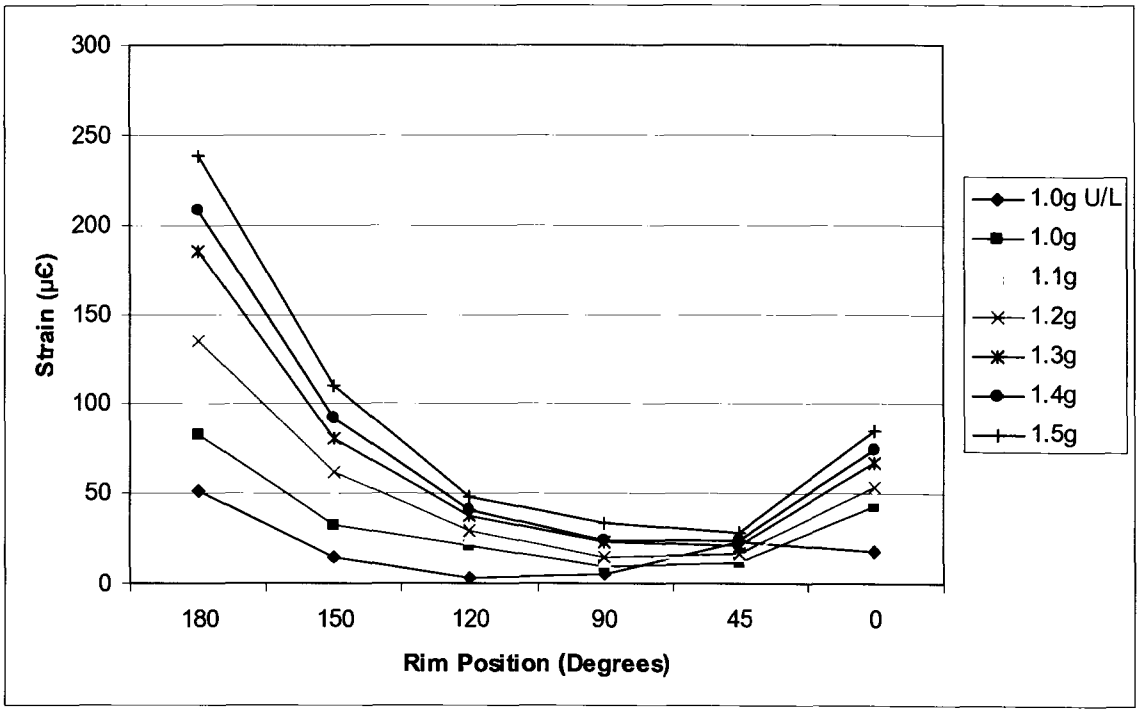

Figure 4-1: Outside Flange Radial Strain, 100psi Tire Pressure

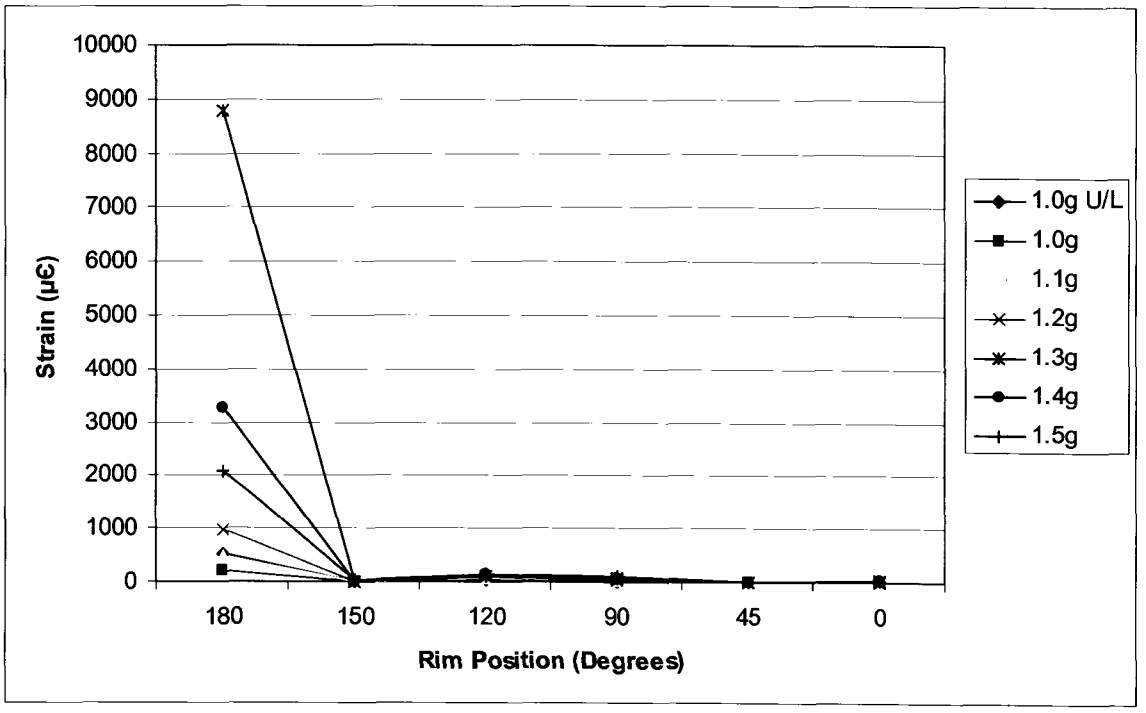

Figure 4-2: Outside Flange Tangential Strain, 100psi Tire Pressure

Figure 4-1 provides a visual representation of the results obtained for the radial strain in the outside flange of the rim. With the exception of the 1.0g unloaded value at the 45° location all of the strains follow a consistent decrease in relation to decrease in load. The highest values occur at the 180° location for each load value and follow a parabolic shape towards the base of the rim, or the 0° point. Having peak values of strain occur at the top and bottom of the rim is expected from a vertical load as these points would be subject to the greatest amount of displacement from their original position as a result of the rim ovalizing. Conversely, the results displayed in figure 4-2 are hard to interpret due to the relatively large values of strain observed at the 180° location which skews the scale of the plot. However, the results for the tangential strain of the outside flange will be discussed more in depth in Section 4.2, where the filtered data will be presented.

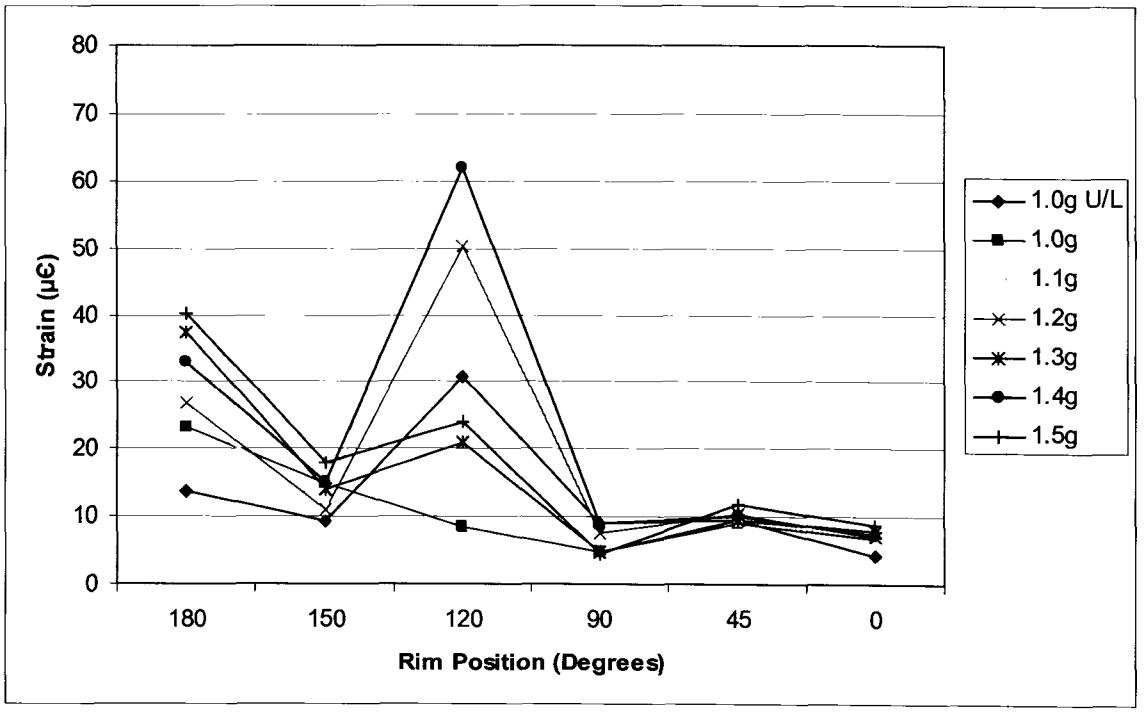

Figure 4-3: Inside Flange Radial Strain, 100psi Tire Pressure

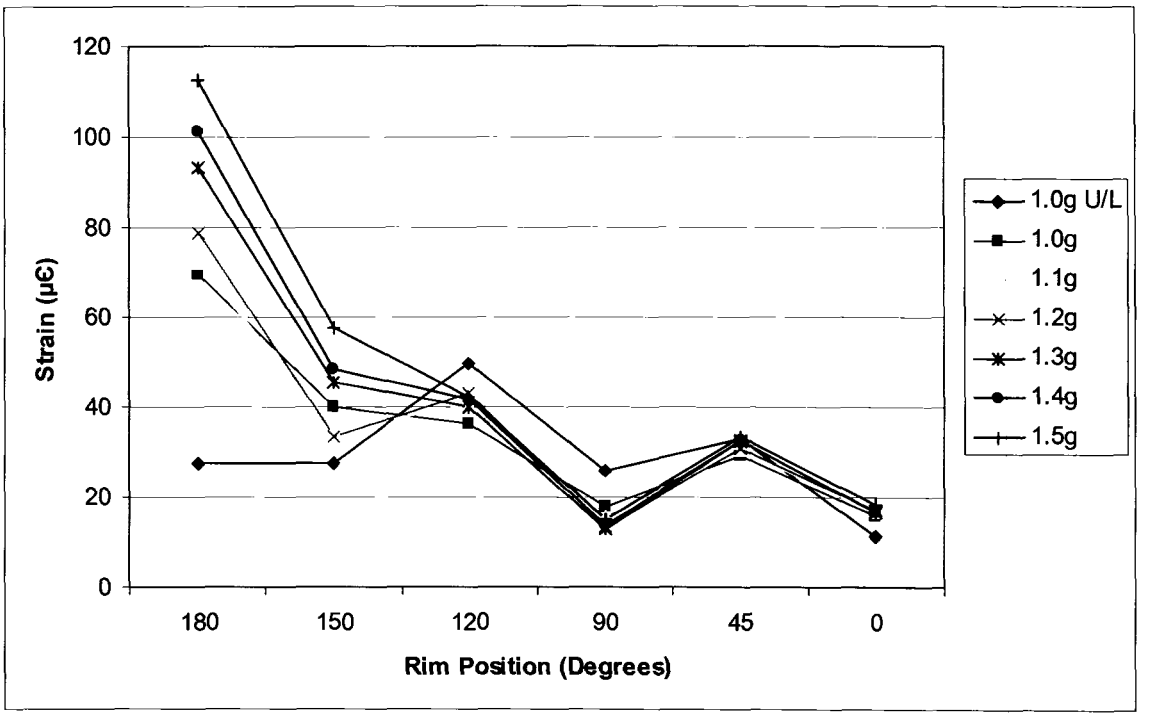

Figure 4-4: Inside Flange Tangential Strain, 100psi Tire Pressure

As for the results obtained for the inside flange, both figures 4-3 and 4-4 show relatively consistent results in terms of decrease in strain versus decrease in load. Aside from the 120° location, the results obtained for radial strain were all relatively low when compared to the outside flange, and slowly decreased from 180° to 0°. Similarly, the results for the tangential strain follow a similar pattern, with the exception of a higher peak value (approximately three times as large) being measured at the 180° location. The lack of consistency for the radial strain results at the 120° location is most likely the result of a damage strain gauge or data channel, as this lack of consistency is observed for the results of the 90psi and 80psi tests as well, as shown in Appendix A.

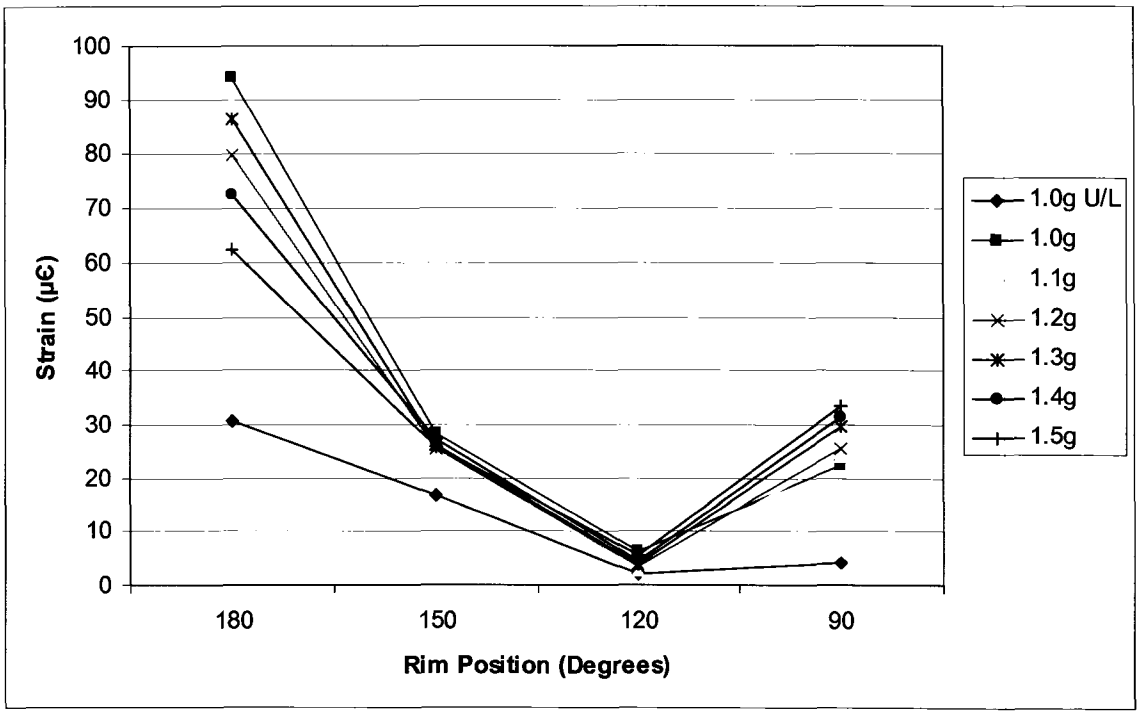

Figure 4-5: Outside Band Radial Strain, 100psi Tire Pressure

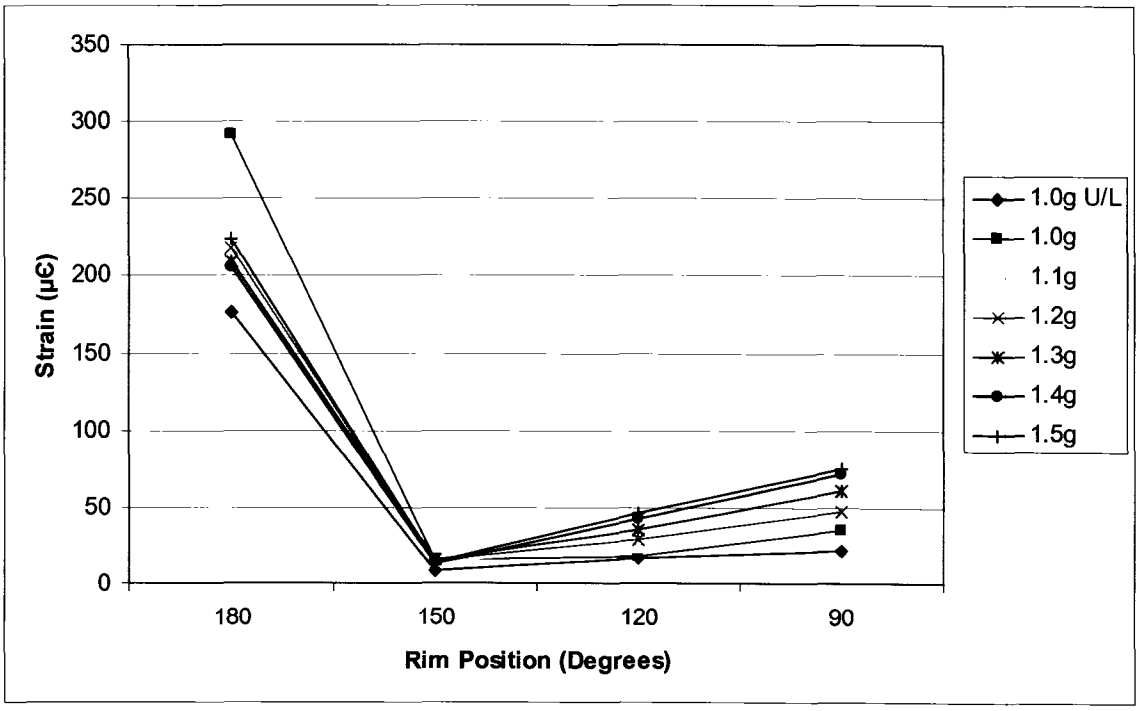

Figure 4-6: Outside Band Tangential Strain, 100psi Tire Pressure

The results for the strain on the outside edge of the center band only show data from the 180° location to the 90° location, missing both the 45° and 0° points. This is a result of the strain gauges at these positions not properly bonding to the rim steel and becoming damaged prior to commencement of testing. However, even with only four data points figures 4-5 and 4-6 seem to indicate a consistent trend in strain level versus position, with peak values occurring at the 180° location and a significant decrease in strain at the other three positions in both the radial and tangential directions.

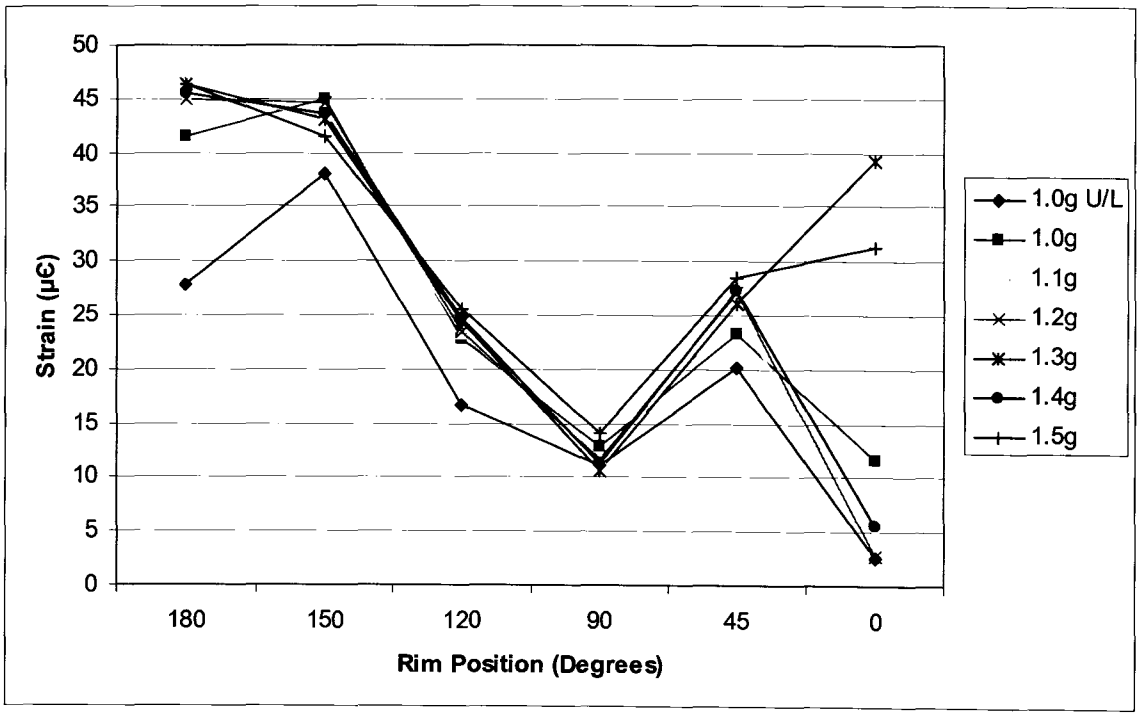

Figure 4-7 Center Band Radial Strain, 100psi Tire Pressure

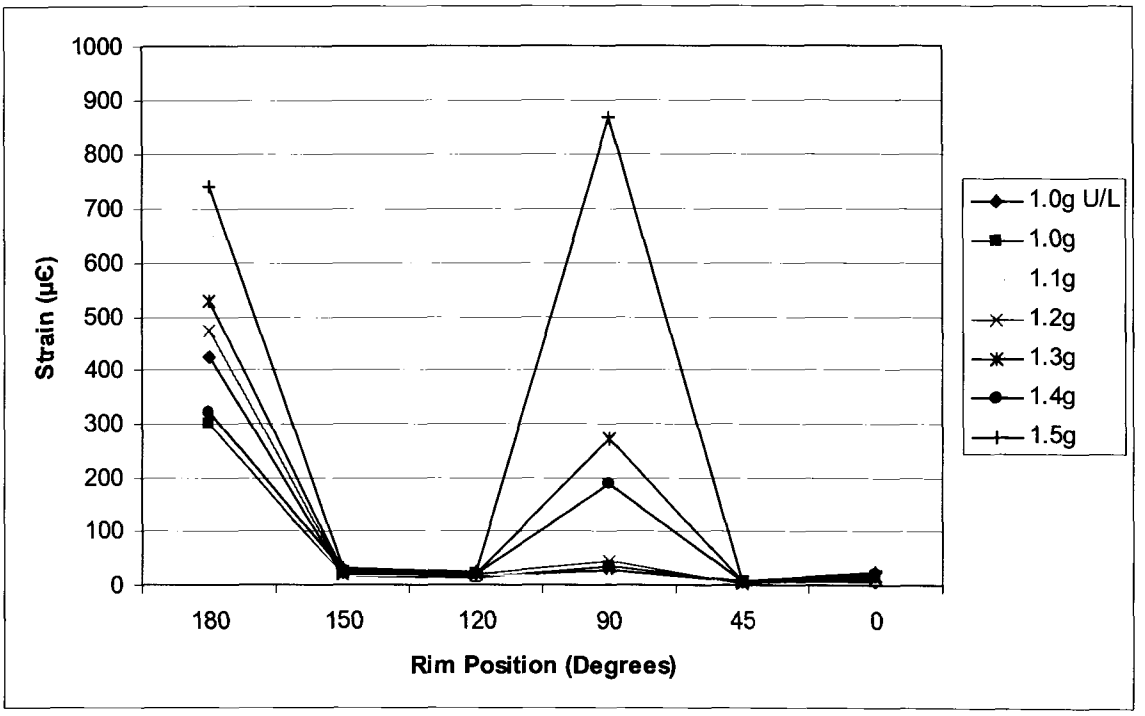

Figure 4-8: Center Band Tangential Strain, 100psi Tire Pressure

The results obtained for the radial and tangential strain in the center band, shown in figures 4-7 and 4-8 respectively, both show low levels of strains being measured in comparison to the other components. While the 180° and the 90° positions for the tangential strain plot indicate higher values of strain, it can be deduced that these values are most likely the result of a defunct strain gauge or data channel, as the values obtained have no correlation with respect to the load applied. Therefore, the results shown in figure 4-8 will be discussed in further detail in the filtered data section, similar to figure 4-2.

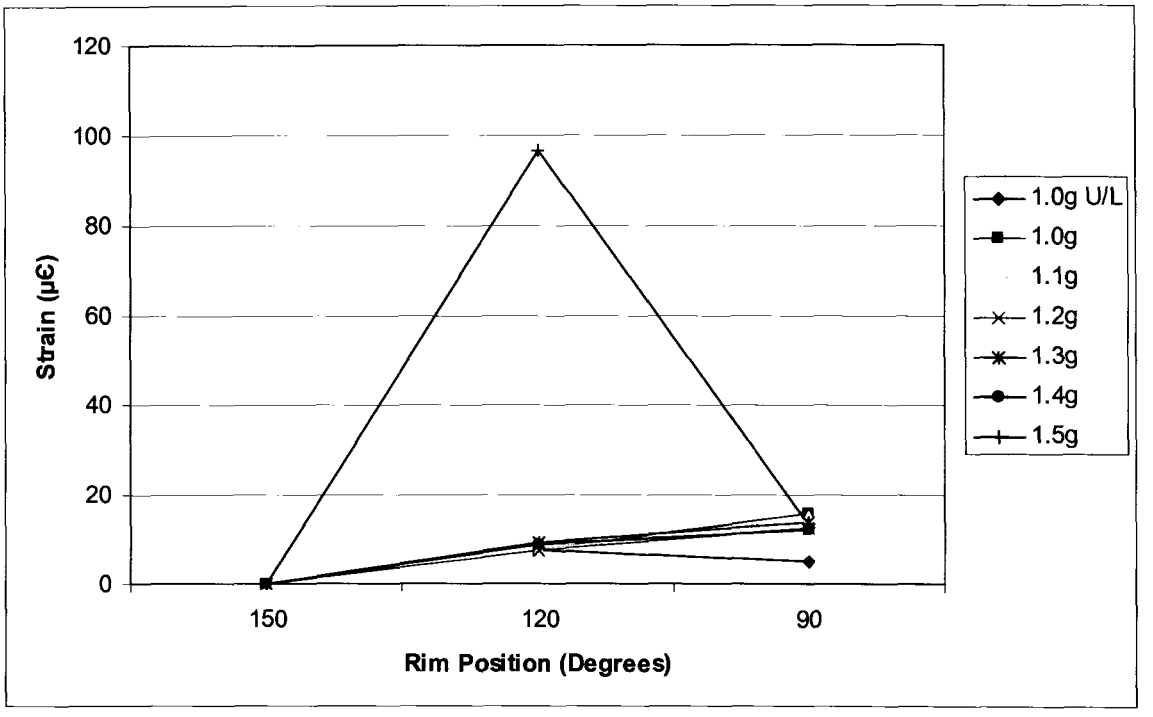

Figure 4-9: Lock Ring Radial Strain, 100psi Tire Pressure

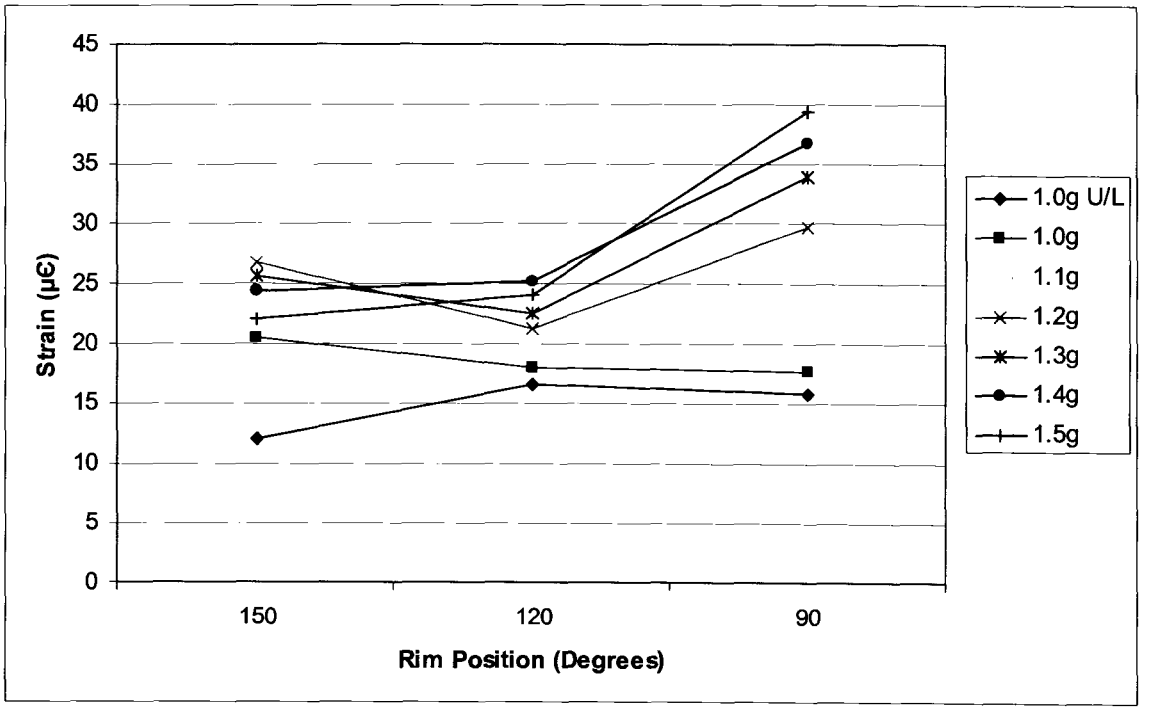

Figure 4-10: Lock Ring Tangential Strain, 100psi Tire Pressure

The results for the radial and tangential strain of the lock ring have the least data of any of the rim components shown so far. This lack of data is a result of the strain gauges at the 180°, 45° and 0° locations being damaged due to rim grease seeping out from the rim on the lock ring during dry test runs. This grease caused the tape holding the communication cables connected to the gauges to slip off and caused the gauges to be torn from the lock rings due to the unsupported weight of the cables. As a result of the missing data points, it is very difficult to draw any correlations between levels of strain and load on the rim, however it can be observed that all of the data collected for the lock ring indicates very low levels of strain with the exception of an outlier value of almost 100με radial strain measured at the 120° location for the 1.5g test.

4.2 Filtered Rim Strain Results

As it can be observed from figures 4-2 and 4-8, the data is hard to interoperate due to uncharacteristically high values skewing the graphs. These high values are a result of corrupted strain gauges, damaged wires, or faulty nodes and therefore, are no longer accurate. With these values removed a more demonstrative result of what is happening is presented in figures 4-11 and 4-12.

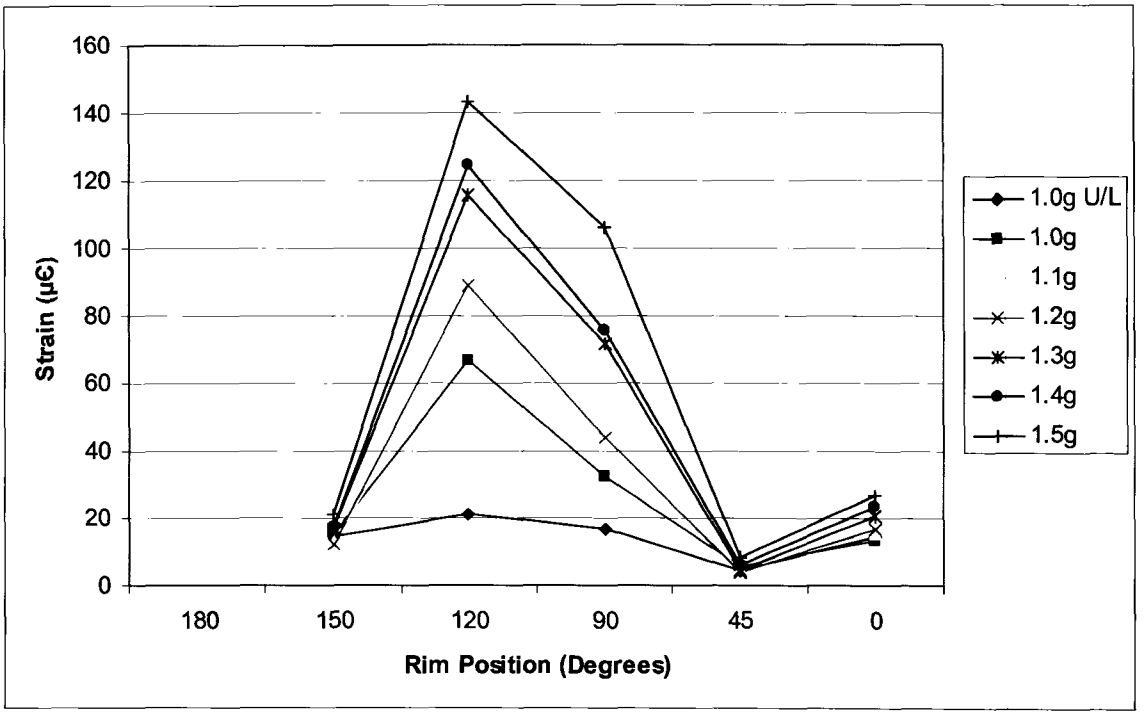

Figure 4-11: Outside Flange Tangential Strain, Filtered Data, 100psi Tire Pressure

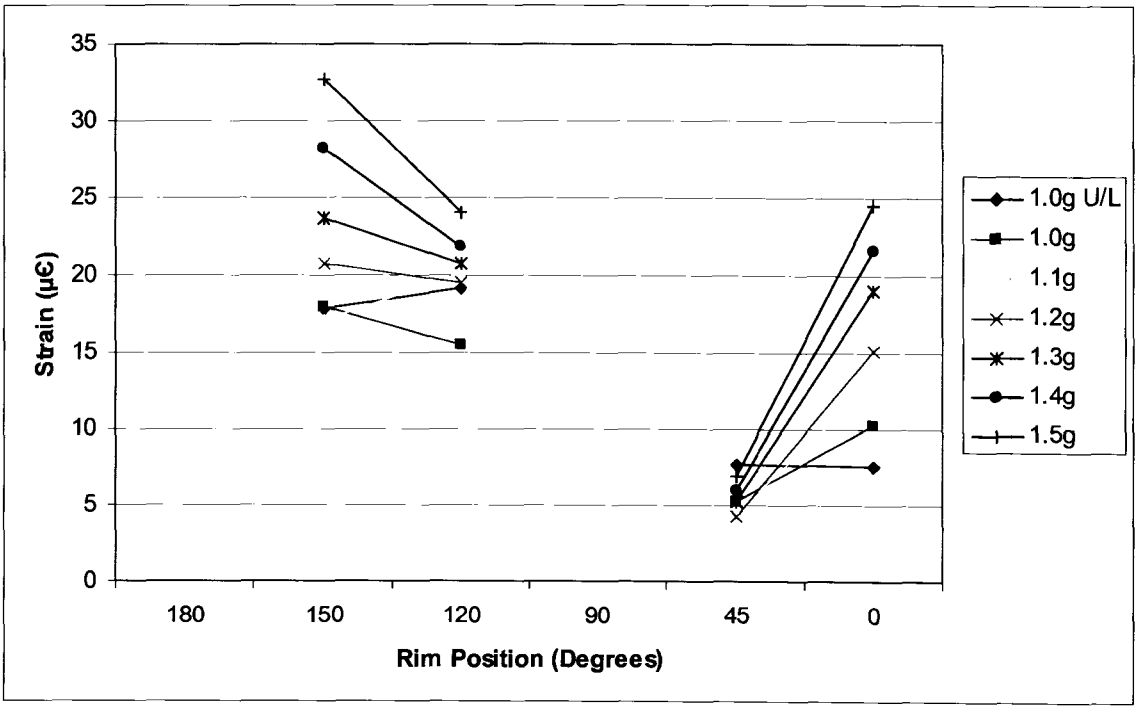

Figure 4-12: Center Band Tangential Strain, Filtered Data, 100psi Tire Pressure

Removing the data collected from the 180° strain gauge helps to provide a clearer picture of how the tangential strain is influenced by an increase in g-loading. Minimal values can be observed at the 150°, 45° and 0° locations, with maximum values occurring at the 120° and 90° points, which is to be expected as these points will experience an increase in tangential load as ovalization of the rim occurs due to load.

In contrast to the results shown in figure 4-11, the filtered results for the tangential strain of the center band shown in figure 4-12 do not provide a clearer picture in terms of rim strain versus g-loading. By filtering out the data from the 180° and 90° strain gauges a disconnect occurs in the data, leaving interpolation between two points for developing trends. While it is possible to observe the slight increase in strain compared to load with the more focused scale, it is not possible to accurately determine the relationship between the strain at the various points along the circumference of the inner surface of the center band.

4.3 Comparison of Rim Strains for Various Tire Pressures

The figures presented in Section 4.1 are from the 100psi tests, however, as stated previously, the same tests were conducted for 100psi, 90psi, and 80psi. Due to the fact there was not a significant difference in the shape of the plots resulting from the testing of each pressure, it was decided to just display the results from the 100psi test to cut down on the redundancy of the presented results. However, while the shapes of the plots remained consistent, there were differences in the values of strain measured, and therefore it was decided to present the results for the different tire pressures for one rim component to demonstrate this. The results for the outside flange were selected as they had the more consistent results and none of the strain gauges or data appeared to have been damaged. See figures 4-13 and 4-14 for a comparison of the 90psi and 80psi tests to the 100psi test (figure 4-1). The remainder of the results from the 90psi and 80psi tests can be found in Appendix A.

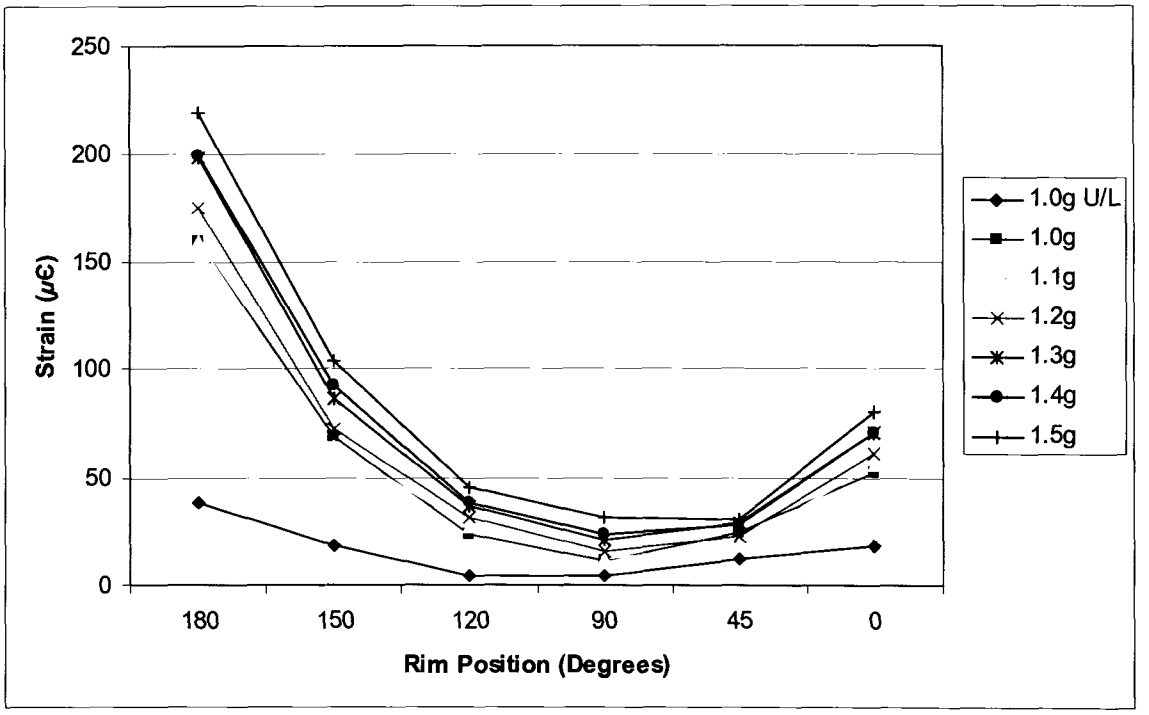

Figure 4-13: Outside Flange Radial Strain, 90psi Tire Pressure

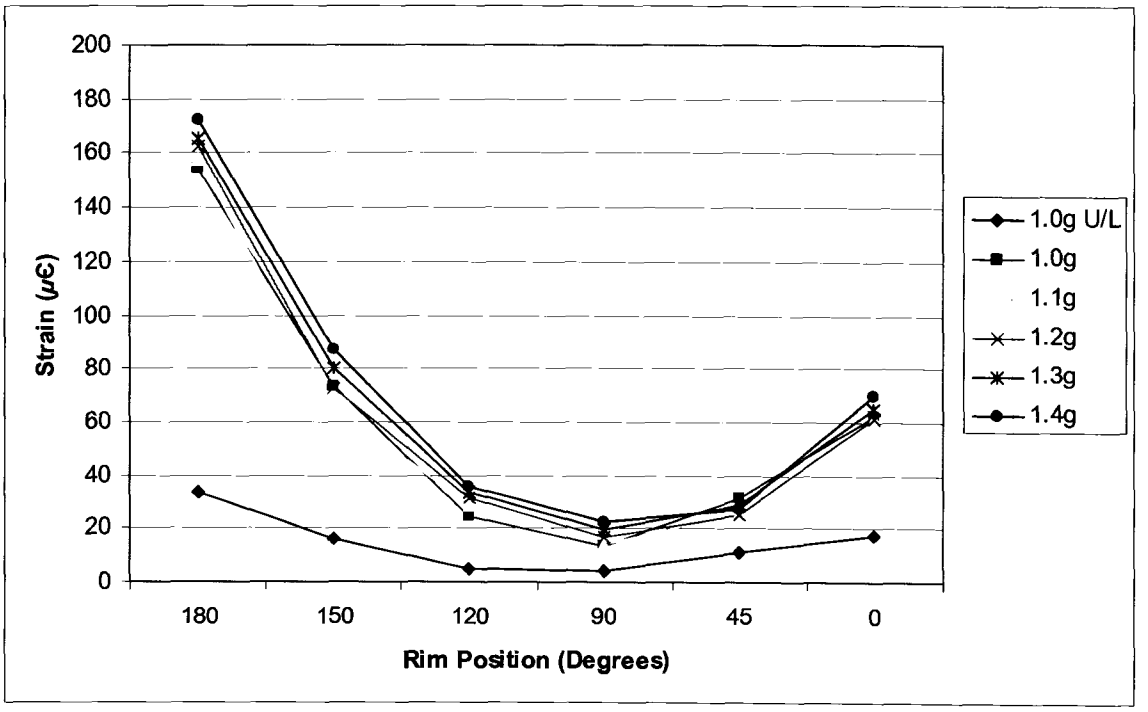

Figure 4-14: Outside Flange Radial Strain, 80psi Tire Pressure

From a comparison of figures 4-1 to figures 4-13 and 4-14 it can be observed that there is a significant decrease in strain (approximately 30με) for the various g-loads as the tire pressure decreased by 10psi intervals. This stands to reason as a lower tire pressure should result in a smaller reaction pressure as more of the normal load on the tire would be absorbed by the tire rather than transferred to the surface below.

Another point of interest when comparing the 100psi, 90psi and 80psi plots is that the results for each load in the lower tire pressure plots appear to have less dispersion when compared to the 100psi results. This however is not believed to be a result of lower tire pressure. Due to the sloped geometry of bottom surface of the flanges as well as their mating surfaces (the inside edge of the center band and the bead band for the inside and outside flanges respectively, see figure 2-6 for reference), the rim components can become pre-stressed after an initial load. This is due to the flanges being forced outwards up the sloped surfaces of the center band and the bead band when a load is applied to the tire and the tire bead pushes the flanges outwards, however, due to friction forces between the surfaces the flanges do not return to their starting position prior to the load occurring. This phenomonen was confirmed by respresentatives from Kal Tire (discussions with Glenn Clarke, 2004) and is believed to be the cause for the results obtained.

It would be possible to test this theory by repeating the 100psi test after an initial load was placed on the rim and tire, and theoretically, the strain results for the 100psi test would have far less dispersion then those shown in figure 4-1. However, as it was very difficult to coordinate with Kal-Tire to inflate the tire, a service vehicle and technician had to be sent to the testing location and had to be booked several weeks in advance, it was decided to fully inflate the tire to 100psi and then reduce the pressure from there after each test. Therefore, for future testing it is recommended that the rim and tire be preloaded prior to recording data to ensure consistent results for all of the rim components.

4.4 Tire Deformation Results

The previous results from the physical test reflected to the strain experienced at various points of the different rim components, whereas the results below have to do with the reaction of the tire to the various degrees of loading. As mentioned previously in the description of the loading test it was desirable to obtain information on the size of the footprint area (figure 4-15), the bugle of the sidewall (figure 4-16), as well as the total vertical displacement of the rim and tire during changes in load (figure 4-17).

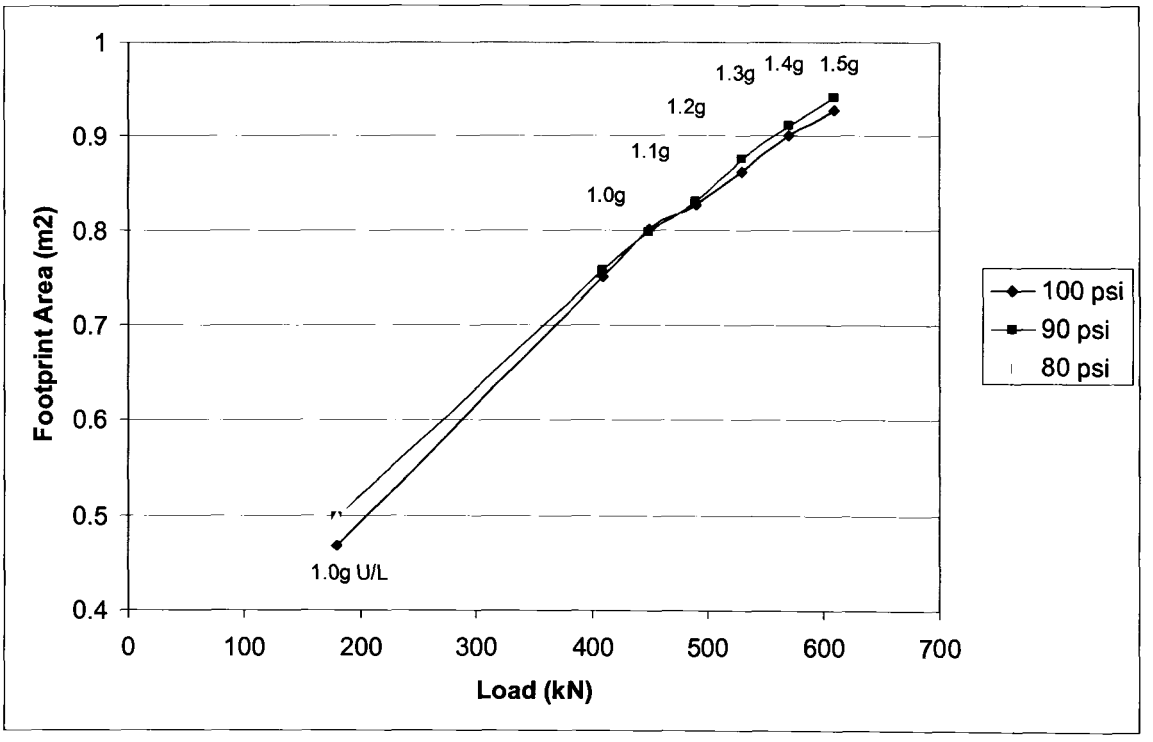

Figure 4-15: Footprint Area Versus Load at Various Tire Pressures

From figure 4-15 it can be observed that all three tire pressures result in an approximate linear increase in footprint area as load increases up to 1.5g. It does appear that for the 80psi tire pressure that the footprint area is beginning to level off at the 1.3g and 1.4g loads, however without further testing this cannot be verified. And unfortunately, as stated previously, the loading rams used did not have enough stroke to produce a load higher than the equivalent of 1.35g for 80psi tire pressure, due to the lack of bearing capacity of the tire. Another interesting note about figure

4-15 is that at low loads there is a large difference in area between 90psi and 100psi compared to 90psi and 80psi, however, as the loads increases this trend reverses and there is a significant difference in area between 80psi and 90psi while the 90psi and 100psi tire pressures almost have identical footprint areas.

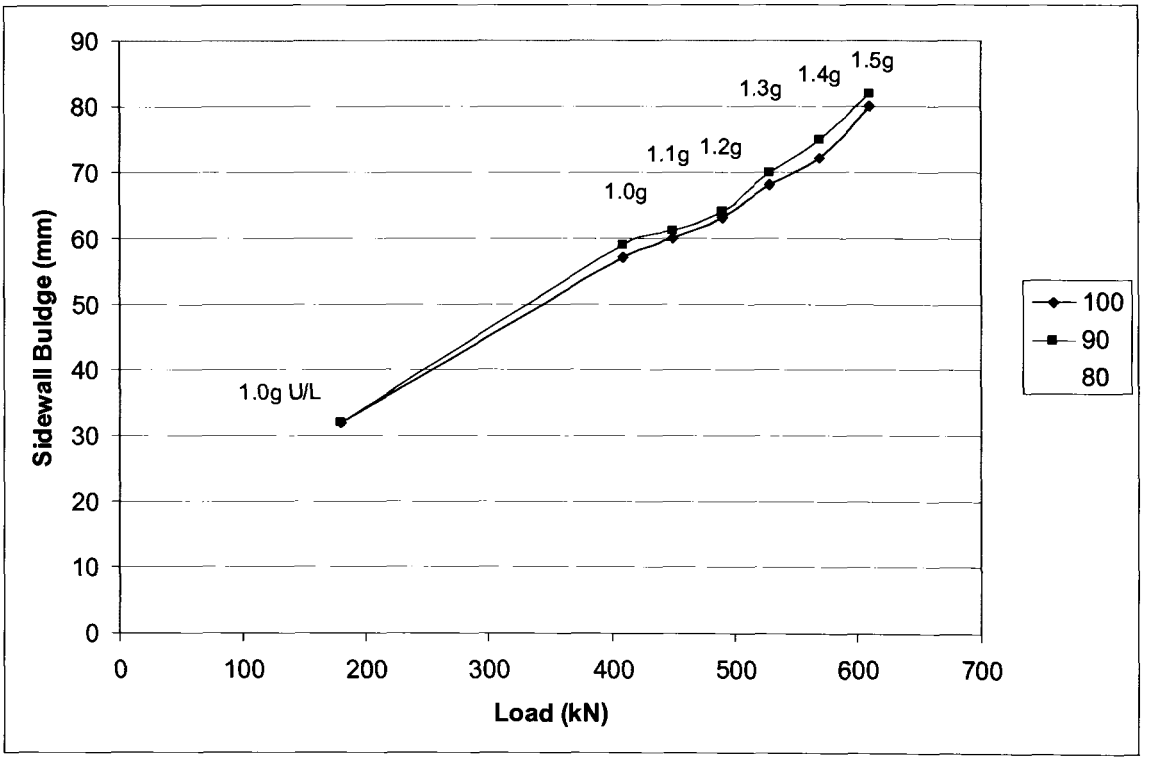

Figure 4-16: Tire Sidewall Bulge Versus Load at Various Tire Pressures

Similar to figure 4-15, figure 4-16 indicates an overall linear relationship between sidewall bulge and applied load. Unlike the footprint area however, none of the tire pressures indicate that the sidewall bulge is beginning to level off at the high g loadings, so it is not possible to determine how far this relationship will continue without further testing at higher loading levels. In terms of the relationship between tire pressures, there is a definite increase in the sidewall bulge between 80psi and 90psi compared to 90psi and 100psi, which remains constant throughout the loading spectrum.

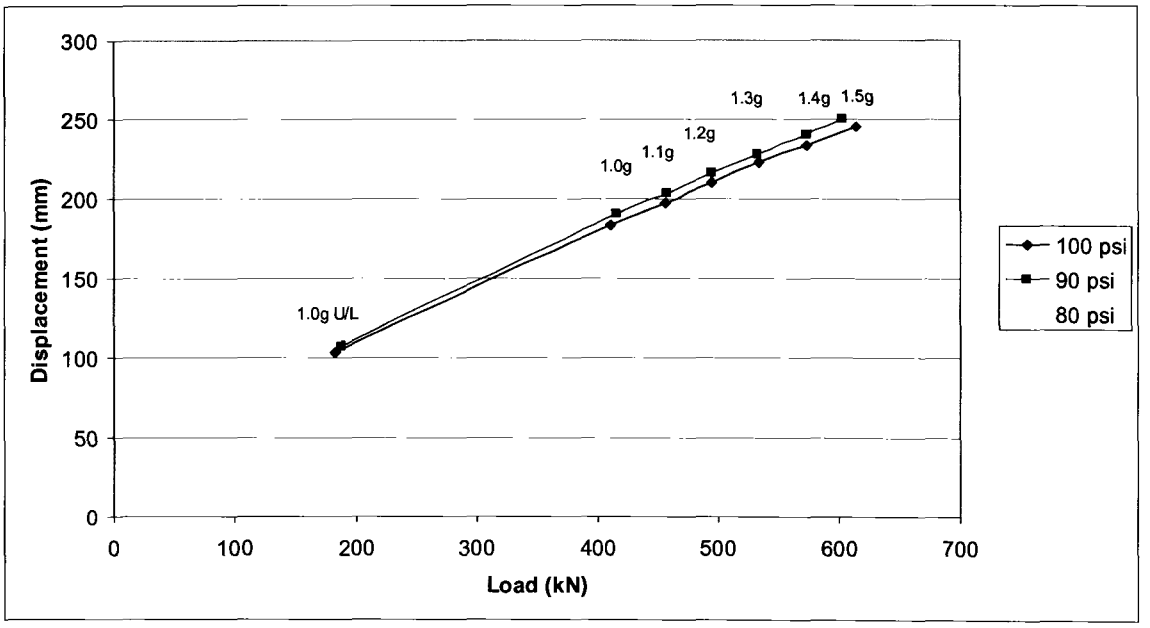

Figure 4-17: Vertical Tire Displacement Versus Load at Various Tire Pressures

Finally, figure 4-17 shows the relationship between vertical displacement and loading and it can be clearly seen that the relationship is linear for all three of the tested tire pressures. While the plots for footprint area and sidewall bulge had an overall linear shape to them, there were slight fluctuations in the trend, especially at the higher levels of load. The same is not true for the vertical displacement, as shown by the completely straight line relationship with no observable variances. Also, once again there is a more visible difference in the displacement when comparing 80psi and 90psi to 90psi and 100psi tire pressures.

5 Analysis of Physical Loading Test

It can be observed from the plots shown in Chapter 4 that there are definite trends in regards to the load that a tire and rim are subjected to. The same patterns of strain are observed at different magnitudes around the circumference for the various loads and tire pressures. Similarly, the physical properties of the tires seem to follow similar patterns as the load and tire pressure varies. Therefore, a closer examination of the results of the reactions of the rim and tire to various loading is required.

5.1 Analysis of Physical Loading Test Rim Results

While it is possible to recognize the patterns that result from the various loads and tire pressures that were used during testing, it is difficult to discern what the rim components are experiencing with the current format of the results. Another problem with the current form of the results is that units of strain are hard to contemplate, as they are not as commonly used as units such as stress. Therefore, to make the results more understandable two things were done: the values of strain were converted to units of stress, and these values of stress were plotted along a diagram of a rim section to give a more visual representation of the results obtained.

To obtain the values of stress for each strain measurement, Equation 5-1 was used, assuming an Elastic Modulus of 200,000MPa, which is a common value for steels.

$$E = \sigma / \varepsilon \qquad 5\text{-}1$$

Where E = Elastic Modulus (MPa)

σ = Stress (MPa)

ε = Microstrain (mm/mm)10^{-6}

To develop the stress plots the value measured at each corresponding point was plotted and curves were fitted between them to estimate the value of the stress in between the measured points. Each of the instrumented rim components was initially

considered independently to gain an understanding of the impact of high g loading for the different parts of the rim. Following this analysis, a comparison of the results of the tests with the different tire pressures was conducted to gain a better understanding of the effect of tire pressure in terms of stress/strain forming from high g loading.

5.1.1 Analysis of Outer Flange Loading Test Results

Figures 5-1 and 5-2 show the stress plots for the 1.0g and 1.5g cases respectively for the outside flange at 100psi, giving a close up view of the stress patterns at the nominal load and the highest load tested. Figure 5-3 shows the range of stress plots for the outside flange at 100psi to give an overall representation of the stress change as the load increases.

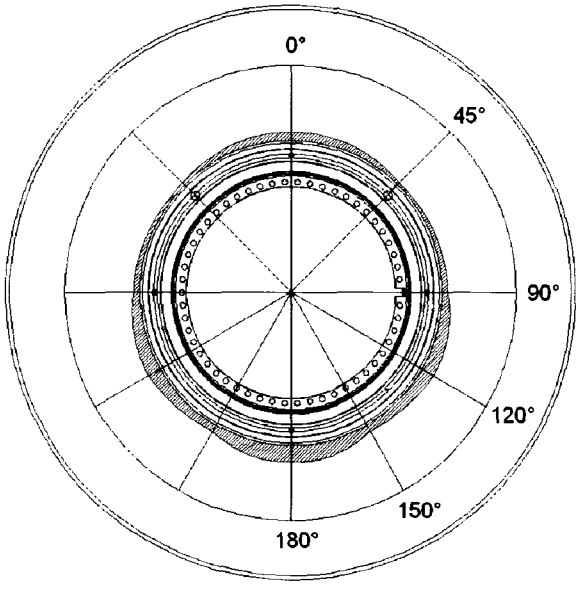

Tire Position	Stress (MPa)
0	9.0
45	2.5
90	6.7
120	14.0
150	7.2
180	16.5

Figure 5-1: Outside Flange Stress Plot, 1.0g, 100psi

Figure 5-1 shows the stress is consistent around the flange at 1.0g. Very little variation at the various points that were measured except at the 180° and 120° point where slightly larger values are observed, though no significant differences.

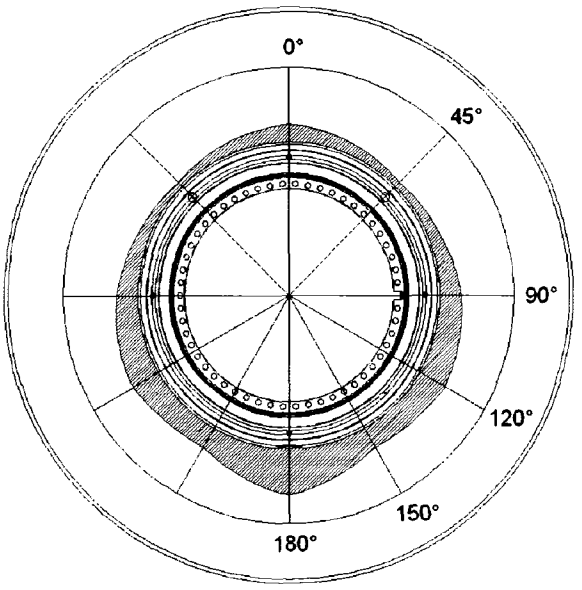

Tire Position	Stress (MPa)
0	17.7
45	5.9
90	22.3
120	30.2
150	22.4
180	47.7

Figure 5-2: Outside Flange Stress Plot, 1.5g, 100psi

Figure 5-2 shows large stress concentrations at the 0°, 120°, and 180° points, with the largest being observed at the 180° point. The value at 45°, while having increased from the value at 1.0g, has not changed significantly. Another point of interest is the value at 150°, while it has increased from 1.0g; it has not done so at the rate of the 120° and 180° points, creating peaks and valleys along the lowest portion of the rim circumference.

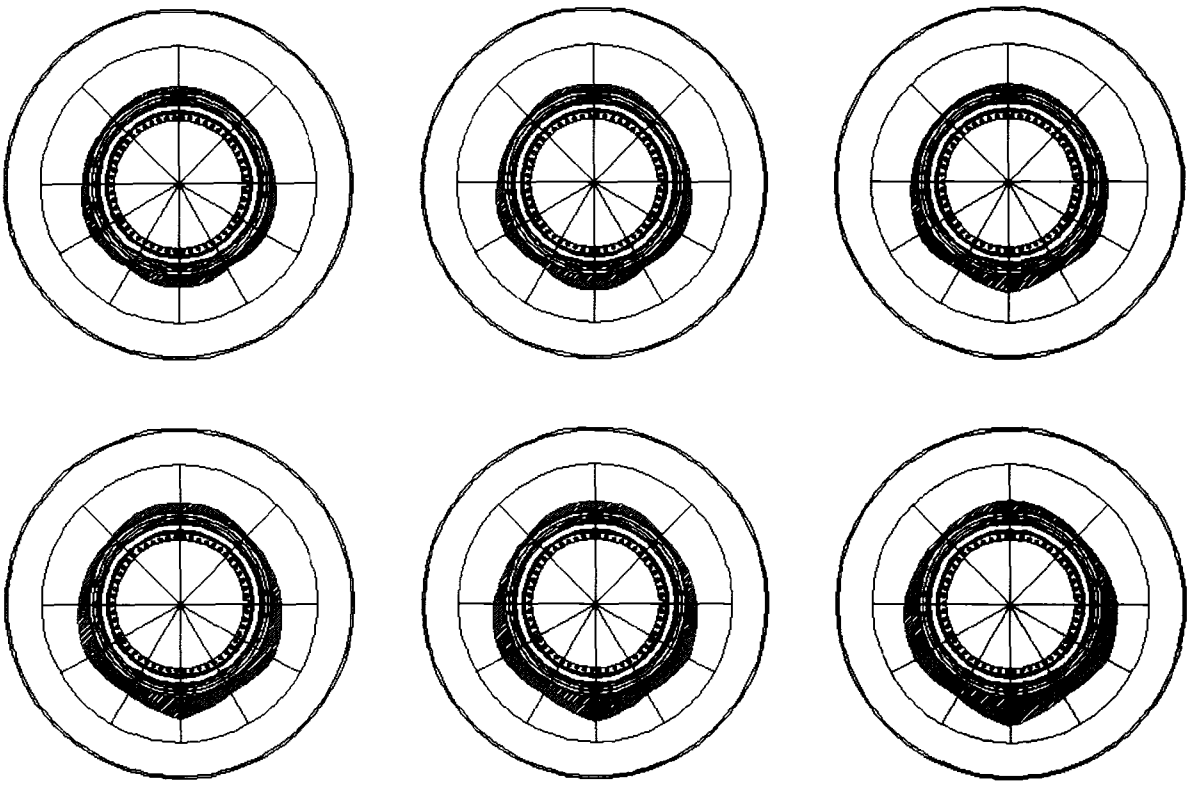

Figure 5-3: Outside Flange Stress Plots, from 1.0g to 1.5g Left to Right, 100psi

Figure 5-3 shows the full range of stress increases throughout the 100 psi test for the outside flange. At the 0° point the stress increases slowly, but at the higher g-levels it can be observed that the stress begins to change from a curve to a peak. At the 45° point there is very little change, as stated previously. For the 90° and 120° points there is a fair amount of increase in stress and the increases appear relatively consistent at the two points. At the 150° point the rate of stress increase is fairly large, about the same as at the 0° point, however, in contrast to the 90°, 120°, and 180° points there is definitely less of an increase in stress. Finally, at the 180° point the largest increases in stress are observed, and at the higher values of g-level a definite point load formation can be observed.

From these changes in stress level the formation of peaks and valleys mentioned previously can be observed. There is a small peak at the 0° point, leading to a an overall low point at the 45° point, rising towards a rounded peak spanning the 90° and 120° points, followed by a shallow peak at 150°, and finally a large peak at 180°. This figure clearly demonstrates the effect of a high g load on the outside flange shown by the large variations in stress, especially when compared to the consistent values at the 1.0g load, for which the rims were designed.

It is important to note that these values of stress are experienced for a stationary load, and during actual operation the tire and rim would be rotating, as would the observed stress curves. While this means that the same point would not always be experiencing high stress levels, it does mean that these points around the outer flange are being subjected to the range of values displayed, which can be detrimental in terms of cyclic fatigue and could eventually lead to rim cracking if left unchecked for too long.

5.1.2 Analysis of Inner Flange Loading Test Results

While the stress plots for the outer flange varied significantly with change in load the values measured for the inner flange show much less of an impact. Figures 5-4, 5-5, and 5-6 show the results for the 100psi test of the inner flange at 1.0g, 1.5g, and for each g-level increment respectively.

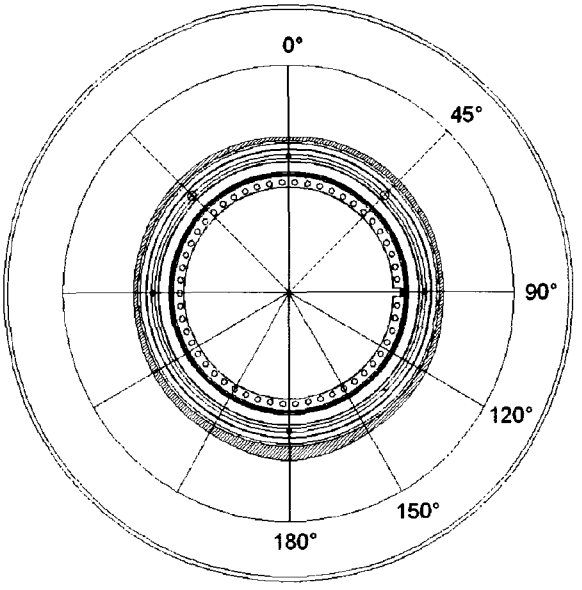

Tire Position	Stress (MPa)
0	3.4
45	6.1
90	3.7
120	7.3
150	8.5
180	14.7

Figure 5-4: Inside Flange Stress Plot, 1.0g, 100psi

At 1.0g load the stress distribution for the inner flange is similar to that for the outer flange, with the stress levels measured being fairly consistent around the circumference of the rim.

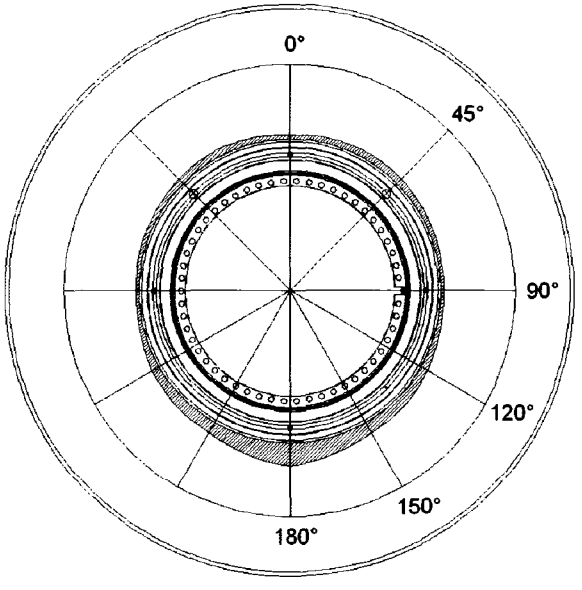

Tire Position	Stress (MPa)
0	4.1
45	7.1
90	3.1
120	8.4
150	12.0
180	23.9

Figure 5-5: Inside Flange Stress Plot, 1.5g, 100psi

At the 1.5g load the formation of a stress peak at the 180° point can be observed, however it is of nearly half the magnitude of the one measured for the outer flange. For the rest of the values measured there does appear to be significant change from those measured at 1.0g.

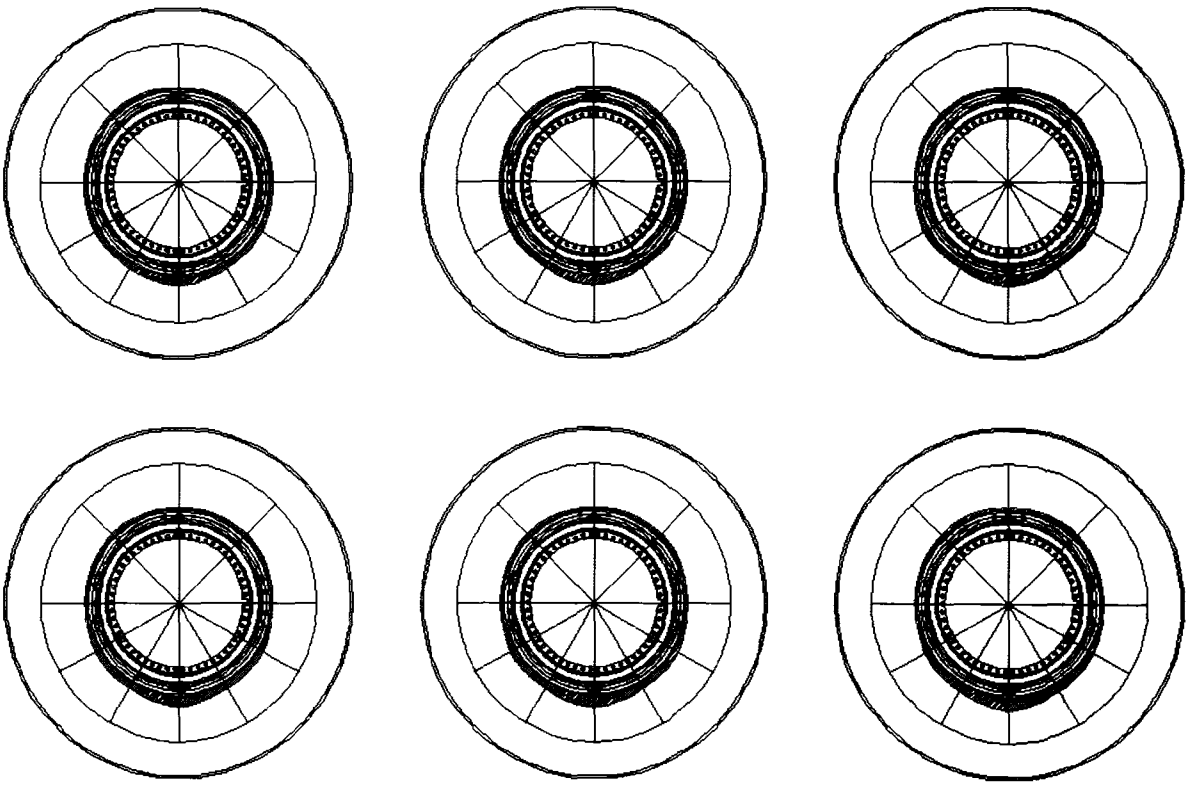

Figure 5-6: Inside Flange Stress Plots, from 1.0g to 1.5g Left to Right, 100psi

The series of stress plots at 100psi for the inner flange show the development of a peak at 180°, similar to the outer flange, but of approximately one third the magnitude. Also of interest, at the 0° point where a large peak was formed on the outer flange with higher g-loads, there was little to no change in the values measured. Similarly, where a large peak formed at the 90° and 120° points on the outer flange, there was only a minor increase at these locations for the inner flange. While there were some similarities between the inner

and outer flanges, such as the formation of a peak load at the 180° point, figures 5-3 and 5-6 clearly indicate that the inner flange is not impacted as much as the outer flange from high g loading.

5.1.3 Analysis of Center of Rim Band Loading Test Results

Whereas the stresses on the outer flange were severely influenced, and there were some increases in the stress profiles of the inner flange due to high g loading, as a result there was very little change for the values measured along the inner surface of the center band. Figures 5-7, 5-8, and 5-9 show the results for the 100psi test of the inner center band at 1.0g, 1.5g, and for each g-level increment respectively.

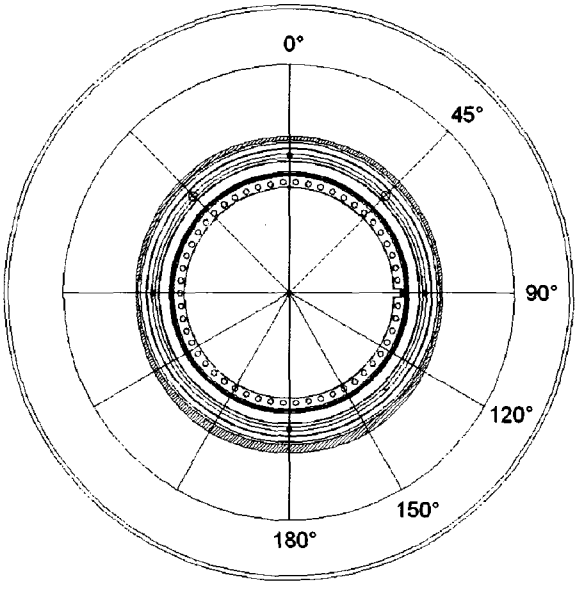

Tire Position	Stress (MPa)
0	3.1
45	4.8
90	2.6
120	5.5
150	9.7
180	8.3

Figure 5-7: Center Band Stress Plot, 1.0g, 100psi

The results for the 1.0g test at 100psi for the inside of the center band are similar to the results for the inner and outer flanges: very consistent stress distributions around the circumference of the rim.

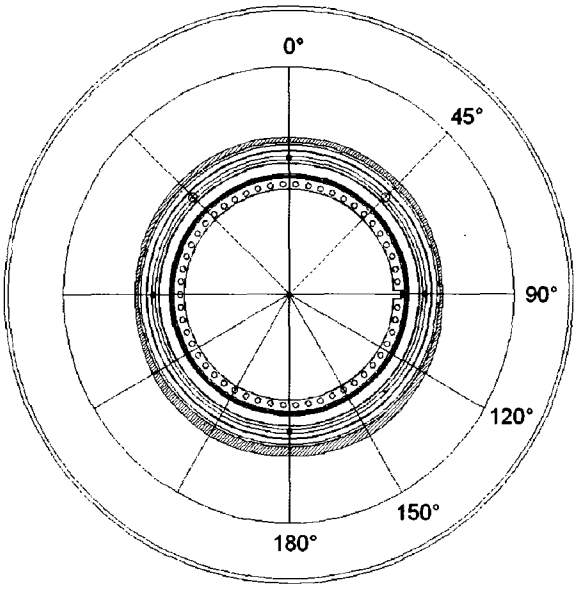

Tire Position	Stress (MPa)
0	4.9
45	5.9
90	2.8
120	7.0
150	10.6
180	9.3

Figure 5-8: Center Band Stress Plot, 1.5g, 100psi

Similarly to the results for the 1.0g test, the results for the 1.5g test at 100 psi show no significant increase in stress at any of the measured points.

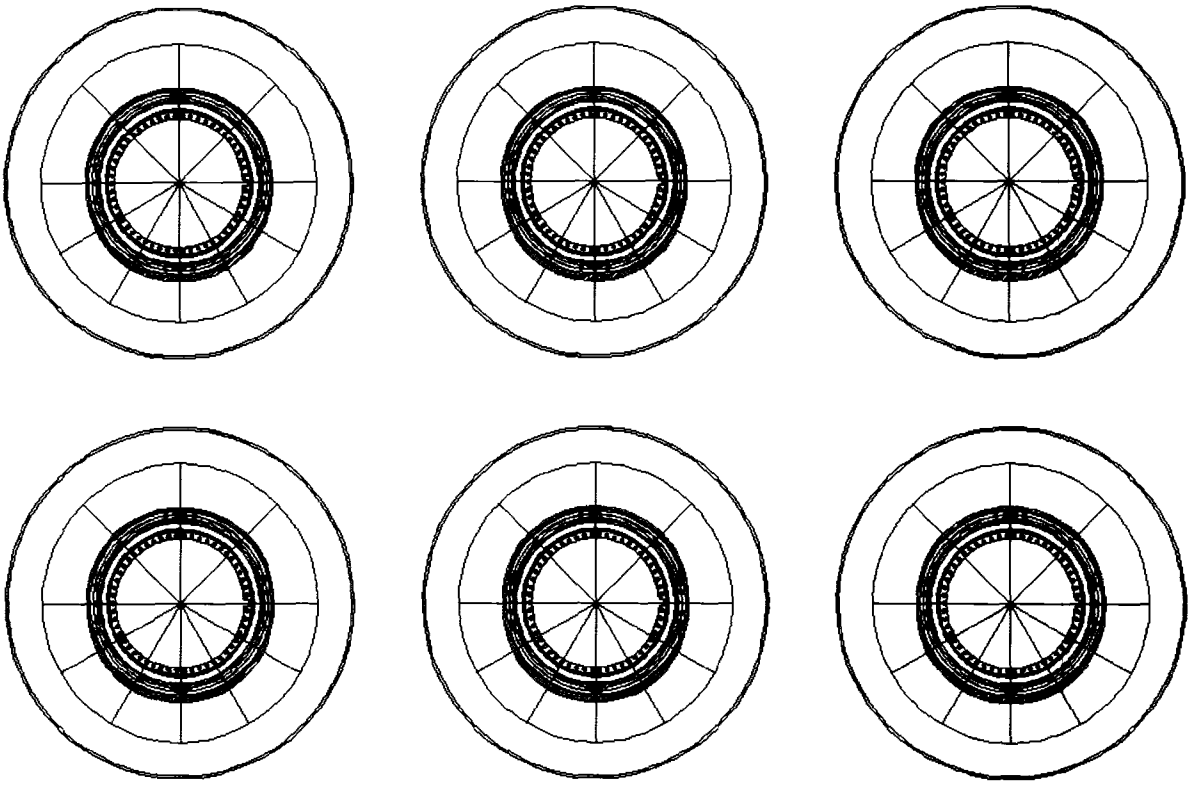

Figure 5-9: Center Band Stress Plots, from 1.0g to 1.5g Left to Right, 100psi

Figure 5-9 clearly shows the trend of minimal stress change with load increase. This can be attributed to the fact that the center of the band piece is not in direct contact with the rim beading, which transfers the load from the tire to the rim. Whereas the components on the inner and outer sides area very close to the beading contacts and definitely seem to be influenced by an increase in loading, as shown previously by the stress plots in figures 5-1 through 5-6.

5.1.4 Analysis of Outer Edge of Rim Band Loading Test Results

After the strain gauges were installed it was found that the channels for which the 0° and the 45° points were connected to on the outer edge of the rim band were malfunctioning.

Unfortunately, there were no extra data channels and therefore it was not possible to obtain data for the top half of the outer edge of the band. Therefore, the stress plots shown in figures 5-10, 5-11, and 5-12 show only the distributions for the bottom half of the rim.

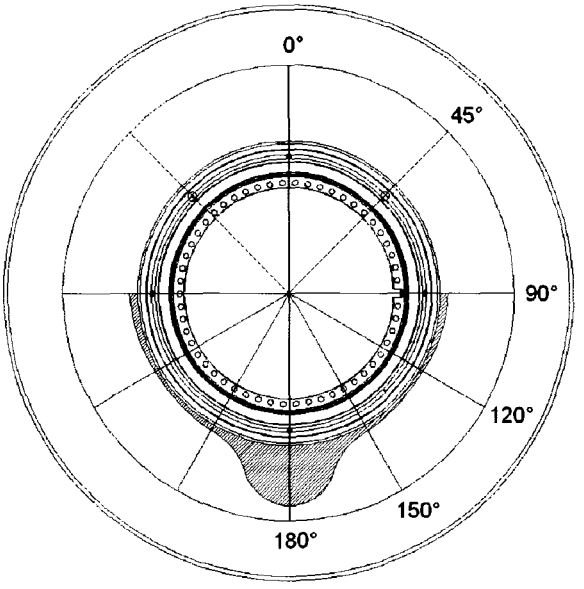

Tire Position	Stress (MPa)
0	N/A
45	N/A
90	8.0
120	4.0
150	6.0
180	61.0

Figure 5-10: Outer Band Stress Plot, 1.0g, 100psi

The results shown in figure 5-10 are somewhat consistent with those shown for the other components located near the tire beading. For the 90°, 120°, and 150° points there is a consistent low value of stress, similar to what was measured for the other components. However at the 180° point, there is already the formation of a large peak stress value, even at 1.0g, which was not observed for any of the other components.

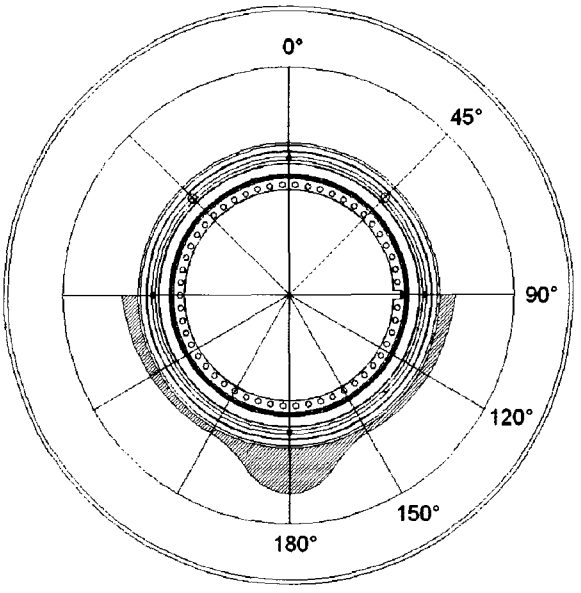

Tire Position	Stress (MPa)
0	N/A
45	N/A
90	17.0
120	9.0
150	6.0
180	46.0

Figure 5-11: Outer Band Stress Plot, 1.5g, 100psi

Again, the results shown in figure 5-11 are somewhat consistent with what would be expected based on the results of the other components. The stress values at the 90°, 120°, and 150° points have increased slightly with load, which is to be expected. However, the stress at the 180° has actually decreased with an increase in load, which is most likely an anomaly in the data based on the data measured for the other components at this point.

From figure 5-12 it can be observed that an increase in loading does not have much of an effect on the stress around the outer portion of the band. There is a noticeable increase at the 90°, and slight variations at the 120° and 150° points, and aside from the large value measured during the 1.0g test, small changes at the 180° point. The values for the 90°, 120°, and 150° points do seem to give results that are consistent with the other components, however the stress at the 180° point, especially at the lower levels of loading, do not coincide with those of the other components. This however is most likely a result of a malfunctioning strain gauge or data channel, as it will be shown that measurements at this point for the other tests produced inconsistent results as well. Therefore, with the lack of data for the top half of the distribution, and the questionable

results obtained for the 180° point, there is definitely a need for more data to be able to understand how the stress on the outer band is influenced by an increase in loading.

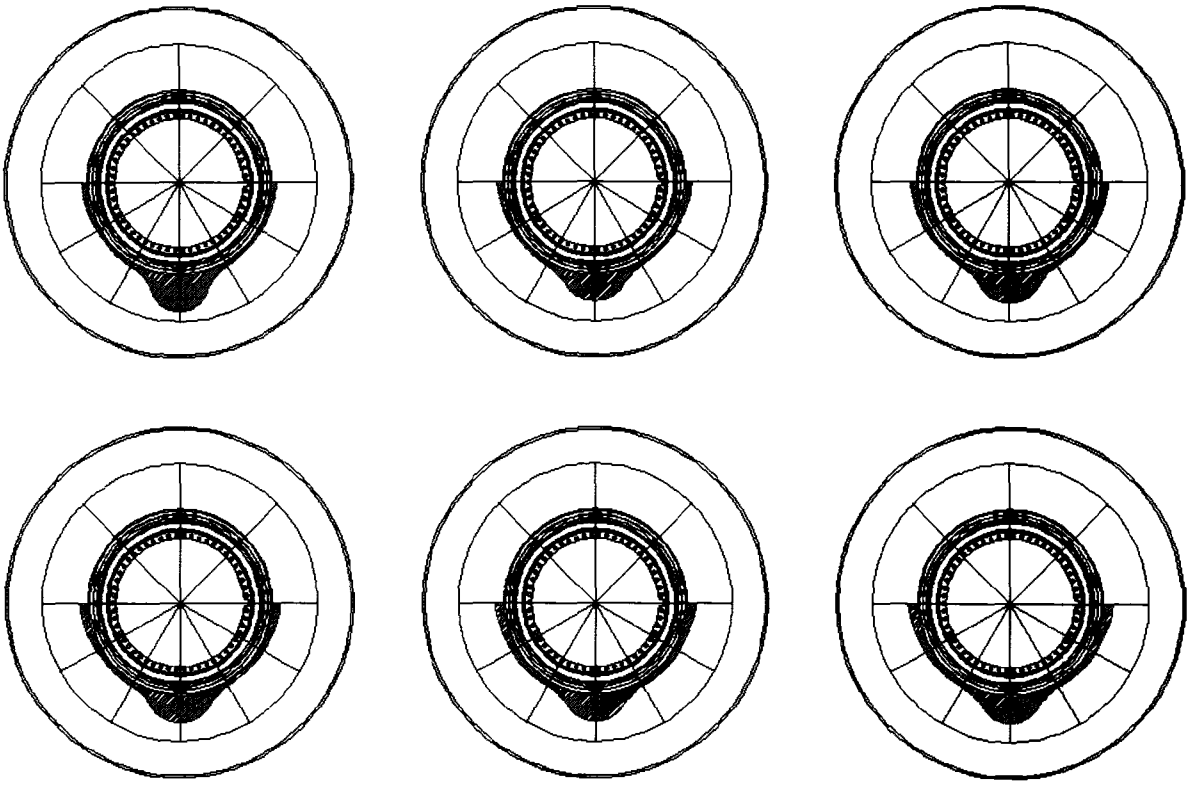

Figure 5-12: Outer Band Stress Plots, from 1.0g to 1.5g Left to Right, 100psi

5.1.5 Analysis of Lock Ring Loading Test Results

While the results from the other components provided enough data to produce a stress distribution around the rim, or around half of it for the outer edge of the band, there was not enough data to produce any plots of value for the change in stress around the lock ring for increased loading. This can be observed from the lack of data displayed in figures 4-9 and 4-10. As discussed previously the lack of results for the lock ring was due to the rim lubrication that seeped from the rim during loading and covered the majority of the strain gauges on the lock ring. This caused the tape that was protecting the gauges and supporting the wires to come off, resulting in damage to most of the strain

gauges. Therefore, without further testing, it is not possible to produce stress distribution plots for the lock ring, as will be discussed in the future work section of Chapter 7.

5.2 Analysis of the Effect of Tire Pressure on the Physical Loading Test Rim Results

The stress plots that have been presented and discussed so far were all for the 100psi test. Now, a comparison of the results for the 100psi test to that of the 90psi and 80psi tests will be made to determine the effects on the rim components from varying internal tire pressures as loading on the rim and tire increases. The following figures show the results for the stress distributions for outside flange for the three tire pressures tested: 100psi, 90psi, and 80psi.

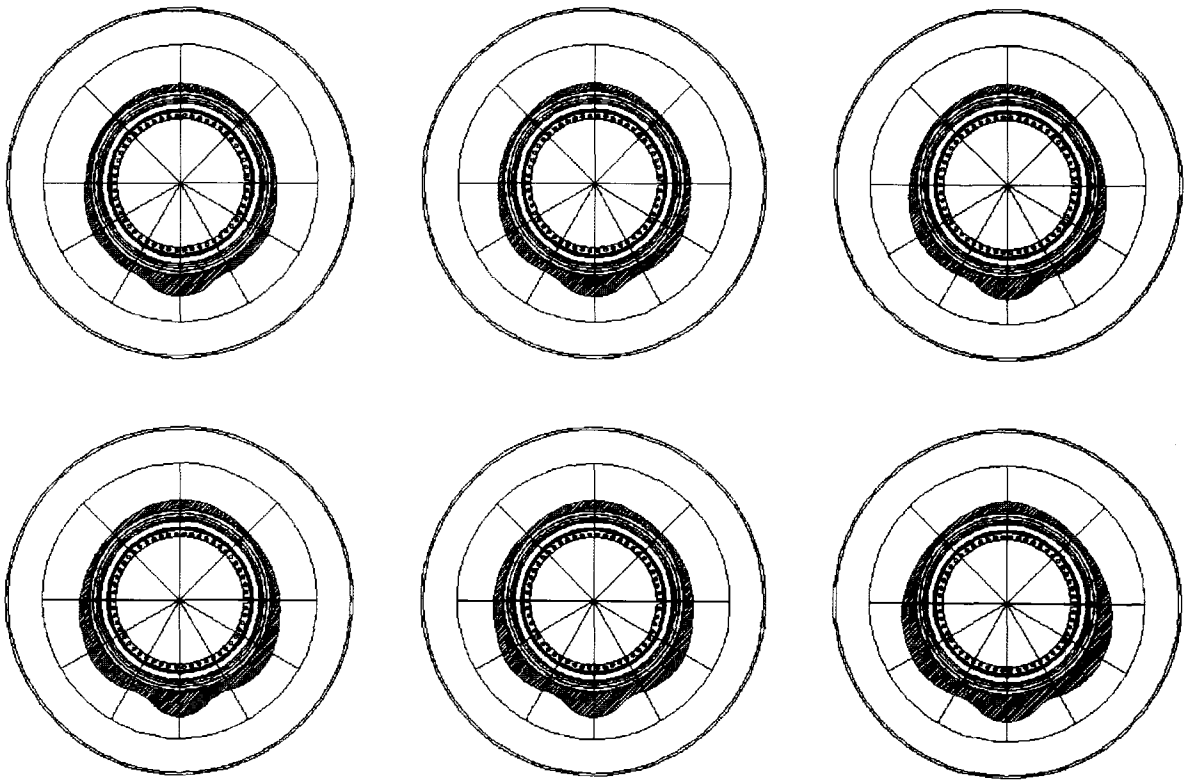

Figure 5-13: Outside Flange Stress Plots, from 1.0g to 1.5g Left to Right, 90psi

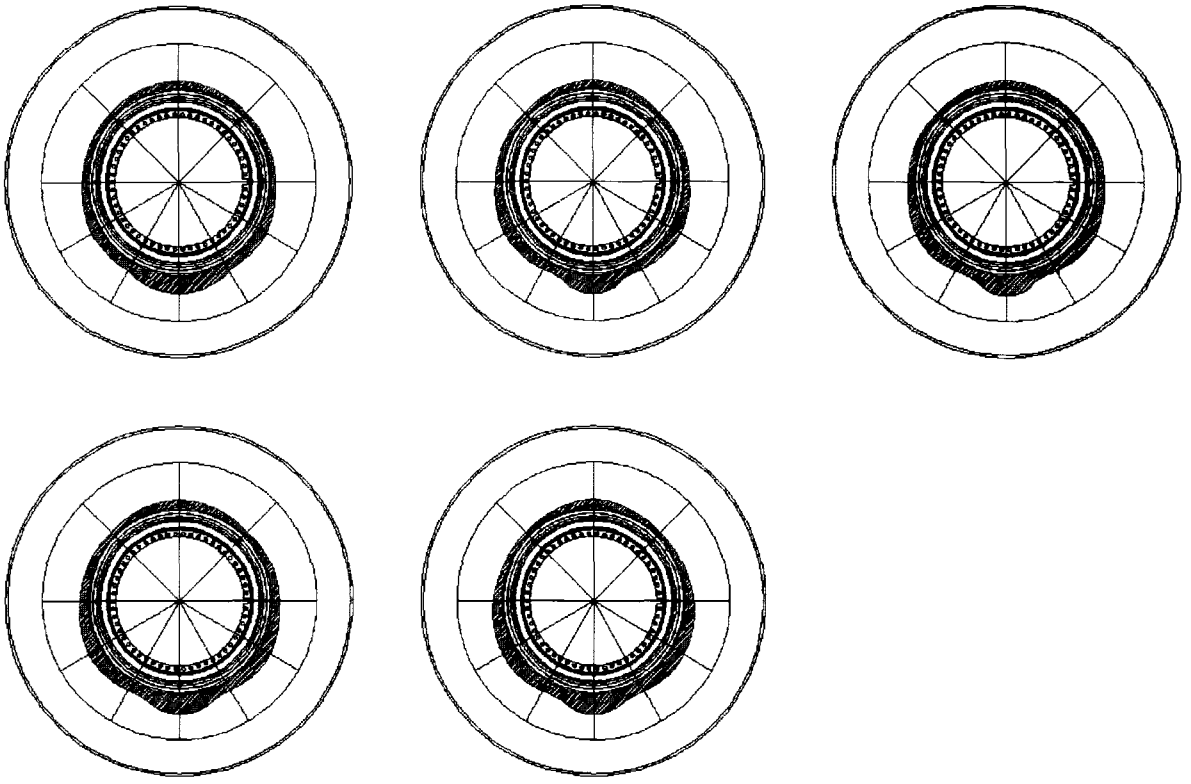

Figure 5-14: Outside Flange Stress Plots, from 1.0g to 1.4g Left to Right, 80psi

From figures 5-3, 5-13, and 5-14 it can be observed that there is small change in the stress distributions for the outside flange as a result of tire pressure change. There is a slight decrease in stress as the pressure is lowered, with the highest change occurring at the 180° point. The drop in stress at this point with a decrease in pressure of 10psi is in the order of 10MPa- 20MPa.

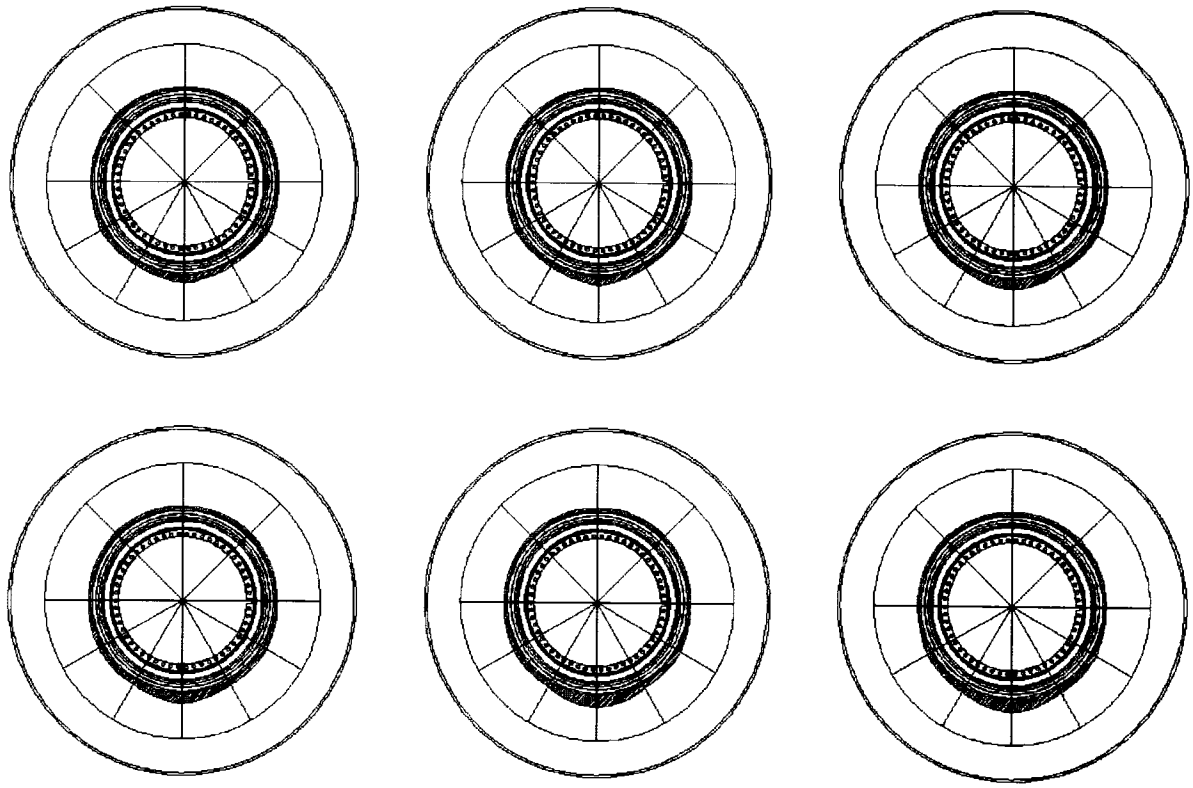

Figure 5-15: Inside Flange Stress Plots, from 1.0g to 1.5g Left to Right, 90psi

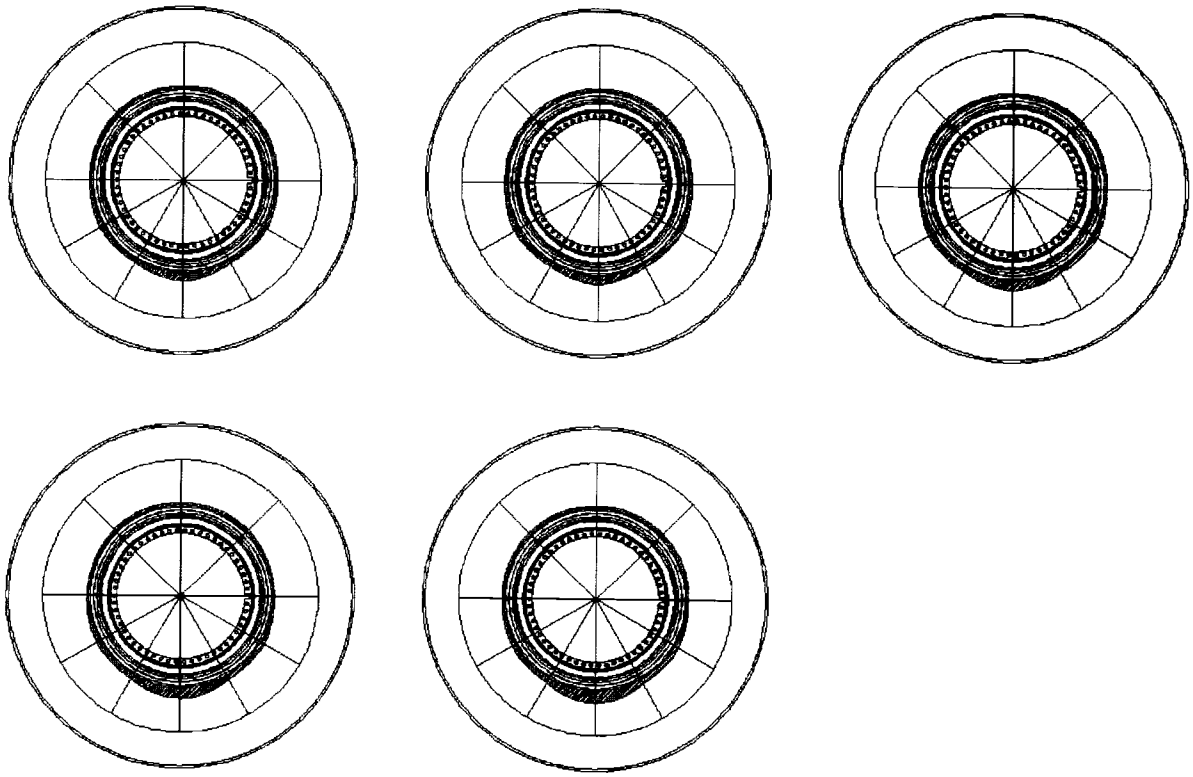

Figure 5-16: Inside Flange Stress Plots, from 1.0g to 1.4g Left to Right, 80psi

Similar to the outer flange, the results for the inner flange, shown in figures 5-6, 5-15, and 5-16 show a relation between tire pressure and the stress/strain measured. As the pressure is decreased there is a slight drop in the value of stress/strain measured. At the 180° point there is an approximately 5MPa drop as the tire pressure is decreased by 10psi. However, with changes in pressure of such a small magnitude, it is not possible to positively determine that the change in stress in the rim is a result of the tire pressure change due to the inaccuracy of the equipment used. Further testing with more accurate methods of measurement would be required to validate this relationship.

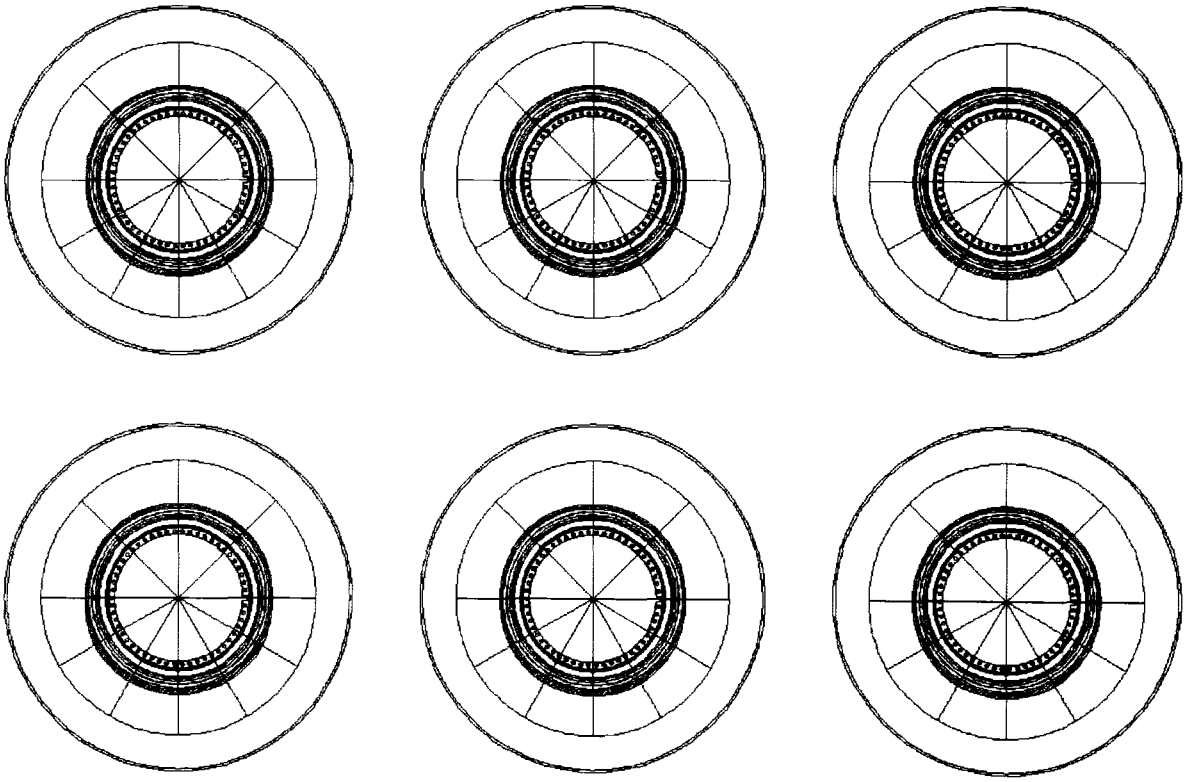

Figure 5-17: Center Band Stress Plots, from 1.0g to 1.5g Left to Right, 90psi

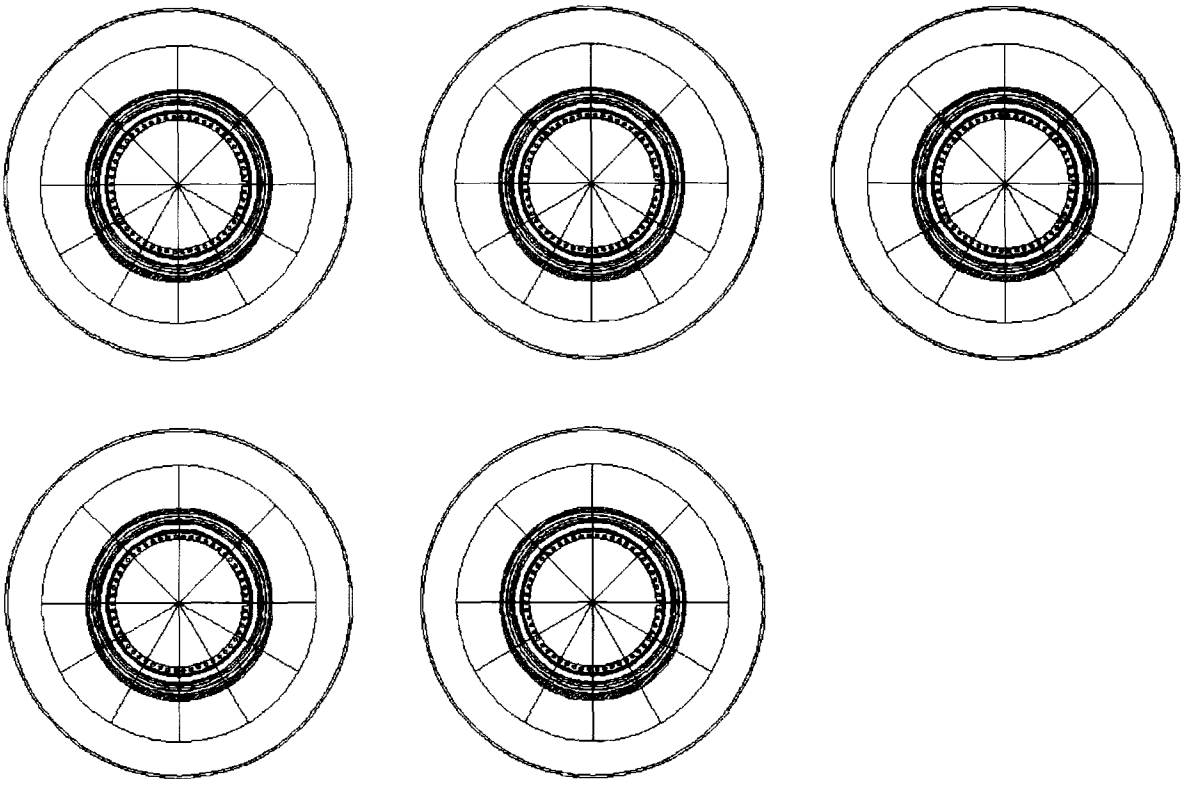

Figure 5-18: Center Band Stress Plots, from 1.0g to 1.4g Left to Right, 80psi

For the results of the inner surface of the center of the rim band, figures 5-9, 5-17, and 5-18 it again can be observed that there is a small correlation between tire pressure and the amount of stress due to load, with similar values of change to that of the inside flange. It stands to reason that the stress in center portion of the rim band would be influenced by the pressure in the tire, as the center of the rim band is the furthest point from both bead contact points, making the impact of the loading minimal. Therefore, the only force have any significant impact in the center of the rim would be the tire pressure. However, due to the values of change being of the same order of those measured for the inside flange, and the lack of data points (3 tests), it again is hard to confidently state that there is a definite relationship between tire pressure and stress in the rim band center without further testing with more accurate equipment.

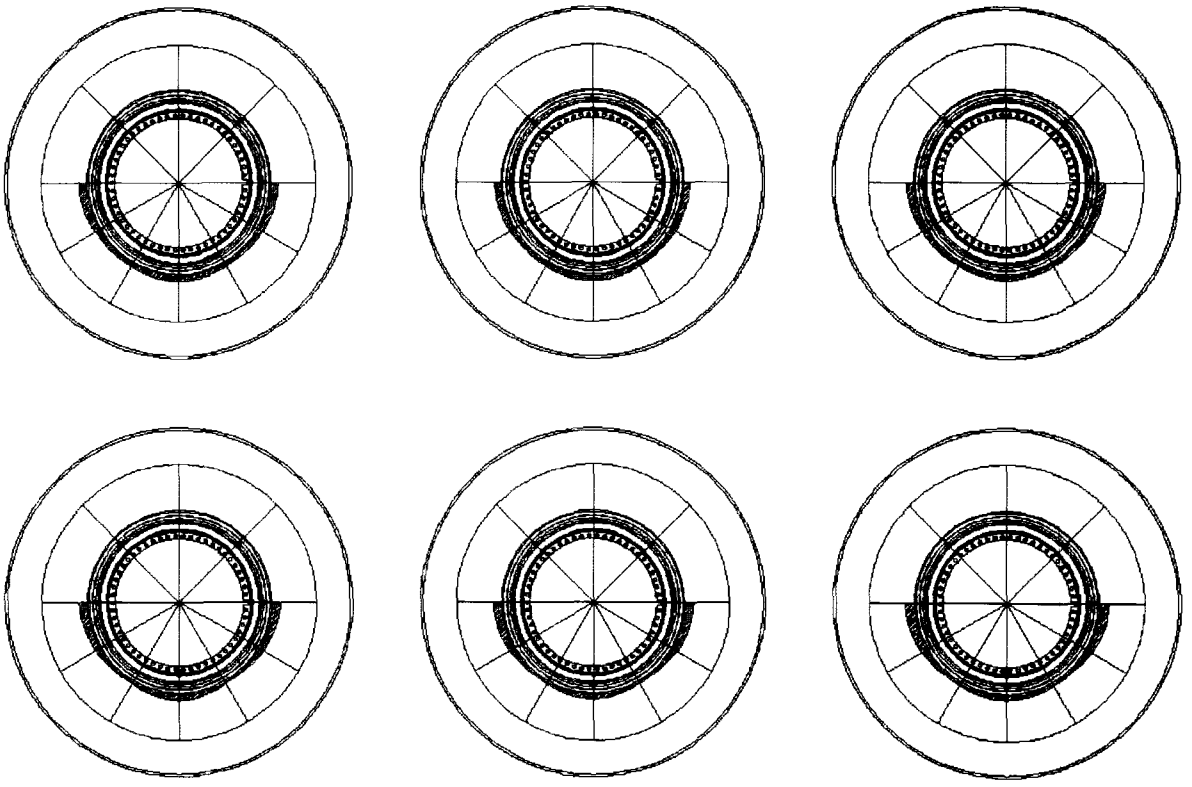

Figure 5-19: Outer Band Stress Plots, from 1.0g to 1.5g Left to Right, 90psi

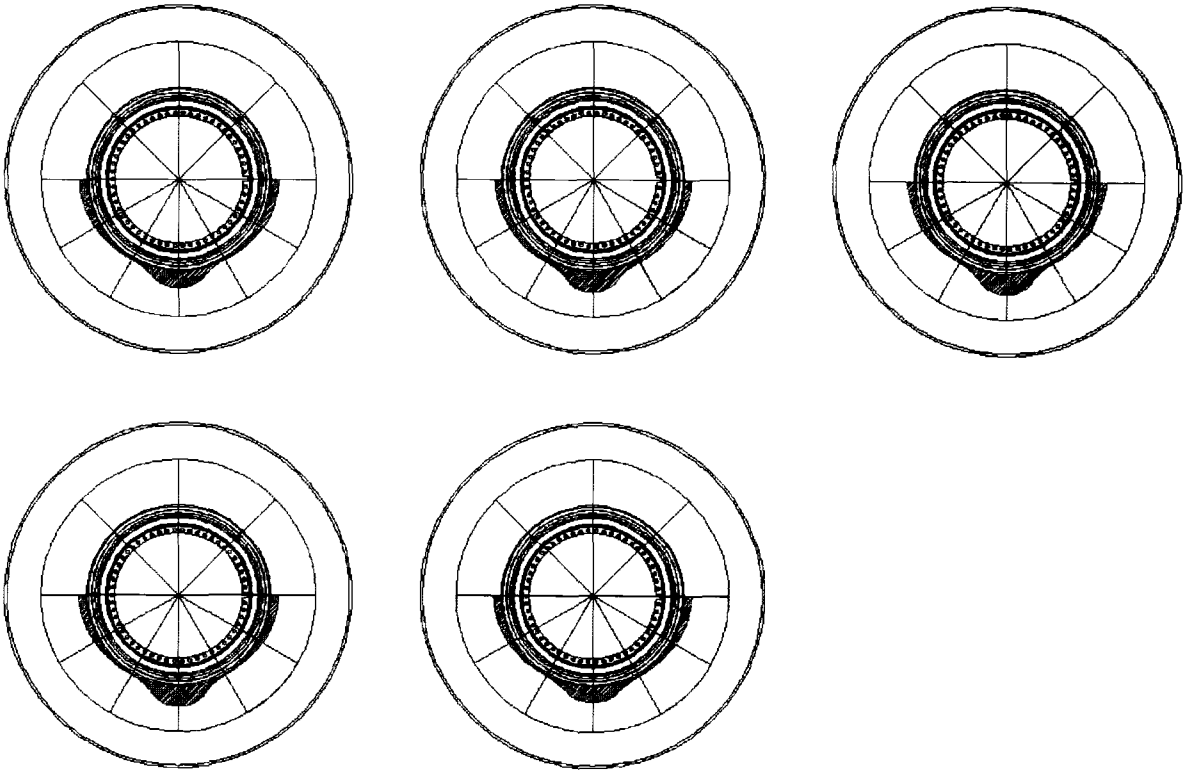

Figure 5-20: Outer Band Stress Plots, from 1.0g to 1.4g Left to Right, 80psi

The results for the outer edge of the rim band, shown in figures 5-12, 5-19, and 5-20 show the least amount of consistency for the value of stress compared to load. Whereas there were small variations in the values recorded for the other three rim pieces, there was consistency in the shape of the stress distributions, which is not true for the outer edge of the rim band. The values for 90°, 120°, and 150° do have some consistency, similar to those measured for the flanges, however the values for the 180° position appear to be completely independent of tire pressure and vary significantly. As stated previously in the analysis of the impact of increased load on the outer rim band, this variation in the values for the 180° point is more than likely the result of a defective strain gauge or faulty data channel, and therefore, without more information it is not possible to determine the relationship between tire pressure and stress for the outer edge of the rim band.

Overall, there appears to be a relationship between the change in tire pressure and the stress/strain values measured at the various points of the four rim components. However, as previously stated, without more testing and more accurate measurement it is hard to quantify exactly what that relationship is. For the data from this set of tests, the only change in stress that was significant was at the 180° position for the outside flange, with the rest being less than 10MPa. Therefore, from the data available it can be inferred that the relationship between rim stress and tire pressure is not significant as that of the effect of increasing the impact load or even the comparison of the rim components.

5.3 Analysis of Physical Loading Test Rim Results

From figures 4-15, 4-16, and 4-17, it can be observed that the footprint area, the sidewall bulge, and the vertical displacement of the tire follow a linear relationship for the values of load measured. However, this linear relationship cannot possibly define the behavior of the tire at higher values of g-level/loads for the values of g-loading measured during operations (4g). It seems reasonable that at higher levels of load the relationship between footprint area, sidewall bulge, and vertical displacement should flatten off following a logarithmic trend. This means that the values measured for these tests define the tire behavioral properties for the lower end of the elastic region, and to obtain a further

understanding of where and how these relationships transform from linear to logarithmic, further testing at higher g-levels must be conducted. Unfortunately, the University of Alberta does not have the equipment or expertise to properly and safely perform these tests at the loads required. Therefore, without further industry help, it is not currently possible to measure and predict the effect of high g-loading on the tire itself.

6 Predictions from the Physical Loading Test

As stated previously, certain mine sites with soft ground conditions have experienced upwards of 4g's of load as measured by on-board monitoring of strut pressures. And while the testing done for this research project has provided some valuable information in terms of stress distributions along the rim and corresponding physical reactions of the tire, they have been in response to a maximum load of 1.5g. Therefore, using the data obtained from the testing, it is hoped to be able to develop a relationship between load and the values measured to predict what happens in terms of rim stress/strain and tire deformation at loads upwards of 4g. To this end only the data for the 100psi test will be discussed here as an example. For the graphs developed for the other tire pressures see Appendix B.

6.1 Predictions of Rim Strain/Stress by Orientation for High-g Loading

The first component of the rim to be discussed is the outside flange. Figure 6-1 shows the data measured for the outer flange at 100psi converted to a Strain ($\mu\epsilon$) versus Applied Load (kN) form, with the associated g value indicated on the plot at the appropriate load level. From this plot it can be observed that the strain/stress for each of the measured points around the circumference increase in a linear matter with an increase in load. While this trend may taper off with higher loads it is not currently feasible to test higher g levels at the University of Alberta due to safety concerns and the limitations of the equipment available. Therefore, based on the data obtained, the predictions for the stress/strain at higher g loads than 1.5g, shown in figure 6-2, were determined by continuing the linear relationship shown in figure 6-1.

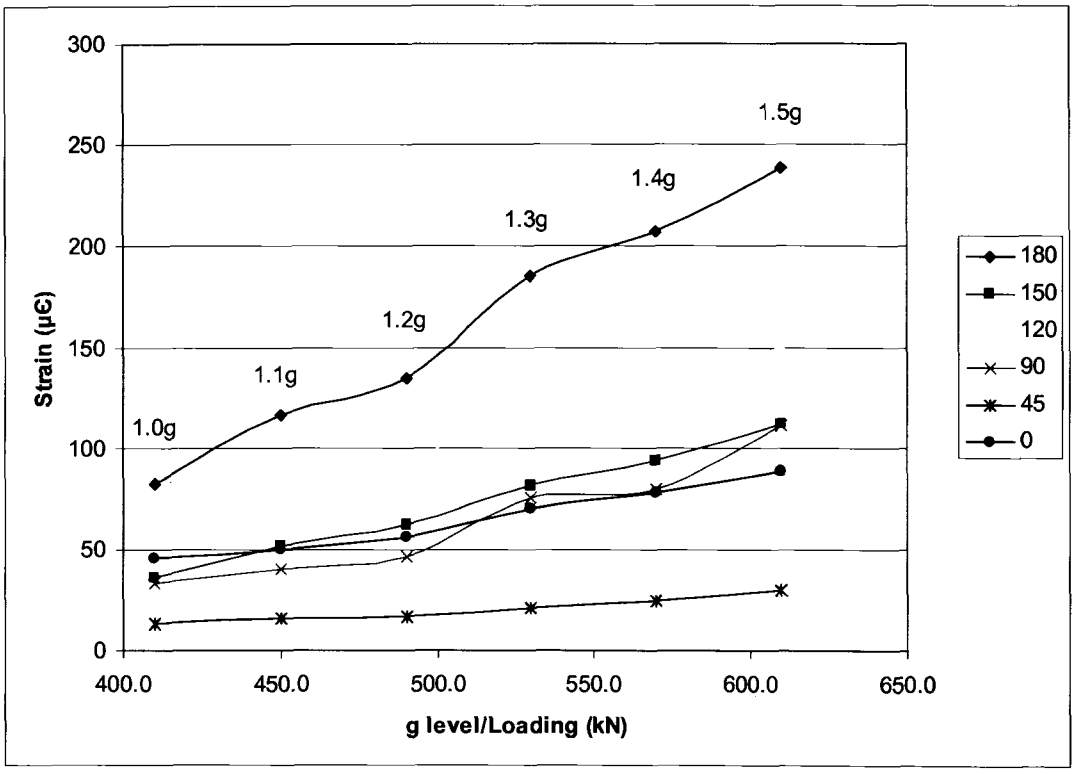

Figure 6-1: Outside Flange Strain vs. g level/Loading Actual (100psi)

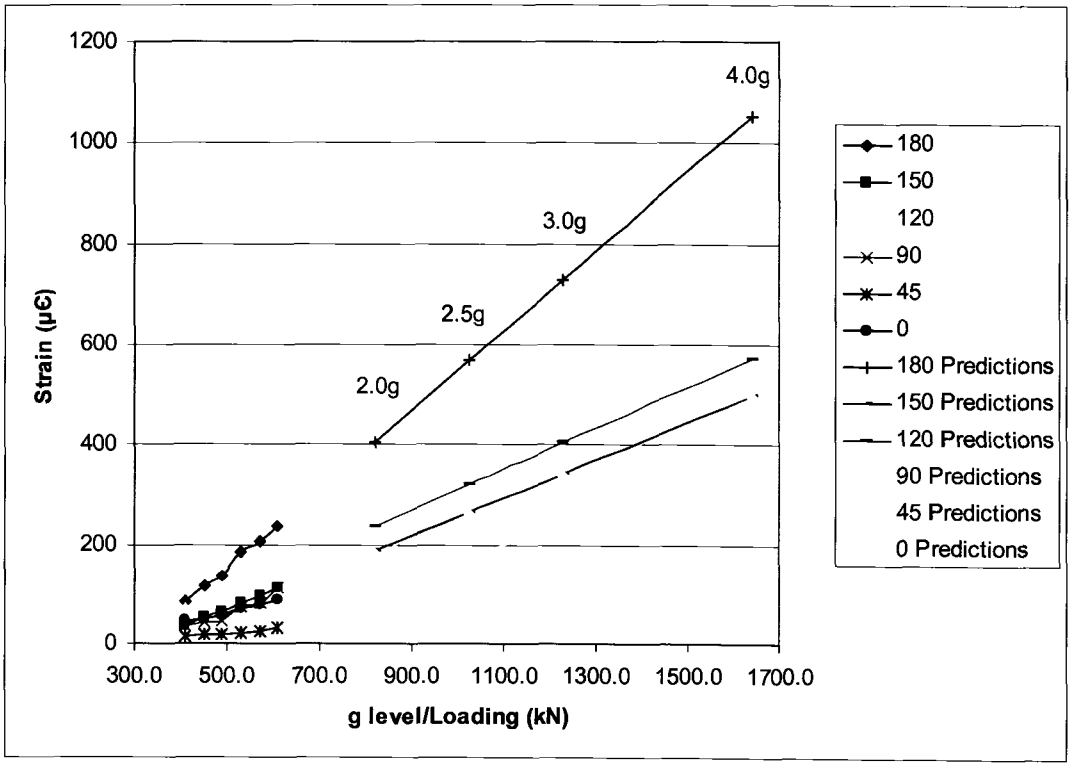

Figure 6-2: Outside Flange Strain vs. g level/Loading Predictions (100psi)

As it can be observed from figure 6-2, the point along the outer rim flange most affected by high g loading is the 180°, or the bottom sector. This is expected based on the results and analysis shown in Chapters 4 and 5, as the stress at this point increased at the highest rate with an increase in load compared to all other points measured during testing. Based on the relationship measured, when a 4.0g load is experienced, it is predicted that the 180° position of the outer rim will experience a strain of 1053$\mu\epsilon$, equivalent to a stress of 210.6MPa. This value, compared to a normal operating strain/stress at 1.0g of 83$\mu\epsilon$ or 16.5MPa respectively, is an increase of over 12.5 times.

Conversely the results found for the 180° position, the magnitude of the strain/stress measured at the 45° point was minor. The value predicted for a 4.0g load at the 45° point was a strain of 112$\mu\epsilon$ or a stress of 22.5MPa. This results in a difference in magnitude of over 9.4 times for stress/strain being measured at two different points along the outer rim for the same wheel load. Meaning that not only does a point along the outer rim experience a change in stress/strain of 12.5 times for an impact load that is equivalent to 4.0g, but it also can experience a difference in stress/strain of 9.4 times depending on its rotational position during this load. In order to obtain a better understanding visually of the stress field created by a 4.0g load, see figure 6-3, which is in the same format as the stress plots shown for the lower values of load in Chapter 5.

Similar to the outer flange, the results for the inner flange of the rim indicate that the strain versus load follows a linear relationship, as shown in figure 6-4. However, unlike the results for the outer flange, the increase of stress/strain in the rim as load increases is not as drastic for the inner flange, as shown by the stress/strain predictions in figure 6-5.

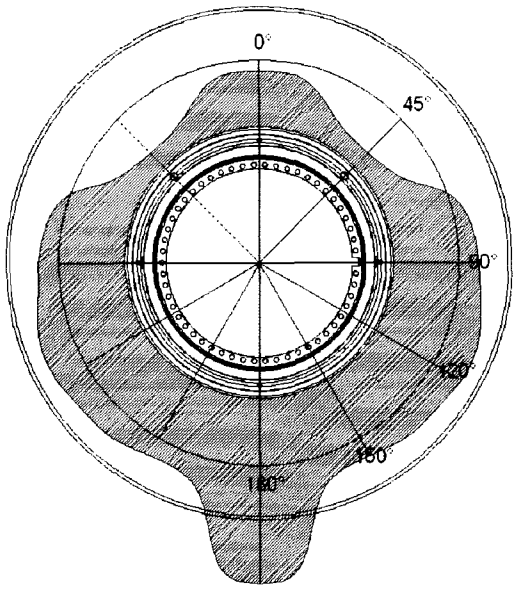

Tire Position	Stress (MPa)
0	63.6
45	22.5
90	99.2
120	114.6
150	99.4
180	210.0

Figure 6-3: Outside Flange Stress Plot, 4.0g, 100psi

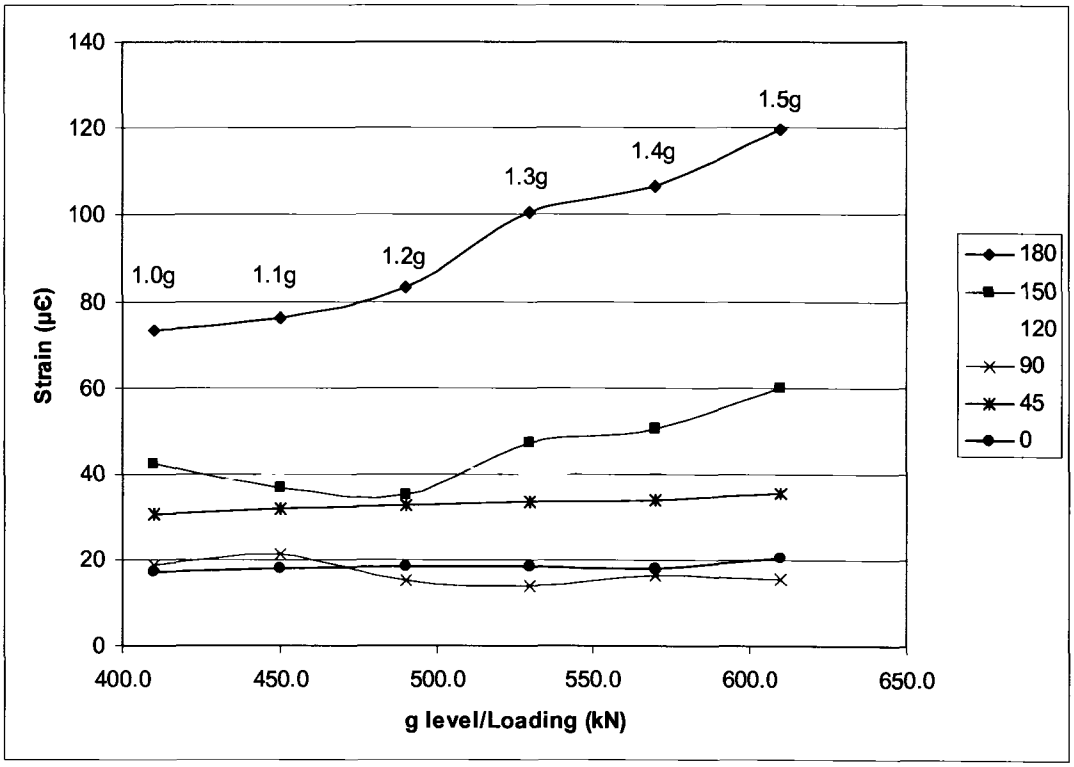

Figure 6-4: Inside Flange Strain vs. g level/Loading Actual (100psi)

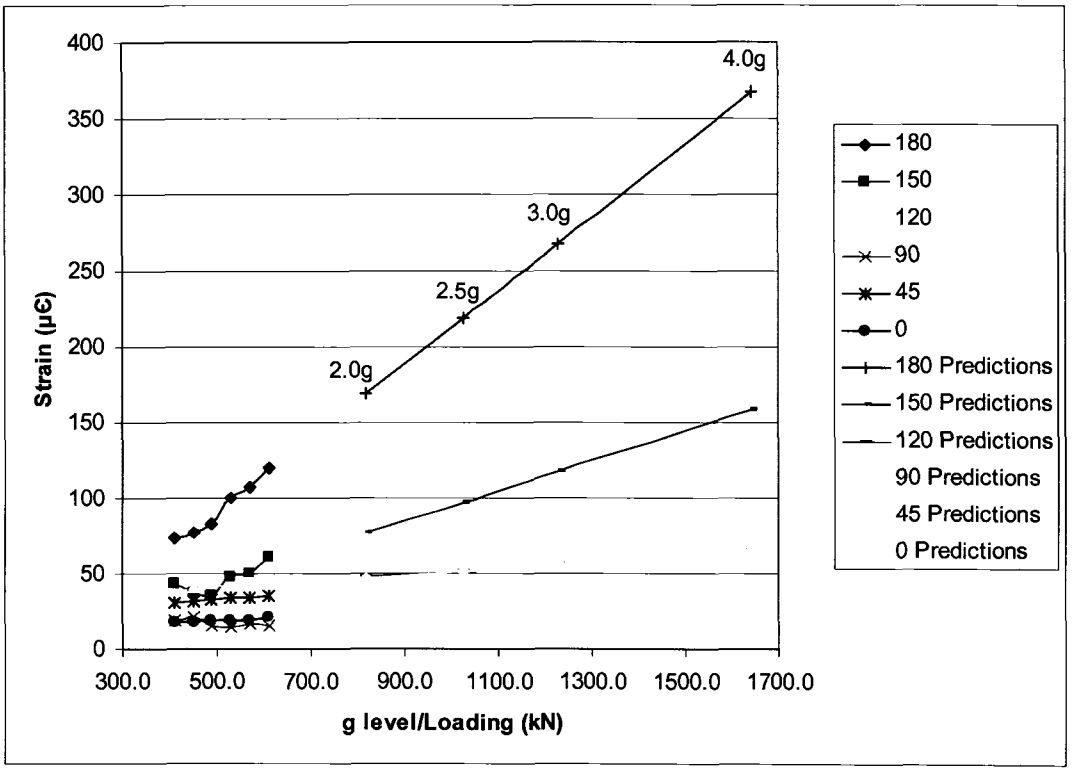

Figure 6-5: Inside Flange Strain vs. g level/Loading Predictions (100psi)

From figure 6-5 it can be observed that the 180° point again has the highest rate of increase, though not as high as that found on the outside flange. The least increase occurs at the 0° and 45° points, again lower than the increases observed on the outer flange for the same points. The change predicted for the 180° points from a 1.0g to a 4.0g load is from 73με to 367με strain or 14.7MPa to 73.4MPa in terms of stress, not as significant of a change as that predicted for the outer flange, but still an increase of 5.0 times. Similarly, the values predicted for the 45° point are a strain of 30με or a stress of 6.0MPa, lower than those predicted for the outer flange, and vastly lower (a factor of 12.2) than the value measured at the 180° point. For a complete predicted stress plot of the inner flange for a 4.0g load at 100psi see figure 6-6.

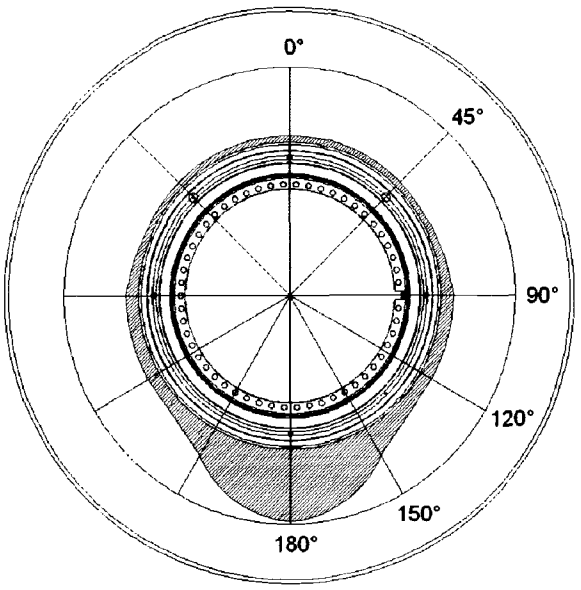

Tire Position	Stress (MPa)
0	6.4
45	6.0
90	13.0
120	13.0
150	31.7
180	73.4

Figure 6-6: Inner Flange Stress Plot, 4.0g, 100psi

As discussed previously in Chapters 4 and 5, the data for the top half of the outer rim band was lost due to damaged strain gauges. Also, the data recorded for the 180° point appears to be suspect as there is no consistency in the results as the load increases or as the tire pressure changes, as was the case with every other point measured during the testing. This lack of consistency, shown in figure 6-7, is also most likely the result of a damaged strain gauge or data channel, and is the reason why predictions for higher g levels, shown in figure 6-8, were only made for the three remaining points on the outside edge of the rim band: 150°, 120°, and 90°.

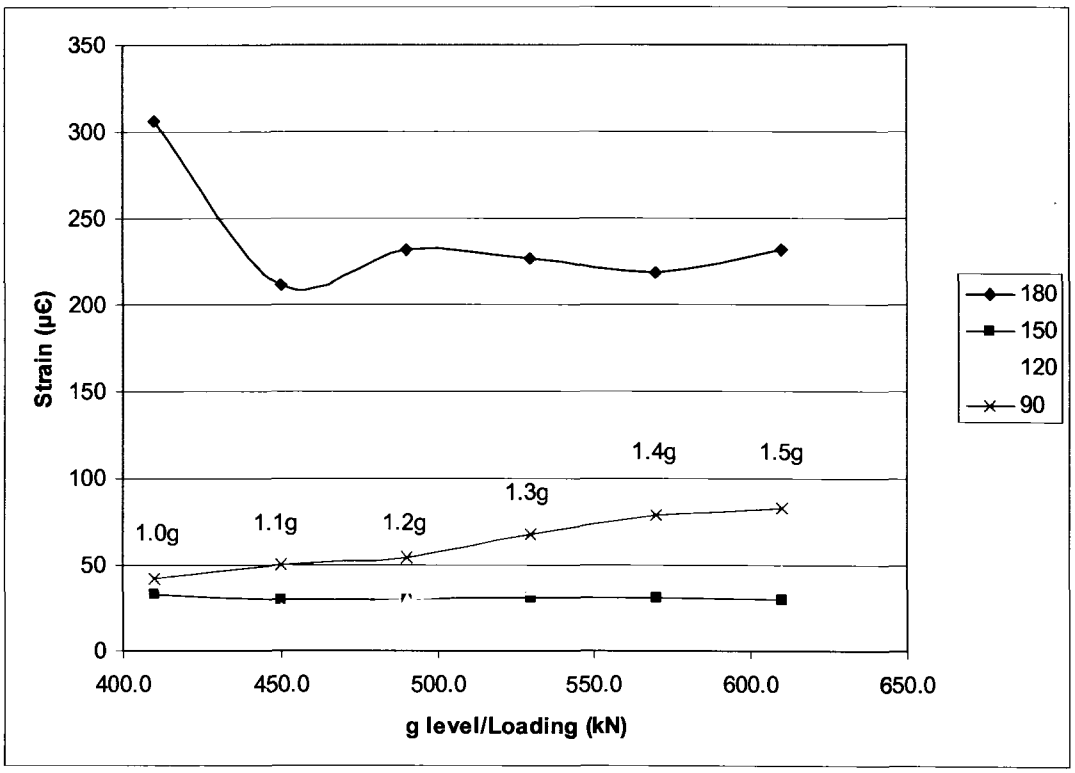

Figure 6-7: Outside Rim Band Strain vs. g level/Loading Actual (100psi)

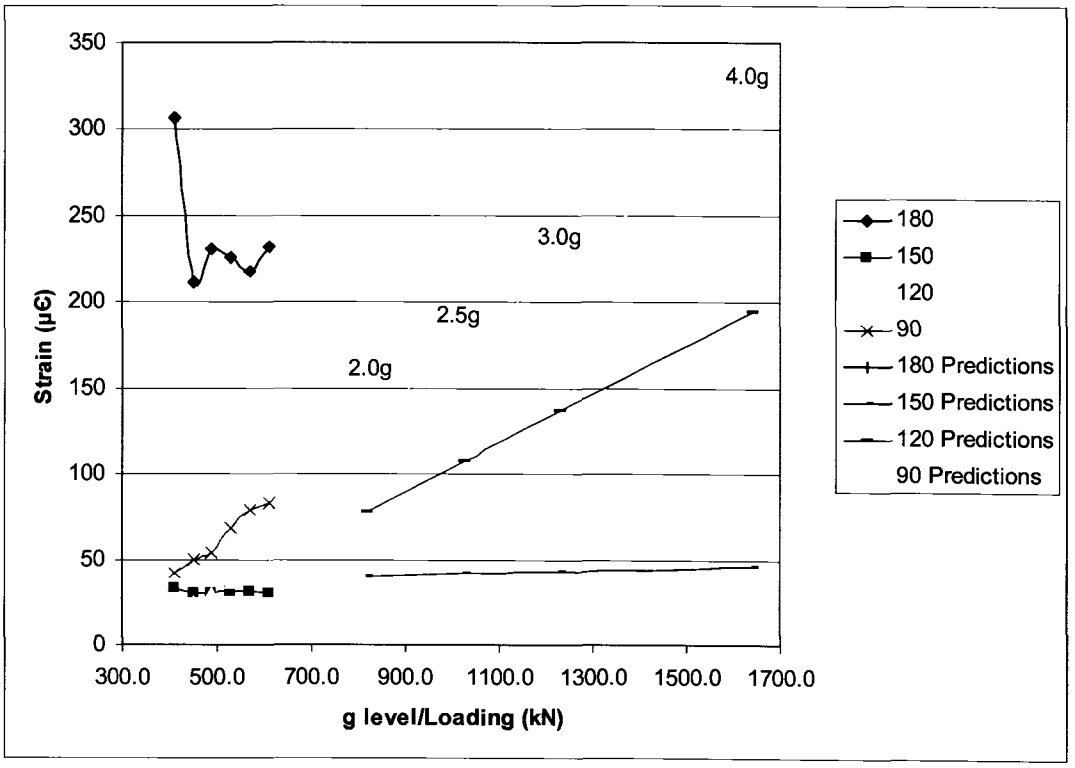

Figure 6-8: Outside Rim Band Strain vs. g level/Loading Predictions (100psi)

The prediction for the 90° point shows the highest rate of increase, similar to the values measured for the lower region of the flanges. Conversely, the values measured for the 150° point are relatively stagnant, and the values for the 120° fell in between. Unfortunately, with half the data missing it is not possible to properly predict a stress distribution without further testing and proper data collection.

Finally, the results from the center of the rim band, shown in figure 6-9, show little to no increase in stress/strain with an increase in loading. And therefore, with an increase in loading of up to 4g's the expected values for stress/strain based on the continuation of the linear relationship developed for the data recorded, there are very small increases in stress strain, see figure 6-10. The increase in strain predicted for a 4.0g load range from less than 1MPa to approximately 10MPa, which are far less than the increases in magnitude measured for on the rim flanges. See figure 6-11 for a stress plot of the center of the rim band at 4.0g.

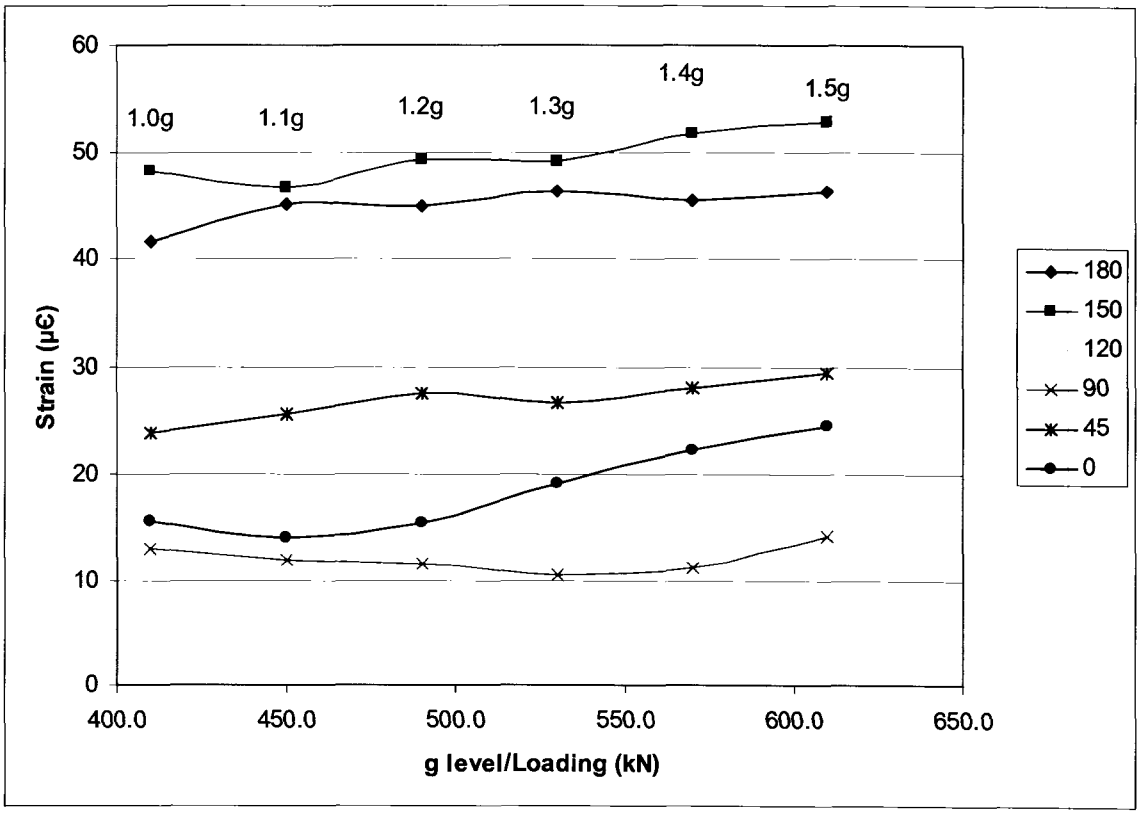

Figure 6-9: Center Rim Band Strain vs. g level/Loading Actual (100psi)

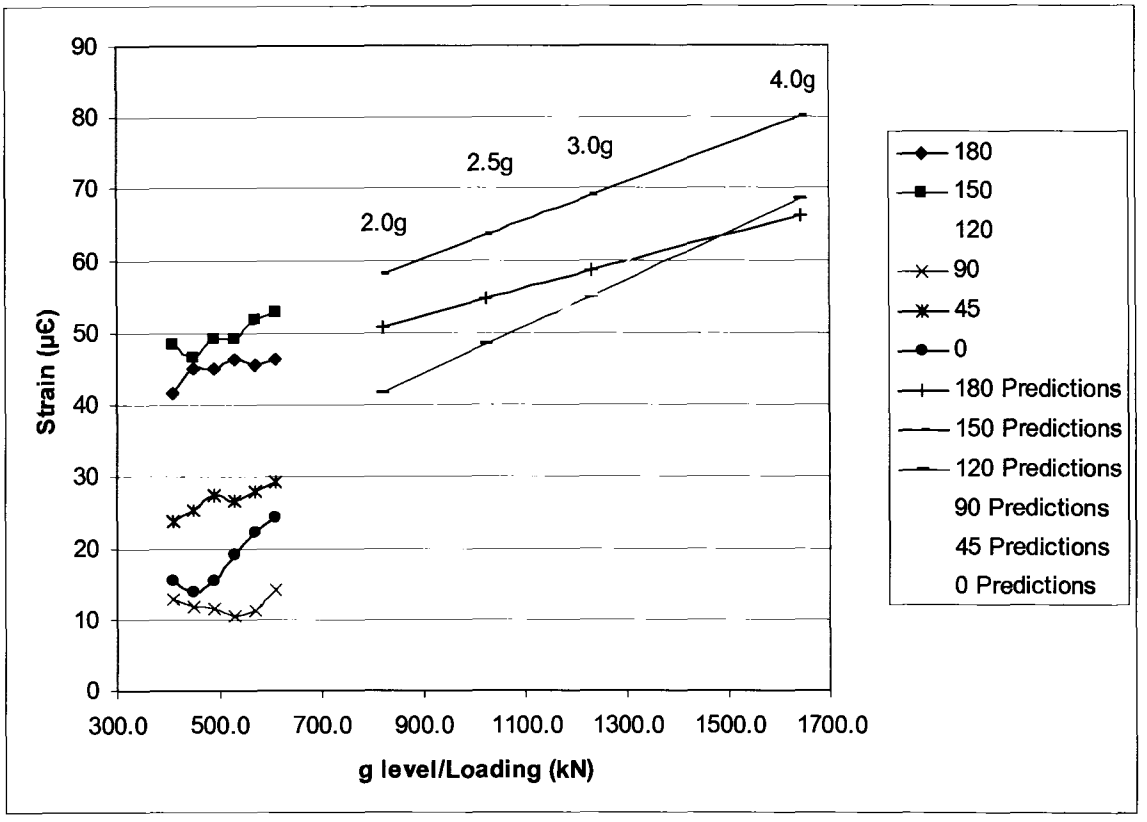

Figure 6-10: Center Rim Band Strain vs. g level/Loading Predictions (100psi)

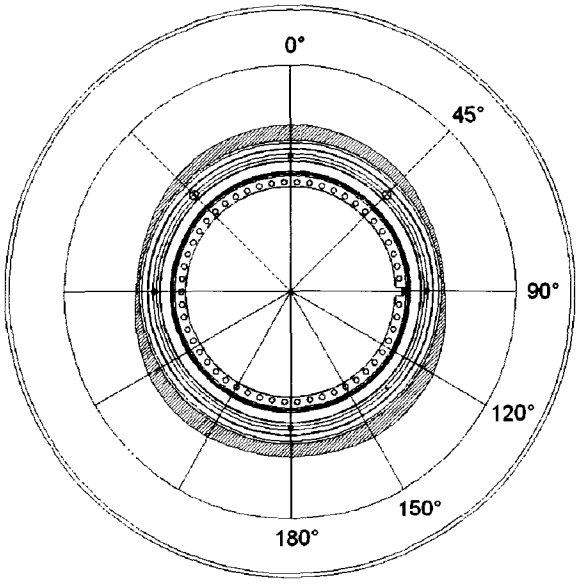

Tire Position	Stress (MPa)
0	15.5
45	10.9
90	2.9
120	13.7
150	16.0
180	13.3

Figure 6-11: Center Rim Band Stress Plot, 4.0g, 100psi

6.2 Development of Stress Prediction Relationships for Rim Components

As stated in Chapter 1 the ultimate goal of this thesis project was to develop a tool to predict the effects of high g loading on the rim and tires of ultra-class haul trucks. Unfortunately for tires, it is currently not possible to accurately predict these adverse effects as the linear relationships that were measured during testing and discussed in Chapter 5 for the footprint area, vertical displacements and sidewall bulge cannot physically hold true for higher values of g loading. Therefore, without further testing of the tire at higher g loads, which is not currently feasible at the University of Alberta, this goal is not possible for ultra-class tires.

Conversely however, for ultra-class rims it is not unreasonable to assume that the linear relationships determined for the various components would hold true at higher levels of g loading as steel, which the rims are composed of, will remain in the elastic region for significantly higher loading as compared to rubber compounds of tires. Therefore, using the linear relationships shown in the figures 6-2, 6-5 and 6-10 a graphical analysis of the slope of strain/load curve versus position can be developed to provide a method of predicting the stress/strain at a given orientation and applied load for each of the tested rim components.

In order to develop these prediction tools each rim component will be examined individually. Unfortunately, due to the lack of data collected for the lock ring and the outside edge of the rim band these components were ignored for this analysis, leaving the outside flange, inside flange and the center of the rim band. The slopes of the predictions equations for each of these three components were taken from their respective plots above and graphed versus the relevant rim position. The intercept values for the slope equations were set to zero for each plot, as for each rim component zero loading on the rim/tire arrangement should ideally produce zero stress/strain measured in the rim. Also, for these plots the results were mirrored to give a visual representation of the entire circumference of the rim rather than just the instrumented half as has been examined so far in the previous strain versus load plots presented. From this analysis the following

plots in figures 6-12, 6-13 and 6-14 were produced for the outside flange, the inside flange and the center of the rim band respectively for the 100psi loading test. The results for the same three components for the 90psi and 80psi loading tests can be found in Appendix C.

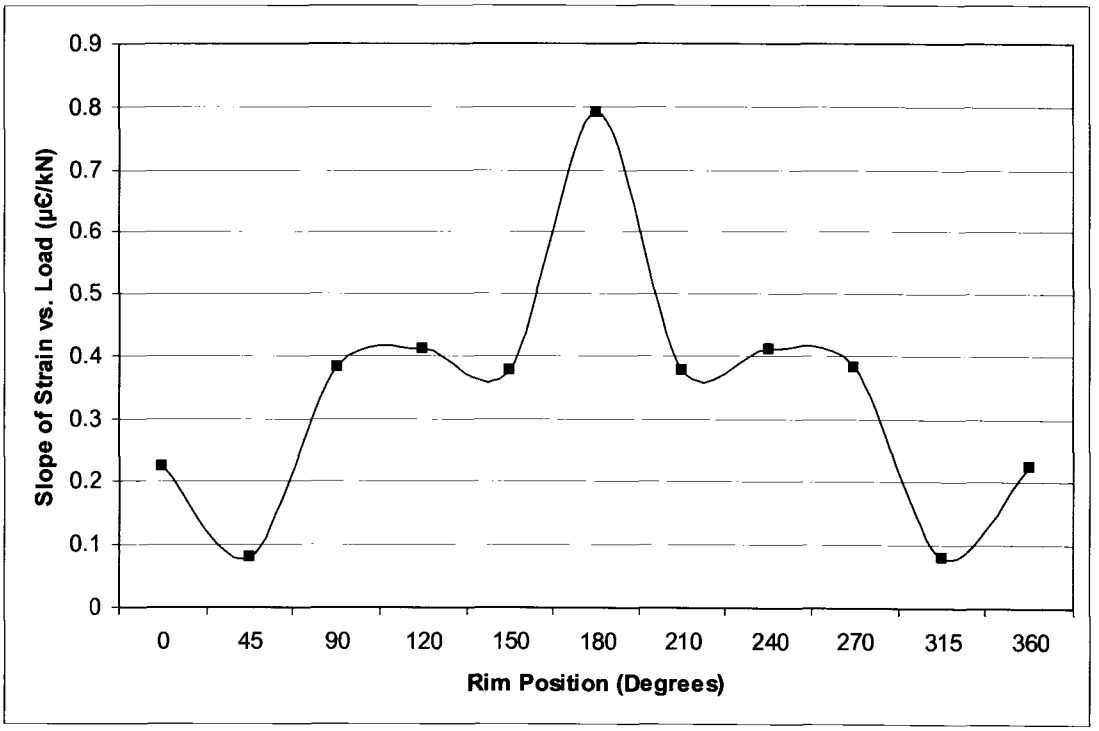

Figure 6-12: Outside Flange Rate of Change of Strain w.r.t. Change in Load versus Rim Position 100psi

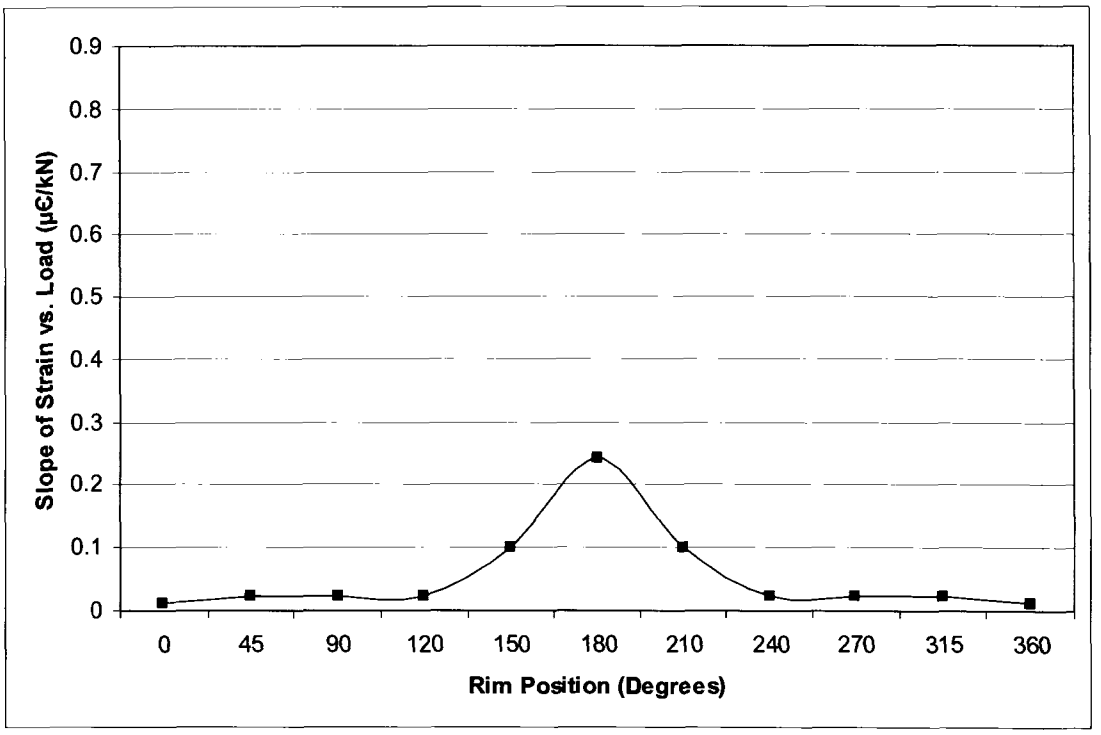

Figure 6-13: Inside Flange Rate of Change of Strain w.r.t. Change in Load versus Rim Position 100psi

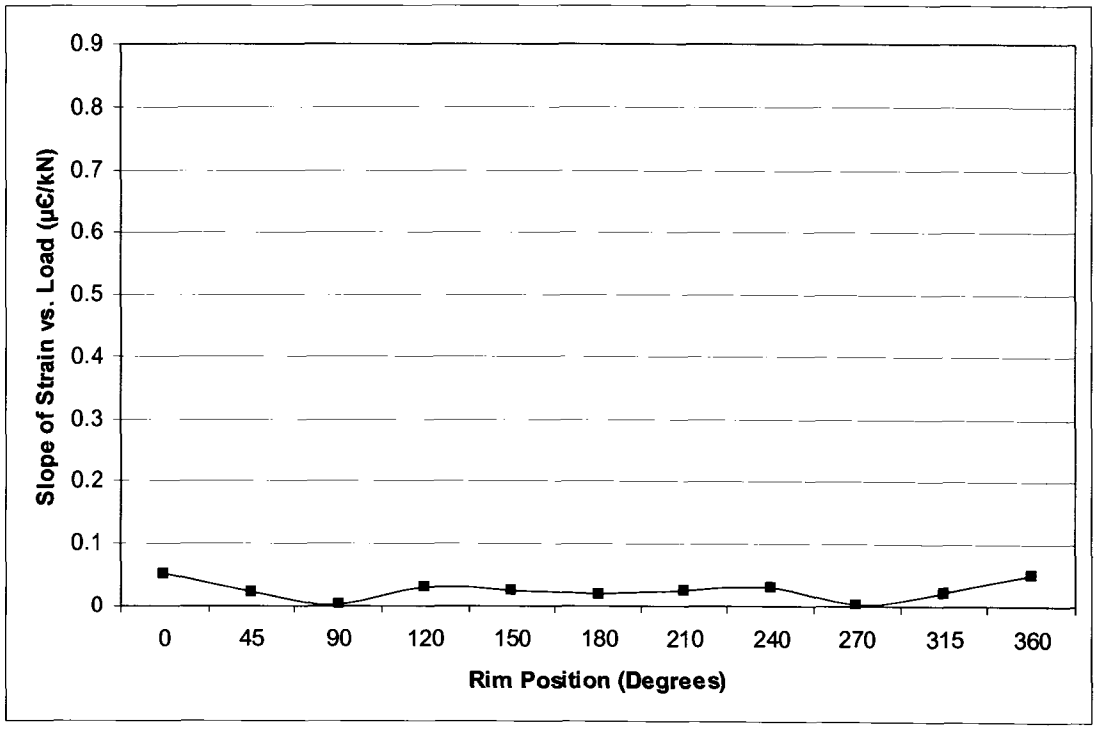

Figure 6-14: Center Rim Band Rate of Change of Strain w.r.t. Change in Load versus Rim Position 100psi

From these plots similar trends can be observed as compared to the previous results shown: peak values occurring at 180° for both the flanges, a large variability occurring in the outside flange as compared to the inside flange, as well as a relatively flat curve for the center of the rim band when compared to the flanges. It is important to note that each of these plots are given the same scale, so that while focus was lost somewhat for the inside flange plot as well as the center of the rim band plot, this allowed for an accurate visual comparison of the effect of the slope of strain versus load by rim position for each of the components.

These graphs allow for a quick calculation of resultant stress/strain at a given location along a rim due to a given load. An example follows:

If this 30.00 series rim and tire is subjected to a 1.5g load, which is an equivalent force of approximately 600kN (see Table 3-1). The 180° location on the outside flange has a strain over load slope value of 0.8$\mu\epsilon$/kN, and the strain and stress values would be (assuming E = 200,000MPa):

(600kN) * (0.8$\mu\epsilon$/kN) = 480$\mu\epsilon$ or 96MPa

For the same load at the 45° location with strain over load slope value of approximately 0.1$\mu\epsilon$/kN the equivalent strain and stress values would be:

(600kN) * (0.1$\mu\epsilon$/kN) = 60$\mu\epsilon$ or 12MPa

For another rim component, the inner flange, for the same g-loading, the following results are obtained for the same locations of 180° and 45°:

@ 180°: (600kN) * (0.25$\mu\epsilon$/kN) = 150$\mu\epsilon$ or 30MPa

@ 45°: (600kN) * (0.025$\mu\epsilon$/kN) = 15$\mu\epsilon$ or 3MPa

Using these plots, the equivalent stress and strain values were quickly calculated for two different rim components, each at two separate locations. By making use of on-board monitoring systems which monitor the loads experienced by the trucks via the suspension measurement above each wheel set which the majority of ultra-class haulers currently have installed, the loads that are measured could be used to quickly develop a stress distribution for the three rim components described above continuously for a given haul cycle.

As demonstrated, these plots are a useful graphical method for quickly determining stress/strain and comparing the values of the different rim components. However, they do not completely define the entire relationship between stress/strain in the rim versus loading, as only certain components and locations of the rim could be instrumented due to the lack of available data channels as described in Chapter 3, as well as the fact that 2 of the 5 components that were instrumented had a large amount of corrupted data that prevented an accurate analysis from taking place. However as stated previously, these plots do provide an excellent visual and mathematical tool for quickly quantifying the stress/strain for a given impact load and rim position for three of the key rim components of an ultra-class hauler, providing a baseline for future, more complete research in this area.

7 Conclusions

With the development of the change of strain with respect to load versus rim position plots developed (Chapter 6 for the 100psi test, Appendix C for the 90psi and 80psi tests) for the outside flange, inside flange and inside surface of the centerband, the goals of this project were partially achieved. The plots developed provide an excellent graphical tool for estimating the amount of stress/strain induced along the rim for a given impact load for the three components listed. However, as stated previously a significant amount of data was lost due to faulty data channels and damaged strain gauges, which resulted in the inability to develop such plots for the outside edge of the centerband and the lock ring. Also, the decision to gauge these components at the given locations was made as a compromise in determining the most vital areas the gauge based on the limited number of data channels available. It would be ideal to gauge more components, at multiple locations on those components than was done for this test to gain an even greater understanding of the effect of high-g loading on ultra class rims.

Similarly, data obtained to understand the effect of high-g loading on ultra-class tires provided great insights, but was somewhat incomplete. The data showed large increases in the vertical displacement of the tire, the bulge of the sidewalls and the footprint area, all of which were expected with an increase in impact load. However, the data obtained showed that each of these trends followed a linear relationship (the data points would fall in the elastic portion of a stress-strain curve), and as discussed previously in Chapter 5, it would be physically impossible for these relationships to continue at the high-g loads that have been measured on mine sites (upwards of 4g's) due to the physical structural limitations of the tire. It can be conceived that at some point the tire material would change from behaving elastically to elastically restricted in movement. This is how a tire would react in response to high-g loads, and due to the fact that the tire manufacturers are reluctant to provide information in regards to the material properties of their tires, this change in material behavior must be determined via further testing at higher loads.

In general, there was a significant amount of data obtained and information learned in regards to the effect of high-g impact loads on rims and tires, however, further testing is required to gain a more complete understanding. Therefore, this chapter will provide a framework for future testing by providing a summary of the thesis results to provide a baseline and prevent any re-work, by discussing "lessons learned" in regards to this research to aid future work; and finally to discuss the requirements of such future work and what ultimately can be achieved if the correct data is obtained in regards to prevention of rim and tire failures that currently occur due to high-g loads; a discussion requiring extensive safe testing practice considerations.

7.1 Summary of Thesis Results

In testing the 30.00R51 rim and tire configuration against a rigid surface, several key pieces of information were learned as well as trends of rim and tire behavior. First of all, it was determined that the internal tire pressure did not play a significant role in terms of rates of stress/strain for an increase in loading. There were noticeable differences in terms of the tire properties measured (vertical displacement, sidewall bulge and footprint area) as would be expected, but overall the effect of internal tire pressure appeared to be minimal.

Where as the effect of tire pressure was observed to be minimal, the impact of increasing the loading value played a significant role in terms stress/strain measured in the rim components as well as the physical displacements of the tires that were tested. All of the test aspects measured followed linear trends for the loading conditions that were applied. For the rim these trends allowed prediction of results at high g-loads due to the fact that it is expected that steel would remain in the elastic region at these predicted loads due its high modulus value. The rubber of the tires however could not remain in the elastic region due to the physical restrictions it would encounter at high g-loads, and therefore, there was no analysis done of the impact of loading on tire behavior for the extreme values of g-loading. As trends provided reasonable assumptions witin the material properties of steel, an analysis was conducted to predict results at g-levels up to 4g's.

Another important result of the effect of high-g loading was the performance of the rim components and the relative position of that component in terms of the values measured for stress and strain. Of the five components strain gauged (outer flange, inner flange, inside surface of the centerband, outer edge of the centerband and the lock ring), the outer edge of the centerband and the lock ring did not provide useful results due to a combination of corrupted data channels and damaged strain gauges. For the other three components, the highest overall values were measured on the outer flange, with the peak value for the outer flange occurring at the 180° locale (bottom of the rim). The inside flange followed a similar trend to the outside flange, with a peak value occurring at the 180° location and significant undulations in loading occurring prominently along the base of the rim. Conversely, the data for the inner surface of the centerband show a consistent lack of increase in stress/strain as the load increased throughout the rim circumference.

As mentioned previously, predictions of stress values in the rim were estimated for a 4g load using the linear relationships of stress/strain versus loading that were developed. At the 180° point it is estimated that a stress value of approximately 210.0MPa would occur with a minimum value of 22.5MPa occurring at the 45° location. Similarly, a peak value for the inner flange was estimated to occur at the 180° point as well, this time with a value of 73.4MPa, and again a minimum value occurring at the 45° location, of 6.0MPa. Again the shape of the stress undulations of the inner flange followed a similar trend compared to that of the outer flange with smaller peak and valley values occurring. For the inside surface of the centerband, a peak value of 16.0MPa was estimated to occur at the 150° location for a 4g load, with a minimum value of 2.9MPa occurring at the 90° point, showing the large decrease in range of stress values expected for each of the three analyzed components to their proximity to tire loading interaction.

The last analysis of the test data was performed to create a graphical plot of the change in strain with respect to load for a given rim position for each of the three previously discussed rim components. These plots allow for the quick determination of the strain (or stress for a known steel modulus value) for a given load and rim position, as well as provide a visual tool for comparing the effect of wheel load and rim position with respect

to the different components. Again it was found that the highest values occurred on the plot for the outer flange, with a peak value of almost 0.8με/kN occurring at the 180° point, and a minimum value of just under 0.1με/kN occurring at the 150° location. Whereas the plot for the outer flange has large fluctuations occurring between the strain gauge locations, the plot for the inner flange shows a relative consistent, low, upwards trend between the 0° and 120° points, followed by a slightly large increase to a value of approximately 0.25με/kN at the 180° location. And again for the inside surface of the centerband, the slope values of strain versus load are all consistently low, ranging from approximately 0.05με/kN at the 0° point to almost 0με/kN at the 90° location

7.2 Lessons Learned

As this project was the first of its kind outside of the tire-rim manufacturing industry there was a fairly steep learning curve associated with it. There were several obstacles that had to be overcome throughout the entire length of the project, and some of them, if known in advance could have saved a great deal of time and effort and helped to produce more complete, accurate results.

The first of these lessons learned is in regards to the selection of the loading rams used for testing. For this project the rams were selected based on their load capability, which far exceeded the requirements needed to apply the loads to get to 1.5g. However, it was soon discovered that for the 80psi loading test, even though the loading rams were capable of exerting the required amount of force, they did not have a long enough stroke to produce an equivalent 1.5g load, as with the tire only having 80psi pressure, it did not produce enough of a bearing reaction to get that high before the rams bottomed out. It was fortunate however that this only resulted in the loss of one test run, and therefore, only resulted in the loss of one data point for each of the components at 80psi. Had the loading rams' stroke been shorter, it could have resulted in the loss of too much data at the 80psi tire pressure tests, voiding their usefulness, or even for the 90psi tests if the stroke was too short. Therefore, for future testing it is recommended that it be checked that the loading rams, or testing frame, have enough stroke to reach all of the desired test

loads for each of the desired tire pressures. This can now be done given our new knowledge on overall tire stiffness.

Another aspect of the testing that impeded results was the limited number of data channels available for strain gauges and LVDT's. Unfortunately, for this particular set of tests this was the only option as it was the only data logger that was available given the limited time that the tire and rim were available. This limited number of data channels required that only certain portions of the rim could be strain gauged; and while a representative from Kal-Tire was consulted as to most optimal use of the available strain gauges to ensure the vital areas of the rim were sampled, more data would always be preferred. For future testing, it is recommended that the maximum number of data channels be made available, as this not only provides redundancy in the results in case data is lost, but also provides a more complete picture of the effect of high-g loading on a tested rim.

Similar to the lack of available data channels, there was a large amount of test data lost from damage to strain gauges as a result of rim grease seeping out from behind the lock ring after the rim and tire were subjected to loading. Rim grease is applied to rim components during assembly and when these components compress together after loading some of the grease is forced out and seeps onto the outer edge of the rim, primarily the lock ring. This rim grease loosened the tape that was protecting some of the strain gauges resulting in damage. Moreover, the grease caused some of the tape which supported the cable connection to the strain gauges to slip, resulting in the weight of the cable hanging on the strain gauges for an extended period of time, causing them to be pulled off the rim surface. For future testing it is recommended that strain gauges be covered with an epoxy, or equivalent coating, which will prevent rim grease from damaging the stain gauges. Also, if the cables attached to the strain gauges require support it is recommended that an alternative method be used to attach them to the rim, such as magnets or an alternative structural support.

An impact of the rim components being forced together during loading was the possible decrease in strain/stress results for the 90psi and 80psi test runs. Due to the tapered nature of the inside edge of the center band as well as the bead band (the landing surfaces of the inside and outside flanges respectively), the flanges are forced up these surfaces as the rim is loaded and are subjected to the reduced stress/strain associated with the resultant elongation experienced. Due to the tapered nature, as the load is relaxed the flanges do not return back to their original position as a result of the frictional forces holding them in place. Therefore, once the rim is subjected to a load and the flanges are held up on the tapered surfaces, they become pre-stressed when compared to the original configuration. And due to the fact that the test results were taken by examining the difference between the initial and peak loads (as the loading was applied gradually, not as an impact due to safety concerns), it is possible that the difference between the peak and initial stress/strain values measured was actually lower than the values experienced in the pre-stressed flanges. Therefore, for further testing it is recommended that prior to testing taking place that a dry-run be performed to the maximum load that will be tested to pre-stress the flange components equally for all the test scenarios, resulting in consistent values throughout.

While the previously mentioned lessons learned were in regards to the testing and data collection associated with the rim, the final one is with respect to the tire. As previously stated at the load range that the tire and rim assembly was tested for this thesis project the rubber material of the tire stayed within the elastic region. Therefore, when developing the plots in order to predict the effects of the high-g loading on the tire all the relationships that were determined were linear. These linear relationships provide insight as to the effect of high-g loading for the lower impact loads experienced by ultra-class trucks, however, in terms of the high-g loads that have been measured by several onboard truck monitoring systems, they do not provide much insight due to the physical restrictions that the tire will experience. Therefore, for future testing it is recommended that higher loads be tested to determine where the tire material enters the restricted region and to obtain several data points at those loads in order to develop a graphical tool for analysis at higher loads. Due to the fact that it is not known at what loads the tire

material will reach this transition, as the manufacturers remain reluctant to release information, it must be determined via trial and error. And due to the high loads that could be experienced with such testing, it is recommended that the tests be conducted with a tire cage, similar to those used for tire maintenance, due to safety concerns associated with the repeated high-g loading of the tire that would be required.

7.3 Future Work

The initial step in terms of future work for this project would be conduct another set of tests utilizing the lessons learned above. Firstly, this would provide a set redundant data in terms of the information collected and the plots developed for the outside flange, the inside flange and the insider surface of the centerband. This redundant data would be useful in terms of checking and verification of the initial test done. Also, this second set of tests would allow for further understanding of the effect of high-g loading on the rim by being able to develop more of the component graphical models that were initially developed. By following the lessons learned, it should be possible to create similar plots for the lock ring and outer surface of the centerband, as well as another other components/locations that could be instrumented with available data channels. And finally, by performing the testing again, this would allow for the opportunity to test at high loadings as described in the lessons learned in order to determine when the tire material reaches the restricted loading region which would allow for more accurate predictions of the impact of high-g loading on tires. This information is especially useful in terms of determining how the size of the tire footprint changes with respect to high impact loading, as the footprint area is instrumental in determining the transfer of load to the ground, which becomes very important once rims and tires are tested on surfaces with different stiffness values, which will be discussed next.

Performing additional tests will help to build a more complete rim/tire interaction model for high-g loading. However, as stated previously, this is a model for a 30.00R51 rim and tire, which is not a commonly used size in today's mining industry (generally limited to water and small operation haul trucks). However, by completing this model it will provide a baseline set of results for future testing. It will be possible to develop the same

models by testing of the various different rims that are most commonly used (including variations in manufacturer, size and aspect ratio). Also, it will then be possible to perform future testing on various ground surfaces too, this will help develop specific models in terms of different ground responses. By developing the baseline model it will allow for comparison and verification of future models that can be any combination of rim and ground response properties, allowing specific models to be developed for individual mine sites that would cater to their specific needs.

Following the development of mine site-specific rim/tire interaction models, including specific rim size, rim profile, rim manufacturer and ground material properties, the next step will be an evaluation of data from a cycle of an actual haul truck rim. By configuring the rim/tire loading model to read onboard truck monitoring data the number and values of impact loads experienced by the truck can be determined and from these it can be predicted what stress/strains are being experienced by the rims and what deformations the tires are being subjected to during day to day operation. This can be done either in real time as a haul truck operates, or by examining logged data and determining the effect of past results. This will make it possible to examine the data of trucks that experienced tire and rim failures and examine the number and the magnitude of high-g loads that were experienced prior to failure. By correlating the information of impact loads experienced compared to the predicted stress/strain values it will aid in prediction of premature rim and tire failures and allow the subsequent preventative maintenance to prevent them, which would meet the ultimate goal of this project: to decrease rim and tire failures on ultra-class haul trucks and therefore reduce the safety risks and the economic losses that are associated with them.

8 References

Berezan, J. J., 2003. Conversations with Jarrett Berezan about truck frames at Syncrude.

Bridgestone 2001. Bridgestone data book off-the-road tires. pp. 27.

Caterpillar Inc. 2004. Caterpillar performance handbook edition 35. pp. 9-5.

Cunagin, W.D. and Grubbs A.B. 1984. Automated acquisition of truck tire pressure data. Transportation Research Record. 1123: pp. 112 – 121.

Joseph, T.G. 2002. OsEIP: The oil sands – equipment interactions program. Canadian Institute of Mining and Metallurgy Bulletin. 95: pp. 58 – 61.

Joseph, T.G. & Hansen, G.W. 2002. Oil sands reaction to cable shovel motion. Canadian Institute of Mining and Metallurgy Bulletin. 95: pp. 62 – 64.

Joseph, T.G., 2003. Large mobile equipment operating on soft ground. 18th International Mining Conference and Exhibition of Turkey. pp. 143 – 147.

LTUG, 2005. Various contributors. Proceedings and discussions from large tire user group meeting. Phoenix.

North Queensland Tyre Fitters Workshop Meeting, 2004. Brief history of accidents involving tyres & rims.
http://www.nrm.qld.gov.au/mines/inspectorate/pdf/tyre_fitters_workshop2.pdf

Michelin Earthmover, 2001. Technical data book. Michelin Earthmove & Industrial Tires. pp 21 – 23.

Michelin Earthmover, 2005. Tire size information.
http://earthmover.webmichelin.com/na_eng/tires/XDR/details.html

Occupational Safety and Health Service, Department of Labour, New Zealand 2004. Accident alert – tyre fitter killed by exploding tyre.
http://www.osh.dol.govt.nz/publications/series/aa-tyreexplosion.html

Ronai, D. & Shmulevich I. 1995. Tire footprint characteristics as a function of soil properties and tire operations. Journal of Terramechanics. 32: No 6. pp: 311 – 323.

SAE J751, 1997. Off-road tire and rim classification – construction machines. SAE Standard., 3: pp. 40.458 - 40.462.

SAE J1315, 1991. Off-road tire and rim selection and application. SAE Standard., 3: pp. 40.463.

SAE J1337, 1997. Off-road tire and rim classification – construction machines. SAE Standard., 3: pp. 40.458 - 40.462.

Tielking, J.T. 1994. Force transmissibility of heavy truck tires. Tire Science and Technology. 22: No. 1 pp. 60 – 74.

Tielking J.T. & Abraham M.A. 1990. Measurement of truck tire footprint pressures. Transportation Research Record 1435: pp. 92 – 99.

Wiermann, C., Way, T.R., Horn, R., Bailey, A.C., and Burt, E.C. 1999. Effect of various dynamic loads on stress and strain behavior of a Norfolk sandy loam. Soil & Tillage Research. 50: pp. 127 – 135.

Appendix A Laboratory Results

A.1 Test Results, 100psi Tire Pressure

Radial Strain (με)

Rim Position	1.0g U/L	1.0g	1.1g	1.2g	1.3g	1.4g	1.5g
180	51.44	82.58	116.08	134.40	185.21	207.51	238.56
150	14.27	32.71	50.09	61.19	79.98	92.08	110.13
120	3.51	20.44	25.46	29.12	37.56	41.10	47.64
90	4.89	9.76	12.24	14.66	22.74	24.24	33.62
45	23.46	11.30	15.18	16.49	20.83	23.52	28.57
0	17.50	43.19	47.75	53.13	66.79	74.26	84.36

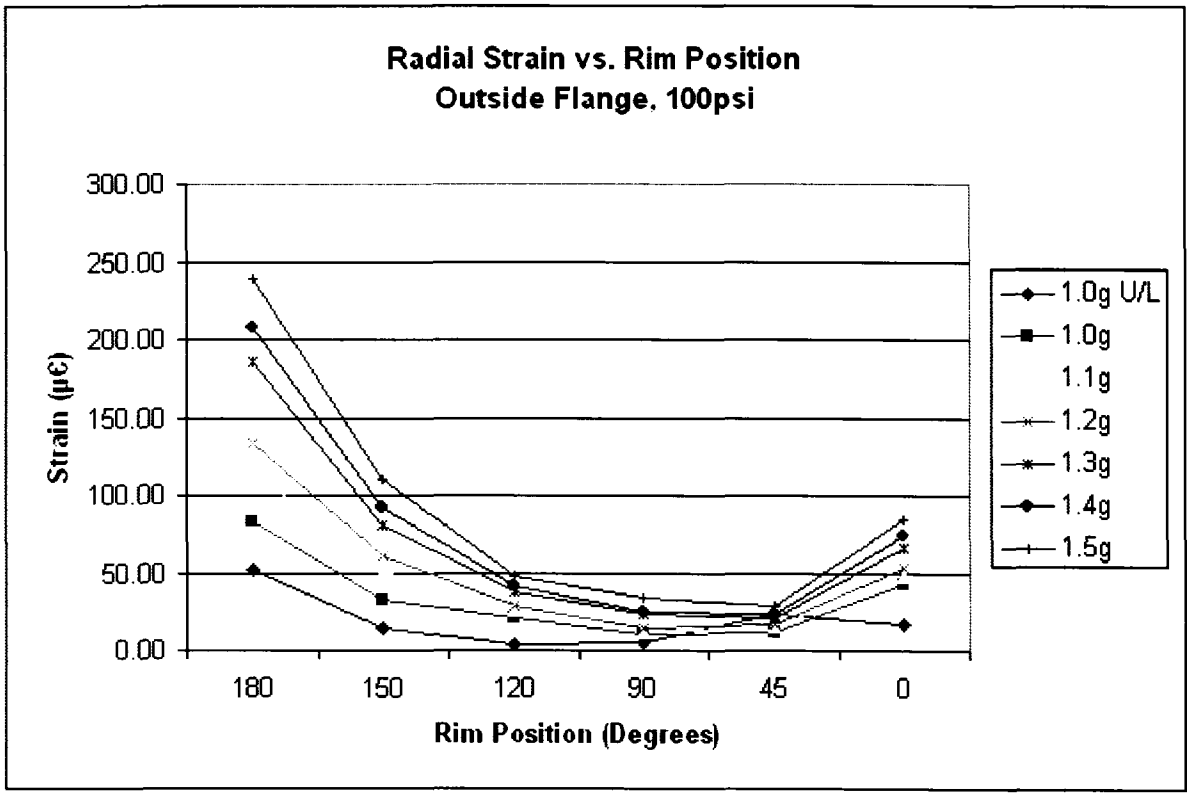

$\sigma = \varepsilon E$

where E = 200,000MPa

Radial Stress (MPa)

Rim Position	1.0g U/L	1.0g	1.1g	1.2g	1.3g	1.4g	1.5g
180	10.29	16.52	23.22	26.88	37.04	41.50	47.71
150	2.85	6.54	10.02	12.24	16.00	18.42	22.03
120	0.70	4.09	5.09	5.82	7.51	8.22	9.53
90	0.98	1.95	2.45	2.93	4.55	4.85	6.72
45	4.69	2.26	3.04	3.30	4.17	4.70	5.71
0	3.50	8.64	9.55	10.63	13.36	14.85	16.87

Perpendicular Strain (με)

Rim Position	1.0g U/L	1.0g	1.1g	1.2g	1.3g	1.4g	1.5g
180	527.69	194.07	487.71	967.97	8768.27	3257.47	2100.32
150	14.27	15.22	12.63	12.06	16.48	17.14	20.84
120	21.24	66.83	79.33	89.08	115.55	124.47	143.12
90	16.91	32.03	38.48	43.77	71.46	75.39	106.16
45	4.51	5.80	4.86	3.98	4.67	6.04	8.12
0	14.47	13.15	15.61	16.73	20.69	23.32	26.85

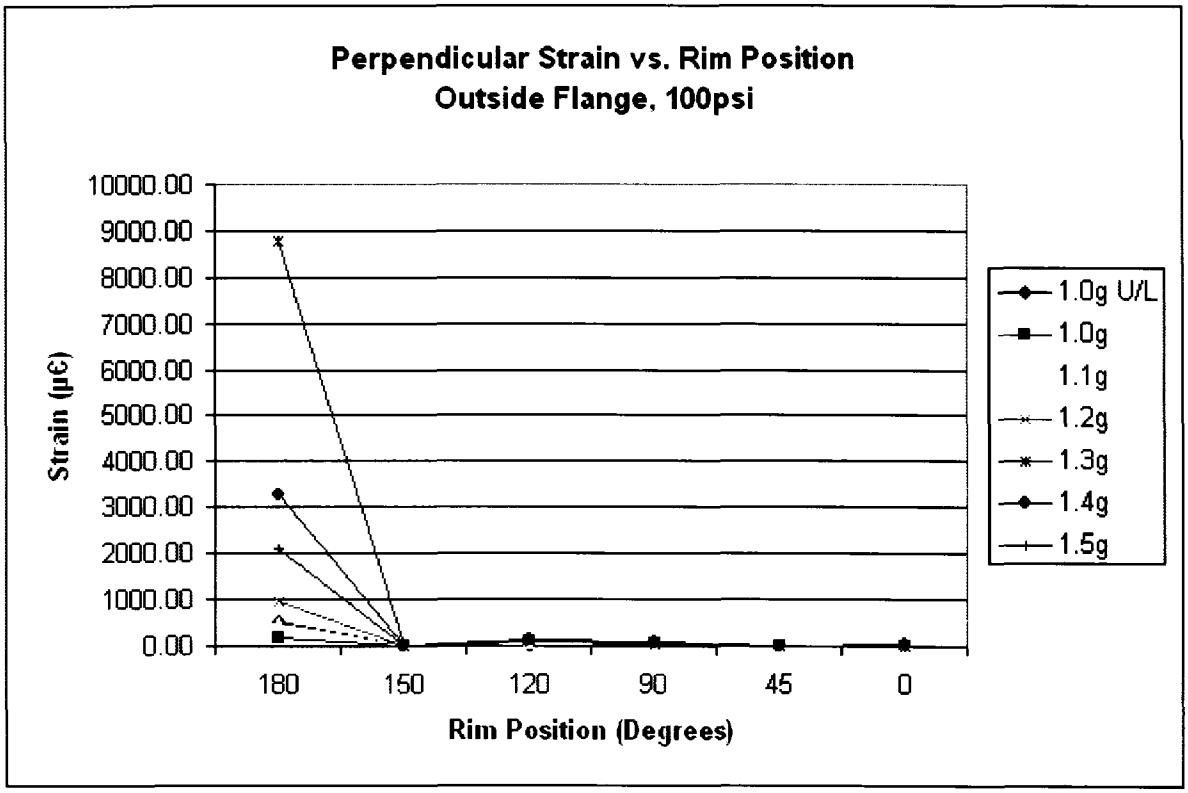

$\sigma = \varepsilon E$

where E = 200,000MPa

Perpendicular Stress (MPa)

Rim Position	1.0g U/L	1.0g	1.1g	1.2g	1.3g	1.4g	1.5g
180	105.54	38.81	97.54	193.59	1753.65	651.49	420.06
150	2.85	3.04	2.53	2.41	3.30	3.43	4.17
120	4.25	13.37	15.87	17.82	23.11	24.89	28.62
90	3.38	6.41	7.70	8.75	14.29	15.08	21.23
45	0.90	1.16	0.97	0.80	0.93	1.21	1.62
0	2.89	2.63	3.12	3.35	4.14	4.66	5.37

Radial Strain (με)

Rim Position	1.0g U/L	1.0g	1.1g	1.2g	1.3g	1.4g	1.5g
180	13.77	23.11	25.18	26.89	37.38	32.89	40.22
150	9.31	14.65	11.77	10.98	13.86	15.00	17.82
120	30.68	8.33	69.95	50.18	20.87	61.79	24.06
90	8.97	4.71	13.93	7.47	4.70	8.95	4.45
45	9.38	8.91	9.46	10.32	9.47	10.15	11.74
0	4.20	6.67	6.92	6.94	7.89	7.19	8.64

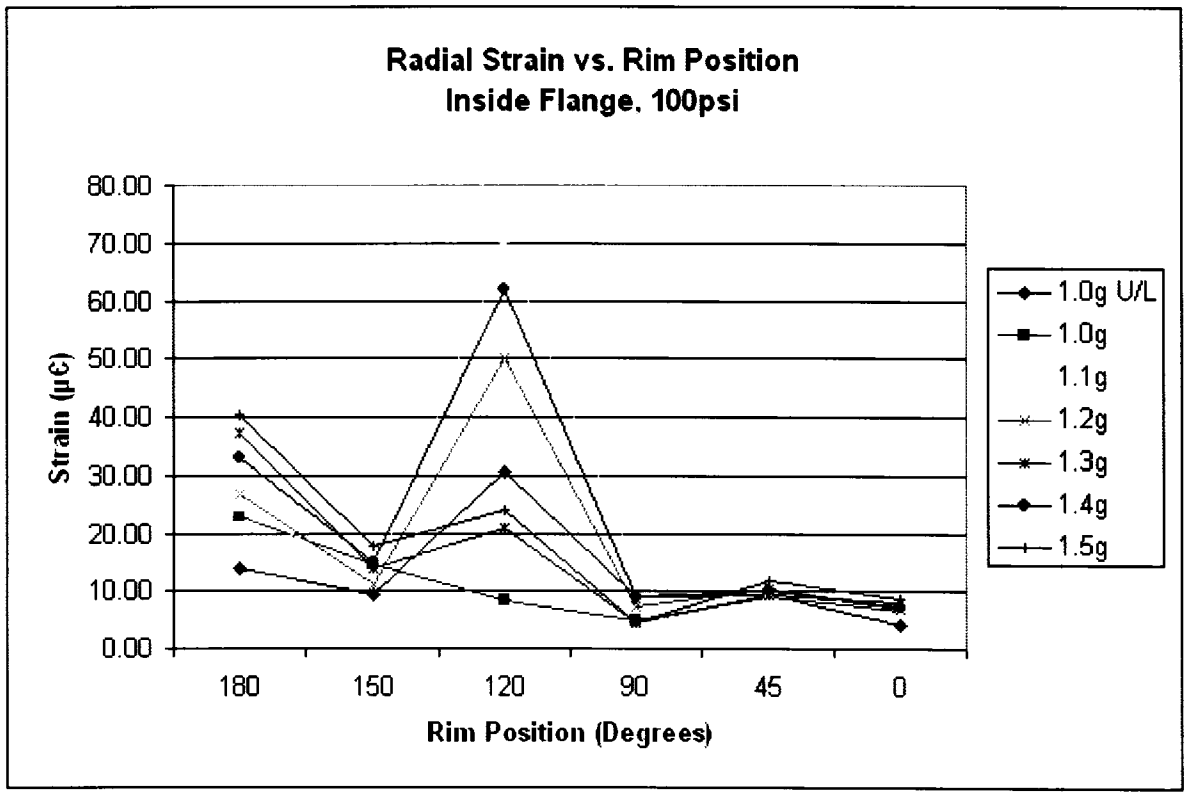

$\sigma = \varepsilon E$

where E = 200,000MPa

Radial Stress (MPa)

Rim Position	1.0g U/L	1.0g	1.1g	1.2g	1.3g	1.4g	1.5g
180	2.75	4.62	5.04	5.38	7.48	6.58	8.04
150	1.86	2.93	2.35	2.20	2.77	3.00	3.56
120	6.14	1.67	13.99	10.04	4.17	12.36	4.81
90	1.79	0.94	2.79	1.49	0.94	1.79	0.89
45	1.88	1.78	1.89	2.06	1.89	2.03	2.35
0	0.84	1.33	1.38	1.39	1.58	1.44	1.73

Perpendicular Strain (με)

Rim Position	1.0g U/L	1.0g	1.1g	1.2g	1.3g	1.4g	1.5g
180	27.44	69.69	71.93	78.67	93.33	101.27	112.68
150	27.52	40.05	34.87	33.16	45.24	48.16	57.30
120	49.67	36.35	40.23	43.02	40.03	41.63	42.15
90	25.82	18.04	15.86	13.31	13.07	13.59	14.92
45	32.88	29.31	30.43	30.79	32.31	32.31	33.45
0	11.11	15.80	16.54	16.89	16.75	16.58	18.46

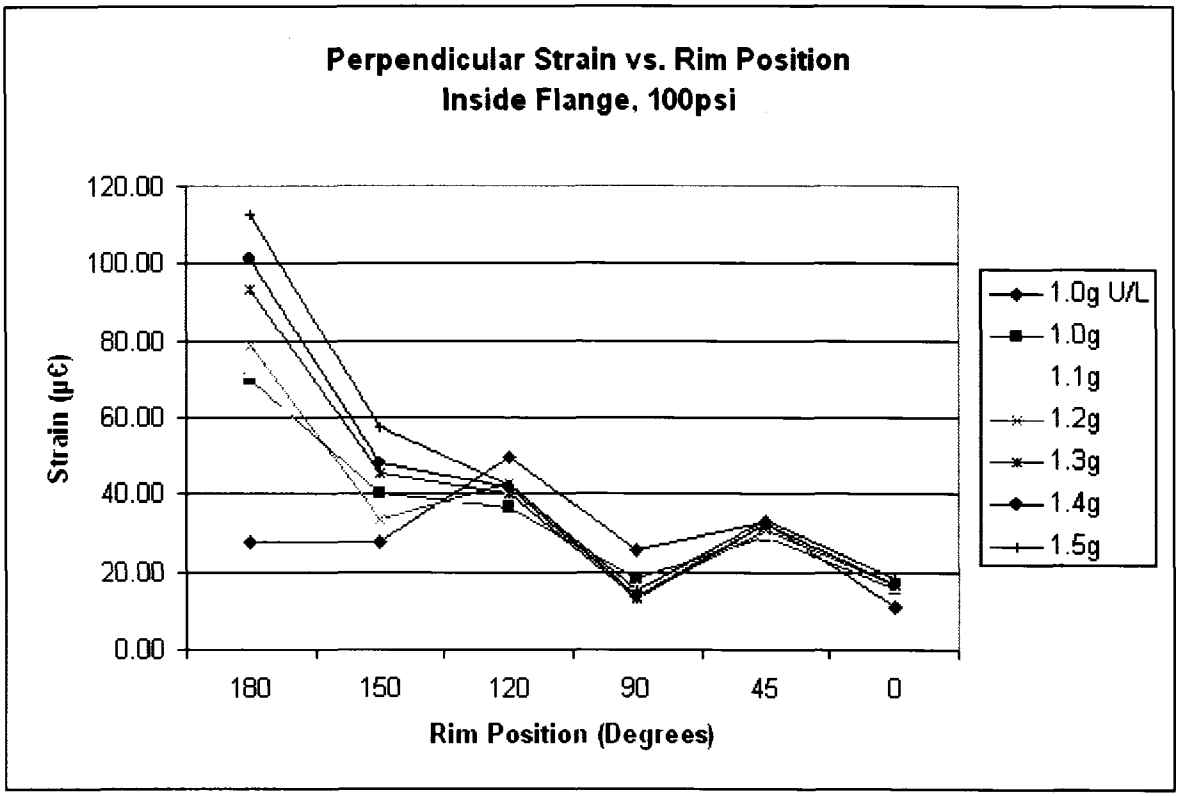

$\sigma = \varepsilon E$

where E = 200,000MPa

Perpendicular Stress (MPa)

Rim Position	1.0g U/L	1.0g	1.1g	1.2g	1.3g	1.4g	1.5g
180	5.49	13.94	14.39	15.73	18.67	20.25	22.54
150	5.50	8.01	6.97	6.63	9.05	9.63	11.46
120	9.93	7.27	8.05	8.60	8.01	8.33	8.43
90	5.16	3.61	3.17	2.66	2.61	2.72	2.98
45	6.58	5.86	6.09	6.16	6.46	6.46	6.69
0	2.22	3.16	3.31	3.38	3.35	3.32	3.69

Radial Strain (με)

Rim Position	1.0g U/L	1.0g	1.1g	1.2g	1.3g	1.4g	1.5g
180	30.76	94.06	89.54	79.95	86.33	72.49	62.53
150	16.65	28.12	25.39	25.33	26.14	27.23	25.86
120	1.93	6.25	2.92	3.58	3.99	4.66	5.45
90	4.03	22.25	23.99	25.56	29.78	31.36	33.45
45	-	-	-	-	-	-	-
0	-	-	-	-	-	-	-

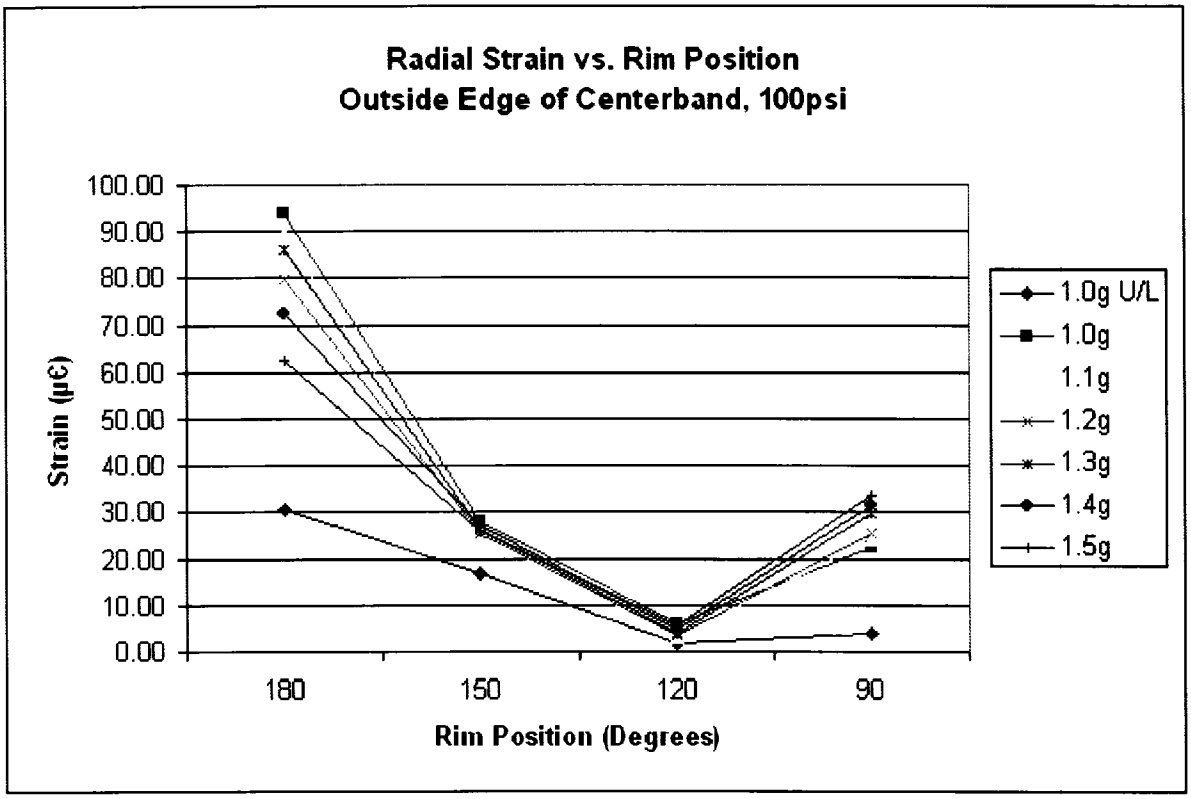

$\sigma = \varepsilon E$

where E = 200,000MPa

Radial Stress (MPa)

Rim Position	1.0g U/L	1.0g	1.1g	1.2g	1.3g	1.4g	1.5g
180	6.15	18.81	17.91	15.99	17.27	14.50	12.51
150	3.33	5.62	5.08	5.07	5.23	5.45	5.17
120	0.39	1.25	0.58	0.72	0.80	0.93	1.09
90	0.81	4.45	4.80	5.11	5.96	6.27	6.69
45	-	-	-	-	-	-	-
0	-	-	-	-	-	-	-

Perpendicular Strain (με)

Rim Position	1.0g U/L	1.0g	1.1g	1.2g	1.3g	1.4g	1.5g
180	176.60	291.50	191.29	217.01	209.16	205.47	223.56
150	8.86	16.21	14.62	15.42	15.68	13.49	14.41
120	16.42	17.94	24.11	28.94	35.51	42.41	46.39
90	22.19	34.98	43.49	47.21	60.90	71.87	75.77
45	-	-	-	-	-	-	-
0	-	-	-	-	-	-	-

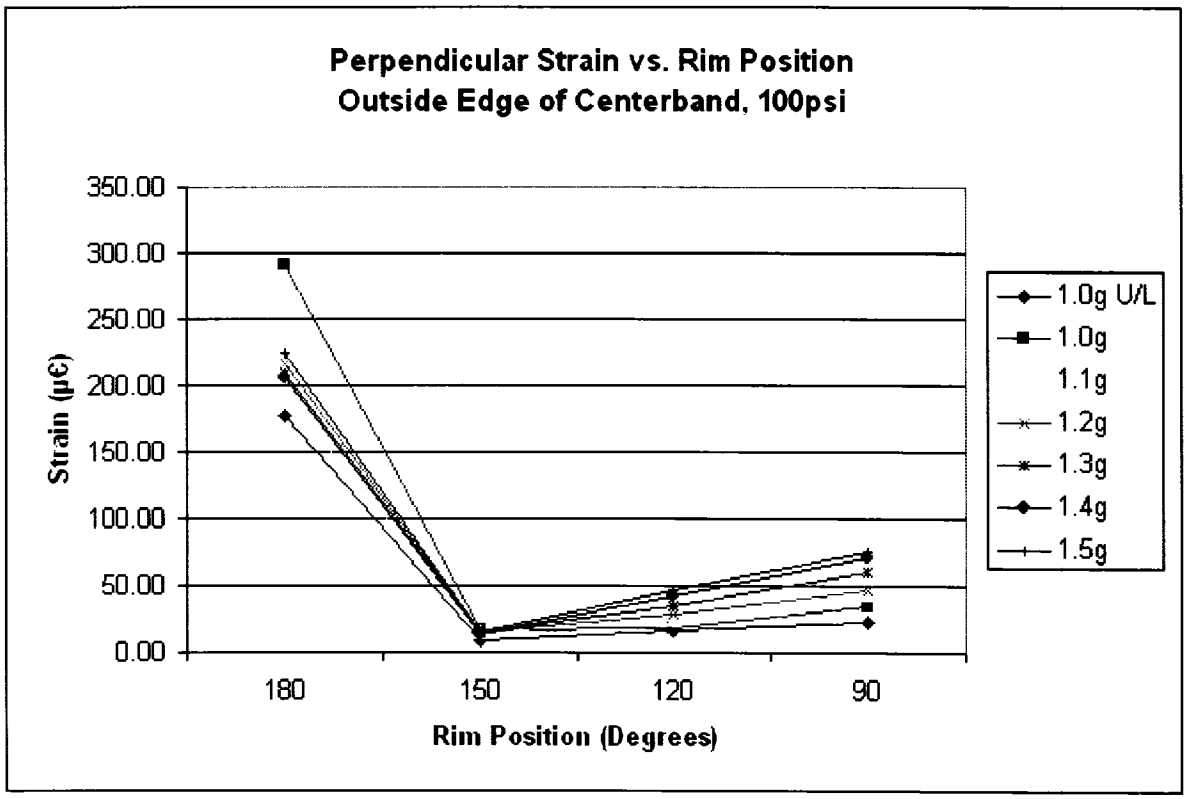

$\sigma = \varepsilon E$

where E = 200,000MPa

Perpendicular Stress (MPa)

Rim Position	1.0g U/L	1.0g	1.1g	1.2g	1.3g	1.4g	1.5g
180	35.32	58.30	38.26	43.40	41.83	41.09	44.71
150	1.77	3.24	2.92	3.08	3.14	2.70	2.88
120	3.28	3.59	4.82	5.79	7.10	8.48	9.28
90	4.44	7.00	8.70	9.44	12.18	14.37	15.15
45	-	-	-	-	-	-	-
0	-	-	-	-	-	-	-

Radial Strain (με)

Rim Position	1.0g U/L	1.0g	1.1g	1.2g	1.3g	1.4g	1.5g
180	27.75	41.55	45.08	45.04	46.37	45.55	46.31
150	37.94	44.88	43.43	44.70	43.09	43.57	41.51
120	16.62	22.72	23.28	23.38	24.25	24.70	25.54
90	11.03	12.86	11.85	11.60	10.54	11.20	14.11
45	20.20	23.29	25.09	27.15	26.13	27.30	28.55
0	2.63	11.67	5.07	2.77	39.28	5.56	31.27

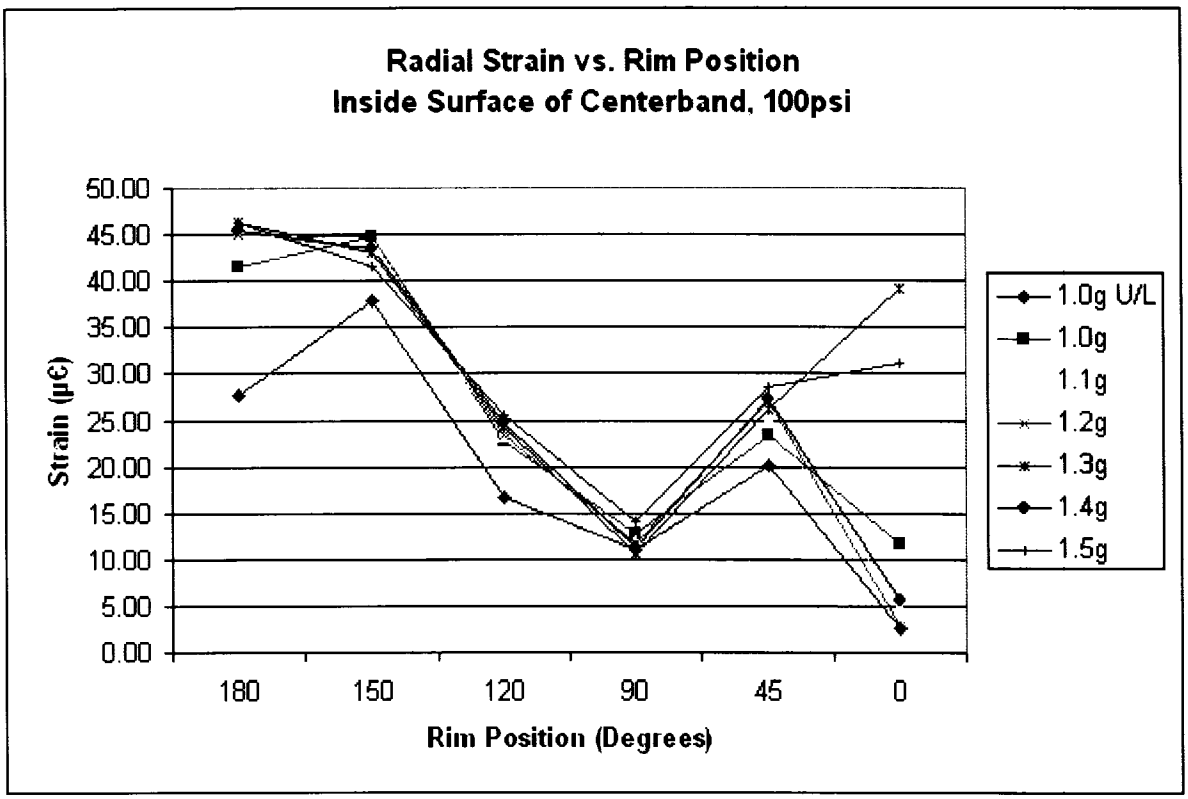

$\sigma = \varepsilon E$

where E = 200,000MPa

Radial Stress (MPa)

Rim Position	1.0g U/L	1.0g	1.1g	1.2g	1.3g	1.4g	1.5g
180	5.55	8.31	9.02	9.01	9.27	9.11	9.26
150	7.59	8.98	8.69	8.94	8.62	8.71	8.30
120	3.32	4.54	4.66	4.68	4.85	4.94	5.11
90	2.21	2.57	2.37	2.32	2.11	2.24	2.82
45	4.04	4.66	5.02	5.43	5.23	5.46	5.71
0	0.53	2.33	1.01	0.55	7.86	1.11	6.25

Perpendicular Strain (με)

Rim Position	1.0g U/L	1.0g	1.1g	1.2g	1.3g	1.4g	1.5g
180	424.45	298.94	279.54	473.31	529.52	318.83	741.12
150	17.76	17.96	17.11	20.71	23.68	28.13	32.66
120	19.16	15.46	20.16	19.50	20.77	21.78	24.04
90	26.17	35.68	14.74	46.26	271.23	189.44	869.25
45	7.70	5.26	4.51	4.32	5.26	6.01	6.95
0	7.60	10.23	13.00	15.09	19.01	21.54	24.46

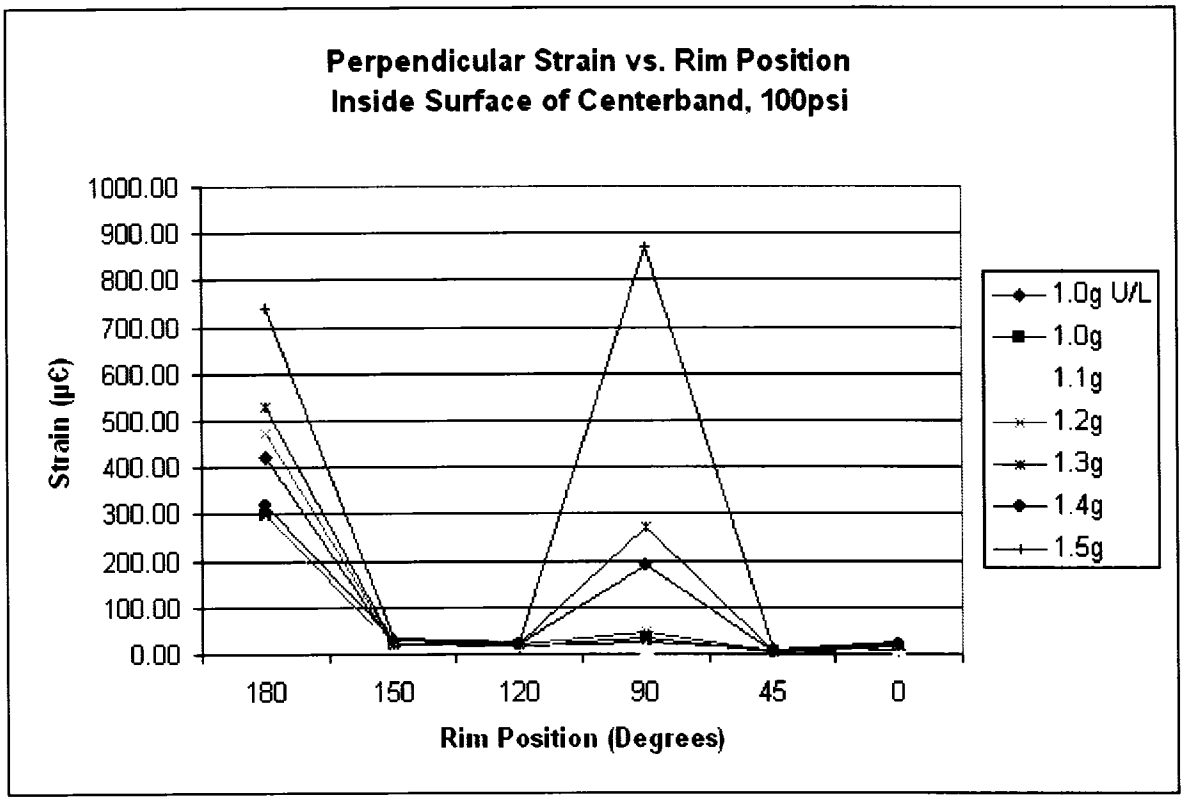

$\sigma = \varepsilon E$

where E = 200,000MPa

Perpendicular Stress (MPa)

Rim Position	1.0g U/L	1.0g	1.1g	1.2g	1.3g	1.4g	1.5g
180	84.89	59.79	55.91	94.66	105.90	63.77	148.22
150	3.55	3.59	3.42	4.14	4.74	5.63	6.53
120	3.83	3.09	4.03	3.90	4.15	4.36	4.81
90	5.23	7.14	2.95	9.25	54.25	37.89	173.85
45	1.54	1.05	0.90	0.86	1.05	1.20	1.39
0	1.52	2.05	2.60	3.02	3.80	4.31	4.89

Radial Strain (με)

Rim Position	1.0g U/L	1.0g	1.1g	1.2g	1.3g	1.4g	1.5g
180	-	-	-	-	-	-	-
150	0.01	0.01	0.02	0.01	0.01	0.02	0.01
120	7.51	7.70	7.51	7.70	9.02	8.63	96.50
90	5.14	15.89	15.26	12.70	13.83	12.21	13.56
45	-	-	-	-	-	-	-
0	-	-	-	-	-	-	-

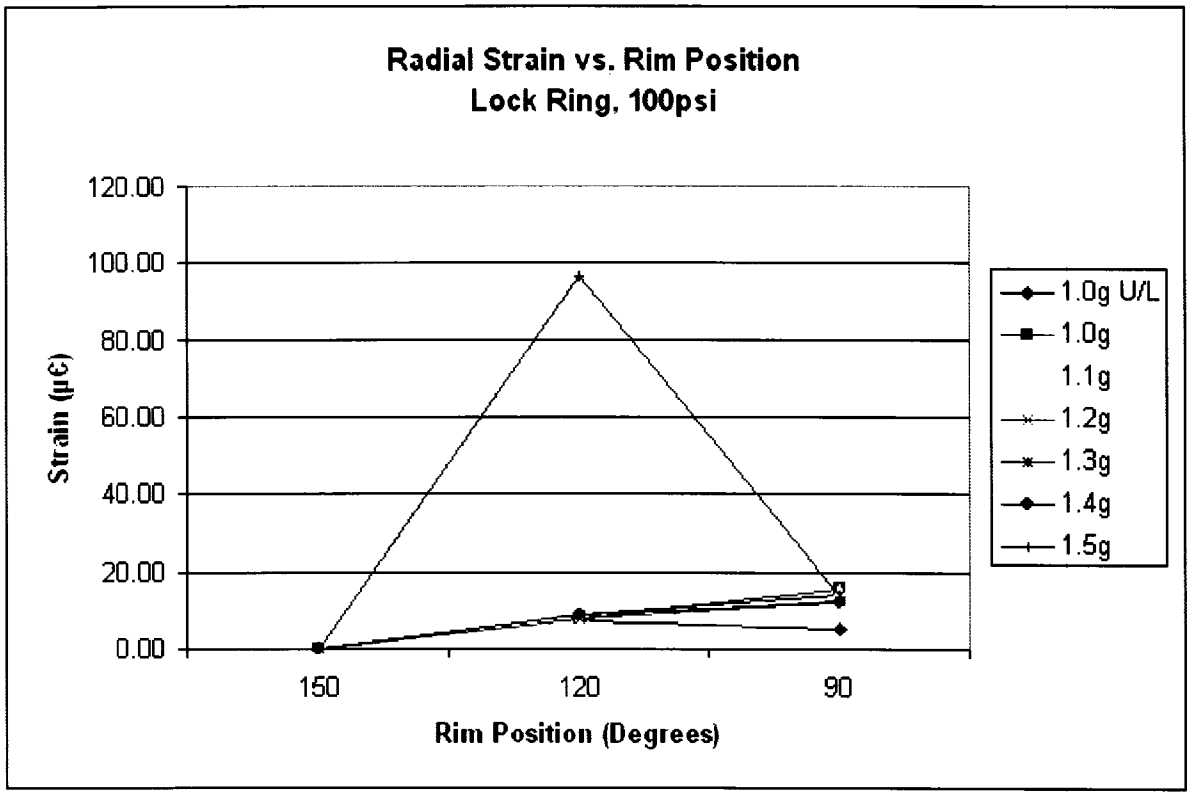

$\sigma = \varepsilon E$

where E = 200,000MPa

Radial Stress (MPa)

Rim Position	1.0g U/L	1.0g	1.1g	1.2g	1.3g	1.4g	1.5g
180	-	-	-	-	-	-	-
150	0.00	0.00	0.00	0.00	0.00	0.00	0.00
120	1.50	1.54	1.50	1.54	1.80	1.73	19.30
90	1.03	3.18	3.05	2.54	2.77	2.44	2.71
45	-	-	-	-	-	-	-
0	-	-	-	-	-	-	-

Perpendicular Strain (με)

Rim Position	1.0g U/L	1.0g	1.1g	1.2g	1.3g	1.4g	1.5g
180	-	-	-	-	-	-	-
150	12.00	20.50	24.55	26.69	25.55	24.34	22.07
120	16.52	18.00	19.87	21.26	22.56	25.19	24.07
90	15.79	17.62	26.84	29.73	33.97	36.65	39.44
45	-	-	-	-	-	-	-
0	-	-	-	-	-	-	-

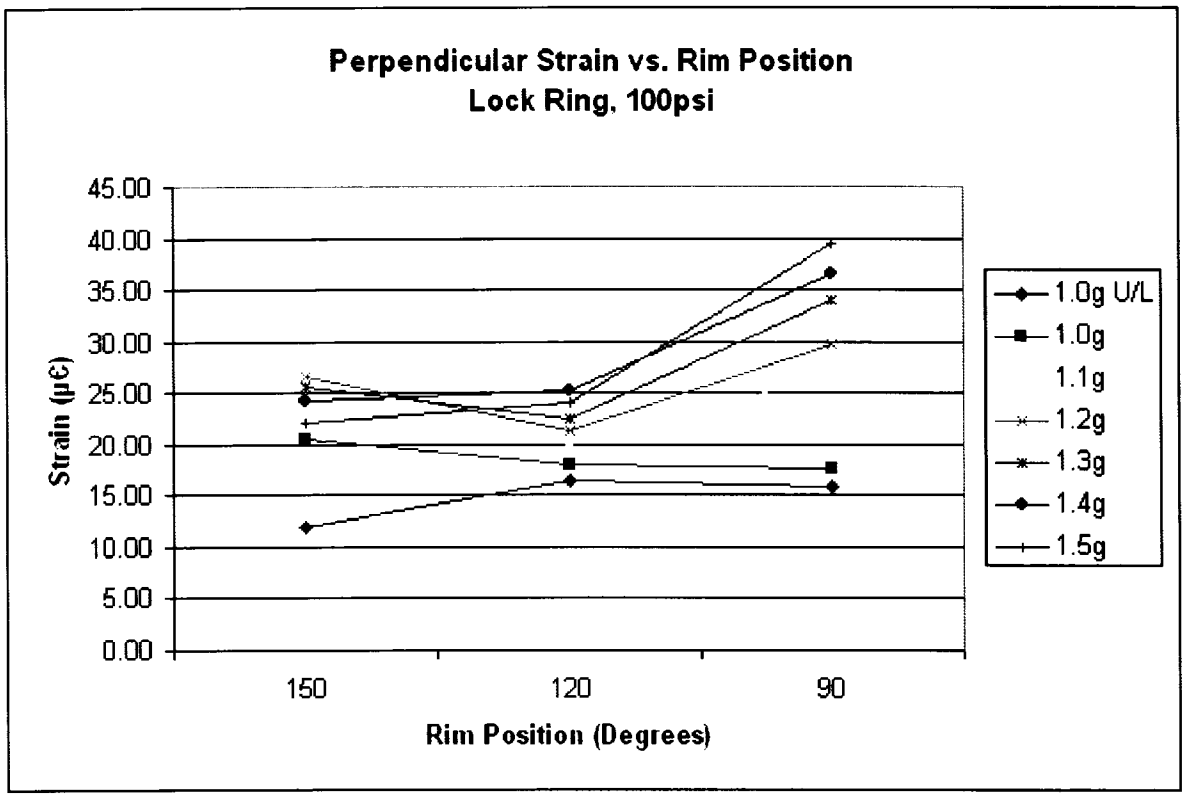

$\sigma = \varepsilon E$

where E = 200,000MPa

Perpendicular Stress (MPa)

Rim Position	1.0g U/L	1.0g	1.1g	1.2g	1.3g	1.4g	1.5g
180	-	-	-	-	-	-	-
150	2.40	4.10	4.91	5.34	5.11	4.87	4.41
120	3.30	3.60	3.97	4.25	4.51	5.04	4.81
90	3.16	3.52	5.37	5.95	6.79	7.33	7.89
45	-	-	-	-	-	-	-
0	-	-	-	-	-	-	-

A.2 Filtered Test Results, 100psi Tire Pressure

Perpendicular Strain (με)

Rim Position	1.0g U/L	1.0g	1.1g	1.2g	1.3g	1.4g	1.5g
180							
150	14.27	15.22	12.63	12.06	16.48	17.14	20.84
120	21.24	66.83	79.33	89.08	115.55	124.47	143.12
90	16.91	32.03	38.48	43.77	71.46	75.39	106.16
45	4.51	5.80	4.86	3.98	4.67	6.04	8.12
0	14.47	13.15	15.61	16.73	20.69	23.32	26.85

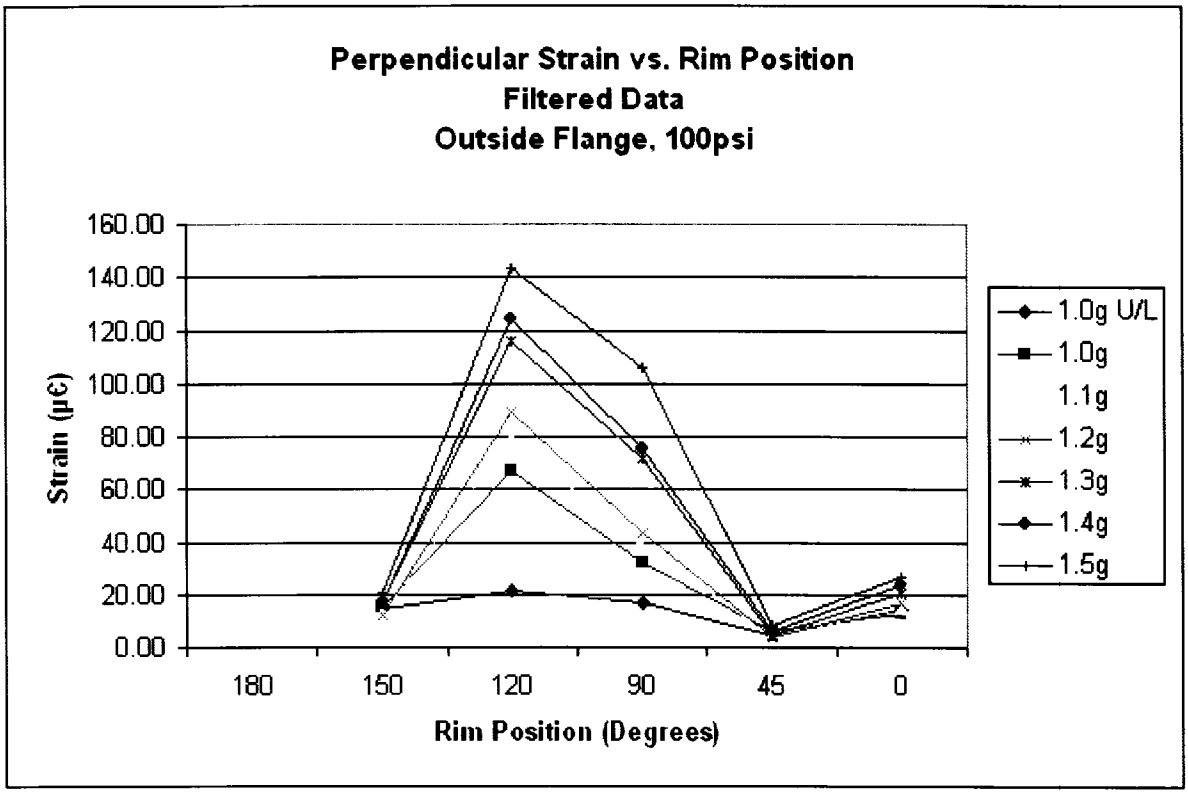

$\sigma = \varepsilon E$

where E = 200,000MPa

Perpendicular Stress (MPa)

Rim Position	1.0g U/L	1.0g	1.1g	1.2g	1.3g	1.4g	1.5g
180	-	-	-	-	-	-	-
150	2.85	3.04	2.53	2.41	3.30	3.43	4.17
120	4.25	13.37	15.87	17.82	23.11	24.89	28.62
90	3.38	6.41	7.70	8.75	14.29	15.08	21.23
45	0.90	1.16	0.97	0.80	0.93	1.21	1.62
0	2.89	2.63	3.12	3.35	4.14	4.66	5.37

Perpendicular Strain (με)

Rim Position	1.0g U/L	1.0g	1.1g	1.2g	1.3g	1.4g	1.5g
180							
150	17.76	17.96	17.11	20.71	23.68	28.13	32.66
120	19.16	15.46	20.16	19.50	20.77	21.78	24.04
90							
45	7.70	5.26	4.51	4.32	5.26	6.01	6.95
0	7.60	10.23	13.00	15.09	19.01	21.54	24.46

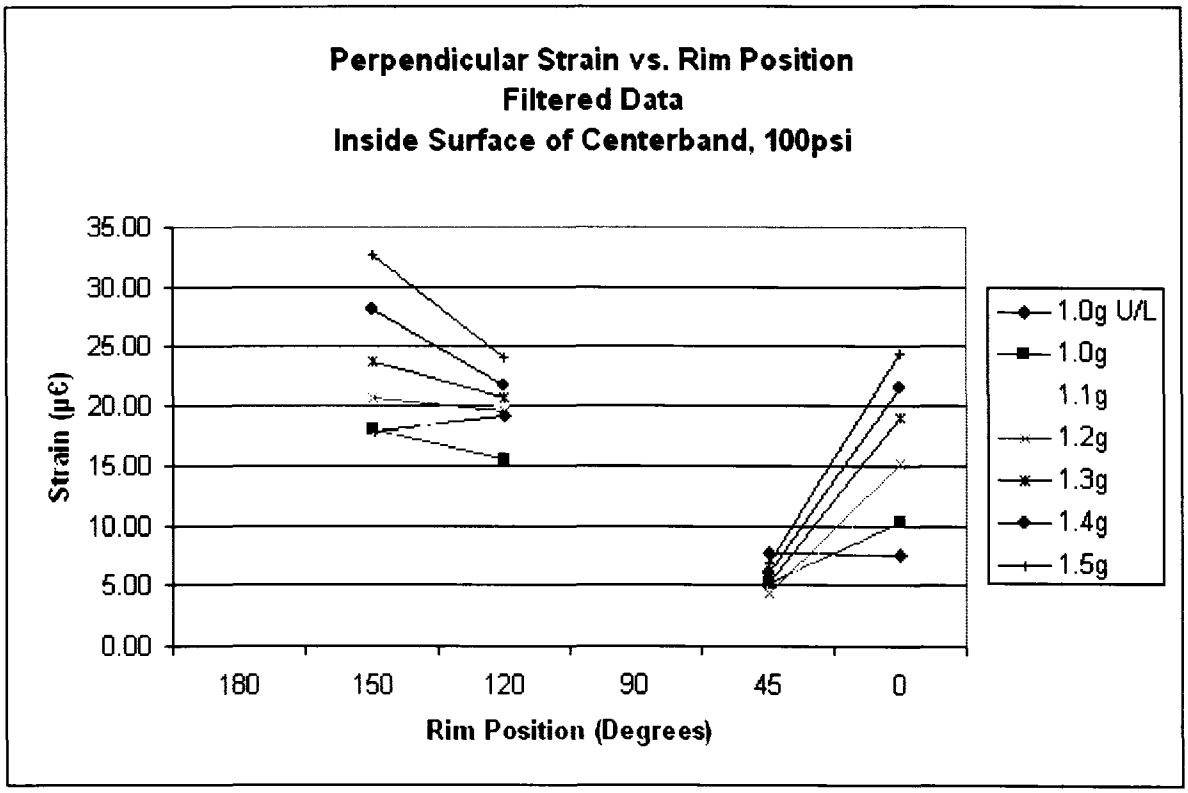

$\sigma = \varepsilon E$

where E = 200,000MPa

Perpendicular Stress (MPa)

Rim Position	1.0g U/L	1.0g	1.1g	1.2g	1.3g	1.4g	1.5g
180	-	-	-	-	-	-	-
150	3.55	3.59	3.42	4.14	4.74	5.63	6.53
120	3.83	3.09	4.03	3.90	4.15	4.36	4.81
90	-	-	-	-	-	-	-
45	1.54	1.05	0.90	0.86	1.05	1.20	1.39
0	1.52	2.05	2.60	3.02	3.80	4.31	4.89

A.3 Test Results, 90psi Tire Pressure

Radial Strain (με)

Rim Position	1.0g U/L	1.0g	1.1g	1.2g	1.3g	1.4g	1.5g
180	38.42	159.41	159.58	174.72	198.83	199.71	219.44
150	18.05	68.99	64.15	72.73	85.97	92.70	103.78
120	4.35	23.60	27.39	31.47	36.65	38.75	45.27
90	4.50	11.46	12.58	15.97	21.22	23.10	31.18
45	12.00	24.42	19.56	22.36	28.42	27.99	30.70
0	17.87	52.60	55.55	60.73	70.64	70.85	80.40

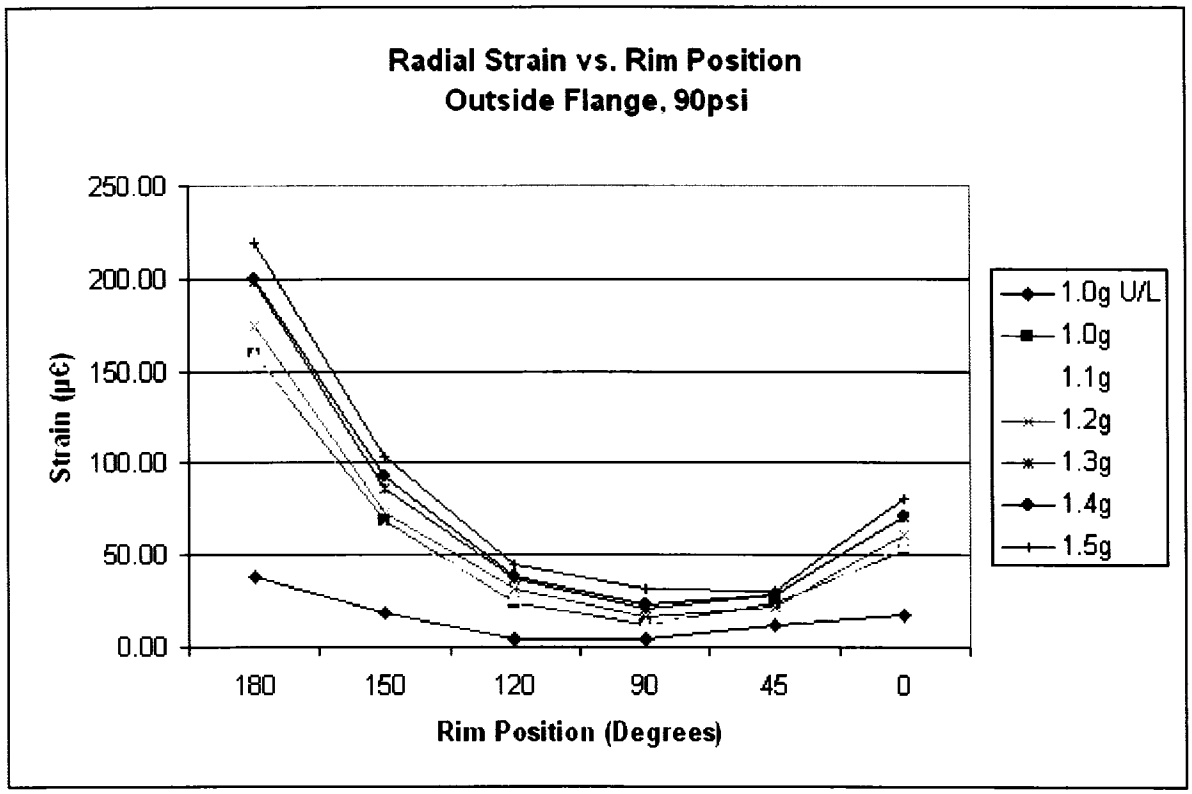

$\sigma = \varepsilon E$

where E = 200,000MPa

Radial Stress (MPa)

Rim Position	1.0g U/L	1.0g	1.1g	1.2g	1.3g	1.4g	1.5g
180	7.68	31.88	31.92	34.94	39.77	39.94	43.89
150	3.61	13.80	12.83	14.55	17.19	18.54	20.76
120	0.87	4.72	5.48	6.29	7.33	7.75	9.05
90	0.90	2.29	2.52	3.19	4.24	4.62	6.24
45	2.40	4.88	3.91	4.47	5.68	5.60	6.14
0	3.57	10.52	11.11	12.15	14.13	14.17	16.08

Perpendicular Strain (με)

Rim Position	1.0g U/L	1.0g	1.1g	1.2g	1.3g	1.4g	1.5g
180	64.30	760.86	1718.57	952.93	6151.45	1815.34	4270.56
150	7.74	7.46	11.46	12.83	16.62	15.68	20.48
120	11.59	72.17	83.27	94.16	110.44	114.66	135.40
90	14.16	29.29	34.78	43.68	64.03	67.22	98.23
45	3.17	5.99	6.96	8.29	9.27	10.54	12.10
0	6.75	16.53	17.48	20.09	24.02	22.87	26.49

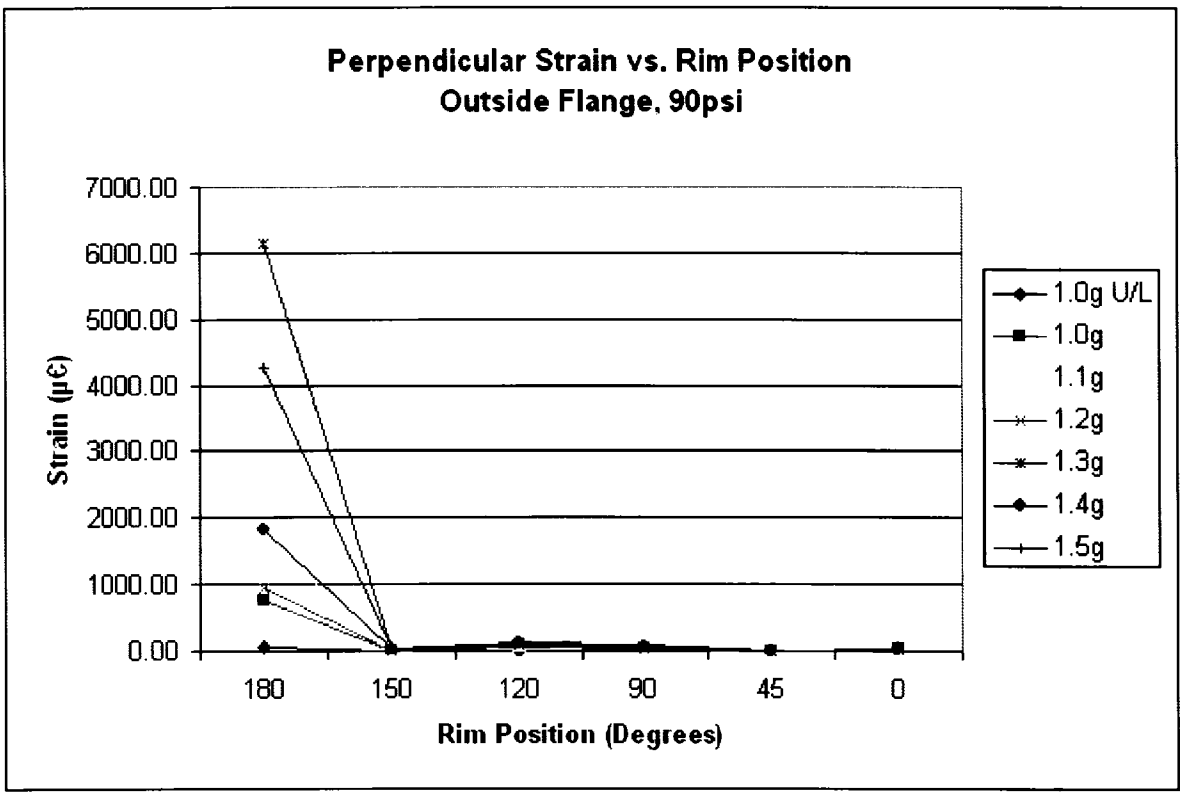

$\sigma = \varepsilon E$

where E = 200,000MPa

Perpendicular Stress (MPa)

Rim Position	1.0g U/L	1.0g	1.1g	1.2g	1.3g	1.4g	1.5g
180	12.86	152.17	343.71	190.59	1230.29	363.07	854.11
150	1.55	1.49	2.29	2.57	3.32	3.14	4.10
120	2.32	14.43	16.65	18.83	22.09	22.93	27.08
90	2.83	5.86	6.96	8.74	12.81	13.44	19.65
45	0.63	1.20	1.39	1.66	1.85	2.11	2.42
0	1.35	3.31	3.50	4.02	4.80	4.57	5.30

Radial Strain (με)

Rim Position	1.0g U/L	1.0g	1.1g	1.2g	1.3g	1.4g	1.5g
180	10.68	21.53	30.20	26.26	29.38	32.68	35.70
150	7.79	9.01	9.17	9.77	12.03	12.55	15.17
120	10.73	15.35	12.23	92.84	87.15	17.40	15.40
90	4.62	4.55	5.82	7.72	6.67	6.23	5.57
45	7.55	9.58	9.47	9.30	9.42	9.18	9.06
0	4.20	6.01	6.35	6.79	7.40	7.73	8.43

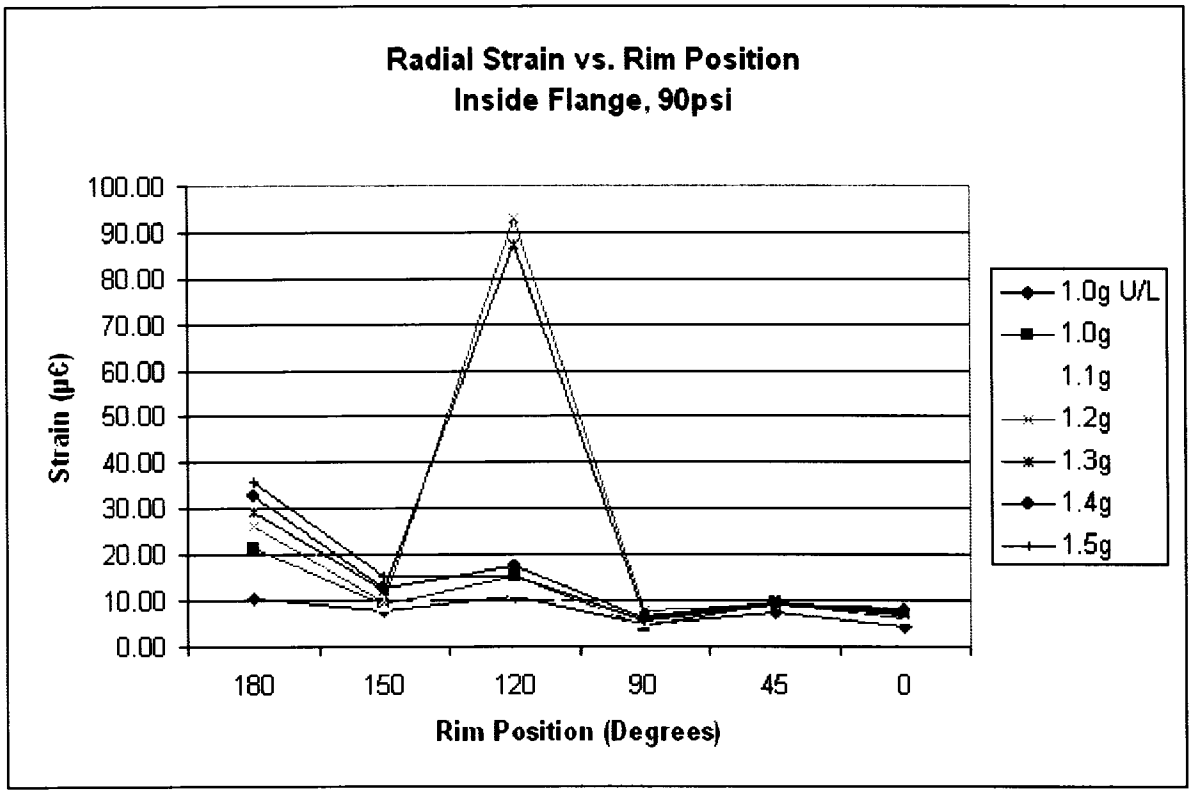

$\sigma = \varepsilon E$

where E = 200,000MPa

Radial Stress (MPa)

Rim Position	1.0g U/L	1.0g	1.1g	1.2g	1.3g	1.4g	1.5g
180	2.14	4.31	6.04	5.25	5.88	6.54	7.14
150	1.56	1.80	1.83	1.95	2.41	2.51	3.03
120	2.15	3.07	2.45	18.57	17.43	3.48	3.08
90	0.92	0.91	1.16	1.54	1.33	1.25	1.11
45	1.51	1.92	1.89	1.86	1.88	1.84	1.81
0	0.84	1.20	1.27	1.36	1.48	1.55	1.69

Perpendicular Strain (με)

Rim Position	1.0g U/L	1.0g	1.1g	1.2g	1.3g	1.4g	1.5g
180	24.62	63.67	70.27	77.00	87.54	95.87	101.25
150	24.14	27.67	27.58	32.31	40.06	41.55	49.67
120	31.08	37.61	37.55	36.90	37.62	36.61	37.16
90	11.10	13.27	13.15	12.46	14.74	13.71	13.34
45	22.37	28.74	28.18	27.61	29.12	27.63	27.41
0	10.03	14.42	15.07	16.86	18.82	18.76	19.89

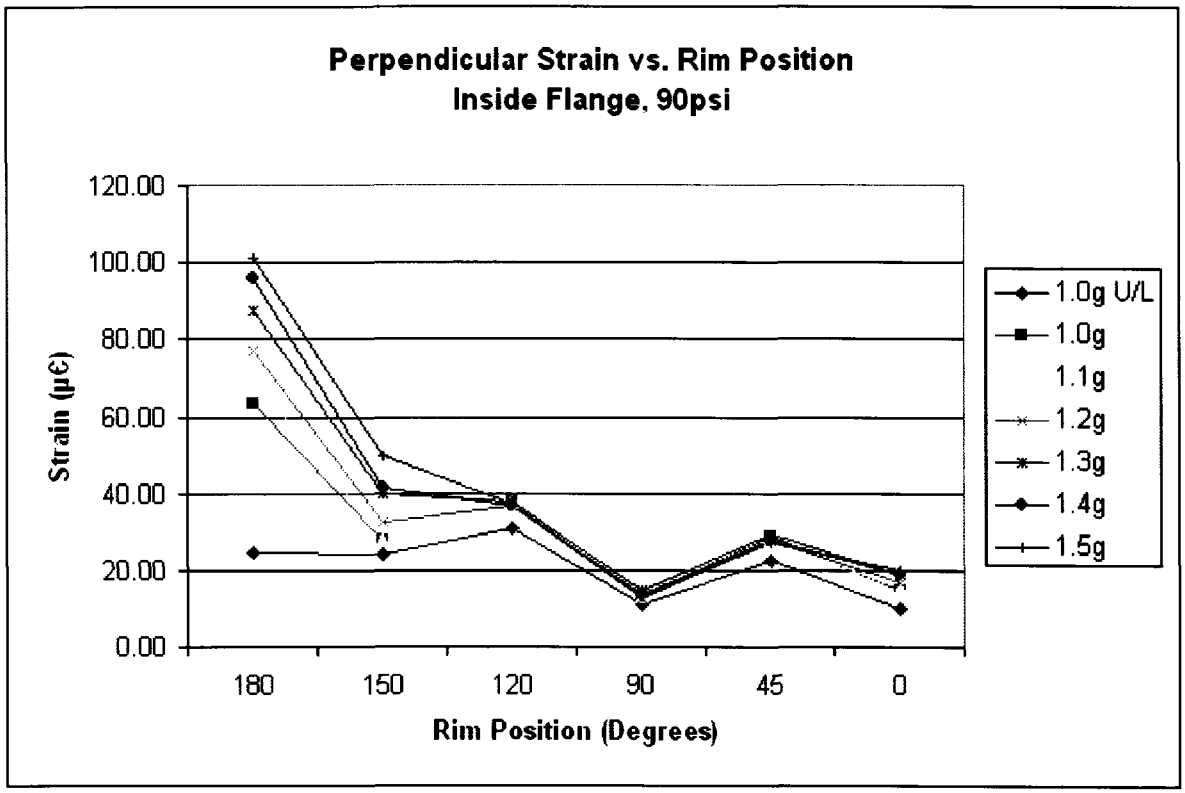

$\sigma = \varepsilon E$

where E = 200,000MPa

Perpendicular Stress (MPa)

Rim Position	1.0g U/L	1.0g	1.1g	1.2g	1.3g	1.4g	1.5g
180	4.92	12.73	14.05	15.40	17.51	19.17	20.25
150	4.83	5.53	5.52	6.46	8.01	8.31	9.93
120	6.22	7.52	7.51	7.38	7.52	7.32	7.43
90	2.22	2.65	2.63	2.49	2.95	2.74	2.67
45	4.47	5.75	5.64	5.52	5.82	5.53	5.48
0	2.01	2.88	3.01	3.37	3.76	3.75	3.98

Radial Strain (με)

Rim Position	1.0g U/L	1.0g	1.1g	1.2g	1.3g	1.4g	1.5g
180	22.08	44.54	46.41	44.83	53.05	41.46	35.72
150	3.50	24.06	23.51	24.17	6.00	3.50	4.70
120	2.39	4.37	4.63	5.97	6.11	6.64	6.59
90	3.05	20.64	19.52	21.89	27.84	27.17	30.59
45	-	-	-	-	-	-	-
0	-	-	-	-	-	-	-

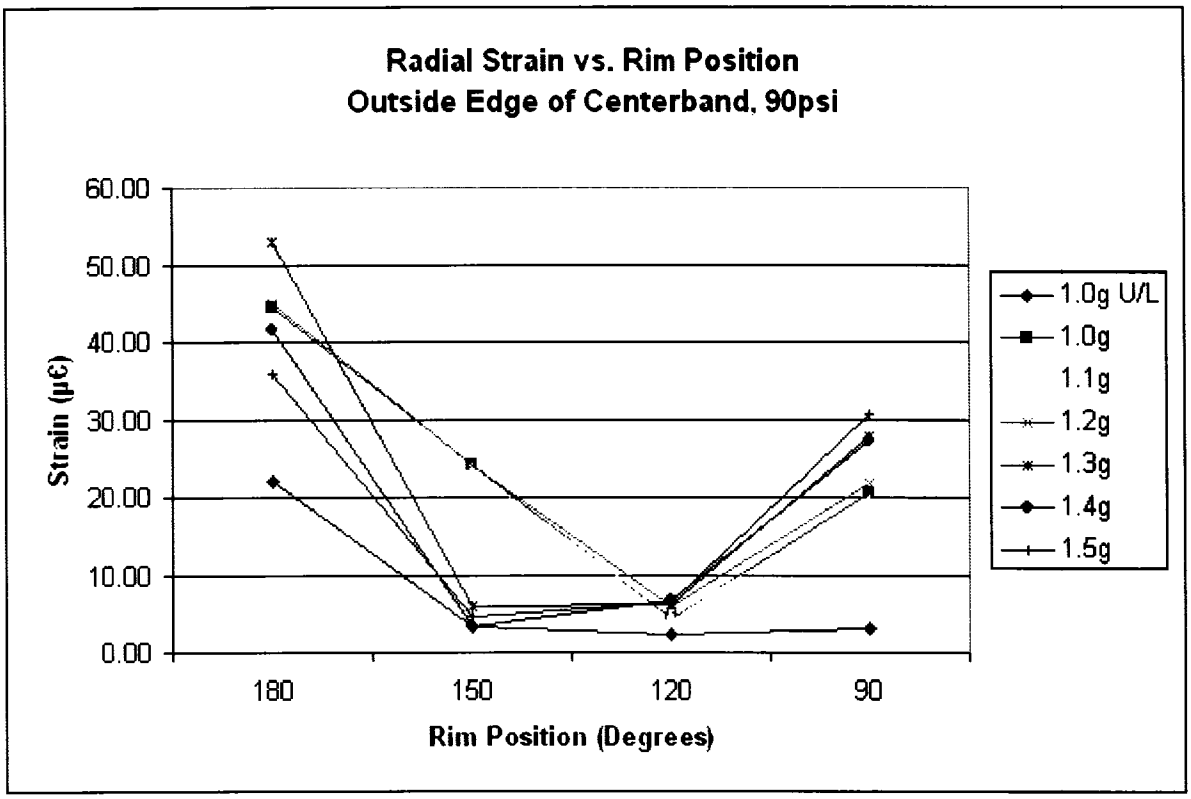

$\sigma = \varepsilon E$

where E = 200,000MPa

Radial Stress (MPa)

Rim Position	1.0g U/L	1.0g	1.1g	1.2g	1.3g	1.4g	1.5g
180	4.42	8.91	9.28	8.97	10.61	8.29	7.14
150	0.70	4.81	4.70	4.83	1.20	0.70	0.94
120	0.48	0.87	0.93	1.19	1.22	1.33	1.32
90	0.61	4.13	3.90	4.38	5.57	5.43	6.12
45	-	-	-	-	-	-	-
0	-	-	-	-	-	-	-

Perpendicular Strain (με)

Rim Position	1.0g U/L	1.0g	1.1g	1.2g	1.3g	1.4g	1.5g
180	141.30	467.01	190.49	117.28	185.52	135.55	146.62
150	5.49	10.16	9.15	8.79	10.02	10.95	13.66
120	9.19	39.85	38.86	40.95	44.82	46.10	48.41
90	9.27	58.75	52.93	58.98	70.27	70.75	76.51
45	-	-	-	-	-	-	-
0	-	-	-	-	-	-	-

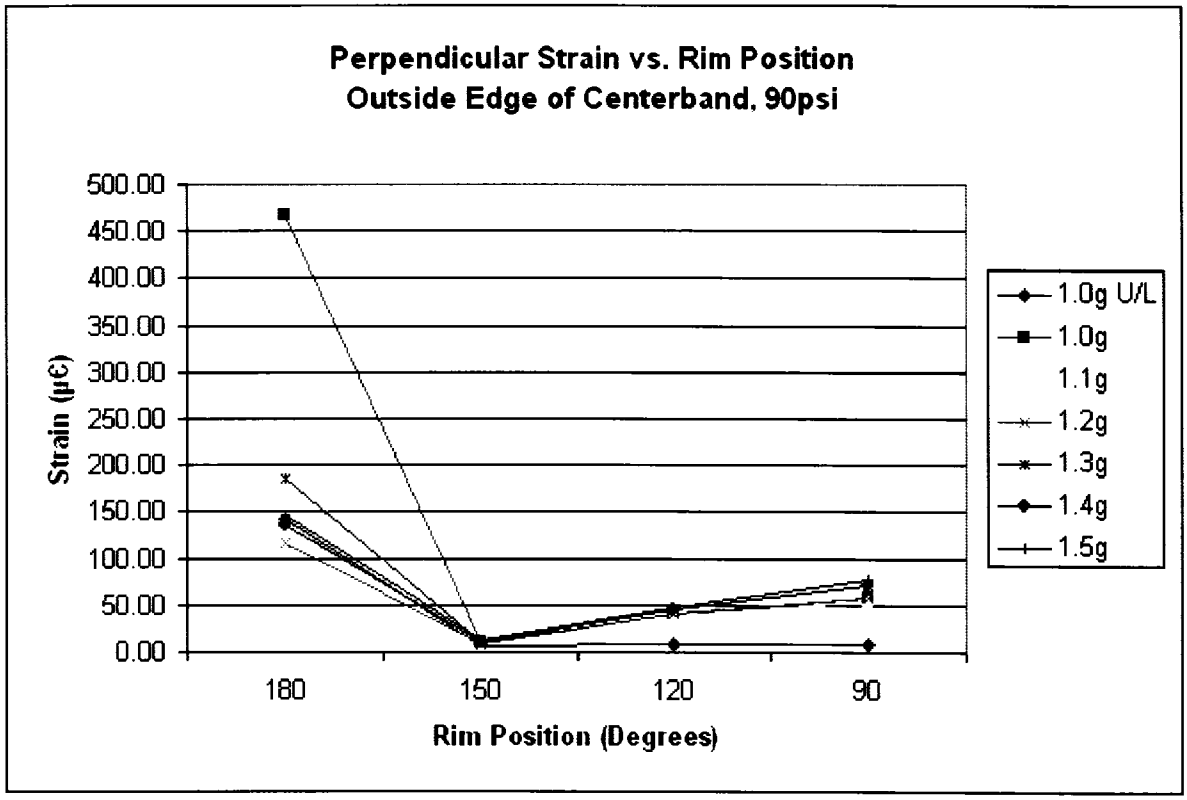

$\sigma = \varepsilon E$

where E = 200,000MPa

Perpendicular Stress (MPa)

Rim Position	1.0g U/L	1.0g	1.1g	1.2g	1.3g	1.4g	1.5g
180	28.26	93.40	38.10	23.46	37.10	27.11	29.32
150	1.10	2.03	1.83	1.76	2.00	2.19	2.73
120	1.84	7.97	7.77	8.19	8.96	9.22	9.68
90	1.85	11.75	10.59	11.80	14.05	14.15	15.30
45	-	-	-	-	-	-	-
0	-	-	-	-	-	-	-

Radial Strain (με)

Rim Position	1.0g U/L	1.0g	1.1g	1.2g	1.3g	1.4g	1.5g
180	26.81	38.76	39.53	40.97	42.94	43.95	44.31
150	35.07	39.99	39.86	41.55	40.78	40.00	39.17
120	15.58	22.60	21.57	21.89	21.66	22.99	22.76
90	9.49	11.69	10.64	10.80	12.23	11.83	13.76
45	19.56	25.27	25.86	26.56	26.85	27.06	26.42
0	1.43	2.02	1.53	1.62	9.15	4.27	3.20

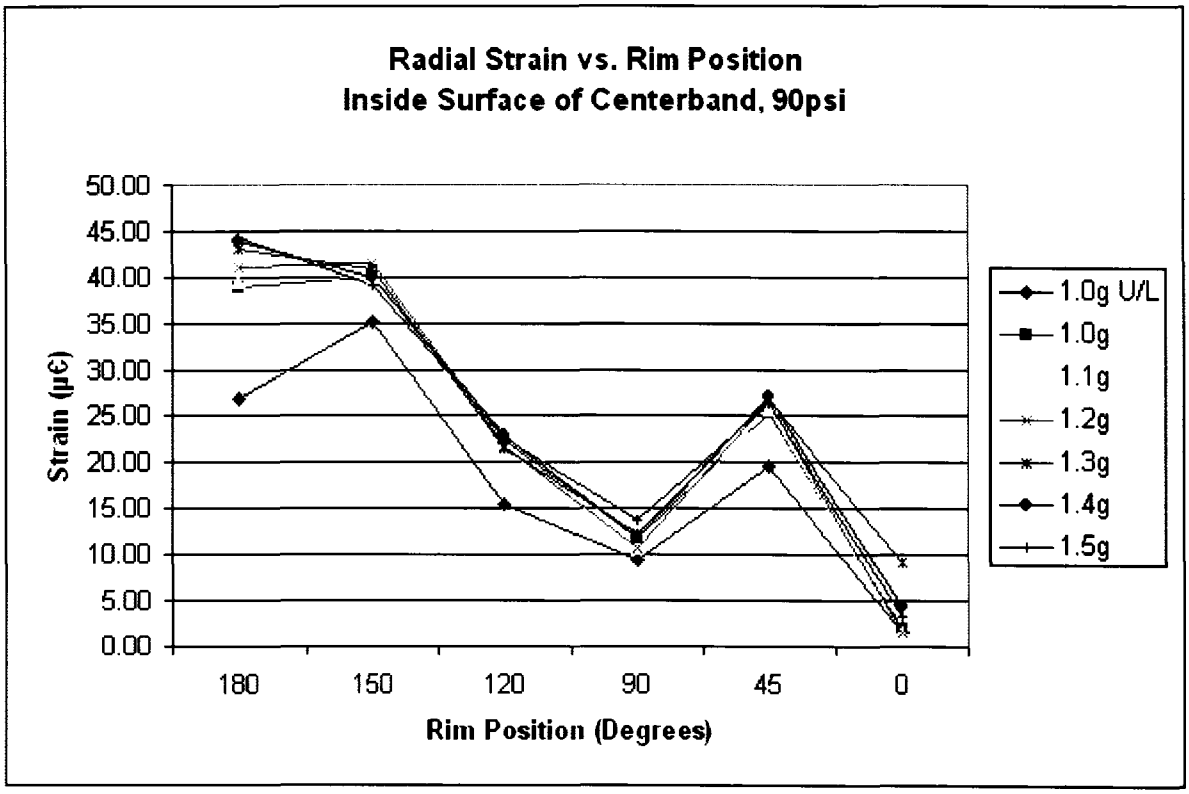

$\sigma = \varepsilon E$

where E = 200,000MPa

Radial Stress (MPa)

Rim Position	1.0g U/L	1.0g	1.1g	1.2g	1.3g	1.4g	1.5g
180	5.36	7.75	7.91	8.19	8.59	8.79	8.86
150	7.01	8.00	7.97	8.31	8.16	8.00	7.83
120	3.12	4.52	4.31	4.38	4.33	4.60	4.55
90	1.90	2.34	2.13	2.16	2.45	2.37	2.75
45	3.91	5.05	5.17	5.31	5.37	5.41	5.28
0	0.29	0.40	0.31	0.32	1.83	0.85	0.64

Perpendicular Strain (με)

Rim Position	1.0g U/L	1.0g	1.1g	1.2g	1.3g	1.4g	1.5g
180	827.02	561.57	743.91	534.73	1161.34	654.23	1186.53
150	13.30	13.83	15.81	18.64	22.08	26.42	27.59
120	7.69	18.28	18.75	26.03	37.50	22.31	20.92
90	364.22	27.76	214.88	288.06	37.82	209.61	8301.52
45	2.63	3.76	4.32	3.94	5.07	5.45	5.82
0	3.67	13.71	15.74	17.57	19.80	21.56	23.43

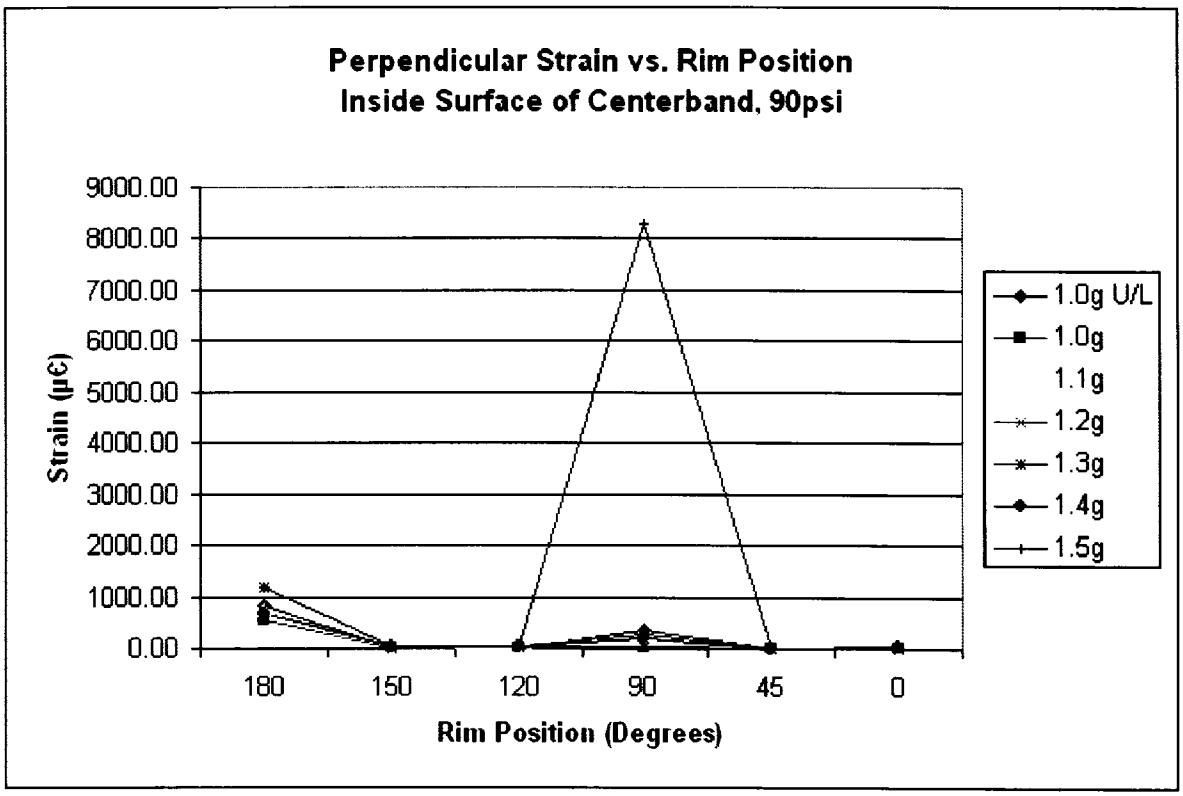

$\sigma = \varepsilon E$

where E = 200,000MPa

Perpendicular Stress (MPa)

Rim Position	1.0g U/L	1.0g	1.1g	1.2g	1.3g	1.4g	1.5g
180	165.40	112.31	148.78	106.95	232.27	130.85	237.31
150	2.66	2.77	3.16	3.73	4.42	5.28	5.52
120	1.54	3.66	3.75	5.21	7.50	4.46	4.18
90	72.84	5.55	42.98	57.61	7.56	41.92	1660.30
45	0.53	0.75	0.86	0.79	1.01	1.09	1.16
0	0.73	2.74	3.15	3.51	3.96	4.31	4.69

Radial Strain (με)

Rim Position	1.0g U/L	1.0g	1.1g	1.2g	1.3g	1.4g	1.5g
180	-	-	-	-	-	-	-
150	0.01	0.01	0.01	0.01	0.01	0.02	0.01
120	2.46	180.55	203.06	82.80	13.52	168.28	14.09
90	6.08	10.67	9.31	9.20	11.42	10.40	13.86
45	-	-	-	-	-	-	-
0	-	-	-	-	-	-	-

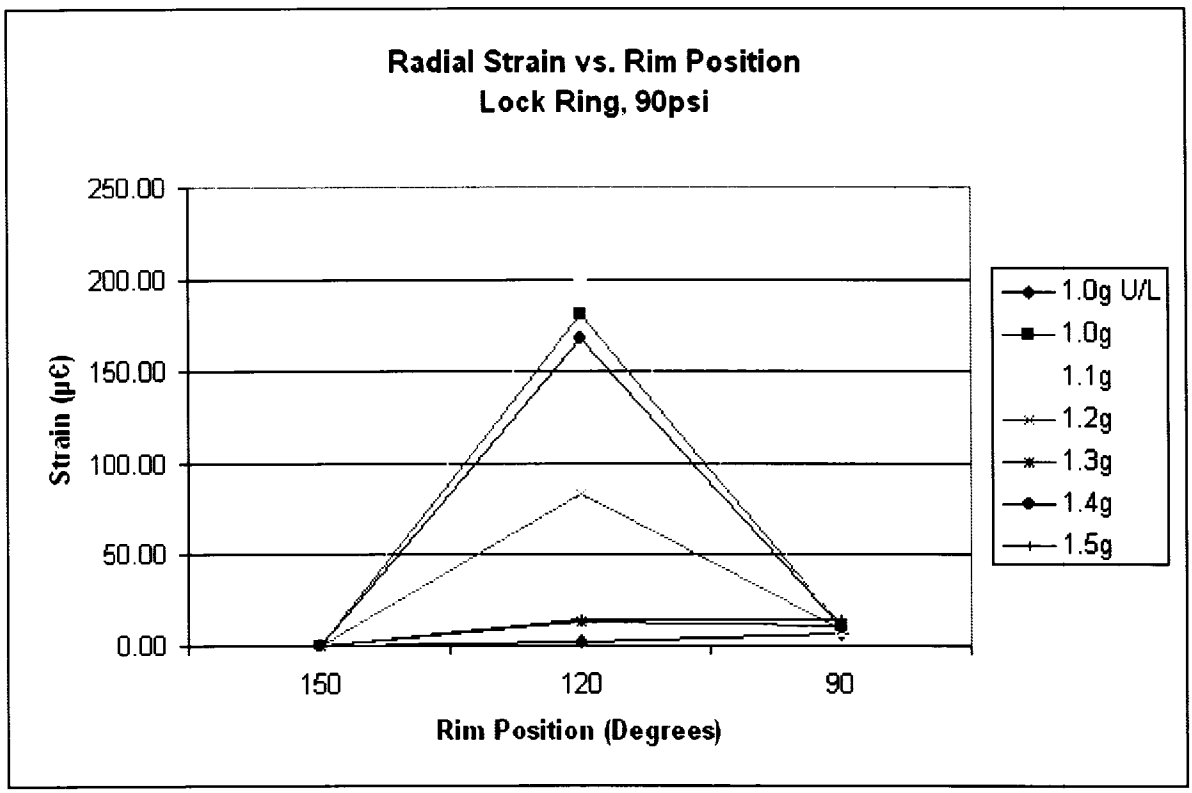

$\sigma = \varepsilon E$

where E = 200,000MPa

Radial Stress (MPa)

Rim Position	1.0g U/L	1.0g	1.1g	1.2g	1.3g	1.4g	1.5g
180	-	-	-	-	-	-	-
150	0.00	0.00	0.00	0.00	0.00	0.00	0.00
120	0.49	36.11	40.61	16.56	2.70	33.66	2.82
90	1.22	2.13	1.86	1.84	2.28	2.08	2.77
45	-	-	-	-	-	-	-
0	-	-	-	-	-	-	-

Perpendicular Strain (με)

Rim Position	1.0g U/L	1.0g	1.1g	1.2g	1.3g	1.4g	1.5g
180	-	-	-	-	-	-	-
150	13.81	21.20	22.65	23.06	23.33	21.58	21.04
120	9.38	18.79	23.48	24.41	28.35	23.31	27.61
90	1.20	27.99	25.38	26.66	9.10	3.80	3.40
45	-	-	-	-	-	-	-
0	-	-	-	-	-	-	-

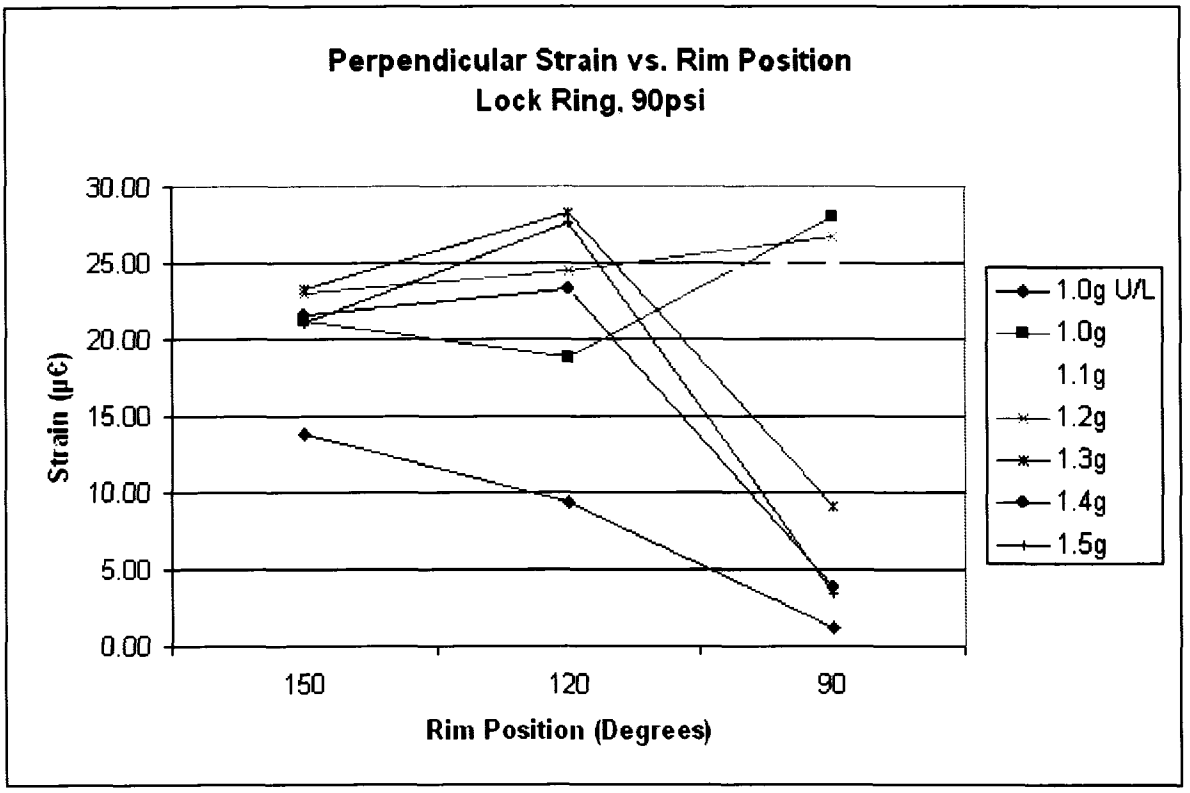

$\sigma = \varepsilon E$

where E = 200,000MPa

Perpendicular Stress (MPa)

Rim Position	1.0g U/L	1.0g	1.1g	1.2g	1.3g	1.4g	1.5g
180	-	-	-	-	-	-	-
150	2.76	4.24	4.53	4.61	4.67	4.32	4.21
120	1.88	3.76	4.70	4.88	5.67	4.66	5.52
90	0.24	5.60	5.08	5.33	1.82	0.76	0.68
45	-	-	-	-	-	-	-
0	-	-	-	-	-	-	-

A.4 Filtered Test Results, 90psi Tire Pressure

Perpendicular Strain (με)

Rim Position	1.0g U/L	1.0g	1.1g	1.2g	1.3g	1.4g	1.5g
180							
150	7.74	7.46	11.46	12.83	16.62	15.68	20.48
120	11.59	72.17	83.27	94.16	110.44	114.66	135.40
90	14.16	29.29	34.78	43.68	64.03	67.22	98.23
45	3.17	5.99	6.96	8.29	9.27	10.54	12.10
0	6.75	16.53	17.48	20.09	24.02	22.87	26.49

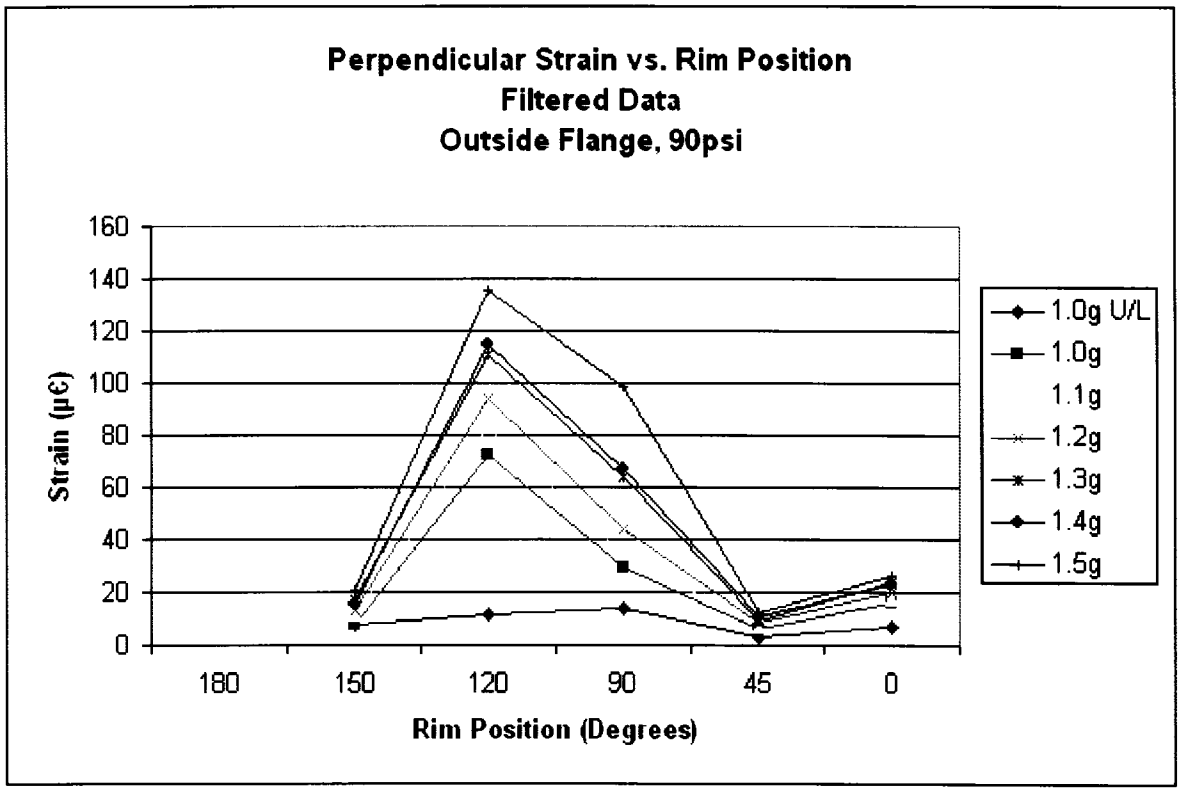

$\sigma = \varepsilon E$

where E = 200,000MPa

Perpendicular Stress (MPa)

Rim Position	1.0g U/L	1.0g	1.1g	1.2g	1.3g	1.4g	1.5g
180	-	-	-	-	-	-	-
150	1.55	1.49	2.29	2.57	3.32	3.14	4.10
120	2.32	14.43	16.65	18.83	22.09	22.93	27.08
90	2.83	5.86	6.96	8.74	12.81	13.44	19.65
45	0.63	1.20	1.39	1.66	1.85	2.11	2.42
0	1.35	3.31	3.50	4.02	4.80	4.57	5.30

Perpendicular Strain (με)

Rim Position	1.0g U/L	1.0g	1.1g	1.2g	1.3g	1.4g	1.5g
180							
150	13.30	13.83	15.81	18.64	22.08	26.42	27.59
120	7.69	18.28	18.75	26.03	37.50	22.31	20.92
90							
45	2.63	3.76	4.32	3.94	5.07	5.45	5.82
0	3.67	13.71	15.74	17.57	19.80	21.56	23.43

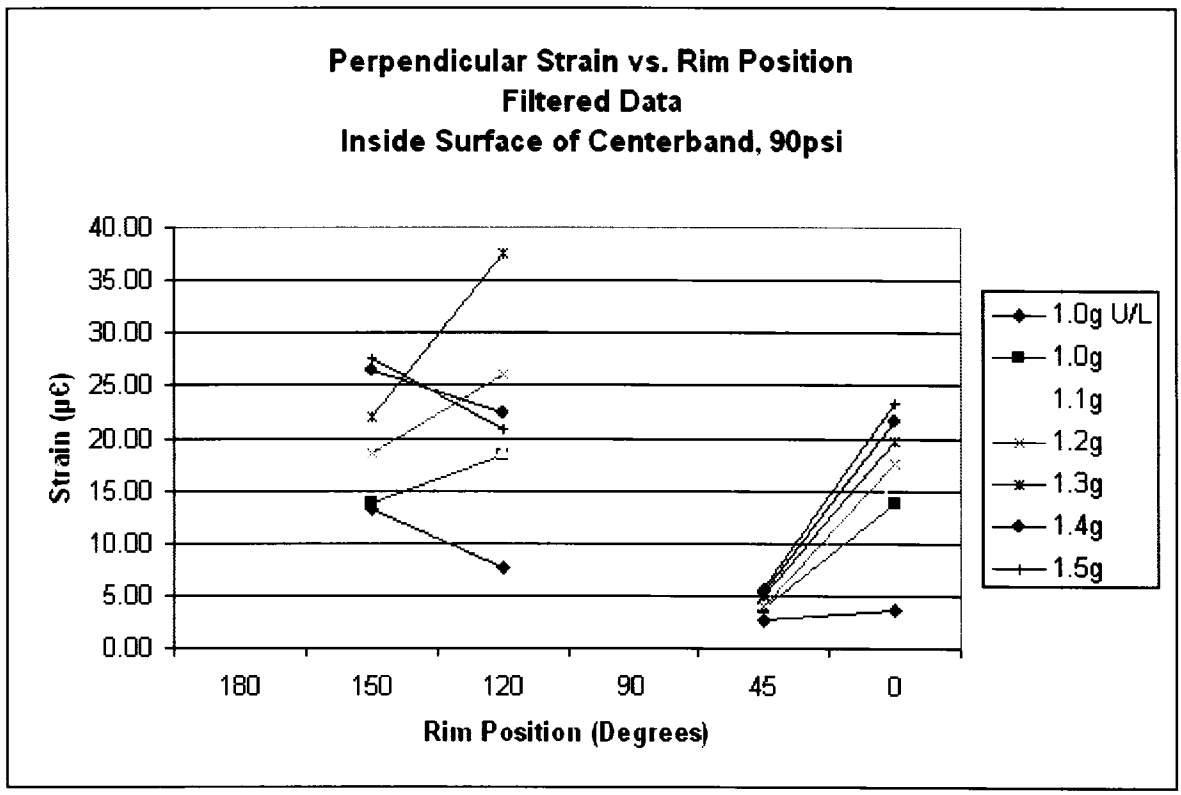

$\sigma = \varepsilon E$

where E = 200,000MPa

Perpendicular Stress (MPa)

Rim Position	1.0g U/L	1.0g	1.1g	1.2g	1.3g	1.4g	1.5g
180	-	-	-	-	-	-	-
150	2.66	2.77	3.16	3.73	4.42	5.28	5.52
120	1.54	3.66	3.75	5.21	7.50	4.46	4.18
90	-	-	-	-	-	-	-
45	0.53	0.75	0.86	0.79	1.01	1.09	1.16
0	0.73	2.74	3.15	3.51	3.96	4.31	4.69

A.5 Test Results, 80psi Tire Pressure

Radial Strain (με)

Rim Position	1.0g U/L	1.0g	1.1g	1.2g	1.3g	1.4g
180	33.68	154.22	157.18	162.61	165.13	172.00
150	16.22	73.10	65.58	72.38	79.90	86.88
120	4.57	24.35	28.40	31.30	33.53	35.84
90	4.15	13.15	13.90	16.54	19.54	22.54
45	11.10	31.41	25.56	25.13	28.36	27.08
0	17.55	62.36	61.18	61.40	65.14	70.00

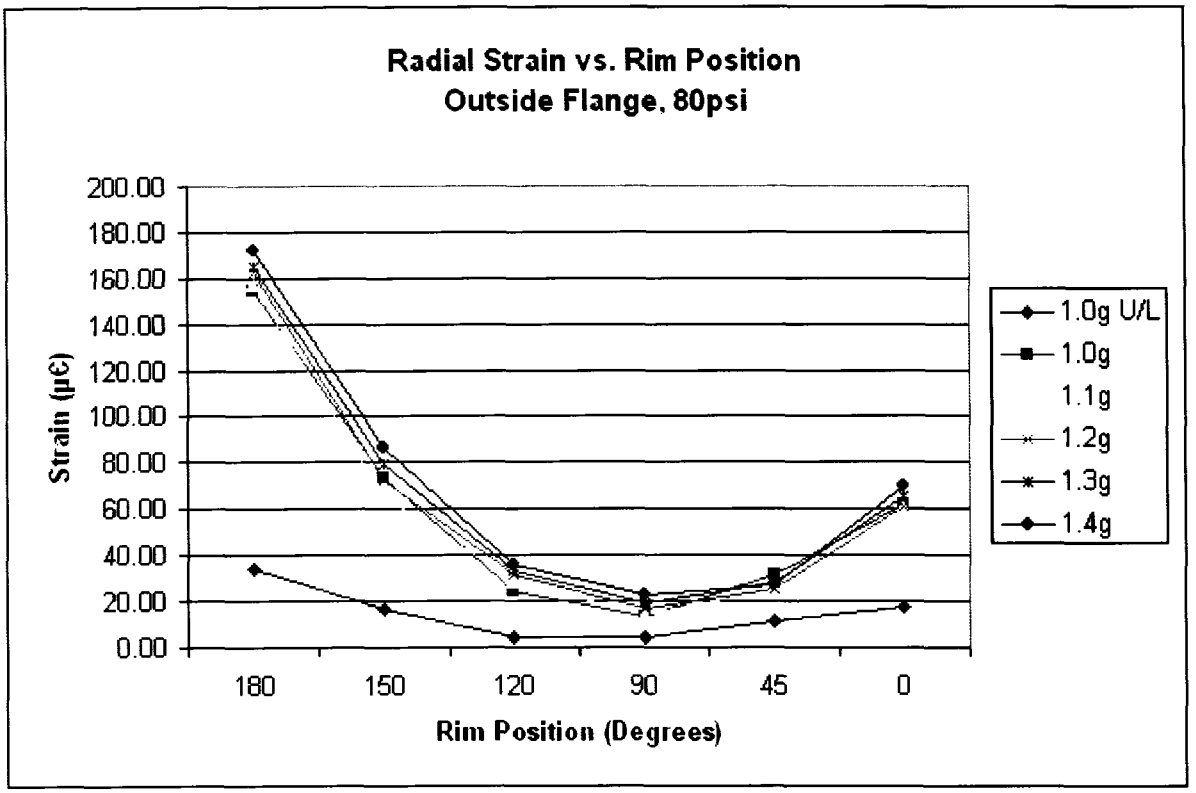

$\sigma = \varepsilon E$

where E = 200,000MPa

Radial Stress (MPa)

Rim Position	1.0g U/L	1.0g	1.1g	1.2g	1.3g	1.4g
180	6.74	30.84	31.44	32.52	33.03	34.40
150	3.24	14.62	13.12	14.48	15.98	17.38
120	0.91	4.87	5.68	6.26	6.71	7.17
90	0.83	2.63	2.78	3.31	3.91	4.51
45	2.22	6.28	5.11	5.03	5.67	5.42
0	3.51	12.47	12.24	12.28	13.03	14.00

Perpendicular Strain (με)

Rim Position	1.0g U/L	1.0g	1.1g	1.2g	1.3g	1.4g
180	-	-	-	-	-	-
150	7.18	8.17	15.40	14.22	16.48	15.30
120	12.81	73.17	84.74	91.48	99.17	103.99
90	13.99	38.04	44.58	47.65	59.96	69.69
45	3.19	8.47	7.53	9.01	10.52	11.64
0	6.98	20.65	21.22	20.69	21.81	23.31

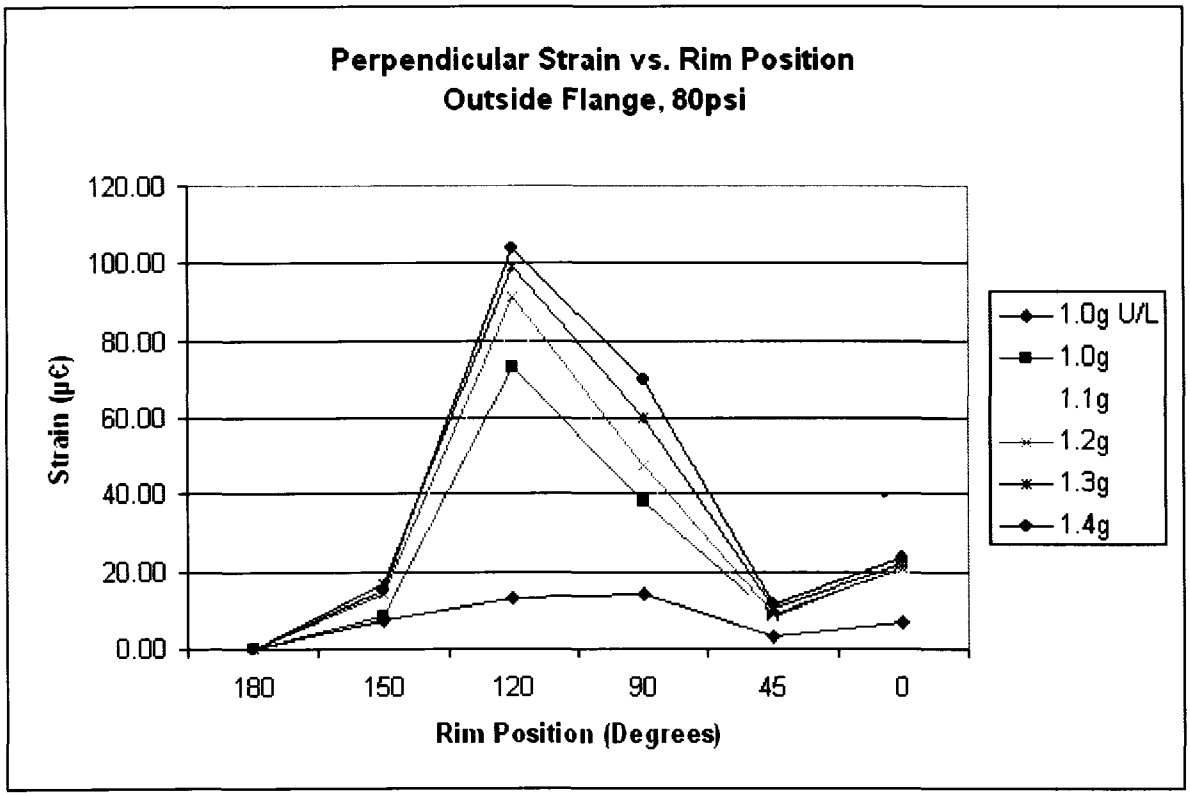

$\sigma = \varepsilon E$

where E = 200,000MPa

Perpendicular Stress (MPa)

Rim Position	1.0g U/L	1.0g	1.1g	1.2g	1.3g	1.4g
180	-	-	-	-	-	-
150	1.44	1.63	3.08	2.84	3.30	3.06
120	2.56	14.63	16.95	18.30	19.83	20.80
90	2.80	7.61	8.92	9.53	11.99	13.94
45	0.64	1.69	1.51	1.80	2.10	2.33
0	1.40	4.13	4.24	4.14	4.36	4.66

Radial Strain (με)

Rim Position	1.0g U/L	1.0g	1.1g	1.2g	1.3g	1.4g
180	9.06	22.00	25.45	27.21	30.04	34.91
150	7.60	7.82	9.64	9.97	12.42	13.12
120	7.44	10.52	25.57	19.57	16.29	13.97
90	4.04	5.62	7.42	5.48	4.57	4.38
45	7.47	8.57	9.45	8.55	8.51	8.35
0	3.77	6.40	6.01	6.80	8.03	7.90

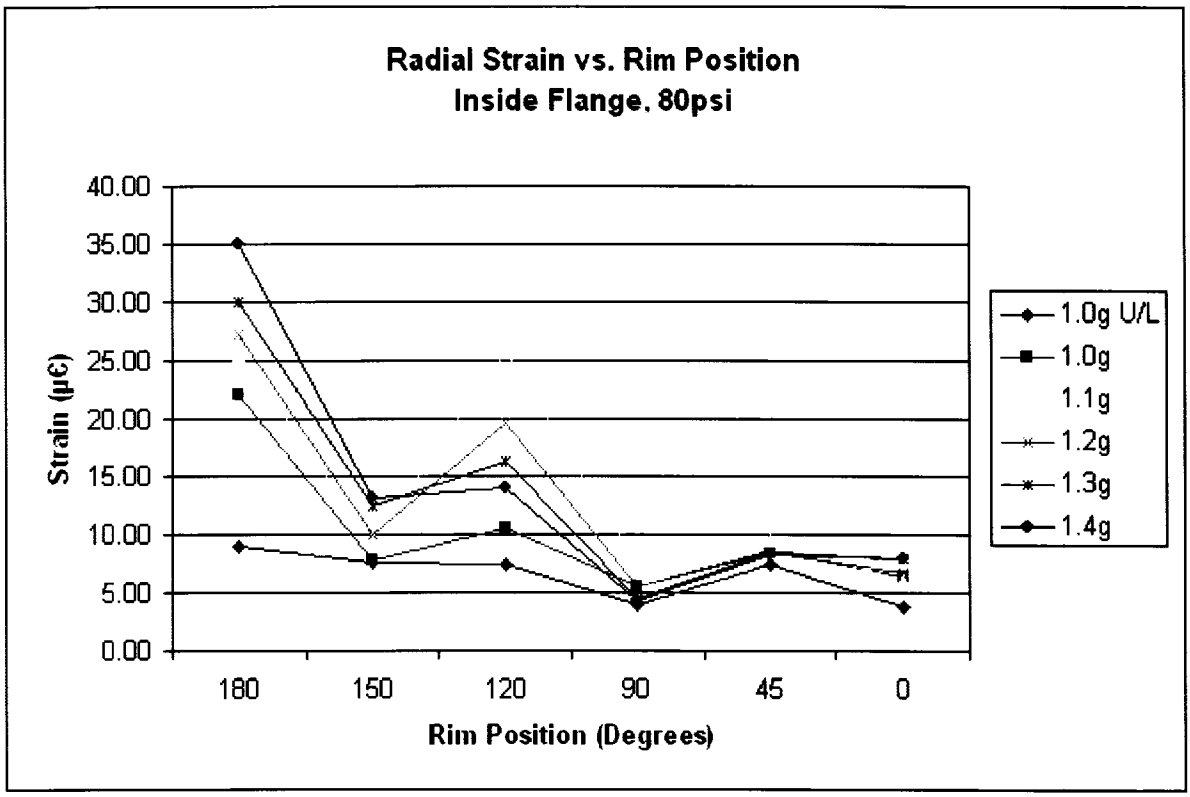

$\sigma = \varepsilon E$

where E = 200,000MPa

Radial Stress (MPa)

Rim Position	1.0g U/L	1.0g	1.1g	1.2g	1.3g	1.4g
180	1.81	4.40	5.09	5.44	6.01	6.98
150	1.52	1.56	1.93	1.99	2.48	2.62
120	1.49	2.10	5.11	3.91	3.26	2.79
90	0.81	1.12	1.48	1.10	0.91	0.88
45	1.49	1.71	1.89	1.71	1.70	1.67
0	0.75	1.28	1.20	1.36	1.61	1.58

Perpendicular Strain (με)

Rim Position	1.0g U/L	1.0g	1.1g	1.2g	1.3g	1.4g
180	24.23	68.18	73.82	82.99	90.70	99.35
150	21.65	24.20	29.70	33.68	39.08	40.94
120	28.90	35.34	37.26	37.52	35.12	36.31
90	10.65	13.82	16.23	10.14	12.16	14.46
45	22.35	26.86	26.10	26.86	27.04	27.05
0	9.54	16.00	17.84	16.67	18.19	18.76

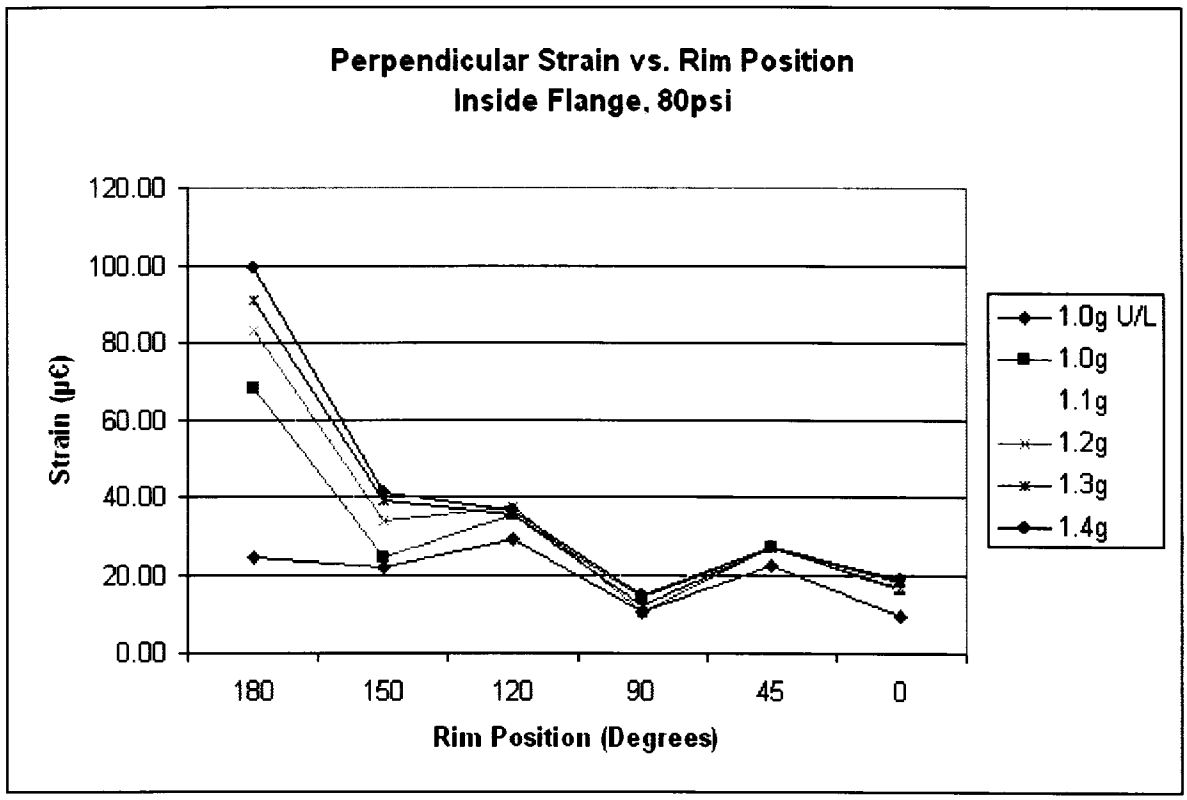

$\sigma = \varepsilon E$

where E = 200,000MPa

Perpendicular Stress (MPa)

Rim Position	1.0g U/L	1.0g	1.1g	1.2g	1.3g	1.4g
180	4.85	13.64	14.76	16.60	18.14	19.87
150	4.33	4.84	5.94	6.74	7.82	8.19
120	5.78	7.07	7.45	7.50	7.02	7.26
90	2.13	2.76	3.25	2.03	2.43	2.89
45	4.47	5.37	5.22	5.37	5.41	5.41
0	1.91	3.20	3.57	3.33	3.64	3.75

Radial Strain (με)

Rim Position	1.0g U/L	1.0g	1.1g	1.2g	1.3g	1.4g
180	19.96	36.02	42.73	37.44	35.82	42.12
150	3.00	2.60	22.20	6.10	5.10	3.00
120	2.27	6.26	5.48	6.01	6.44	5.40
90	2.88	21.67	22.08	23.32	24.76	24.24
45	-	-	-	-	-	-
0	-	-	-	-	-	-

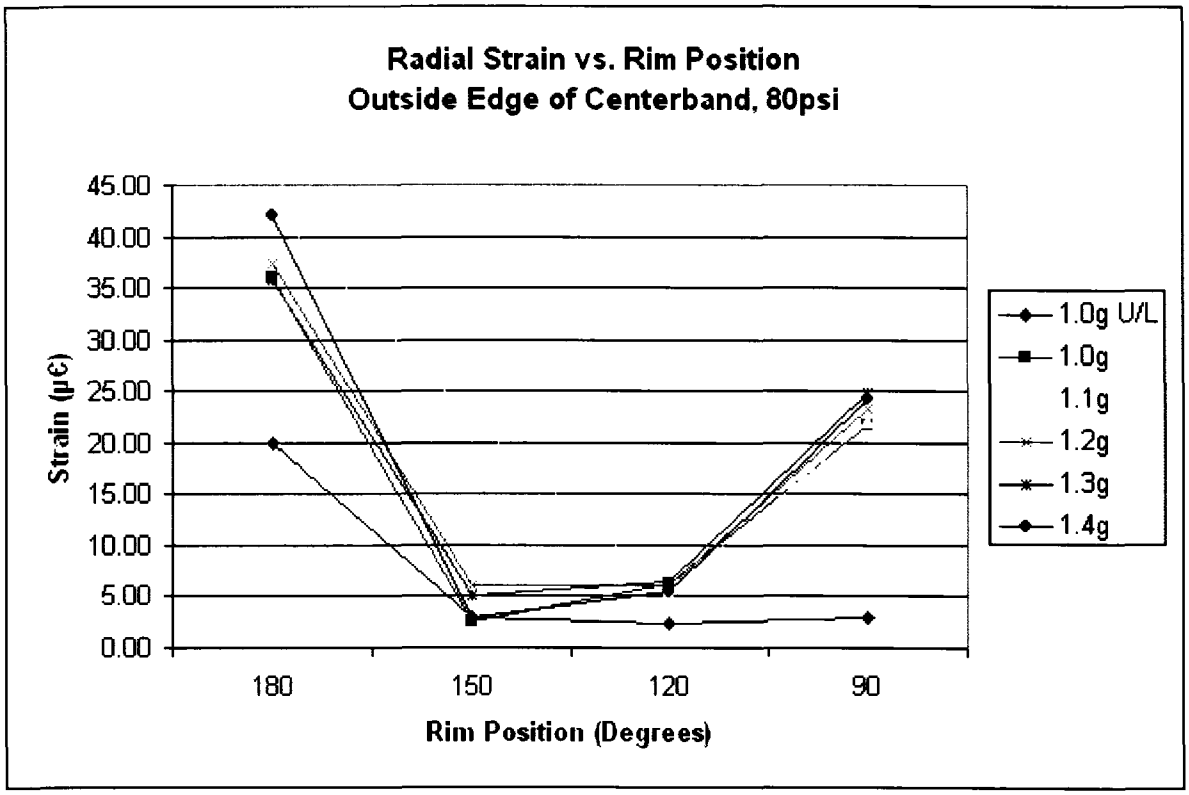

$\sigma = \varepsilon E$

where E = 200,000MPa

Radial Stress (MPa)

Rim Position	1.0g U/L	1.0g	1.1g	1.2g	1.3g	1.4g
180	3.99	7.20	8.55	7.49	7.16	8.42
150	0.60	0.52	4.44	1.22	1.02	0.60
120	0.45	1.25	1.10	1.20	1.29	1.08
90	0.58	4.33	4.42	4.66	4.95	4.85
45	-	-	-	-	-	-
0	-	-	-	-	-	-

Perpendicular Strain (με)

Rim Position	1.0g U/L	1.0g	1.1g	1.2g	1.3g	1.4g
180	107.14	135.14	167.74	166.88	167.56	126.57
150	5.32	9.71	8.08	9.44	11.03	8.86
120	9.45	41.50	39.22	40.43	40.87	40.94
90	9.46	60.46	57.24	59.06	62.31	64.03
45	-	-	-	-	-	-
0	-	-	-	-	-	-

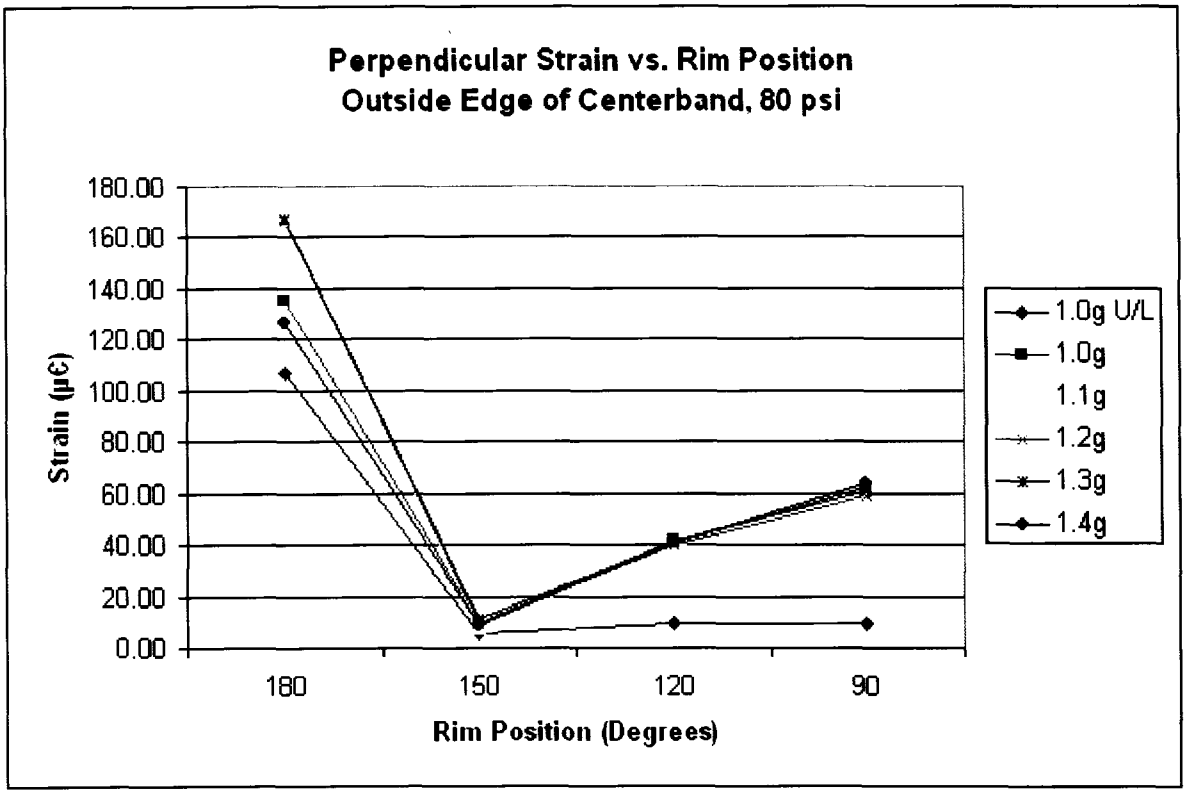

$\sigma = \varepsilon E$

where E = 200,000MPa

Perpendicular Stress (MPa)

Rim Position	1.0g U/L	1.0g	1.1g	1.2g	1.3g	1.4g
180	21.43	27.03	33.55	33.38	33.51	25.31
150	1.06	1.94	1.62	1.89	2.21	1.77
120	1.89	8.30	7.84	8.09	8.17	8.19
90	1.89	12.09	11.45	11.81	12.46	12.81
45	-	-	-	-	-	-
0	-	-	-	-	-	-

Radial Strain (με)

Rim Position	1.0g U/L	1.0g	1.1g	1.2g	1.3g	1.4g
180	26.74	37.28	40.38	40.04	40.05	40.75
150	35.31	42.67	42.58	39.95	38.22	42.69
120	15.99	19.40	21.85	22.90	23.31	24.14
90	9.70	12.00	10.35	10.40	11.08	11.38
45	19.22	24.81	24.32	25.70	25.49	26.63
0	1.52	2.24	40.04	10.77	10.01	2.71

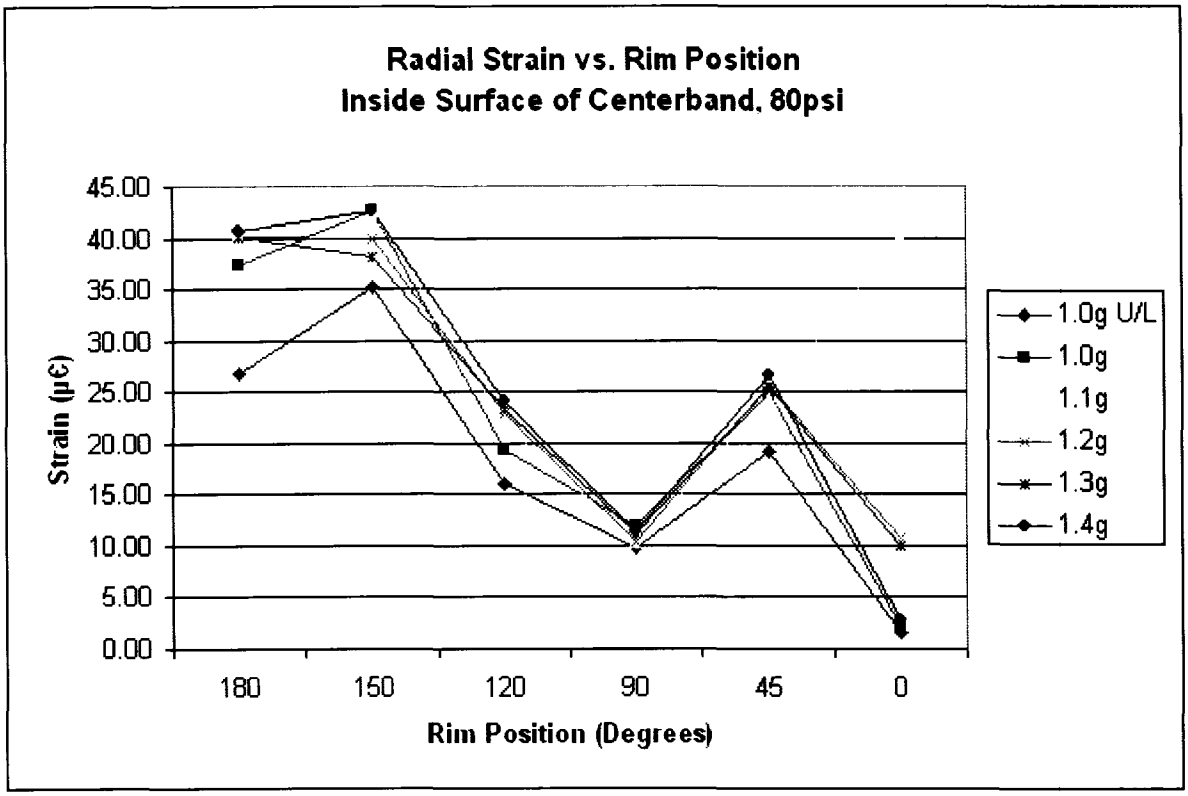

$\sigma = \varepsilon E$

where E = 200,000MPa

Radial Stress (MPa)

Rim Position	1.0g U/L	1.0g	1.1g	1.2g	1.3g	1.4g
180	5.35	7.46	8.08	8.01	8.01	8.15
150	7.06	8.53	8.52	7.99	7.64	8.54
120	3.20	3.88	4.37	4.58	4.66	4.83
90	1.94	2.40	2.07	2.08	2.22	2.28
45	3.84	4.96	4.86	5.14	5.10	5.33
0	0.30	0.45	8.01	2.15	2.00	0.54

Perpendicular Strain (με)

Rim Position	1.0g U/L	1.0g	1.1g	1.2g	1.3g	1.4g
180	539.43	419.24	994.67	661.93	1437.19	1023.94
150	13.64	14.68	17.06	17.64	20.66	23.05
120	7.41	19.15	16.89	20.94	22.40	21.97
90	14.84	693.60	1921.70	215.00	248.60	5924.24
45	2.63	4.13	5.64	4.88	5.45	5.45
0	3.43	14.14	14.69	17.77	19.80	20.99

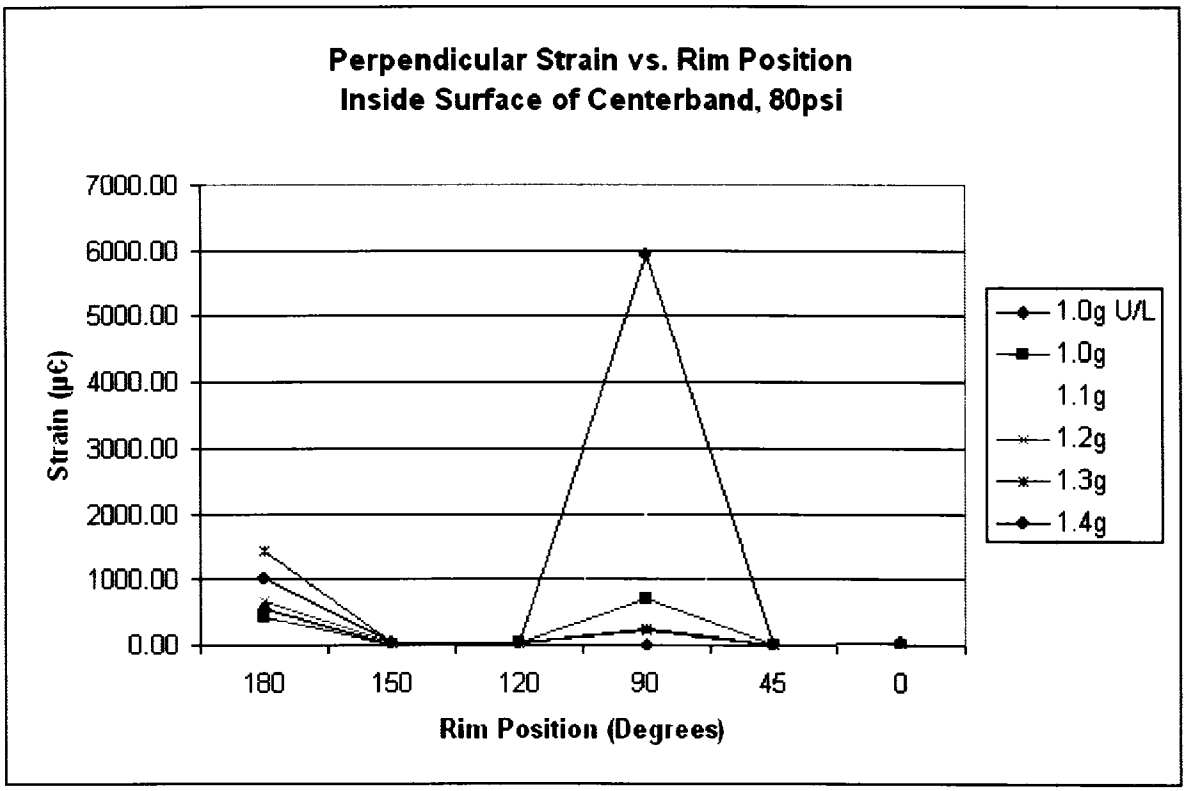

$\sigma = \varepsilon E$

where E = 200,000MPa

Perpendicular Stress (MPa)

Rim Position	1.0g U/L	1.0g	1.1g	1.2g	1.3g	1.4g
180	107.89	83.85	198.93	132.39	287.44	204.79
150	2.73	2.94	3.41	3.53	4.13	4.61
120	1.48	3.83	3.38	4.19	4.48	4.39
90	2.97	138.72	384.34	43.00	49.72	1184.85
45	0.53	0.83	1.13	0.98	1.09	1.09
0	0.69	2.83	2.94	3.55	3.96	4.20

Radial Strain (με)

Rim Position	1.0g U/L	1.0g	1.1g	1.2g	1.3g	1.4g
180	-	-	-	-	-	-
150	0.02	0.02	0.01	0.02	0.02	0.02
120	10.73	8.64	8.63	6.80	8.62	6.42
90	5.72	9.59	9.39	8.49	9.60	9.24
45	-	-	-	-	-	-
0	-	-	-	-	-	-

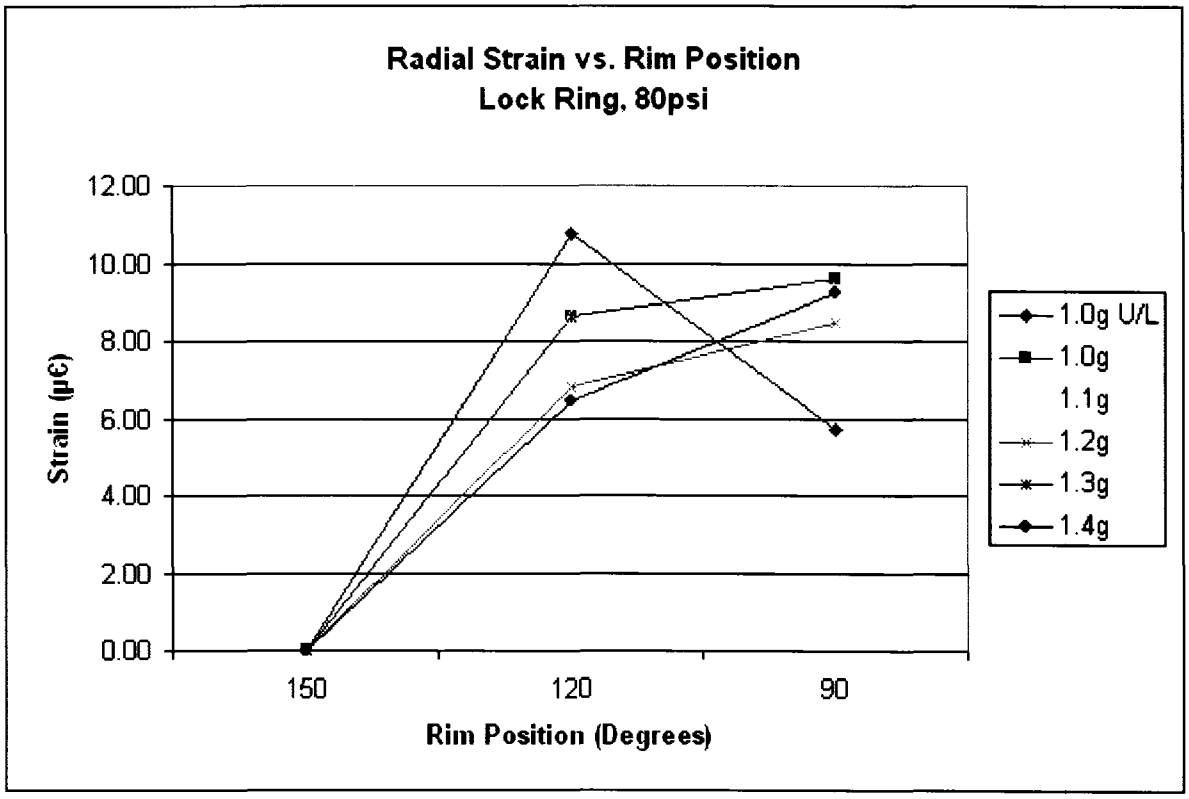

$\sigma = \varepsilon E$

where E = 200,000MPa

Radial Stress (MPa)

Rim Position	1.0g U/L	1.0g	1.1g	1.2g	1.3g	1.4g
180	-	-	-	-	-	-
150	0.00	0.00	0.00	0.00	0.00	0.00
120	2.15	1.73	1.73	1.36	1.72	1.28
90	1.14	1.92	1.88	1.70	1.92	1.85
45	-	-	-	-	-	-
0	-	-	-	-	-	-

Perpendicular Strain (με)

Rim Position	1.0g U/L	1.0g	1.1g	1.2g	1.3g	1.4g
180	-	-	-	-	-	-
150	14.35	21.25	23.34	22.42	22.26	21.98
120	9.96	19.16	26.68	23.46	24.77	21.96
90	1.90	1.70	38.20	10.00	10.00	2.50
45	-	-	-	-	-	-
0	-	-	-	-	-	-

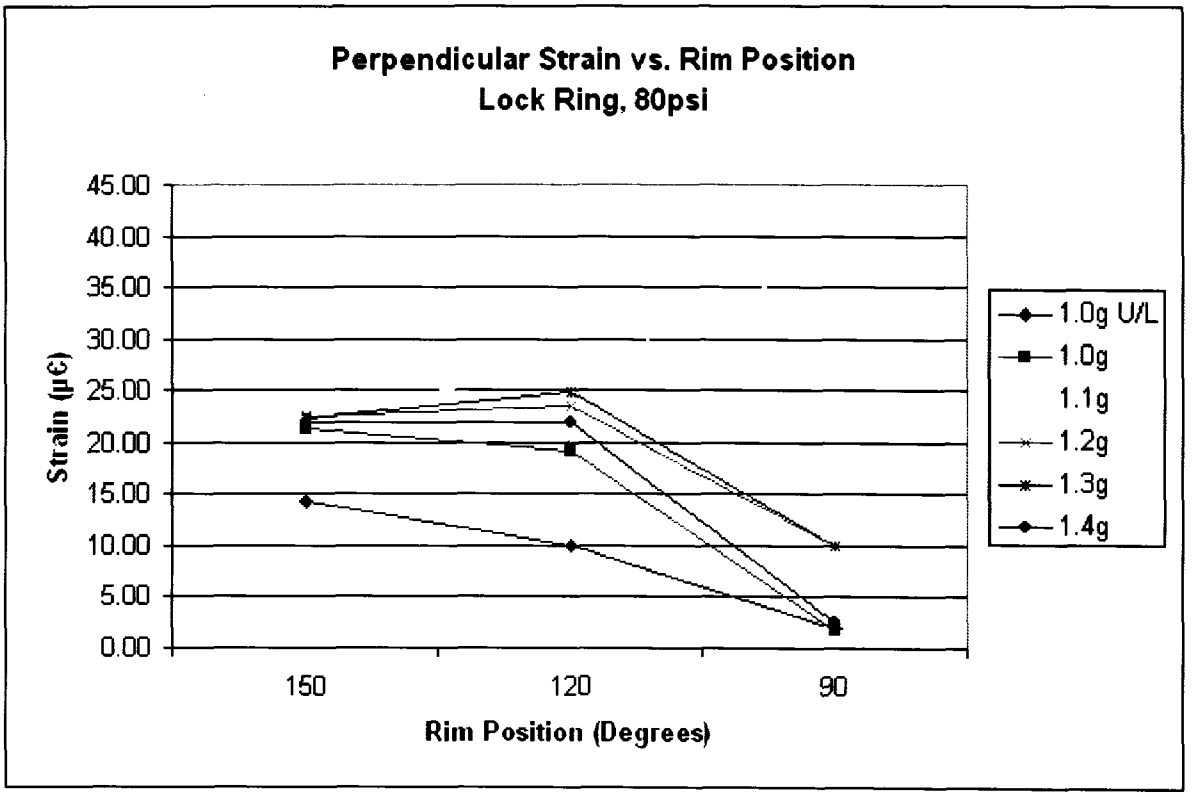

$\sigma = \varepsilon E$

where E = 200,000MPa

Perpendicular Stress (MPa)

Rim Position	1.0g U/L	1.0g	1.1g	1.2g	1.3g	1.4g
180	-	-	-	-	-	-
150	2.87	4.25	4.67	4.48	4.45	4.40
120	1.99	3.83	5.34	4.69	4.95	4.39
90	0.38	0.34	7.64	2.00	2.00	0.50
45	-	-	-	-	-	-
0	-	-	-	-	-	-

A.6 Filtered Test Results, 80psi Tire Pressure

Perpendicular Strain (με)

Rim Position	1.0g U/L	1.0g	1.1g	1.2g	1.3g	1.4g
180						
150	7.18	8.17	15.40	14.22	16.48	15.30
120	12.81	73.17	84.74	91.48	99.17	103.99
90	13.99	38.04	44.58	47.65	59.96	69.69
45	3.19	8.47	7.53	9.01	10.52	11.64
0	6.98	20.65	21.22	20.69	21.81	23.31

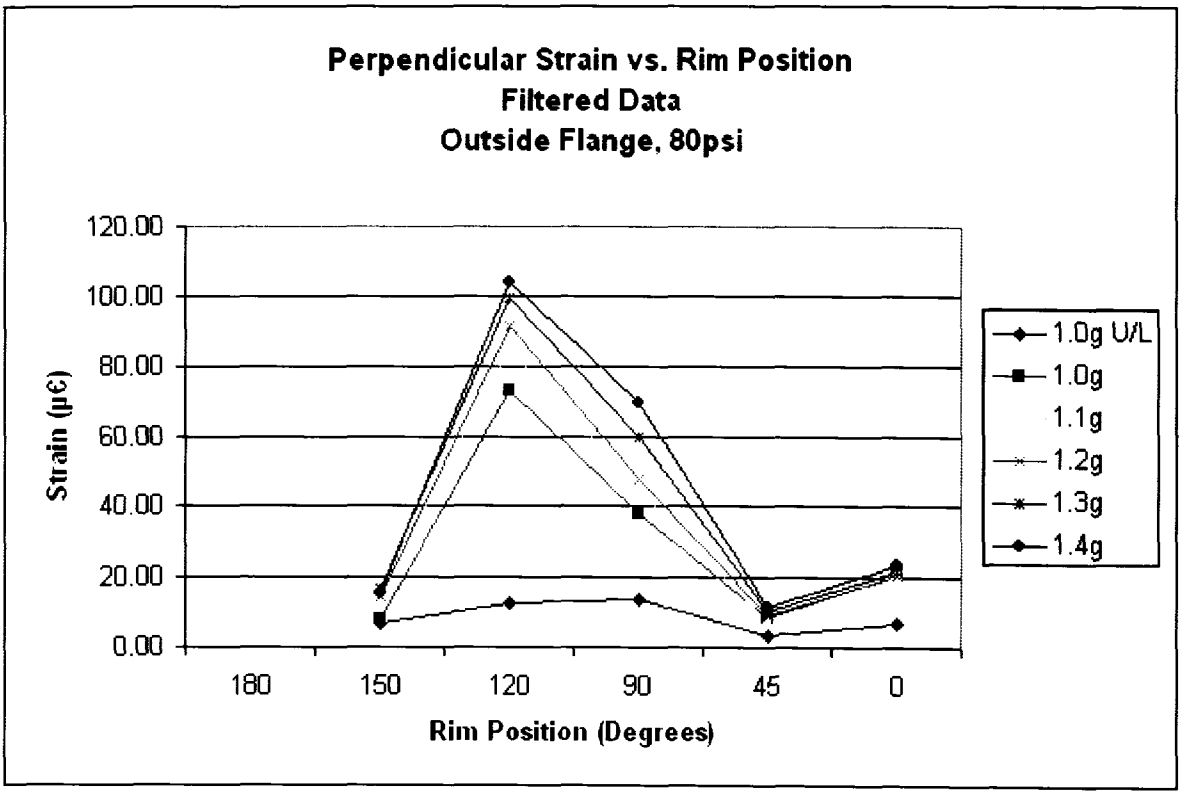

$\sigma = \varepsilon E$

where E = 200,000MPa

Perpendicular Stress (MPa)

Rim Position	1.0g U/L	1.0g	1.1g	1.2g	1.3g	1.4g
180	-	-	-	-	-	-
150	1.44	1.63	3.08	2.84	3.30	3.06
120	2.56	14.63	16.95	18.30	19.83	20.80
90	2.80	7.61	8.92	9.53	11.99	13.94
45	0.64	1.69	1.51	1.80	2.10	2.33
0	1.40	4.13	4.24	4.14	4.36	4.66

Perpendicular Strain (με)

Rim Position	1.0g U/L	1.0g	1.1g	1.2g	1.3g	1.4g
180						
150	13.64	14.68	17.06	17.64	20.66	23.05
120	7.41	19.15	16.89	20.94	22.40	21.97
90						
45	2.63	4.13	5.64	4.88	5.45	5.45
0	3.43	14.14	14.69	17.77	19.80	20.99

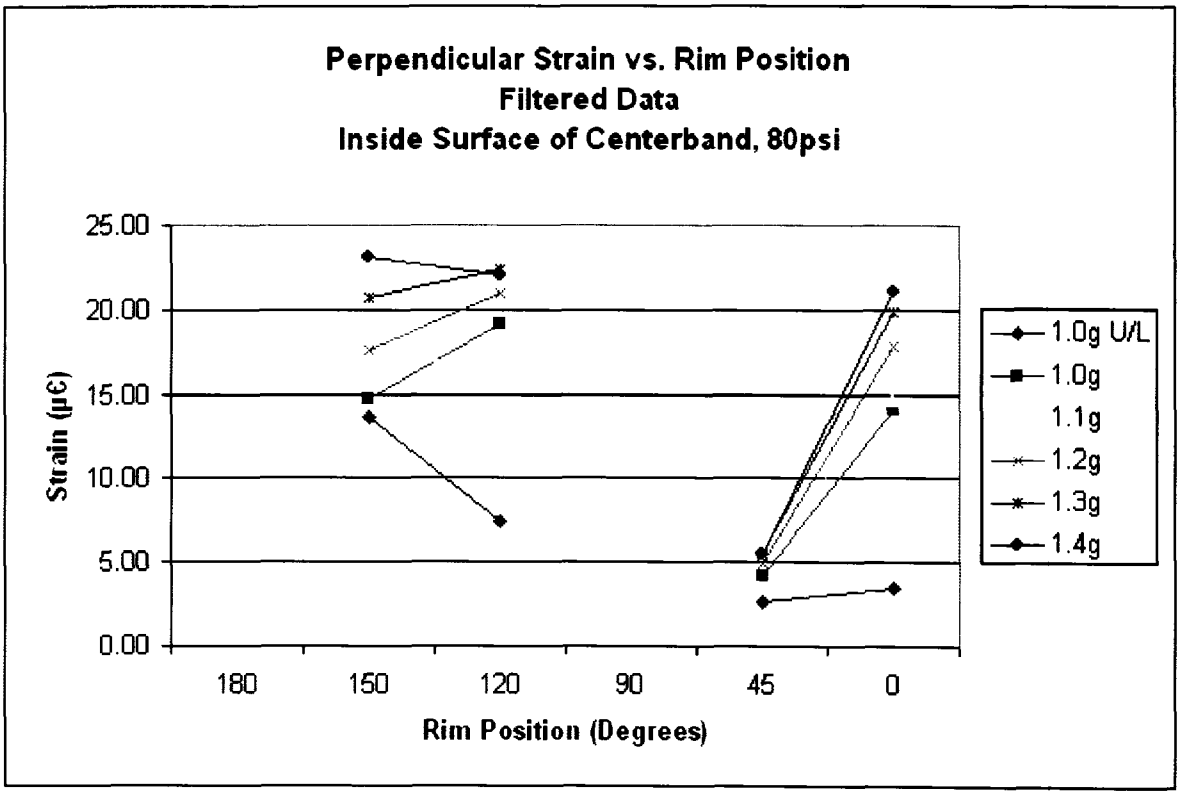

$\sigma = \varepsilon E$

where E = 200,000MPa

Perpendicular Stress (MPa)

Rim Position	1.0g U/L	1.0g	1.1g	1.2g	1.3g	1.4g
180	-	-	-	-	-	-
150	2.73	2.94	3.41	3.53	4.13	4.61
120	1.48	3.83	3.38	4.19	4.48	4.39
90	-	-	-	-	-	-
45	0.53	0.83	1.13	0.98	1.09	1.09
0	0.69	2.83	2.94	3.55	3.96	4.20

Appendix B Analysis and Calculations of Data

B.1 Analysis, Calculations and Equations, 100psi Tire Pressure

Outside Flange Stress/Strain Calcuations, 100psi

Radial Strain ($\mu\varepsilon$)

Tire Position	Load (g level) 1.0g U/L	1.0g	1.1g	1.2g	1.3g	1.4g	1.5g
180	51.44	82.58	116.08	134.40	185.21	207.51	238.56
150	14.27	32.71	50.09	61.19	79.98	92.08	110.13
120	3.51	20.44	25.46	29.12	37.56	41.10	47.64
90	4.89	9.76	12.24	14.66	22.74	24.24	33.62
45	23.46	11.30	15.18	16.49	20.83	23.52	28.57
0	17.50	43.19	47.75	53.13	66.79	74.26	84.36

Perpendicular Strain ($\mu\varepsilon$)

Tire Position	Load (g level) 1.0g U/L	1.0g	1.1g	1.2g	1.3g	1.4g	1.5g
180	-	-	-	-	-	-	-
150	14.27	15.22	12.63	12.06	16.48	17.14	20.84
120	21.24	66.83	79.33	89.08	115.55	124.47	143.12
90	16.91	32.03	38.48	43.77	71.46	75.39	106.16
45	4.51	5.80	4.86	3.98	4.67	6.04	8.12
0	14.47	13.15	15.61	16.73	20.69	23.32	26.85

$$TotalStrain = \sqrt{(RadialStrain)^2 + (PerpendicularStrain)^2}$$

$$y = mx + b$$

Total Strain ($\mu\varepsilon$)	Load (g level/kN) 1.0g U/L	1.0g	1.1g	From Test Data 1.2g	1.3g	1.4g	1.5g	Predicted from Graphed Data 2.0g	2.5g	3.0g	4.0g
Tire Position (Degrees)	180	410	450	490	530	570	610	820	1,025	1,230	1,640
180	51.44	82.58	116.08	134.40	185.21	207.51	238.56	405.42	567.22	729.03	1,052.64
150	20.18	36.08	51.65	62.37	81.86	93.67	112.09	189.35	266.30	343.26	497.16
120	21.53	69.89	83.31	93.72	121.50	131.08	150.84	235.89	320.20	404.52	573.15
90	17.61	33.48	40.37	46.16	74.99	79.19	111.35	182.67	260.96	339.25	495.83
45	23.89	12.70	15.94	16.96	21.35	24.29	29.70	45.47	62.22	78.97	112.47
0	22.71	45.15	50.24	55.70	69.92	77.83	88.53	134.06	180.02	225.98	317.90

$$\sigma = \varepsilon E$$

where E = 200,000MPa

Total Stress (MPa)	Load (g level/kN) 1.0g U/L	1.0g	1.1g	From Test Data 1.2g	1.3g	1.4g	1.5g	Predicted from Graphed Data 2.0g	2.5g	3.0g	4.0g
Tire Position (Degrees)	180	410	450	490	530	570	610	820	1,025	1,230	1,640
180	10.3	16.5	23.2	26.9	37.0	41.5	47.7	81.1	113.4	145.8	210.5
150	4.0	7.2	10.3	12.5	16.3	18.7	22.4	37.9	53.3	68.7	99.4
120	4.3	14.0	16.7	18.7	24.3	26.2	30.2	47.2	64.0	80.9	114.6
90	3.5	6.7	8.1	9.2	15.0	15.8	22.3	36.5	52.2	67.8	99.2
45	4.8	2.5	3.2	3.4	4.3	4.9	5.9	9.1	12.4	15.8	22.5
0	4.5	9.0	10.0	11.1	14.0	15.6	17.7	26.8	36.0	45.2	63.6

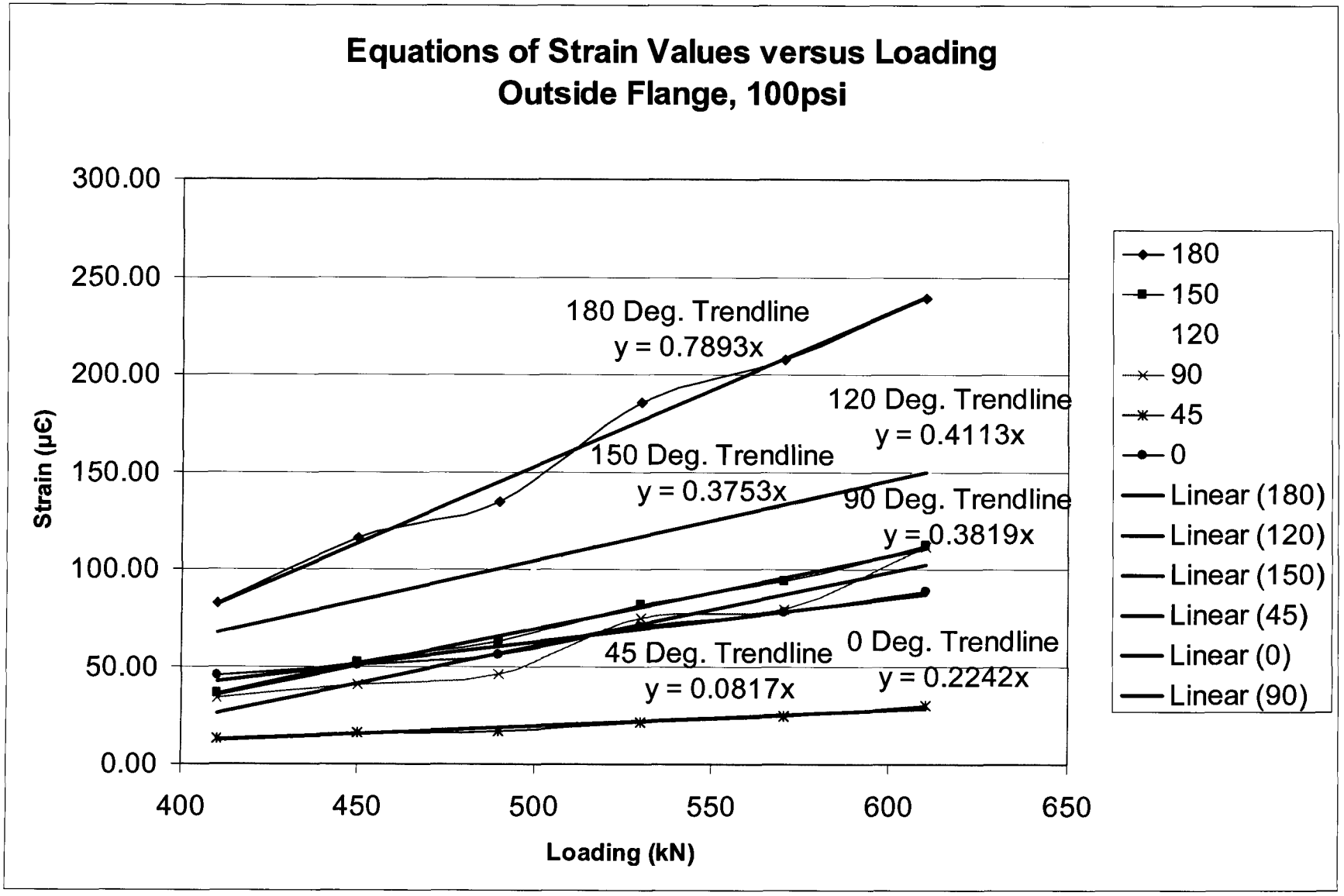

Inside Flange Stress/Strain Calcuations, 100psi

Radial Strain ($\mu\varepsilon$)

Tire Position	Load (g level) 1.0g U/L	1.0g	1.1g	1.2g	1.3g	1.4g	1.5g
180	13.77	23.11	25.18	26.89	37.38	32.89	40.22
150	9.31	14.65	11.77	10.98	13.86	15.00	17.82
120	-	-	-	-	-	-	-
90	8.97	4.71	13.93	7.47	4.70	8.95	4.45
45	9.38	8.91	9.46	10.32	9.47	10.15	11.74
0	4.20	6.67	6.92	6.94	7.89	7.19	8.64

Perpendicular Strain ($\mu\varepsilon$)

Tire Position	Load (g level) 1.0g U/L	1.0g	1.1g	1.2g	1.3g	1.4g	1.5g
180	27.44	69.69	71.93	78.67	93.33	101.27	112.68
150	27.52	40.05	34.87	33.16	45.24	48.16	57.30
120	49.67	36.35	40.23	43.02	40.03	41.63	42.15
90	25.82	18.04	15.86	13.31	13.07	13.59	14.92
45	32.88	29.31	30.43	30.79	32.31	32.31	33.45
0	11.11	15.80	16.54	16.89	16.75	16.58	18.46

$$TotalStrain = \sqrt{(RadialStrain)^2 + (PerpendicularStrain)^2}$$

$$y = mx + b$$

Total Strain ($\mu\varepsilon$)	Load (g level/kN) 1.0g U/L	From Test Data 1.0g	1.1g	1.2g	1.3g	1.4g	1.5g	Predicted from Graphed Data 2.0g	2.5g	3.0g	4.0g
Tire Position (Degrees)	180	410	450	490	530	570	610	820	1,025	1,230	1,640
180	30.70	73.42	76.21	83.14	100.54	106.47	119.65	168.40	218.09	267.78	367.17
150	29.05	42.64	36.81	34.93	47.32	50.45	60.01	76.40	96.92	117.44	158.48
120	49.67	36.35	40.23	43.02	40.03	41.63	42.15	47.27	51.70	56.13	64.98
90	27.33	18.65	21.11	15.26	13.88	16.27	15.56	46.47	51.04	55.61	64.76
45	34.19	30.63	31.86	32.48	33.67	33.87	35.45	25.36	26.46	27.57	29.79
0	11.88	17.15	17.93	18.26	18.51	18.08	20.38	22.09	24.55	27.01	31.93

$$\sigma = \varepsilon E$$ where E = 200,000MPa

Total Stress (MPa)	Load (g level/kN) 1.0g U/L	From Test Data 1.0g	1.1g	1.2g	1.3g	1.4g	1.5g	Predicted from Graphed Data 2.0g	2.5g	3.0g	4.0g
Tire Position (Degrees)	180	410	450	490	530	570	610	820	1,025	1,230	1,640
180	6.1	14.7	15.2	16.6	20.1	21.3	23.9	33.7	43.6	53.6	73.4
150	5.8	8.5	7.4	7.0	9.5	10.1	12.0	15.3	19.4	23.5	31.7
120	9.9	7.3	8.0	8.6	8.0	8.3	8.4	9.5	10.3	11.2	13.0
90	5.5	3.7	4.2	3.1	2.8	3.3	3.1	9.3	10.2	11.1	13.0
45	6.8	6.1	6.4	6.5	6.7	6.8	7.1	5.1	5.3	5.5	6.0
0	2.4	3.4	3.6	3.7	3.7	3.6	4.1	4.4	4.9	5.4	6.4

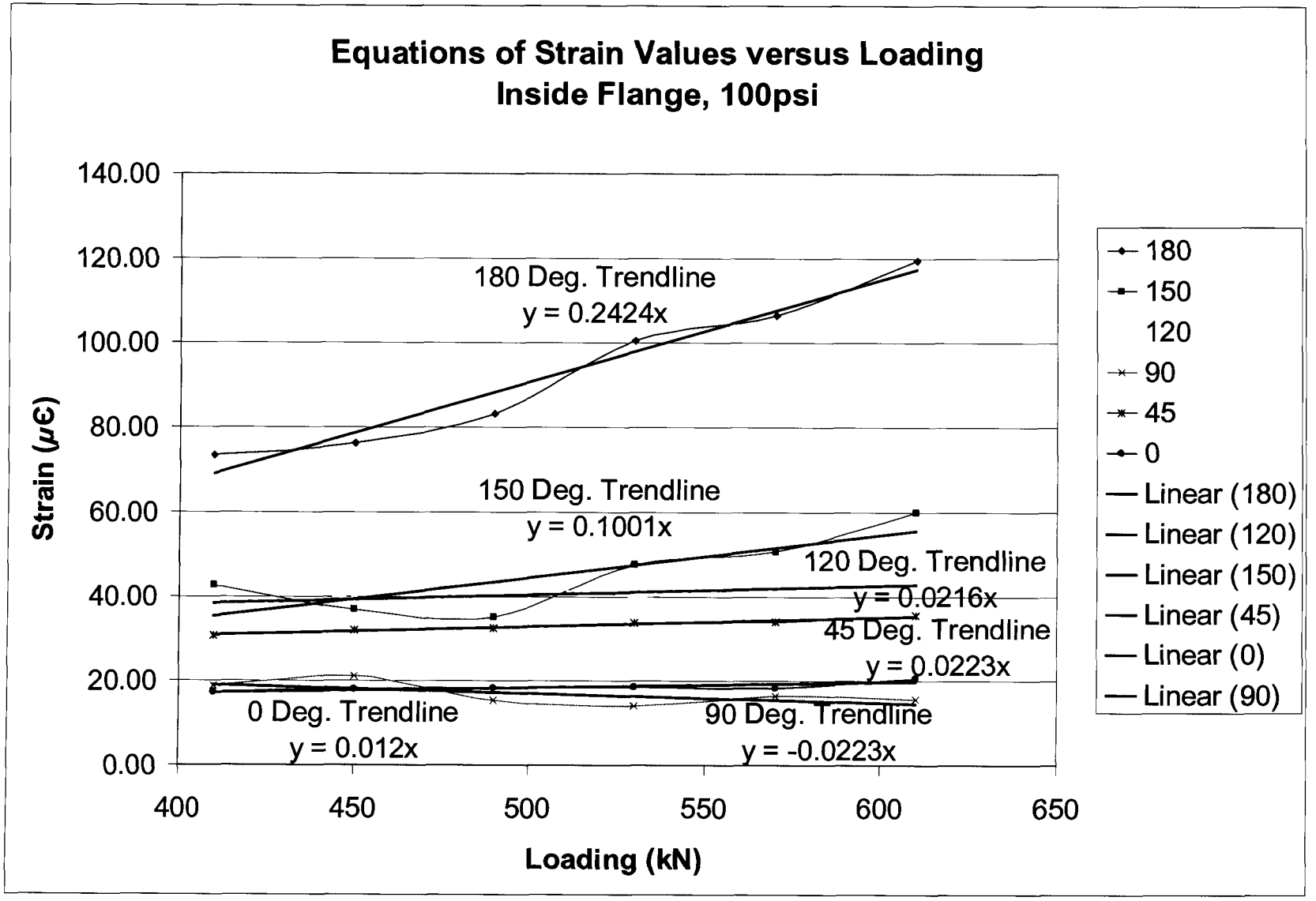

Outside Edge of Centerband Stress/Strain Calcuations, 100psi

Radial Strain ($\mu\varepsilon$)

Tire Position	Load (g level) 1.0g U/L	1.0g	1.1g	1.2g	1.3g	1.4g	1.5g
180	30.76	94.06	89.54	79.95	86.33	72.49	62.53
150	16.65	28.12	25.39	25.33	26.14	27.23	25.86
120	1.93	6.25	2.92	3.58	3.99	4.66	5.45
90	4.03	22.25	23.99	25.56	29.78	31.36	33.45
45	-	-	-	-	-	-	-
0	-	-	-	-	-	-	-

Perpendicular Strain ($\mu\varepsilon$)

Tire Position	Load (g level) 1.0g U/L	1.0g	1.1g	1.2g	1.3g	1.4g	1.5g
180	176.60	291.50	191.29	217.01	209.16	205.47	223.56
150	8.86	16.21	14.62	15.42	15.68	13.49	14.41
120	16.42	17.94	24.11	28.94	35.51	42.41	46.39
90	22.19	34.98	43.49	47.21	60.90	71.87	75.77
45	-	-	-	-	-	-	-
0	-	-	-	-	-	-	-

$$TotalStrain = \sqrt{(RadialStrain)^2 + (PerpendicularStrain)^2}$$

$$y = mx + b$$

Total Strain ($\mu\varepsilon$)

Tire Position (Degrees)	Load (g level/kN) 1.0g U/L 180	1.0g 410	1.1g 450	From Test Data 1.2g 490	1.3g 530	1.4g 570	1.5g 610	Predicted from Graphed Data 2.0g 820	2.5g 1,025	3.0g 1,230	4.0g 1,640
180	179.26	306.30	211.21	231.27	226.27	217.88	232.14	-	-	-	-
150	18.86	32.45	29.30	29.65	30.48	30.39	29.60	40.00	41.49	42.99	45.98
120	16.53	19.00	24.28	29.16	35.74	42.67	46.71	77.30	106.64	135.97	194.64
90	22.56	41.46	49.67	53.68	67.79	78.41	82.82	130.32	175.30	220.27	310.23
45	-	-	-	-	-	-	-	-	-	-	-
0	-	-	-	-	-	-	-	-	-	-	-

$\sigma = \varepsilon E$ where E = 200,000MPa

Total Stress (MPa)

Tire Position (Degrees)	Load (g level/kN) 1.0g U/L 180	1.0g 410	1.1g 450	From Test Data 1.2g 490	1.3g 530	1.4g 570	1.5g 610	Predicted from Graphed Data 2.0g 820	2.5g 1,025	3.0g 1,230	4.0g 1,640
180	35.9	61.3	42.2	46.3	45.3	43.6	46.4	-	-	-	-
150	3.8	6.5	5.9	5.9	6.1	6.1	5.9	8.0	8.3	8.6	9.2
120	3.3	3.8	4.9	5.8	7.1	8.5	9.3	15.5	21.3	27.2	38.9
90	4.5	8.3	9.9	10.7	13.6	15.7	16.6	26.1	35.1	44.1	62.0
45	-	-	-	-	-	-	-	-	-	-	-
0	-	-	-	-	-	-	-	-	-	-	-

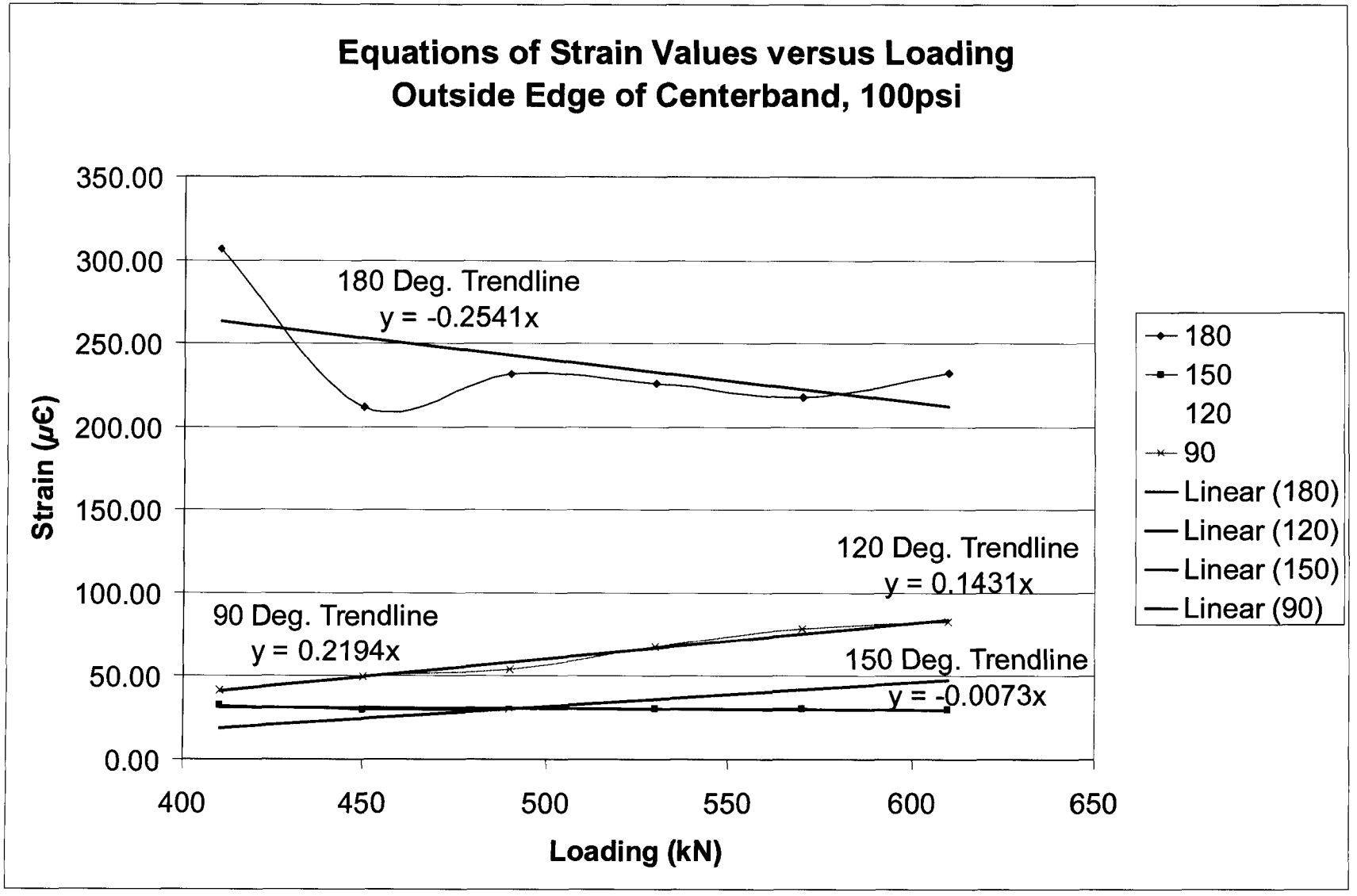

Inside Surface of Centerband Stress/Strain Calcuations, 100psi

Radial Strain ($\mu\varepsilon$)

Tire Position	Load (g level) 1.0g U/L	1.0g	1.1g	1.2g	1.3g	1.4g	1.5g
180	27.75	41.55	45.08	45.04	46.37	45.55	46.31
150	37.94	44.88	43.43	44.70	43.09	43.57	41.51
120	16.62	22.72	23.28	23.38	24.25	24.70	25.54
90	11.03	12.86	11.85	11.60	10.54	11.20	14.11
45	20.20	23.29	25.09	27.15	26.13	27.30	28.55
0	2.63	11.67	5.07	2.77	39.28	5.56	31.27

Perpendicular Strain ($\mu\varepsilon$)

Tire Position	Load (g level) 1.0g U/L	1.0g	1.1g	1.2g	1.3g	1.4g	1.5g
180	-	-	-	-	-	-	-
150	17.76	17.96	17.11	20.71	23.68	28.13	32.66
120	19.16	15.46	20.16	19.50	20.77	21.78	24.04
90	-	-	-	-	-	-	-
45	7.70	5.26	4.51	4.32	5.26	6.01	6.95
0	7.60	10.23	13.00	15.09	19.01	21.54	24.46

$$TotalStrain = \sqrt{(RadialStrain)^2 + (PerpendicularStrain)^2}$$

$$y = mx + b$$

Total Strain ($\mu\varepsilon$)

Tire Position (Degrees)	Load (g level/kN) 1.0g U/L	1.0g	1.1g	1.2g	1.3g	1.4g	1.5g	Predicted from Graphed Data 2.0g	2.5g	3.0g	4.0g
	180	410	450	490	530	570	610	820	1,025	1,230	1,640
180	27.75	41.55	45.08	45.04	46.37	45.55	46.31	50.82	54.70	58.57	66.32
150	41.89	48.34	46.67	49.26	49.17	51.86	52.82	58.03	63.57	69.10	80.17
120	25.36	27.48	30.79	30.45	31.93	32.93	35.08	41.62	48.35	55.07	68.52
90	11.03	12.86	11.85	11.60	10.54	11.20	14.11	12.75	13.22	13.69	14.63
45	21.62	23.87	25.49	27.49	26.65	27.95	29.38	34.40	39.40	44.40	54.40
0	8.04	15.52	13.95	15.34	43.64	22.25	39.70	34.62	45.34	56.06	77.50

$$\sigma = \varepsilon E$$ where E = 200,000MPa

Total Stress (MPa)

Tire Position (Degrees)	Load (g level/kN) 1.0g U/L	1.0g	1.1g	1.2g	1.3g	1.4g	1.5g	Predicted from Graphed Data 2.0g	2.5g	3.0g	4.0g
	180	410	450	490	530	570	610	820	1,025	1,230	1,640
180	5.6	8.3	9.0	9.0	9.3	9.1	9.3	10.2	10.9	11.7	13.3
150	8.4	9.7	9.3	9.9	9.8	10.4	10.6	11.6	12.7	13.8	16.0
120	5.1	5.5	6.2	6.1	6.4	6.6	7.0	8.3	9.7	11.0	13.7
90	2.2	2.6	2.4	2.3	2.1	2.2	2.8	2.5	2.6	2.7	2.9
45	4.3	4.8	5.1	5.5	5.3	5.6	5.9	6.9	7.9	8.9	10.9
0	1.6	3.1	2.8	3.1	8.7	4.4	7.9	6.9	9.1	11.2	15.5

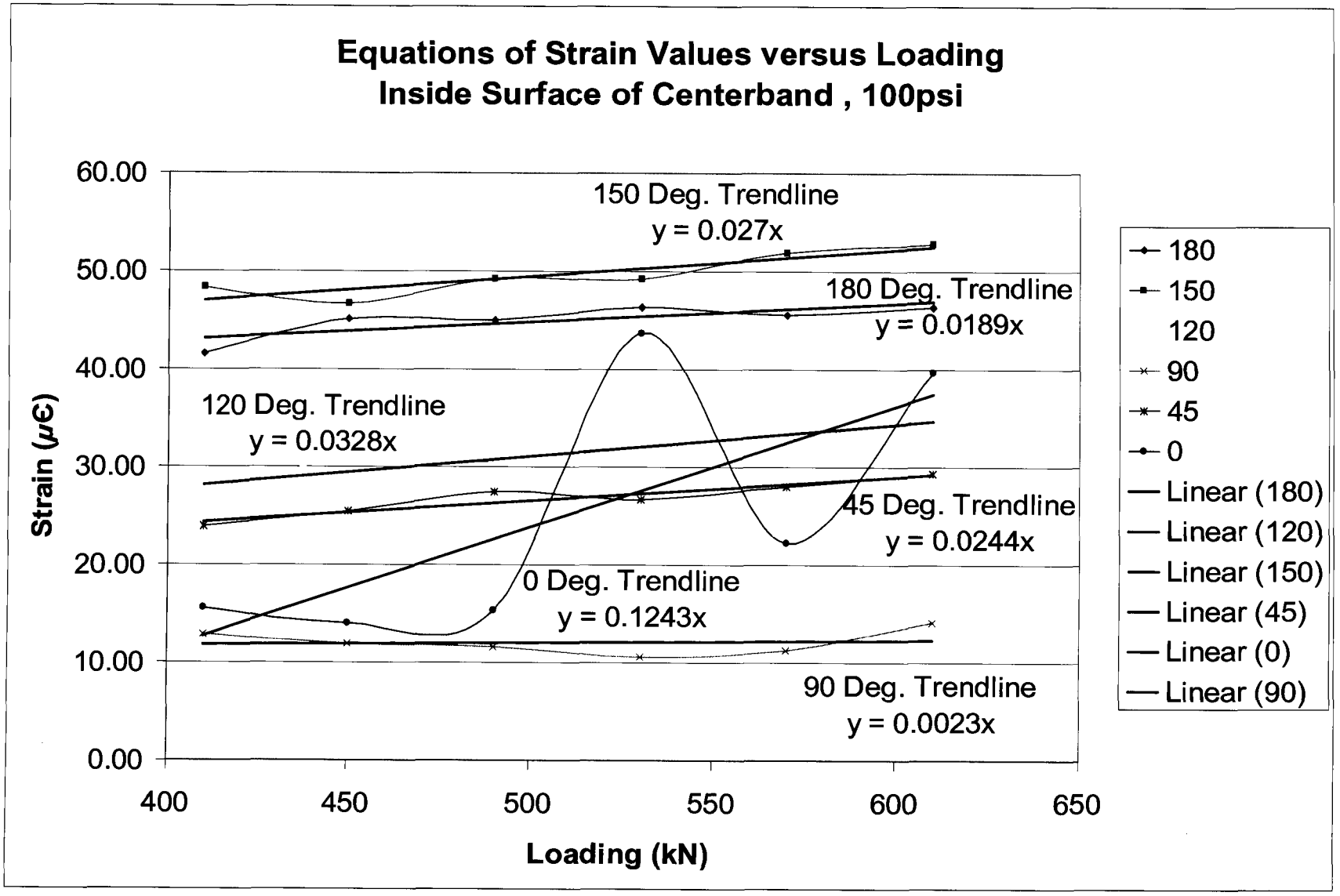

Outside Flange Stress/Strain Calcuations, 90psi

Radial Strain ($\mu\varepsilon$)

Tire Position	Load (g level) 1.0g U/L	1.0g	1.1g	1.2g	1.3g	1.4g	1.5g
180	38.42	159.41	159.58	174.72	198.83	199.71	219.44
150	18.05	68.99	64.15	72.73	85.97	92.70	103.78
120	4.35	23.60	27.39	31.47	36.65	38.75	45.27
90	4.50	11.46	12.58	15.97	21.22	23.10	31.18
45	12.00	24.42	19.56	22.36	28.42	27.99	30.70
0	17.87	52.60	55.55	60.73	70.64	70.85	80.40

Perpendicular Strain ($\mu\varepsilon$)

Tire Position	Load (g level) 1.0g U/L	1.0g	1.1g	1.2g	1.3g	1.4g	1.5g
180	-	-	-	-	-	-	-
150	7.74	7.46	11.46	12.83	16.62	15.68	20.48
120	11.59	72.17	83.27	94.16	110.44	114.66	135.40
90	14.16	29.29	34.78	43.68	64.03	67.22	98.23
45	3.17	5.99	6.96	8.29	9.27	10.54	12.10
0	6.75	16.53	17.48	20.09	24.02	22.87	26.49

$$TotalStrain = \sqrt{(RadialStrain)^2 + (PerpendicularStrain)^2}$$

$$y = mx + b$$

Total Strain ($\mu\varepsilon$)

Tire Position (Degrees)	Load (g level/kN) 1.0g U/L	1.0g	1.1g	From Test Data 1.2g	1.3g	1.4g	1.5g	Predicted from Graphed Data 2.0g	2.5g	3.0g	4.0g
	180	410	450	490	530	570	610	820	1,025	1,230	1,640
180	38.42	159.41	159.58	174.72	198.83	199.71	219.44	283.73	348.83	413.94	544.16
150	19.64	69.39	65.17	73.85	87.56	94.02	105.78	145.12	186.45	227.78	310.43
120	12.38	75.93	87.66	99.28	116.36	121.03	142.77	207.11	273.20	339.29	471.48
90	14.86	31.46	36.98	46.51	67.45	71.08	103.06	165.94	236.40	306.86	447.78
45	12.41	25.14	20.76	23.85	29.89	29.91	33.00	43.21	53.87	64.53	85.85
0	19.10	55.14	58.23	63.96	74.61	74.45	84.65	114.27	144.55	174.83	235.39

$\sigma = \varepsilon E$ where E = 200,000MPa

Total Stress (MPa)

Tire Position (Degrees)	Load (g level/kN) 1.0g U/L	1.0g	1.1g	From Test Data 1.2g	1.3g	1.4g	1.5g	Predicted from Graphed Data 2.0g	2.5g	3.0g	4.0g
	180	410	450	490	530	570	610	820	1,025	1,230	1,640
180	7.7	31.9	31.9	34.9	39.8	39.9	43.9	56.7	69.8	82.8	108.8
150	3.9	13.9	13.0	14.8	17.5	18.8	21.2	29.0	37.3	45.6	62.1
120	2.5	15.2	17.5	19.9	23.3	24.2	28.6	41.4	54.6	67.9	94.3
90	3.0	6.3	7.4	9.3	13.5	14.2	20.6	33.2	47.3	61.4	89.6
45	2.5	5.0	4.2	4.8	6.0	6.0	6.6	8.6	10.8	12.9	17.2
0	3.8	11.0	11.6	12.8	14.9	14.9	16.9	22.9	28.9	35.0	47.1

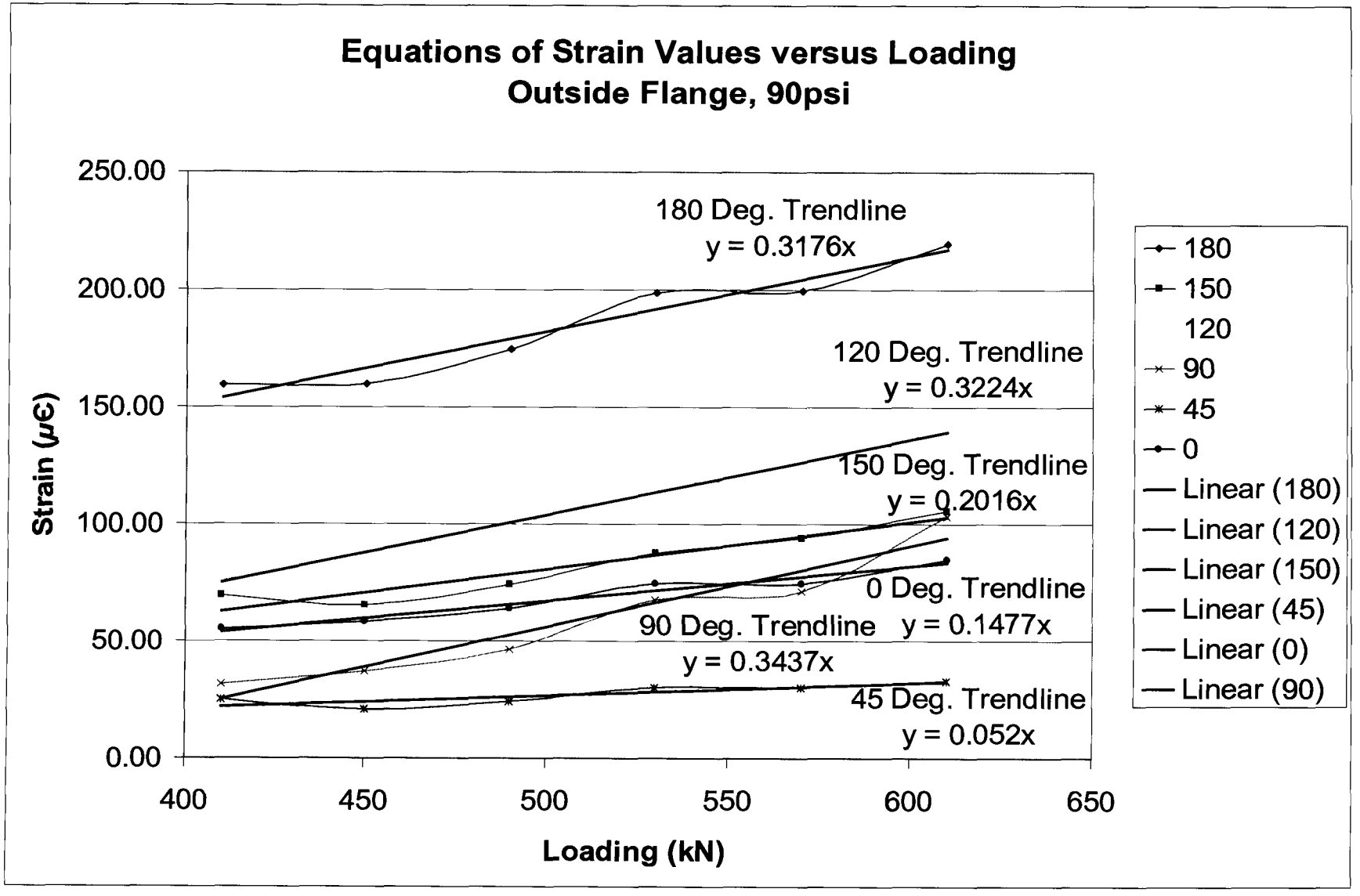

Inside Flange Stress/Strain Calcuations, 90psi

Radial Strain ($\mu\varepsilon$)

Tire Position	Load (g level) 1.0g U/L	1.0g	1.1g	1.2g	1.3g	1.4g	1.5g
180	10.68	21.53	30.20	26.26	29.38	32.68	35.70
150	7.79	9.01	9.17	9.77	12.03	12.55	15.17
120	10.73	15.35	12.23	92.84	87.15	17.40	15.40
90	4.62	4.55	5.82	7.72	6.67	6.23	5.57
45	7.55	9.58	9.47	9.30	9.42	9.18	9.06
0	4.20	6.01	6.35	6.79	7.40	7.73	8.43

Perpendicular Strain ($\mu\varepsilon$)

Tire Position	Load (g level) 1.0g U/L	1.0g	1.1g	1.2g	1.3g	1.4g	1.5g
180	24.62	63.67	70.27	77.00	87.54	95.87	101.25
150	24.14	27.67	27.58	32.31	40.06	41.55	49.67
120	31.08	37.61	37.55	36.90	37.62	36.61	37.16
90	11.10	13.27	13.15	12.46	14.74	13.71	13.34
45	22.37	28.74	28.18	27.61	29.12	27.63	27.41
0	10.03	14.42	15.07	16.86	18.82	18.76	19.89

$$TotalStrain = \sqrt{(RadialStrain)^2 + (PerpendicularStrain)^2}$$

$$y = mx + b$$

Total Strain ($\mu\varepsilon$)	Load (g level/kN)			From Test Data				Predicted from Graphed Data			
	1.0g U/L	1.0g	1.1g	1.2g	1.3g	1.4g	1.5g	2.0g	2.5g	3.0g	4.0g
Tire Position (Degrees)	180	410	450	490	530	570	610	820	1,025	1,230	1,640
180	26.84	67.21	76.49	81.35	92.34	101.29	107.36	151.04	192.94	234.84	318.65
150	25.37	29.09	29.06	33.75	41.83	43.41	51.94	74.79	99.00	123.22	171.64
120	32.88	40.62	39.49	99.90	94.93	40.54	40.22	39.63	39.90	40.16	40.70
90	12.02	14.03	14.38	14.66	16.18	15.06	14.45	16.08	16.92	17.76	19.45
45	23.60	30.29	29.73	29.14	30.60	29.12	28.87	32.27	32.26	32.26	32.25
0	10.87	15.62	16.35	18.18	20.22	20.29	21.60	28.36	34.76	41.15	53.94

$\sigma = \varepsilon E$ where E = 200,000MPa

Total Stress (MPa)	Load (g level/kN)			From Test Data				Predicted from Graphed Data			
	1.0g U/L	1.0g	1.1g	1.2g	1.3g	1.4g	1.5g	2.0g	2.5g	3.0g	4.0g
Tire Position (Degrees)	180	410	450	490	530	570	610	820	1,025	1,230	1,640
180	5.4	13.4	15.3	16.3	18.5	20.3	21.5	30.2	38.6	47.0	63.7
150	5.1	5.8	5.8	6.7	8.4	8.7	10.4	15.0	19.8	24.6	34.3
120	6.6	8.1	7.9	20.0	19.0	8.1	8.0	7.9	8.0	8.0	8.1
90	2.4	2.8	2.9	2.9	3.2	3.0	2.9	3.2	3.4	3.6	3.9
45	4.7	6.1	5.9	5.8	6.1	5.8	5.8	6.5	6.5	6.5	6.5
0	2.2	3.1	3.3	3.6	4.0	4.1	4.3	5.7	7.0	8.2	10.8

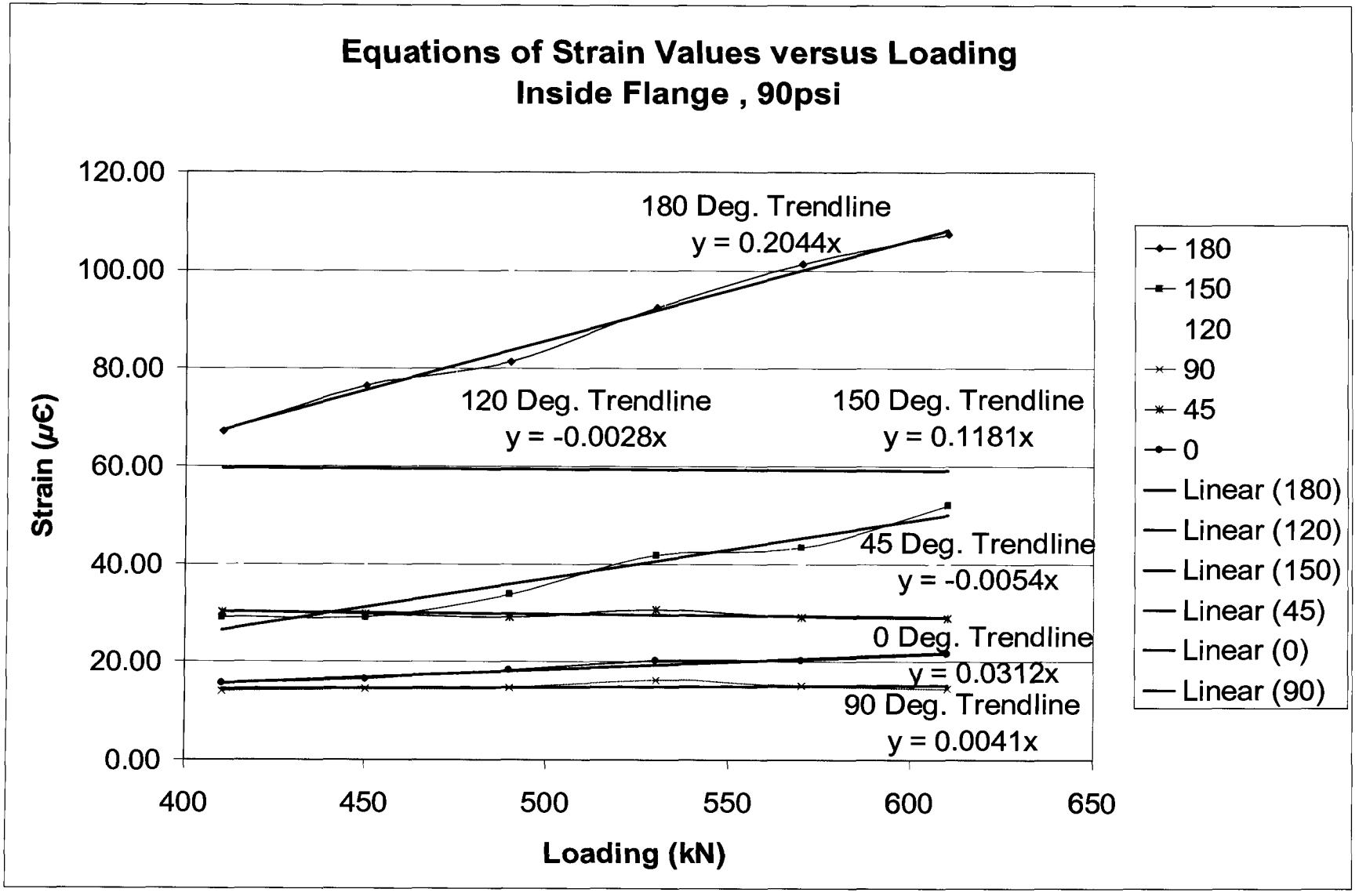

Outside Edge of Centerband Stress/Strain Calcuations, 90psi

Radial Strain ($\mu\varepsilon$)

Tire Position	Load (g level) 1.0g U/L	1.0g	1.1g	1.2g	1.3g	1.4g	1.5g
180	22.08	44.54	46.41	44.83	53.05	41.46	35.72
150	3.50	24.06	23.51	24.17	6.00	3.50	4.70
120	2.39	4.37	4.63	5.97	6.11	6.64	6.59
90	3.05	20.64	19.52	21.89	27.84	27.17	30.59
45	-	-	-	-	-	-	-
0	-	-	-	-	-	-	-

Perpendicular Strain ($\mu\varepsilon$)

Tire Position	Load (g level) 1.0g U/L	1.0g	1.1g	1.2g	1.3g	1.4g	1.5g
180	-	-	-	-	-	-	-
150	5.49	10.16	9.15	8.79	10.02	10.95	13.66
120	9.19	39.85	38.86	40.95	44.82	46.10	48.41
90	9.27	58.75	52.93	58.98	70.27	70.75	76.51
45	-	-	-	-	-	-	-
0	-	-	-	-	-	-	-

$$TotalStrain = \sqrt{(RadialStrain)^2 + (PerpendicularStrain)^2}$$

$$y = mx + b$$

Total Strain ($\mu\varepsilon$)

	Load (g level/kN) 1.0g U/L	1.0g	1.1g	From Test Data 1.2g	1.3g	1.4g	1.5g	Predicted from Graphed Data 2.0g	2.5g	3.0g	4.0g
Tire Position (Degrees)	180	410	450	490	530	570	610	820	1,025	1,230	1,640
180	22.08	44.54	46.41	44.83	53.05	41.46	35.72	33.12	25.70	18.28	3.44
150	6.51	26.11	25.23	25.72	11.68	11.50	14.45	6.01	22.64	39.26	72.52
120	9.50	40.09	39.14	41.39	45.24	46.58	48.86	59.05	69.30	79.55	100.05
90	9.76	62.27	56.42	62.91	75.58	75.79	82.40	107.15	132.24	157.33	207.52
45	-	-	-	-	-	-	-	-	-	-	-
0	-	-	-	-	-	-	-	-	-	-	-

$\sigma = \varepsilon E$ where E = 200,000MPa

Total Stress (MPa)

	Load (g level/kN) 1.0g U/L	1.0g	1.1g	From Test Data 1.2g	1.3g	1.4g	1.5g	Predicted from Graphed Data 2.0g	2.5g	3.0g	4.0g
Tire Position (Degrees)	180	410	450	490	530	570	610	820	1,025	1,230	1,640
180	4.4	8.9	9.3	9.0	10.6	8.3	7.1	6.6	5.1	3.7	0.7
150	1.3	5.2	5.0	5.1	2.3	2.3	2.9	1.2	4.5	7.9	14.5
120	1.9	8.0	7.8	8.3	9.0	9.3	9.8	11.8	13.9	15.9	20.0
90	2.0	12.5	11.3	12.6	15.1	15.2	16.5	21.4	26.4	31.5	41.5
45	-	-	-	-	-	-	-	-	-	-	-
0	-	-	-	-	-	-	-	-	-	-	-

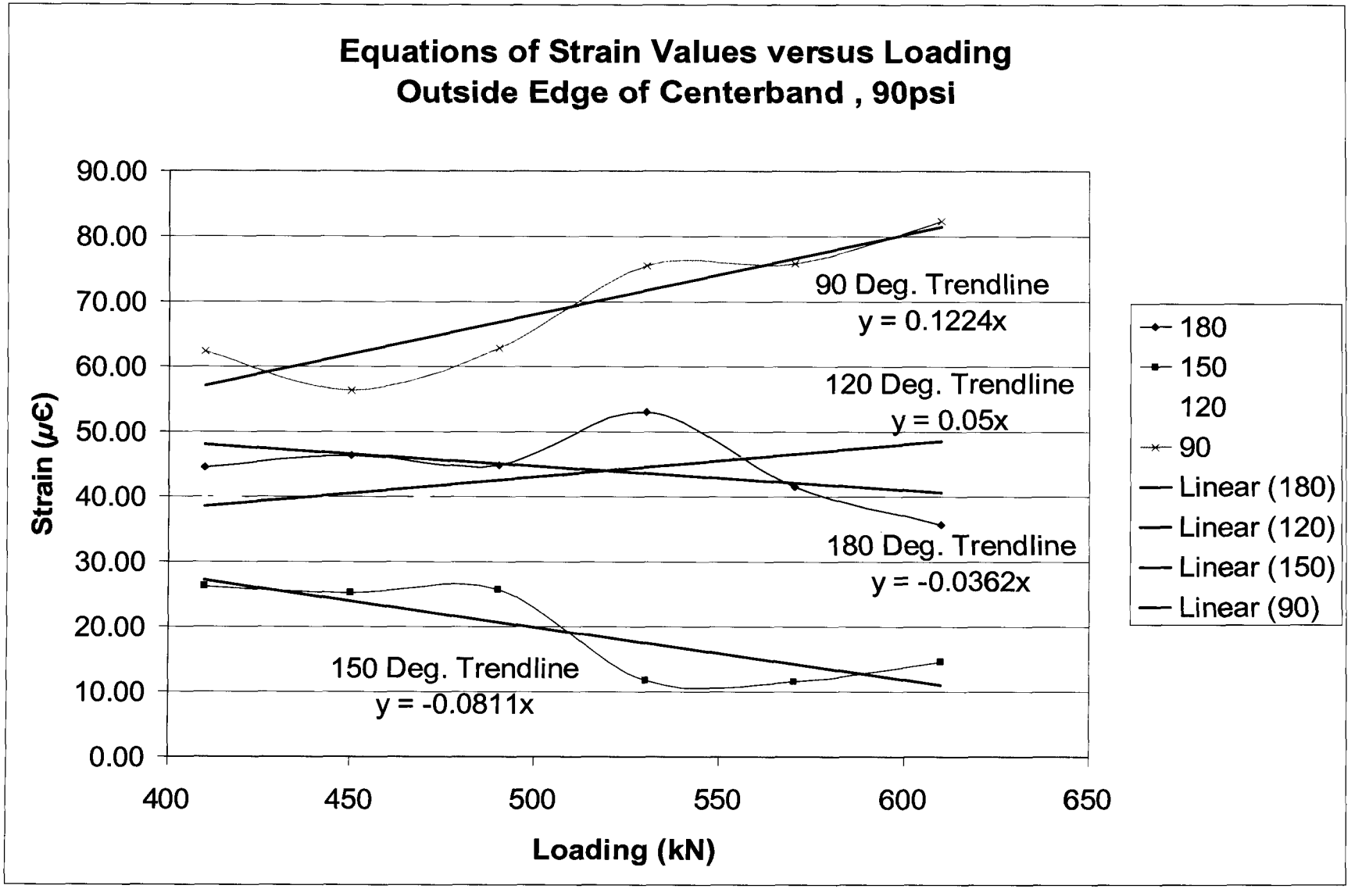

Inside Surface of Centerband Stress/Strain Calcuations, 90psi

Radial Strain ($\mu\varepsilon$)

Tire Position	Load (g level) 1.0g U/L	1.0g	1.1g	1.2g	1.3g	1.4g	1.5g
180	26.81	38.76	39.53	40.97	42.94	43.95	44.31
150	35.07	39.99	39.86	41.55	40.78	40.00	39.17
120	15.58	22.60	21.57	21.89	21.66	22.99	22.76
90	9.49	11.69	10.64	10.80	12.23	11.83	13.76
45	19.56	25.27	25.86	26.56	26.85	27.06	26.42
0	1.43	2.02	1.53	1.62	9.15	4.27	3.20

Perpendicular Strain ($\mu\varepsilon$)

Tire Position	Load (g level) 1.0g U/L	1.0g	1.1g	1.2g	1.3g	1.4g	1.5g
180	-	-	-	-	-	-	-
150	13.30	13.83	15.81	18.64	22.08	26.42	27.59
120	7.69	18.28	18.75	26.03	37.50	22.31	20.92
90	-	-	-	-	-	-	-
45	2.63	3.76	4.32	3.94	5.07	5.45	5.82
0	3.67	13.71	15.74	17.57	19.80	21.56	23.43

$$TotalStrain = \sqrt{RadialStrain^2 + (PerpendicularStrain)^2}$$

$$y = mx + b$$

Total Strain ($\mu\varepsilon$)

Tire Position (Degrees)	Load (g level/kN) 1.0g U/L	From Test Data 1.0g	1.1g	1.2g	1.3g	1.4g	1.5g	Predicted from Graphed Data 2.0g	2.5g	3.0g	4.0g
	180	410	450	490	530	570	610	820	1,025	1,230	1,640
180	26.81	38.76	39.53	40.97	42.94	43.95	44.31	51.26	57.56	63.85	76.44
150	37.51	42.31	42.88	45.54	46.37	47.94	47.91	55.22	61.65	68.09	80.96
120	17.37	29.06	28.58	34.01	43.30	32.03	30.91	39.35	43.57	47.79	56.24
90	9.49	11.69	10.64	10.80	12.23	11.83	13.76	15.26	17.52	19.77	24.28
45	19.73	25.55	26.21	26.85	27.33	27.61	27.05	29.47	31.26	33.04	36.61
0	3.94	13.86	15.81	17.65	21.81	21.98	23.64	48.86	59.34	69.81	90.77

$$\sigma = \varepsilon E$$ where E = 200,000MPa

Total Stress (MPa)

Tire Position (Degrees)	Load (g level/kN) 1.0g U/L	From Test Data 1.0g	1.1g	1.2g	1.3g	1.4g	1.5g	Predicted from Graphed Data 2.0g	2.5g	3.0g	4.0g
	180	410	450	490	530	570	610	820	1,025	1,230	1,640
180	5.4	7.8	7.9	8.2	8.6	8.8	8.9	10.3	11.5	12.8	15.3
150	7.5	8.5	8.6	9.1	9.3	9.6	9.6	11.0	12.3	13.6	16.2
120	3.5	5.8	5.7	6.8	8.7	6.4	6.2	7.9	8.7	9.6	11.2
90	1.9	2.3	2.1	2.2	2.4	2.4	2.8	3.1	3.5	4.0	4.9
45	3.9	5.1	5.2	5.4	5.5	5.5	5.4	5.9	6.3	6.6	7.3
0	0.8	2.8	3.2	3.5	4.4	4.4	4.7	9.8	11.9	14.0	18.2

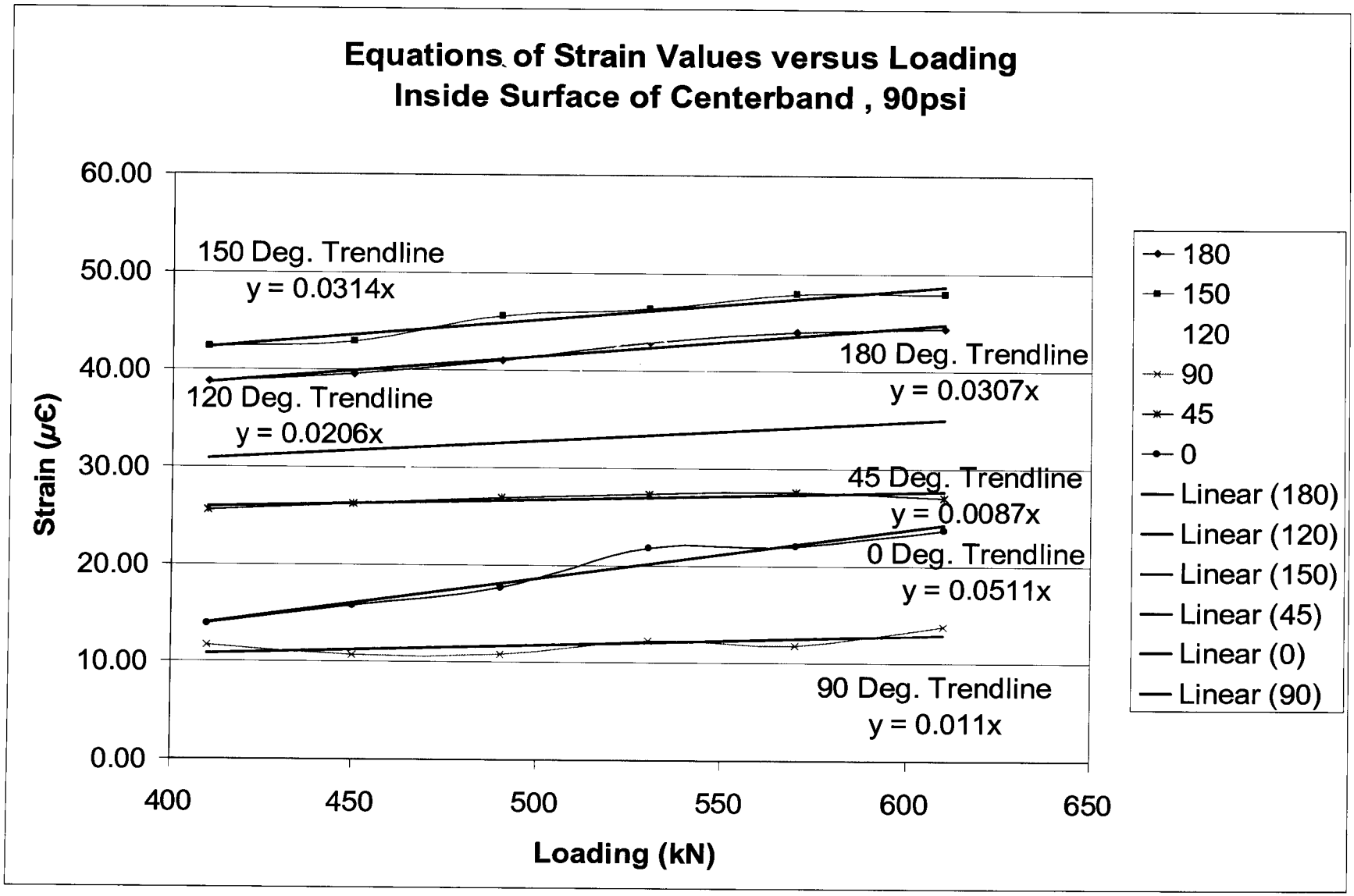

Outside Flange Stress/Strain Calcuations, 80psi

Radial Strain ($\mu\varepsilon$)

Tire Position	Load (g level) 1.0g U/L	1.0g	1.1g	1.2g	1.3g	1.4g	1.5g
180	33.68	154.22	157.18	162.61	165.13	172.00	-
150	16.22	73.10	65.58	72.38	79.90	86.88	-
120	4.57	24.36	28.40	31.30	33.53	35.84	-
90	4.15	13.15	13.90	16.54	19.54	22.54	-
45	11.10	31.41	25.56	25.13	28.36	27.08	-
0	17.55	62.36	61.18	61.40	65.14	70.00	-

Perpendicular Strain ($\mu\varepsilon$)

Tire Position	Load (g level) 1.0g U/L	1.0g	1.1g	1.2g	1.3g	1.4g	1.5g
180	-	-	-	-	-	-	-
150	7.18	8.17	15.40	14.22	16.48	15.30	-
120	12.81	73.17	84.74	91.48	99.17	103.99	-
90	13.99	38.04	44.58	47.65	59.96	69.69	-
45	3.19	8.47	7.53	9.01	10.52	11.64	-
0	6.98	20.65	21.22	20.69	21.81	23.31	-

$$TotalStrain = \sqrt{(RadialStrain)^2 + (PerpendicularStrain)^2}$$

$$y = mx + b$$

Total Strain ($\mu\varepsilon$)

	Load (g level/kN) 1.0g U/L	1.0g	1.1g	1.2g	1.3g	1.4g	1.5g	Predicted from Graphed Data 2.0g	2.5g	3.0g	4.0g
				From Test Data							
Tire Position (Degrees)	180	410	450	490	530	570	610	820	1,025	1,230	1,640
180	33.68	154.22	157.18	162.61	165.13	172.00	-	198.14	220.44	242.74	287.35
150	17.73	73.56	67.36	73.76	81.58	88.22	-	112.85	135.18	157.50	202.15
120	13.60	77.11	89.37	96.69	104.68	109.99	-	162.48	204.03	245.59	328.69
90	14.59	40.25	46.70	50.44	63.07	73.24	-	122.69	164.90	207.11	291.53
45	11.55	32.53	26.65	26.69	30.24	29.48	-	27.04	25.75	24.45	21.87
0	18.89	65.69	64.75	64.79	68.69	73.78	-	84.16	94.47	104.79	125.41

$\sigma = \varepsilon E$ where E = 200,000MPa

Total Stress (MPa)

	Load (g level/kN) 1.0g U/L	1.0g	1.1g	1.2g	1.3g	1.4g	1.5g	Predicted from Graphed Data 2.0g	2.5g	3.0g	4.0g
				From Test Data							
Tire Position (Degrees)	180	410	450	490	530	570	610	820	1,025	1,230	1,640
180	6.7	30.8	31.4	32.5	33.0	34.4	-	39.6	44.1	48.5	57.5
150	3.5	14.7	13.5	14.8	16.3	17.6	-	22.6	27.0	31.5	40.4
120	2.7	15.4	17.9	19.3	20.9	22.0	-	32.5	40.8	49.1	65.7
90	2.9	8.0	9.3	10.1	12.6	14.6	-	24.5	33.0	41.4	58.3
45	2.3	6.5	5.3	5.3	6.0	5.9	-	5.4	5.1	4.9	4.4
0	3.8	13.1	13.0	13.0	13.7	14.8	-	16.8	18.9	21.0	25.1

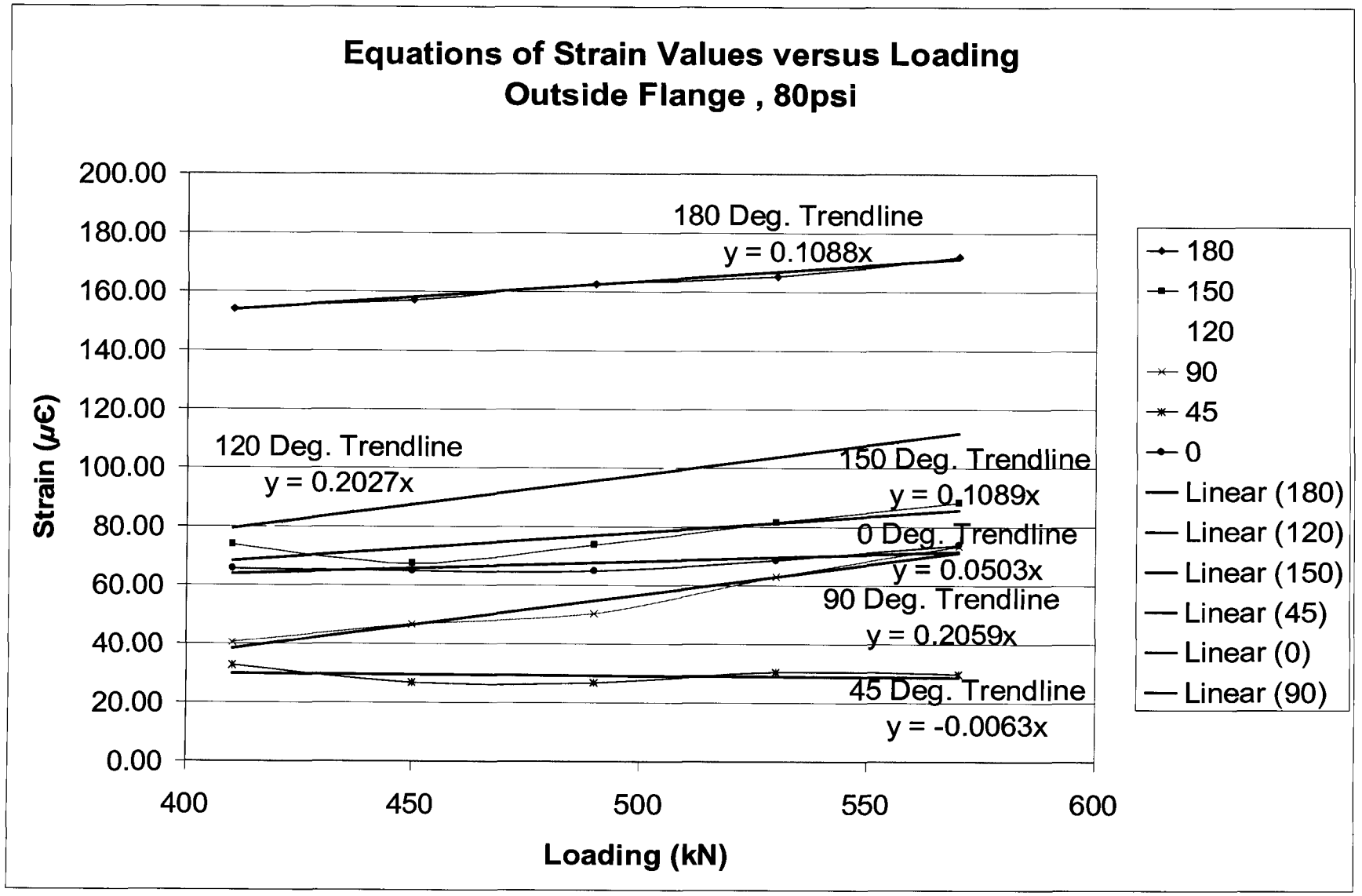

Inside Flange Stress/Strain Calcuations, 80psi

Radial Strain ($\mu\varepsilon$)

Tire Position	Load (g level) 1.0g U/L	1.0g	1.1g	1.2g	1.3g	1.4g	1.5g
180	9.06	22.00	25.45	27.21	30.04	34.91	-
150	7.60	7.82	9.64	9.97	12.42	13.12	-
120	7.44	10.52	25.57	19.57	16.29	13.97	-
90	4.04	5.62	7.42	5.48	4.57	4.38	-
45	7.47	8.57	9.45	8.55	8.51	8.35	-
0	3.77	6.40	6.01	6.80	8.03	7.90	-

Perpendicular Strain ($\mu\varepsilon$)

Tire Position	Load (g level) 1.0g U/L	1.0g	1.1g	1.2g	1.3g	1.4g	1.5g
180	24.23	68.18	73.82	82.99	90.70	99.35	-
150	21.65	24.20	29.70	33.68	39.08	40.94	-
120	28.90	35.34	37.26	37.52	35.12	36.31	-
90	10.65	13.82	16.23	10.14	12.16	14.46	-
45	22.35	26.86	26.10	26.86	27.04	27.05	-
0	9.54	16.00	17.84	16.67	18.19	18.76	-

$$TotalStrain = \sqrt{(RadialStrain)^2 + (PerpendicularStrain)^2}$$

$$y = mx + b$$

Total Strain ($\mu\varepsilon$)	Load (g level/kN) 1.0g U/L	1.0g	1.1g	From Test Data 1.2g	1.3g	1.4g	1.5g	Predicted from Graphed Data 2.0g	2.5g	3.0g	4.0g
Tire Position (Degrees)	180	410	450	490	530	570	610	820	1,025	1,230	1,640
180	25.86	71.64	78.08	87.33	95.54	105.30	-	157.56	201.02	244.48	331.40
150	22.94	25.43	31.22	35.13	41.00	42.99	-	72.16	95.16	118.16	164.16
120	29.85	36.87	45.19	42.32	38.72	38.91	-	38.42	37.19	35.96	33.50
90	11.39	14.92	17.85	11.53	12.99	15.11	-	10.78	8.49	6.19	1.60
45	23.56	28.19	27.76	28.18	28.35	28.31	-	28.87	29.30	29.73	30.59
0	10.26	17.23	18.83	18.00	19.88	20.36	-	24.91	28.66	32.42	39.92

$$\sigma = \varepsilon E$$ where E = 200,000MPa

Total Stress (MPa)	Load (g level/kN) 1.0g U/L	1.0g	1.1g	From Test Data 1.2g	1.3g	1.4g	1.5g	Predicted from Graphed Data 2.0g	2.5g	3.0g	4.0g
Tire Position (Degrees)	180	410	450	490	530	570	610	820	1,025	1,230	1,640
180	5.2	14.3	15.6	17.5	19.1	21.1	-	31.5	40.2	48.9	66.3
150	4.6	5.1	6.2	7.0	8.2	8.6	-	14.4	19.0	23.6	32.8
120	6.0	7.4	9.0	8.5	7.7	7.8	-	7.7	7.4	7.2	6.7
90	2.3	3.0	3.6	2.3	2.6	3.0	-	2.2	1.7	1.2	0.3
45	4.7	5.6	5.6	5.6	5.7	5.7	-	5.8	5.9	5.9	6.1
0	2.1	3.4	3.8	3.6	4.0	4.1	-	5.0	5.7	6.5	8.0

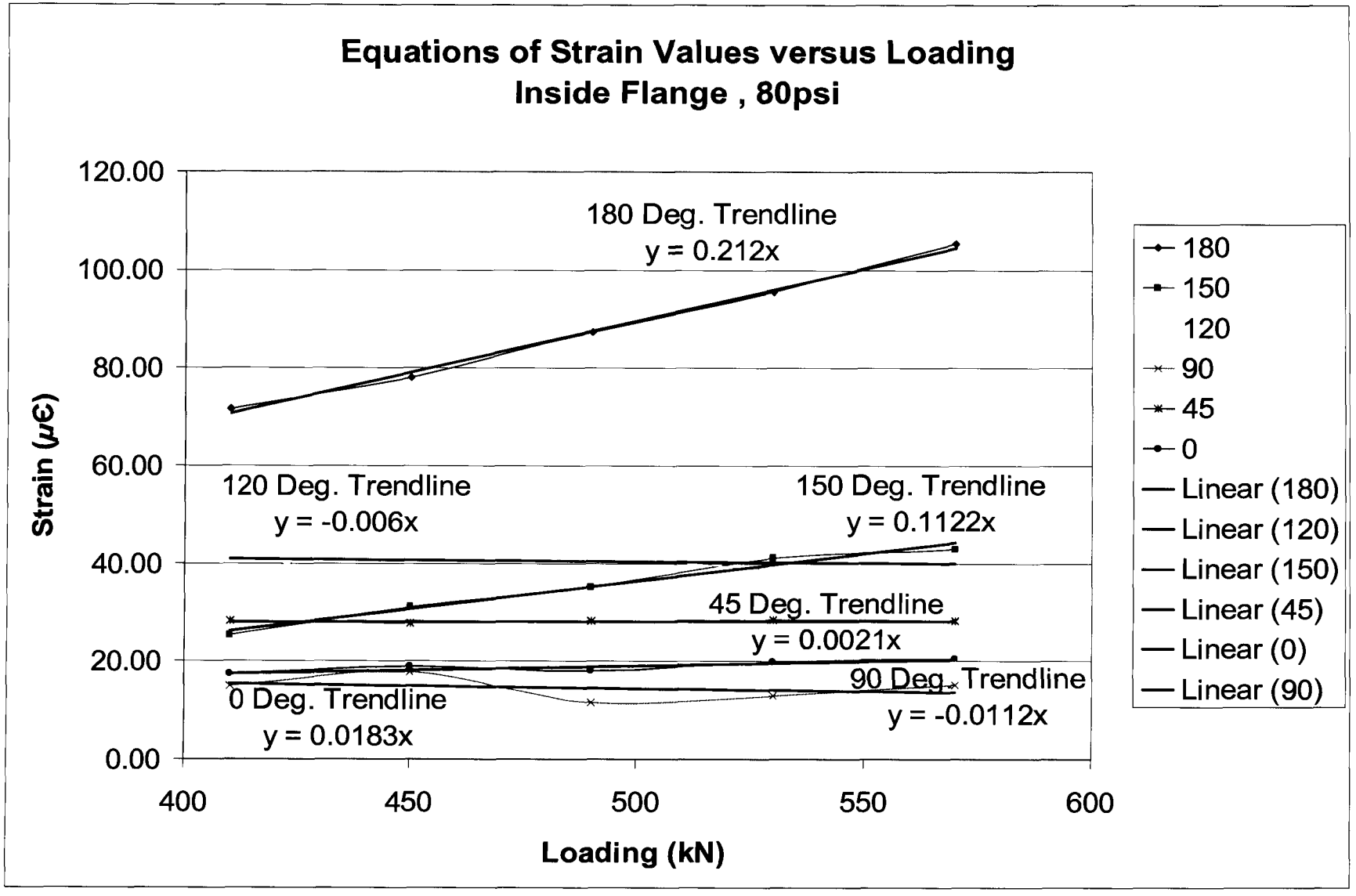

Outside Edge of Centerband Stress/Strain Calcuations, 80psi

Radial Strain ($\mu\varepsilon$)

Tire Position	Load (g level) 1.0g U/L	1.0g	1.1g	1.2g	1.3g	1.4g	1.5g
180	19.96	36.02	42.73	37.44	35.82	42.12	-
150	3.00	2.60	22.20	6.10	5.10	3.00	-
120	2.27	6.26	5.48	6.01	6.44	5.40	-
90	2.88	21.67	22.08	23.32	24.76	24.24	-
45	-	-	-	-	-	-	-
0	-	-	-	-	-	-	-

Perpendicular Strain ($\mu\varepsilon$)

Tire Position	Load (g level) 1.0g U/L	1.0g	1.1g	1.2g	1.3g	1.4g	1.5g
180	107.14	135.14	167.74	166.88	167.56	126.57	-
150	5.32	9.71	8.08	9.44	11.03	8.86	-
120	9.45	41.60	39.22	40.43	40.87	40.94	-
90	9.46	60.46	57.24	59.06	62.31	64.03	-
45	-	-	-	-	-	-	-
0	-	-	-	-	-	-	-

$$TotalStrain = \sqrt{(RadialStrain)^2 + (PerpendicularStrain)^2}$$

$$y = mx + b$$

Total Strain ($\mu\varepsilon$)	Load (g level/kN)			From Test Data				Predicted from Graphed Data			
	1.0g U/L	1.0g	1.1g	1.2g	1.3g	1.4g	1.5g	2.0g	2.5g	3.0g	4.0g
Tire Position (Degrees)	180	410	450	490	530	570	610	820	1,025	1,230	1,640
180	108.99	139.86	173.10	171.02	171.35	133.40	-	146.20	138.82	131.44	116.68
150	6.11	10.05	23.62	11.24	12.15	9.35	-	2.64	3.96	10.56	23.76
120	9.72	41.97	39.60	40.88	41.38	41.29	-	41.33	41.54	41.74	42.15
90	9.89	64.23	61.35	63.50	67.04	68.46	-	76.60	83.85	91.11	105.62
45	-	-	-	-	-	-	-	-	-	-	-
0	-	-	-	-	-	-	-	-	-	-	-

$$\sigma = \varepsilon E$$ where E = 200,000MPa

Total Stress (MPa)	Load (g level/kN)			From Test Data				Predicted from Graphed Data			
	1.0g U/L	1.0g	1.1g	1.2g	1.3g	1.4g	1.5g	2.0g	2.5g	3.0g	4.0g
Tire Position (Degrees)	180	410	450	490	530	570	610	820	1,025	1,230	1,640
180	21.8	28.0	34.6	34.2	34.3	26.7	-	29.2	27.8	26.3	23.3
150	1.2	2.0	4.7	2.2	2.4	1.9	-	0.5	0.8	2.1	4.8
120	1.9	8.4	7.9	8.2	8.3	8.3	-	8.3	8.3	8.3	8.4
90	2.0	12.8	12.3	12.7	13.4	13.7	-	15.3	16.8	18.2	21.1
45	-	-	-	-	-	-	-	-	-	-	-
0	-	-	-	-	-	-	-	-	-	-	-

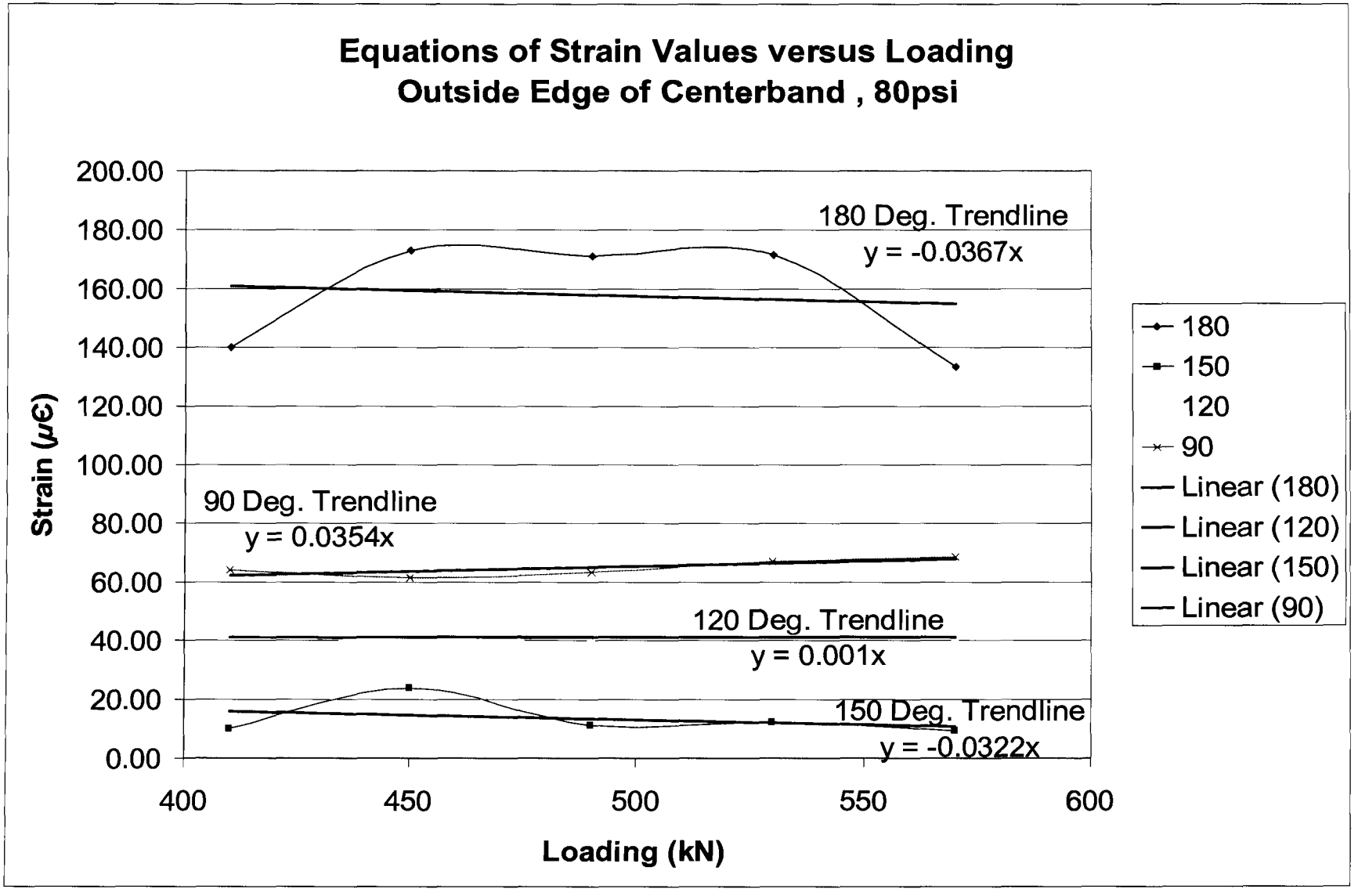

Inside Surface of Centerband Stress/Strain Calcuations, 80psi

Radial Strain ($\mu\varepsilon$)

Tire Position	Load (g level) 1.0g U/L	1.0g	1.1g	1.2g	1.3g	1.4g	1.5g
180	26.74	37.28	40.38	48.04	40.05	40.75	-
150	35.31	42.67	42.58	39.95	38.22	42.69	-
120	15.99	19.40	21.85	22.90	23.31	24.14	-
90	9.70	12.00	10.35	10.40	11.08	11.38	-
45	19.22	24.81	24.32	25.70	25.49	26.63	-
0	1.52	2.24	40.04	10.77	10.01	2.71	-

Perpendicular Strain ($\mu\varepsilon$)

Tire Position	Load (g level) 1.0g U/L	1.0g	1.1g	1.2g	1.3g	1.4g	1.5g
180	-	-	-	-	-	-	-
150	13.64	14.68	17.06	17.64	20.66	23.05	-
120	7.41	19.15	16.89	20.94	22.40	21.97	-
90	-	-	-	-	-	-	-
45	2.63	4.13	5.64	4.88	5.45	5.45	-
0	3.43	14.14	14.69	17.77	19.80	20.99	-

$$TotalStrain = \sqrt{(RadialStrain)^2 + (PerpendicularStrain)^2}$$

$$y = mx + b$$

Total Strain ($\mu\varepsilon$)

Tire Position (Degrees)	Load (g level/kN) 1.0g U/L 180	From Test Data 1.0g 410	1.1g 450	1.2g 490	1.3g 530	1.4g 570	1.5g 610	Predicted from Graphed Data 2.0g 820	2.5g 1,025	3.0g 1,230	4.0g 1,640
180	26.74	37.28	40.38	40.04	40.05	40.75	-	45.20	48.60	52.01	58.81
150	37.85	45.13	45.87	43.67	43.44	48.52	-	48.93	51.16	53.40	57.87
120	17.62	27.27	27.62	31.03	32.33	32.64	-	42.97	50.90	58.84	74.70
90	9.70	12.00	10.35	10.40	11.08	11.38	-	10.59	10.33	10.06	9.53
45	19.40	25.15	24.96	26.16	26.07	27.18	-	30.15	32.60	35.44	40.73
0	3.75	14.32	42.65	20.78	22.19	21.17	-	36.12	46.98	57.85	79.58

$$\sigma = \varepsilon E$$ where E = 200,000MPa

Total Stress (MPa)

Tire Position (Degrees)	Load (g level/kN) 1.0g U/L 180	From Test Data 1.0g 410	1.1g 450	1.2g 490	1.3g 530	1.4g 570	1.5g 610	Predicted from Graphed Data 2.0g 820	2.5g 1,025	3.0g 1,230	4.0g 1,640
180	5.3	7.5	8.1	8.0	8.0	8.2	-	9.0	9.7	10.4	11.8
150	7.6	9.0	9.2	8.7	8.7	9.7	-	9.8	10.2	10.7	11.6
120	3.5	5.5	5.5	6.2	6.5	6.5	-	8.6	10.2	11.8	14.9
90	1.9	2.4	2.1	2.1	2.2	2.3	-	2.1	2.1	2.0	1.9
45	3.9	5.0	5.0	5.2	5.2	5.4	-	6.0	6.6	7.1	8.1
0	0.8	2.9	8.5	4.2	4.4	4.2	-	7.2	9.4	11.6	15.9

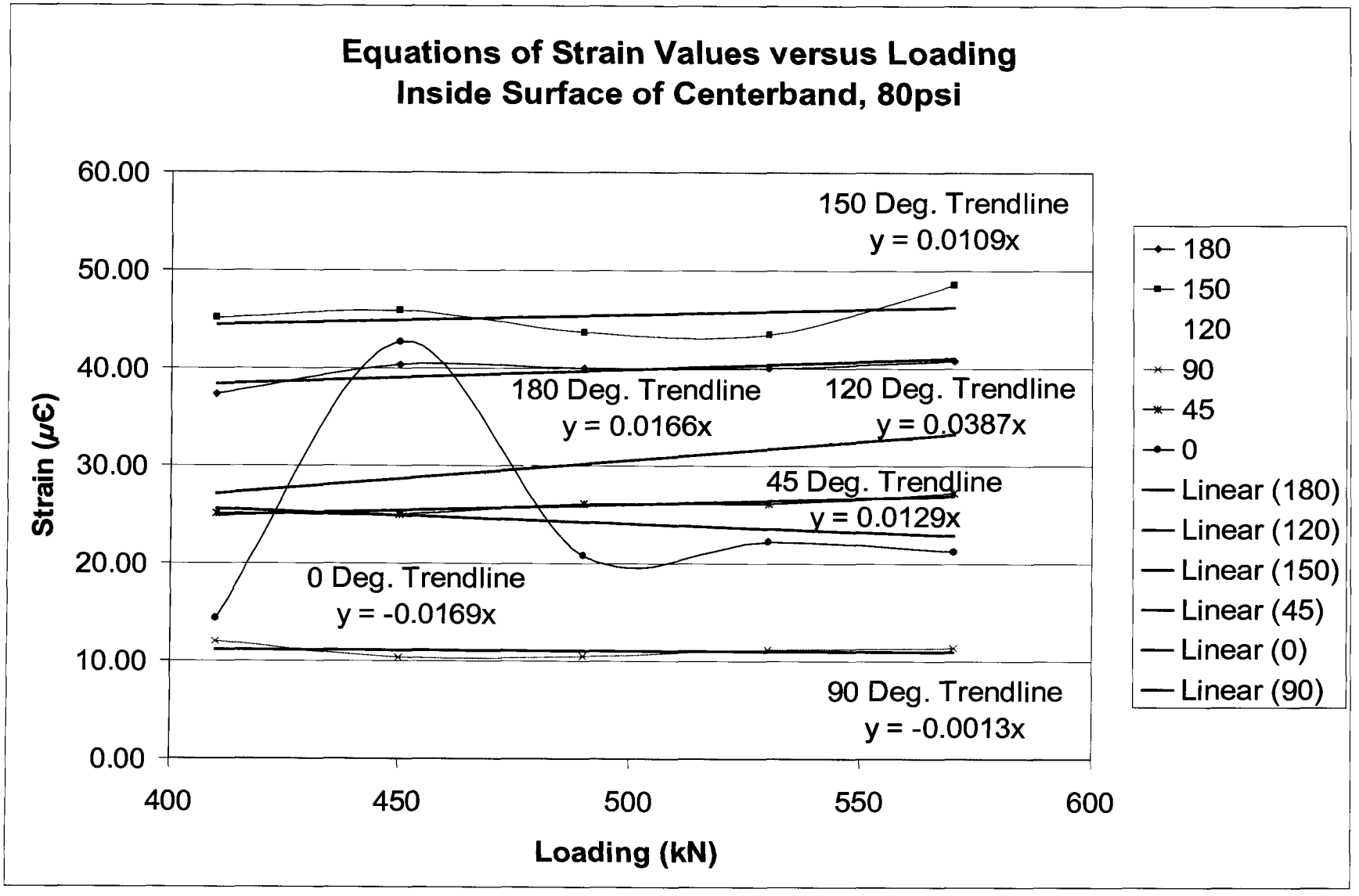

Appendix C Rate of Change of Strain with Respect to Change in Load versus Rim Position

C.1 90psi Tire Pressure

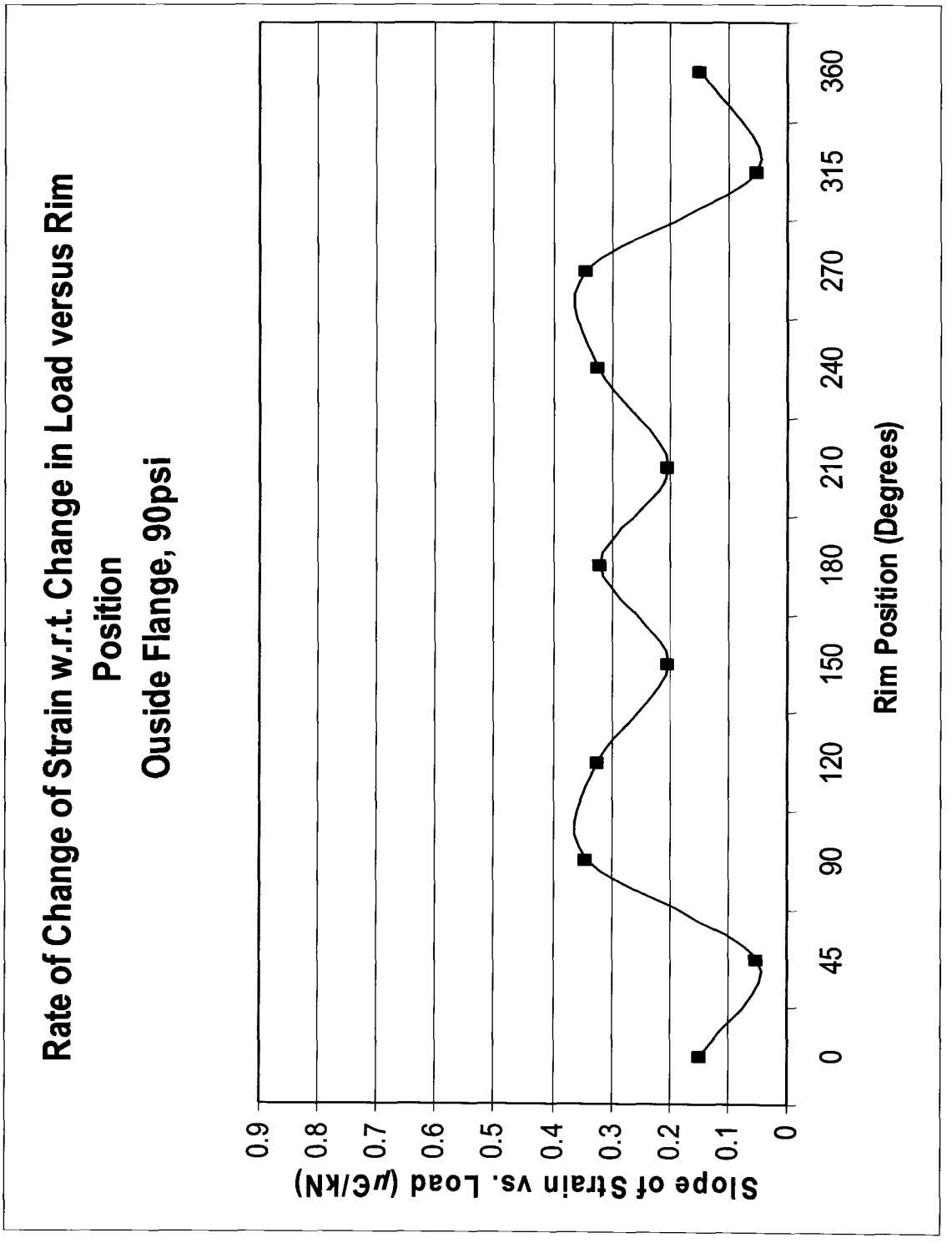

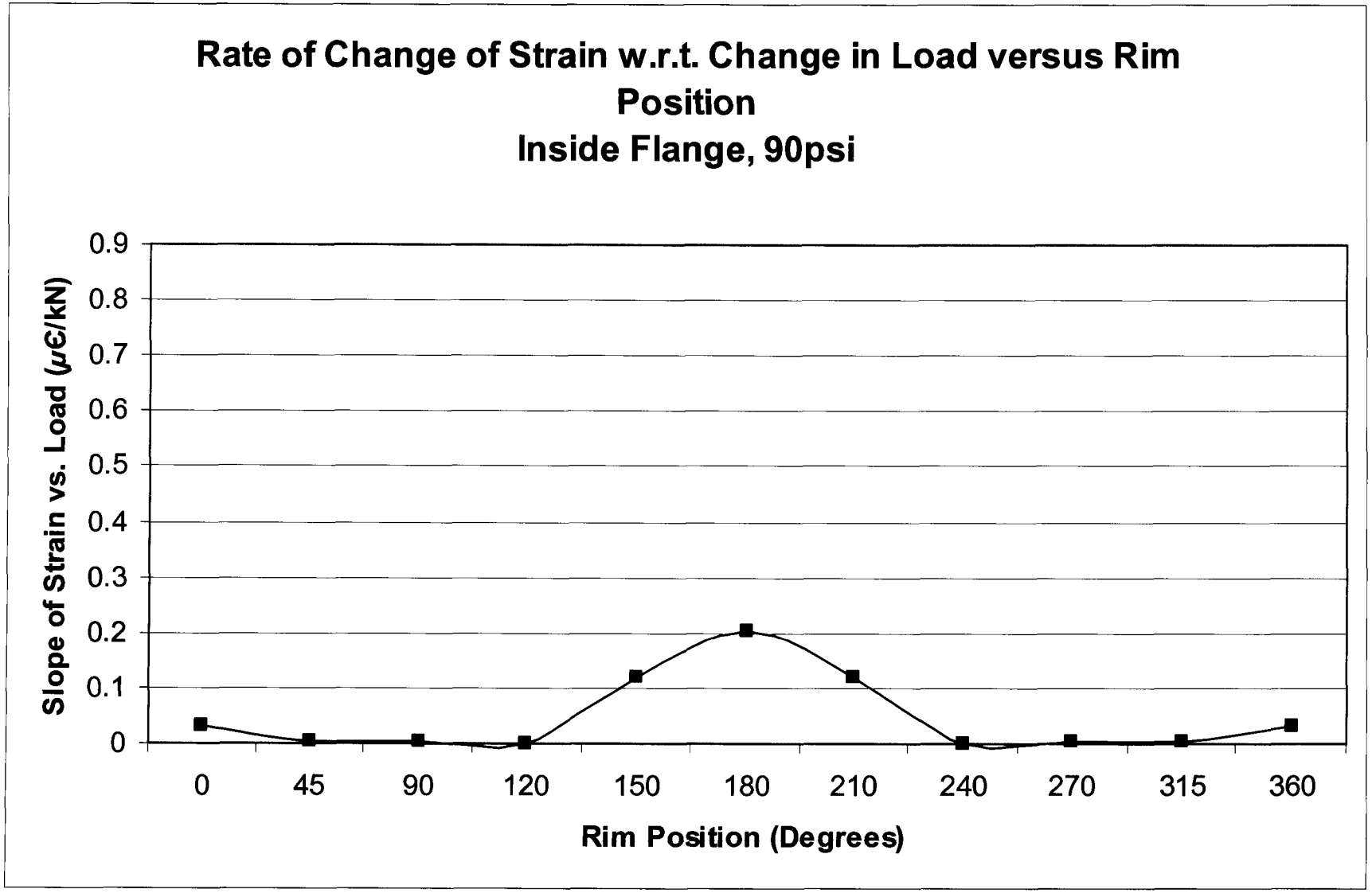

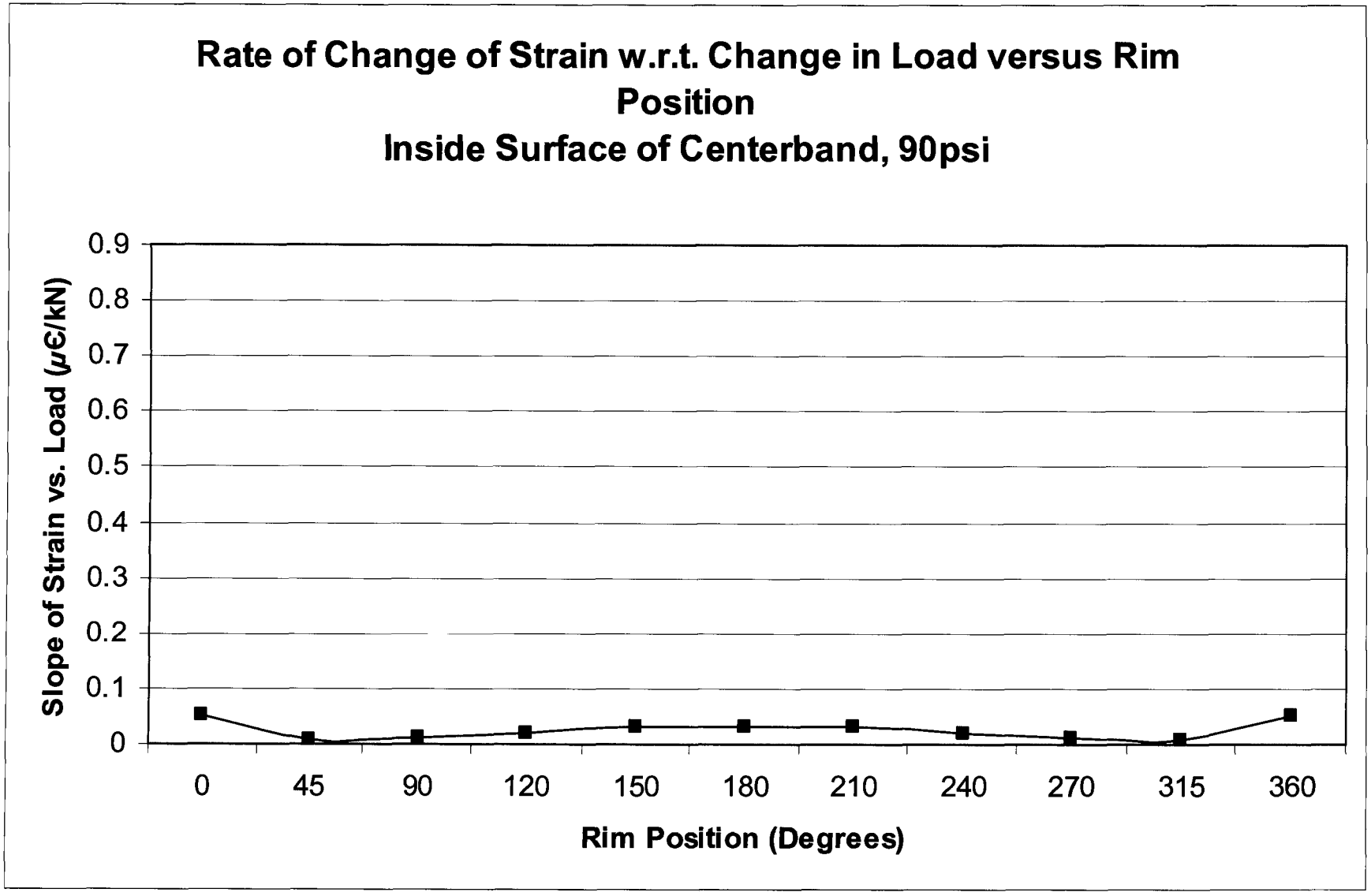

C.2 80psi Tire Pressure

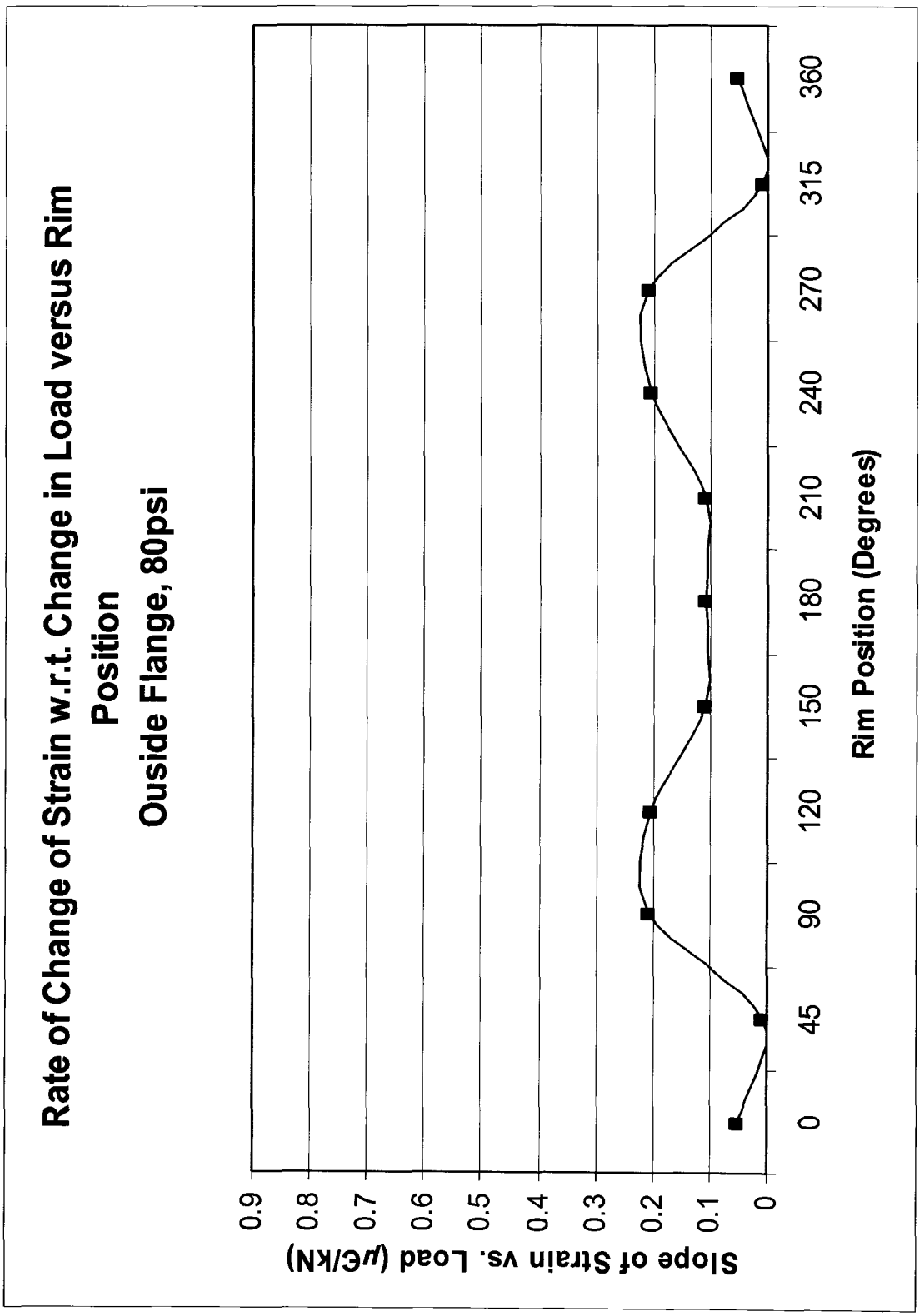

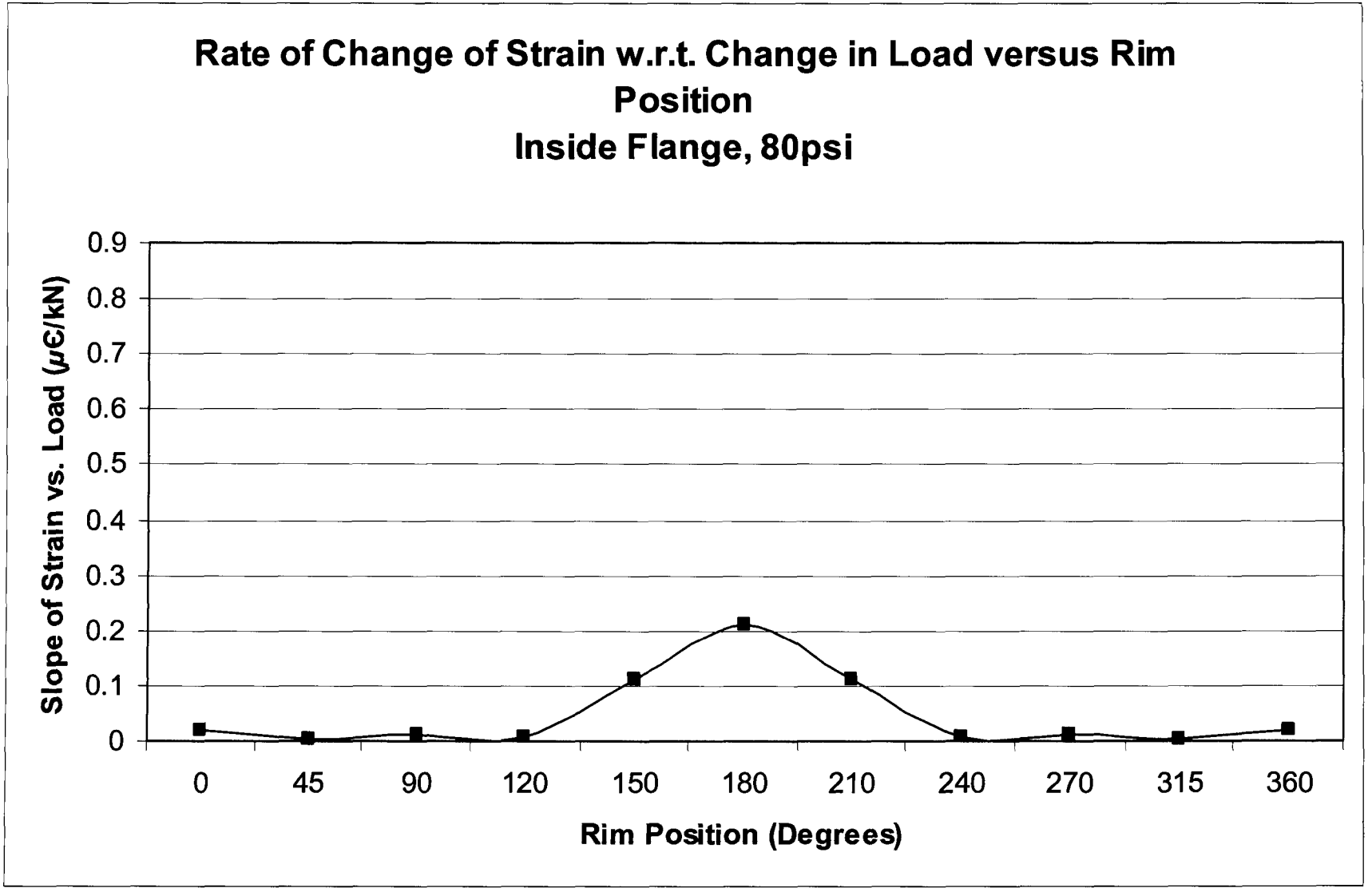

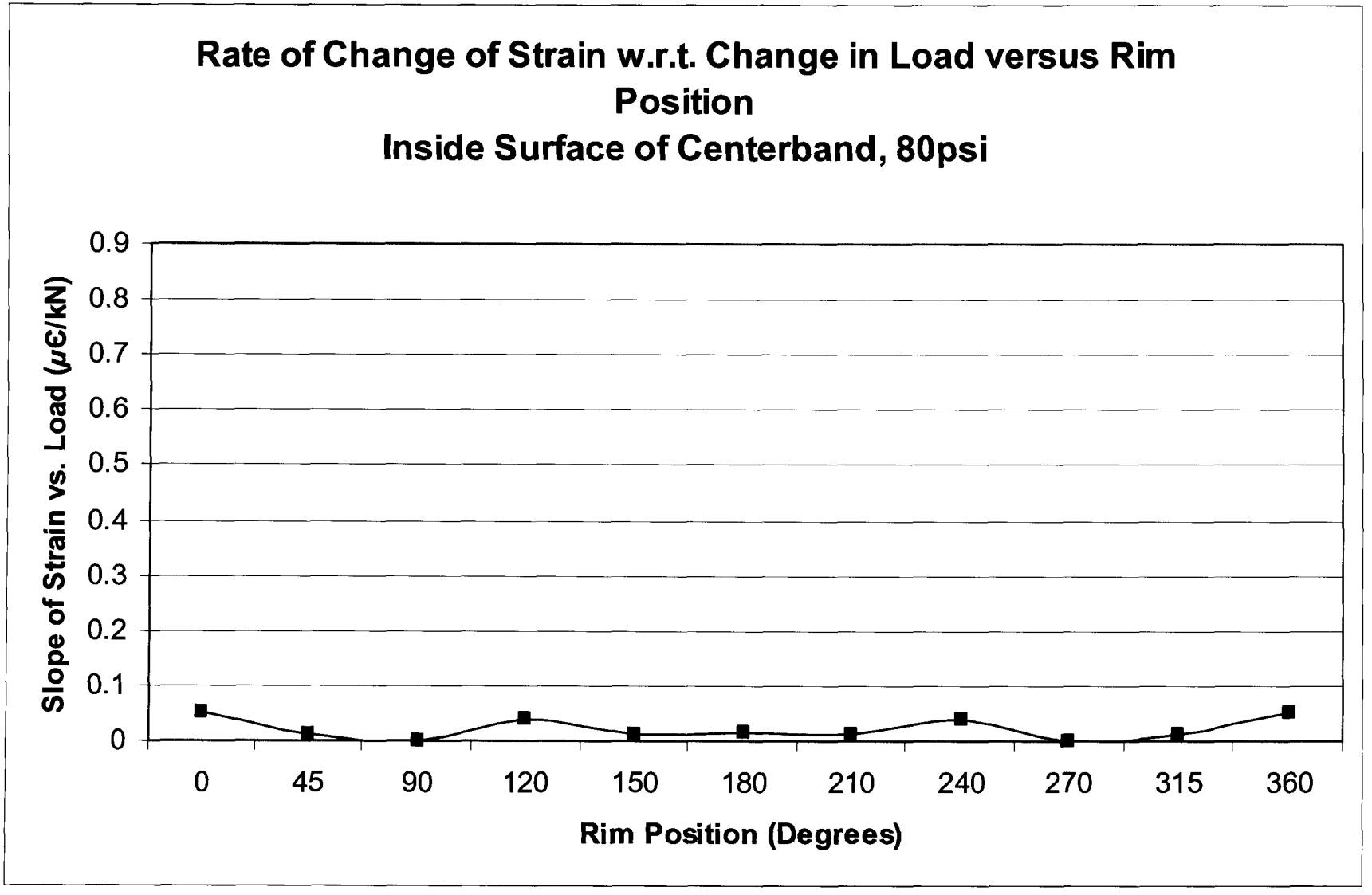

Appendix D Record of Computer Modeling Work

The purpose of this appendix is to summarize the work done in regards to the computer modeling portion of this research project. The original intention for this project was to develop a computer model of an ultra-class rim and tire to provide an alternative set of results to those obtained from the physical testing that was performed. However, due to the complexity of the nature of this project, more specifically, the complexity of the interaction between the rim and tire, it was not possible to accurately develop a model with the software chosen. The notion of starting the computer model portion over with a more customizable piece of software was explored, however, due to the time invested in the initial attempt to model the rim and tire, as well as the time constraints associated with physical testing, it was decided to eliminate the computer model from the scope of the project and focus more on the results of the physical testing.

As a result of this change in scope, a great deal of valid work that was conducted in regards to developing a computer model would no longer be applicable for this thesis. Therefore, instead of abandoning that work completely, it was decided to summarize it in this appendix. This not only provides a record of the work conducted, but also serves as a reference for any future research that will be conducted in this area.

D.1 Description of Computer Model 30 Series

The computer modeling portion of the research project that was completed was conducted using SolidWorks for 3D drafting and COSMOS for finite element analysis. Both software packages are off-the-shelf products and were chosen for their simplicity of application. Drawings of the components were kindly provided by Rimex for the 51" diameter rim that was used for the loading tests outlined above, as well as for 63" diameter rims that Rimex manufactures for Caterpillar Inc.'s 797B ultra-class model and Komatsu Mining Systems 930E ultra-class model.

According to the specifications, each of these rims are entirely constructed using ASTM A36 steel, making modeling of the rim components very easy, as the material properties

of A36 steel can be found with ease, figure D-1. However, accurate modeling of the tire is very difficult, due to its complex material make-up. The tires require radial steel belting for structural support, which have vastly different properties compared to the rubber of the tire. Compounding this large contrast in mechanical properties between the rubber and the steel belting, (almost two orders of magnitude difference for elastic modulus), is the fact that the rubber in the tires is not consistent throughout its form. Starting from the tread, the tire is made up of several different layers of rubber, with properties such as heat absorption, wear resistance, and penetrability changing with the profile. The number and make up of these layers varies depending on the manufacturer, model, and purpose of the tire, making it hard to determine the overall material properties such as elastic modulus, shear modulus, and density. And as mentioned earlier, tire manufacturers, for proprietary reasons, are very reluctant to provide material properties in regards to their tires.

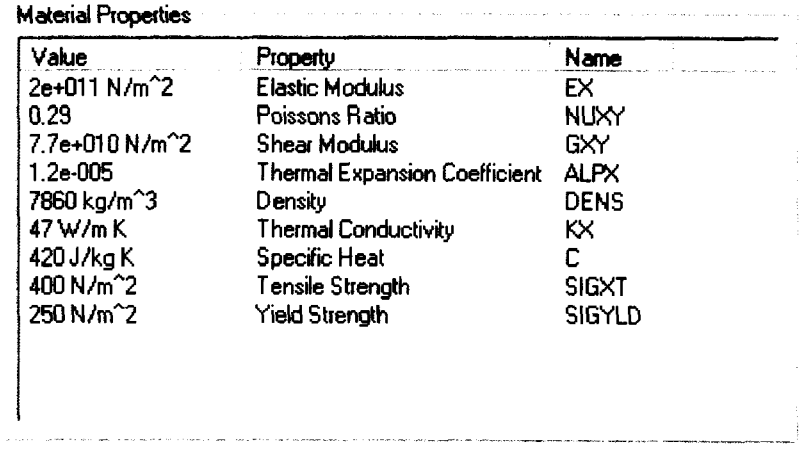

Material Properties

Value	Property	Name
2e+011 N/m^2	Elastic Modulus	EX
0.29	Poissons Ratio	NUXY
7.7e+010 N/m^2	Shear Modulus	GXY
1.2e-005	Thermal Expansion Coefficient	ALPX
7860 kg/m^3	Density	DENS
47 W/m K	Thermal Conductivity	KX
420 J/kg K	Specific Heat	C
400 N/m^2	Tensile Strength	SIGXT
250 N/m^2	Yield Strength	SIGYLD

Figure D-1: Summary of Material Properties for Rim Components

Therefore, it was planned to obtain samples of tread and sidewall materials for an ultra class earthmover tire and to perform material tests to obtain values for elastic modulus, shear modulus, and density. Such samples were kindly donated by Syncurde and Suncor and transported by Kal-Tire, however, they were too large to perform tensile tests on to deduce the values of modulus. It was however possible to determine the density of the

samples which was found to be approximately 979kg/cm^3. In order to establish values for the elastic and shear modulus of the tire, the samples needed to be cut down to much smaller sizes, and the equipment required to cut the tires and produce such samples was not available at or to the University of Alberta. Fortunately, a representative from Goodyear provided modulus values of 3.75MPa and 2.9MPa for a typical tread and sidewall respectively. While these values do not accurately reflex the complexity of the tire make-up they do provide a very good approximation for future attempts at computer modeling. See figures D-2 and D-3 for the complete list of material properties obtained for the modeling of the tire treads and sidewalls respectively.

Material Properties

Value	Property	Name
3.75e+006 N/m^2	Elastic Modulus	EX
0.49	Poissons Ratio	NUXY
2.9e+006 N/m^2	Shear Modulus	GXY
0.00067	Thermal Expansion Coefficient	ALPX
979 kg/m^3	Density	DENS
0.14 W/m K	Thermal Conductivity	KX
1.37871e+007 N/m^2	Tensile Strength	SIGXT
9.23737e+006 N/m^2	Yield Strength	SIGYLD

Figure D-2: Summary of Material Properties for Tire Tread

Material Properties

Value	Property	Name
2.9e+006 N/m^2	Elastic Modulus	EX
0.49	Poissons Ratio	NUXY
2.9e+006 N/m^2	Shear Modulus	GXY
0.00067	Thermal Expansion Coefficient	ALPX
979 kg/m^3	Density	DENS
0.14 W/m K	Thermal Conductivity	KX
1.37871e+007 N/m^2	Tensile Strength	SIGXT
9.23737e+006 N/m^2	Yield Strength	SIGYLD

Figure D-3: Summary of Material Properties for Tire Sidewalls

With the dimensions and physical properties of the rim and tire obtained it was then possible to accurately model the rim and tire combination. To ensure the finite element analysis was as accurate as possible when compared to the physical load test it was decided to completely model the entire test setup. This includes the steel rim plates and I-beam that acted as a hub and an axle respectively. These components were drafted using their measured dimensions and they were given the physical properties of ASTM A36 steel, same as the rim components found in figure D-1. In order to simulate the forces applied to the rim, the equivalent downward force for each g-level (see Table D-1) was applied to the bottom surface of the I-beam. Also, a pressure field was applied to the inside surface of the tire, as well as the rim components that are exposed to the internal pressure of the tire. This pressure was varied from 80psi to 100psi in 10psi increments, the same pressures that were used in the actual loading test.

Table D-1: Summary of Forces used for 30.00R51 Computer Model

g level	Total (lbs)	Per ram (lbs)	Total (kN)	Per ram (kN)	Approx per ram (kN)
1 U/L	40000.0	20000.0	177.9	89.0	90
1.0	91666.0	45833.0	407.8	203.9	205
1.1	100832.6	50416.3	448.5	224.3	225
1.2	109999.2	54999.6	489.3	244.7	245
1.3	119165.8	59582.9	530.1	265.0	265
1.4	128332.4	64166.2	570.9	285.4	285
1.5	137499.0	68749.5	611.6	305.8	305
1.6	146665.6	73332.8	652.4	326.2	325

D.2 Description of Computer Model Large Series

The computer models of the large series tires and rims were setup almost identical to the model described for the 30 series rim and tire in the previous section. The material properties for the rim components and the tires were kept constant, same with the properties of the plate and I-beams. Where the models were mainly different was in terms of scale. As stated previously the CAT 797B and Komatsu 930-E rims and tires were much larger, and therefore, the plate and I-beams had to be increased accordingly. Also, the forces applied to the large series models had to be increased as the forces were

calculated based on the typical gross vehicle weight that the given rim would be subjected to. See Table D-2 for a summary of the forces used in the large series models.

Table D-2: Summary of Forces used for Large Scale Computer Model

g level	Total (lbs)	Per ram (lbs)	Total (kN)	Per ram (kN)	Approx per ram (kN)
1 U/L	92895.3	46447.7	413.2	206.6	210
1.0	229166.7	114583.3	1019.4	509.7	510
1.1	252083.3	126041.7	1121.3	560.7	565
1.2	275000.0	137500.0	1223.3	611.6	615
1.3	297916.7	148958.3	1325.2	662.6	665
1.4	320833.3	160416.7	1427.1	713.6	715
1.5	343750.0	171875.0	1529.1	764.5	765
1.6	366666.7	183333.3	1631.0	815.5	820

Another difference between the models for the large series and the 30.00 series was the geometry of the rim assembly. Obviously the components themselves were larger but there was also a slightly different arrangement of the components when comparing the CAT 797B rim and the 30.00 series rim, as well as a significant difference in the design on the Komatsu 930-E rim compared to the others. See figures 2-6, 2-12 and 2-13 for a representation of the difference in scale and geometry between the three rim designs.

Again, the data presented here is by no means complete, it is presented only as reference material for future research work that will conducted in this field. It is hoped that by summarizing the work completed here that it will not only provide a record of the work that was done, but to also help speed the learning curve for future researchers that will continue on in this field.